Investigating processing body condensation, material properties and function during early *Drosophila* development

This thesis is submitted for the degree of Doctor of Philosophy

Sidney Sussex College
University of Cambridge

Sidney Sussex college

Department of Zoology

July 2020

Sankaranarayanan Meenakshi Sundaram

Personal Declaration

This dissertation is the result of my own work and includes nothing which is the outcome of work done in collaboration except declared in the Preface and specified in the text. Any work from collaborations is duly acknowledged in the beginning of each chapter.

It is not substantially the same as any that I have submitted, or, is being concurrently submitted for a degree, diploma or other qualification at the University of Cambridge or any other University or similar institution except as declared in the Preface and specified in the text. I further state that no substantial part of my dissertation has already been submitted, or, is being concurrently submitted for any such degree, diploma or other qualification at the University of Cambridge or any other University of similar institution except as declared in the Preface and specified in the text. It does not exceed the prescribed word limit for the relevant Degree committee.

Sankaranarayanan Meenakshi Sundaram

12 July 2020

Abstract

Investigating processing body condensation, material properties and function during early *Drosophila* development

This dissertation is submitted for the degree of Doctor of Philosophy

Sankaranarayanan Meenakshi Sundaram

How cells control spatiotemporal protein synthesis is a biological phenomenon with broad implications in physiology, pathology, and therapeutics. Cellular material can be organised into membrane-bound or membrane-less compartments. The latter, commonly known as biomolecular condensates, often contain ribonucleoprotein assemblies that form via liquid-liquid phase separation. Conserved across eukaryotes, Processing bodies (P bodies) are cytoplasmic biomolecular condensates which act as hubs for RNA regulation including storage, translation, and degradation. During *Drosophila* oogenesis, several maternal mRNAs are stored and translationally repressed inside P bodies before they are translated and degraded in the early embryo. How P bodies differentially regulate maternal RNAs is not fully understood.

Using a combination of *in vivo* and *in vitro* assays, I show that P bodies in the mature oocyte exist as multilayered viscoelastic condensates that are regulated by synergistic, multivalent interactions between structurally distinct protein and RNA molecules. I also demonstrate that the gel-like biophysical state of P bodies allows for the storage of *bicoid*, a key maternal transcript needed for embryonic development. Using pharmacological disruption and live imaging, I show that large scale cytoplasmic reorganisation causes P body dispersal during the oocyte to embryo transition to release the stored maternal mRNAs. Finally, in the early embryo, using live imaging and biochemical analyses, I show that P bodies re-form into smaller sized, highly dynamic condensates with altered post-translational and biochemical modifications.

Taken together, developmental cues coordinate synergistic macromolecular interactions and cytoplasmic modifications to differentially regulate RNAs through P body phase transitions during early *Drosophila* development.

Acknowledgements

First and foremost, I would like to acknowledge and thank the limitless and selfless sacrifices of my parents. I am indebted to them for everything they have done for me and whole heartedly appreciate my family for their love and support.

The seeds of my scientific journey were sowed during my undergraduate days and I am particularly grateful to Dr.Saikrishnan Kayarat at the Indian Institute of Science Education and Research, Pune, for introducing me to the world of science and invigorating my scientific curiosity. I would like to also thank my mentors at the National Centre for Biological Sciences, Prof.K. VijayRaghavan, Prof.Mani Ramaswami and Dr.Baskar. B, who have been instrumental in shaping my scientific acumen. I also want to extend my gratitude to my undergraduate lecturers at SASTRA university, Dr.P.R Naren, Dr.Sai Subramanian and Dr.Srinivasan Vedantham, who provided me the moral support and confidence to pursue my interests in life sciences, despite being enrolled in a full-time engineering course!

I would like to express my heartfelt gratitude to Dr.Tim Weil for his constant support and encouragement throughout the duration of my stay in Cambridge. Our discussions, both within and outside of science, have broadened my perspective and vision about life. He gave me immense freedom, independence and support when needed, allowing me to explore brave and interesting trajectories in the project. We had our fair share of differences, but constructive debates and discussions have allowed me to experience and grow as a strong and thinking scientist. I could not have asked for a better person to work with for my PhD, so thank you Tim for believing in my abilities and giving me an opportunity to work in your lab.

I would also like to thank several past and present colleagues and friends in the department for their wonderful support and hospitality in the last three years. All of you made the department a friendly and an enjoyable place to work in! I am particularly grateful to Dr.Paul Conduit, Dr.Matthias Landgraf, Prof.Peter Lawrence and Dr.Matt Wayland for their generous guidance and support whenever I needed. I also have been fortunate to be involved in teaching and supervising undergraduate students at various capacities within the department and I am grateful to the course organisers

Dr.Tim Weil, Dr.Matthias Landgraf, Claudia Lopes and Dr.Paul Conduit for trusting and honing my mentoring skills.

My relationship with the department and Cambridge would be incomplete without acknowledging the countless cricketing memories that I will cherish for a long time. Playing for the Zoology cricket team has been the most fun part of Cambridge life and I would like to thank past and present members of the team for all the lovely times. Additionally, weekend cricket with the Coton cricket club ensured that I made the most of the English summer, playing at different village cricket grounds around south England, all of which have been a truly amazing experience.

My close friends have been an outstanding support system throughout my PhD journey, and I want to particularly thank Lakshmi, Aishwarya, Sridhar, Srinivaas and Swetha for their endless love and support during the good and bad times. This would not have been possible without you guys! I am also grateful to Shipra, Ben, Elise, and Tim for proofreading my thesis.

I would like to thank a few colleagues across the globe, including Dr.Alex Holehouse, Prof.Rohit Pappu and Dr.Amy Gladfelter for their guidance and stimulating discussions at conferences and workshops. A significant portion of my experiments was possible due to the expertise of, and collaboration with the Alberti lab at the Max Planck institute, Dresden (MPI-CBG) and I would like to thank Prof.Simon Alberti, Irmela Trussina and Dr.Titus Franzmann for the support, other members of the Alberti lab for their warmth and hospitality and the MPI-CBG for allowing access to their facilities. I would also like to acknowledge Dr.Marcus Jahnel (Grill lab) and Dr.Anatol Fritsch (Hyman lab) at the MPI-CBG for their insights and technical support with the project.

Last but not the least, my PhD was possible thanks to the generous funding, support, and encouragement from the INLAKS foundation and the Cambridge Trust. I would also like to acknowledge additional sources of financial support from the European Molecular Biology Organization, Company of Biologists, Cambridge philosophical society, Leche Trust, and the Sidney Sussex college, that have enabled collaborations, and my attendance to conferences and workshops across Europe.

Table of contents

Chapter 1

General Introduction

1.1 Introduction

A large volume of the cellular cytoplasm is occupied by macromolecular complexes, which predominantly contain ribonucleic acids (RNA) and proteins. How such a densely packed cytoplasm is organised to perform complex, yet specific cellular reactions in space and time is a fundamental question in cell biology. One way to achieve specificity and spatio-temporal control is to create compartments that function as localised reaction centres. A compartment is generally characterised by the following features: A physical boundary that separates its contents from the surrounding cytoplasm, and mobility of molecules to enable chemical reactions to occur inside the compartment. Compartmentalisation, therefore, not only allows the concentration of components locally but also controls the flux of molecules entering and exiting to regulate reaction kinetics.

Historically, such compartments, commonly referred to as organelles, like the endoplasmic reticulum, Golgi apparatus, nucleus and mitochondria, were thought to be the primary reaction centres for regulating signalling and biochemical processes in the cell (Bard and Chia 2016; Bonifacino and Glick 2004; Heald and Cohen-Fix 2014). Since the physical segregation of these organelles from its surrounding renders these compartments impermeable to most molecules, their biomolecular composition needs to be controlled through specialised membrane transport machineries. Due to the presence of a physical membrane, it is possible to comprehend how membrane-bound organelles coexist with the surrounding cytoplasmic milieu.

In addition to membrane-bound organelles, cells also contain organelles that are devoid of membranes. The nucleolus was the first membrane-less organelle observed within a neuronal cell nucleus in the 1830s (Valentin 1837; Wagner 1835). Since then, several membrane-less organelles have been discovered not only in the nucleus, but also in the cytoplasm, raising the possibility that these organelles may contribute, more generally, to an additional level of cellular organisation (Aguilera-Gomez and Rabouille 2017; Banani et al. 2017; Mitrea and Kriwacki 2016). Examples include RNA-protein complexes such as Cajal bodies, promyelocytic leukaemia (PML nuclear bodies) and paraspeckles in the nucleus, as well as processing bodies (P bodies), stress granules and germ granules in the cytoplasm. However, the lack of a physical membrane in these organelles led scientists to ponder a few questions: (a) How do these organelles

ensure that their interior components do not mix with the surrounding nucleoplasm/cytoplasm?; (b) How is the composition of the organelle maintained and regulated?; (c) How is specificity of molecular interactions and chemical reactions within organelles achieved?.

Some membrane-less compartments such as glycogen granules are an exception. Their formation is aided by cross-linked aggregation of multiple glycogen polymers, thereby forming a stable matrix that separates them from the cytoplasm. Membrane-less organelles in which chemical reactions take place frequently require free diffusion of molecules. Hence, such stable cross-aggregation is less suitable. A novel conceptual framework was, therefore, required to understand the physical and chemical (physicochemical) basis of these membrane-less organelles.

In the last decade, several groups have investigated the assembly and properties of diverse membrane-less organelles. Most, if not all, studies have revealed a common observation about these organelles; they act like tiny droplets of oil in water, retaining their morphology and structure, and possess different physicochemical properties from the surrounding cytoplasm. Their assembly is achieved through a process called liquid-liquid phase separation (LLPS) or condensation (Hyman, Weber, and Jülicher 2014), resulting in the formation of compartments which resemble liquid droplets in the cell. Such RNA-protein droplets that form through condensation have recently been referred to as biomolecular condensates. These condensates have been identified across different species including plants, fungi, bacteria, flies, nematodes, and higher order vertebrates such as zebrafish and mice. Mis-regulation of condensates could lead to aberrant phase transitions such as aggregation (including RNA-protein and RNA-only complexes), which are linked to several neurodegenerative diseases (Aguzzi and Altmeyer 2016; Alberti and Dormann 2019; Jain and Vale 2017). Phase separation has, thus, been described as an emerging paradigm to understand the role and function of membrane-less compartments in cell physiology and disease.

1.2 Chapter objectives

In the first half of this chapter, I provide a brief overview of phase separation and the underlying physicochemical features that regulate condensate assembly and properties. I also discuss the different models postulated in the field to understand the sequence and structural determinants that control condensate assembly, composition, and material properties. In the second half of the chapter, I discuss how *Drosophila* eggs can be a powerful model system to investigate various aspects of ribonucleoprotein (RNP) granule phase separation. I then provide a brief overview of P bodies and their roles during early *Drosophila* development. Finally, I conclude by highlighting some outstanding questions and objectives of my thesis.

1.3 Historical overview

A little over a century ago, American cell biologist E.B Wilson performed a simple yet insightful experiment. He squashed starfish eggs between two glass coverslips and noted that as the contents spilled out, cellular material contained spherical blobs that fused frequently, characteristic of chemically different liquids with similar densities suspended in one another. Based on the colour or apparent density, he observed that only droplets of the same type fused upon contact with each other, highlighting their specificity. He, therefore, proposed that the cytoplasm was a jelly fluid holding cellular material in the form of liquid droplets with distinct chemical and biological characteristics. In his paper titled 'The structure of protoplasm', he reported the following: "To sum up, a critical study of the living protoplasm of echinoderm-eggs shows that it is a liquid, or rather a mixture of liquids, consisting of a continuous substance in which are suspended drops of two general orders of magnitude and of different chemical nature" (Wilson 1899). In 1955, Harry Walter and Donald Brooks, borrowing ideas from the field of polymer chemistry, suggested a phase separation model for cellular compartmentalisation based on macromolecular diversity and concentration in cells. They proposed that macromolecules in the cell could partition and compartmentalise the cytoplasm into physicochemically distinct compartments, analogous to aqueous two-phase systems in which biomaterials with distinct properties partition amongst different phases (Walter and Brooks 1995).

Using electron microscopy, several electron-dense structures which completely lacked a physical membrane continued to be discovered (Figure 1.1), yet what precisely allowed these organelles to form and maintain in the cellular cytoplasm remained a mystery up until recently.

Figure 1.1: Electron micrograph of a *Drosophila* embryo. **(A)** Pole cells (PC) containing nuclear bodies (nb) and polar granules (P). **(B)** Magnified image of a polar granule that illustrates their electron-dense and non-membranous features. Image adapted from: (Mahowald, Illmensee, and Turner 1976).

Half a century later, the idea of cells containing fluid compartments gained renewed interest when Brangwynne and colleagues stumbled upon an unexpected behaviour of membrane-less organelles called P granules inside the embryo of the nematode *Caenorhabditis elegans* (*C.elegans*; Figure 1.2A). They observed that P granules upon contact with one another fused like liquids in a lava lamp (Figure 1.2D), deformed their shape upon shear force and exhibited rapid exchange of molecules, indicating liquid-like behaviour (Figure 1.2B,C). This led to the proposal of a general model of cytoplasmic organisation achieved via several such membrane-less organelles exhibiting liquid-like properties (Brangwynne et al. 2009).

Figure 1.2: Liquid-like characteristics of P granules. (A) Posterior localisation of P granules (green; GFP tagged) in the one cell stage of the *C.elegans* embryo. **(B)** Fluorescence recovery before and after photobleaching of a P granule. Kymograph of intensity profiles (*right*) along the anterior-posterior axis; red colour corresponds to high intensity and blue colour indicates the background intensity. Fluorescence recovery occurs as fast as 5s post bleaching. **(C)** P granule deformation (red outline) upon shear force (white arrowheads indicate directionality). **(D)** Two P granules fusing and relaxing into a single droplet within a minute. Image adapted from: (Hyman et al. 2014).

Their discovery has since led to a dramatic increase in research on diverse biomolecular condensates (Figure 1.3), both nuclear and cytoplasmic (Abbondanzieri and Meyer 2019; Aguzzi and Altmeyer 2016; Al-Husini et al. 2018; Banerjee et al. 2017; Berry et al. 2015; Boeynaems et al. 2017; Brangwynne, Mitchison, and Hyman 2011; Dine et al. 2019; Franzmann et al. 2018; Huizar et al. 2018; Nott et al. 2015; Patel et al. 2015). These studies accumulated strong evidence which established the liquid-like behaviour of most membrane-less organelles and plausible implications for their biological functions. It is possible that cells may have evolved a fine-tuned mechanism for self-organisation through cytoplasmic compartments formed via liquid-liquid phase transitions, enabling reversible assembly and disassembly of compartments in response to cellular and environmental cues.

Figure 1.3: Overview of biomolecular condensates identified in eukaryotic cells. Schematic of the various condensates identified thus far, both in the nucleus and the cytoplasm. While some condensates are specific to certain cell types (eg: Balbiani body and germ granule to germ cells and RNA transport granules and synaptic densities to neuronal cells), this graphic represents the numerous condensates as a whole. Image adapted from: (Banani et al. 2017).

1.4 Many membrane-less organelles assemble by LLPS

Like their membrane-bound counterparts, membrane-less organelles are microenvironments, both in the nucleus and the cytoplasm, that facilitate compartmentalisation of macromolecules and act as reaction centres and signalling clusters within the cell (Boeynaems et al. 2018; Bracha, Walls, and Brangwynne 2019). Mostly composed of protein and RNA molecules, these organelles are also referred to as RNP granules/droplets/condensates. Advances in high-resolution imaging approaches have allowed for the identification of a large pool of RNP condensates, including Cajal bodies (storage sites for small nuclear ribonucleoproteins), Balbiani bodies (segregate germ plasm and vegetal patterning molecules within the oocyte), P bodies (storage and degradation sites for RNA) and stress granules (accumulate RNAs and proteins in response to stress). Although these

structures have been studied for a long time, the mechanism underlying their assembly and disassembly has mostly remained unclear. Research in recent times has shown several protein components that are specific to and/or overlap between different RNP granules that exhibit liquid-like behaviour, suggesting a general mechanism of RNP granule assembly via LLPS, despite variations in their subcellular location and function (Figure 1.4).

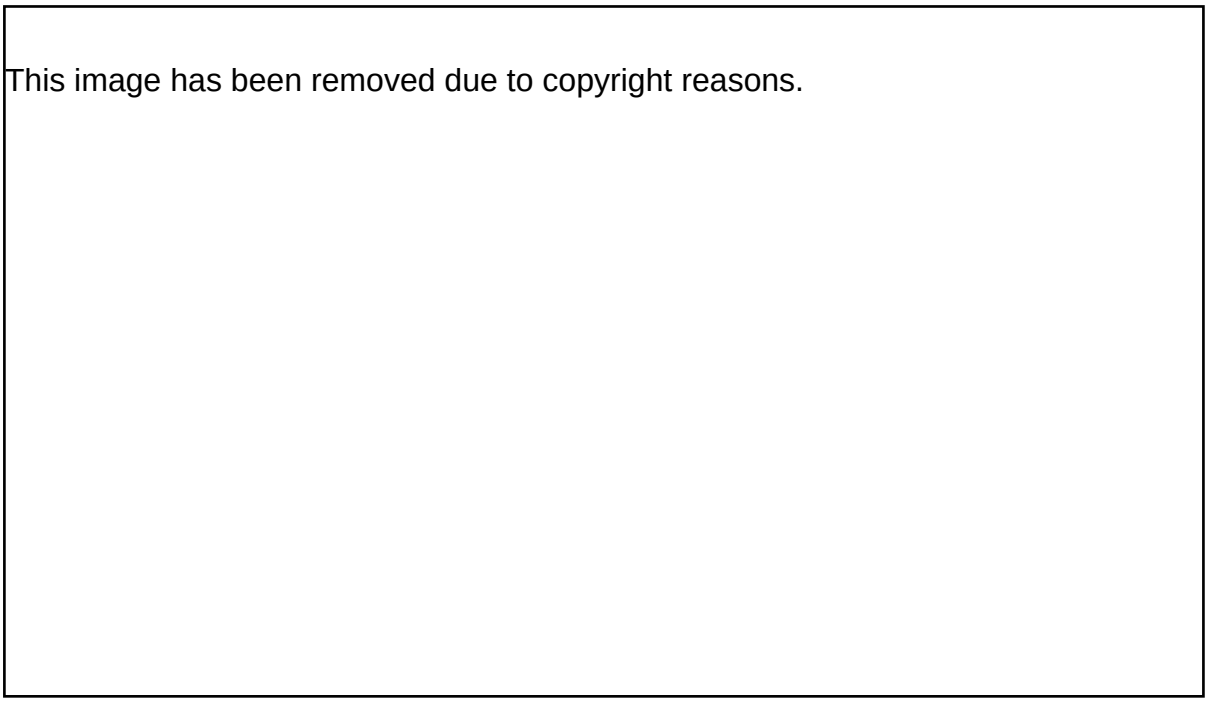

Figure 1.4: Functional diversity of condensates. Schematic highlights the diversity of condensates in different cell types with functions ranging from genome organisation (heterochromatin) to signalling centres (Nephrin-Nck-N-WASP complex). Most, if not all, of the condensates shown in the schematic have been shown to assemble via LLPS. Image adapted from: (Bracha et al. 2019).

LLPS is a physical process that occurs when a homogeneous solution of components spontaneously de-mixes or separates into two phases, a dense phase that is enriched for specific components and a dilute phase that is largely depleted of these same components. During the formation of the dense phase, an interface between the two phases forms a boundary that allows the entry and exit of only selective molecules. This interface allows condensates with liquid-like properties to exist as functionally distinct compartments in the cell (Bentley, Frey, and Deniz 2019; Titus et al. 2020). Several excellent reviews have also discussed the physicochemical basis of LLPS (Berry et al. 2015; Brangwynne, Tompa, and Pappu 2015; Choi, Holehouse, and

Pappu 2020; Lee and Wurtz 2018; Perry 2019; Rosowski et al. 2020; Söding et al. 2020).

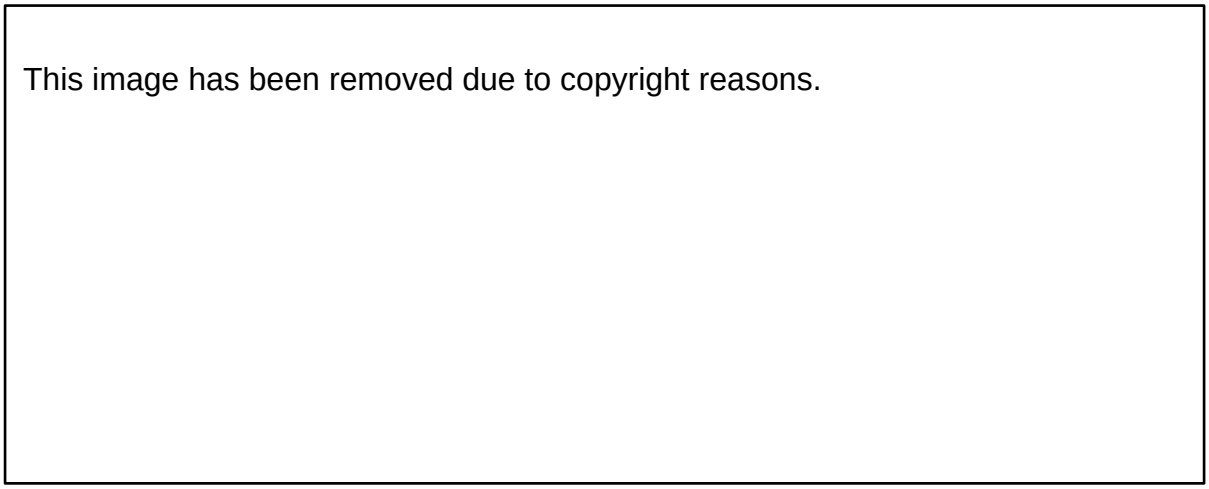

Figure 1.5: Model for condensate assembly and disassembly. Factors such as post-translational modifications (PTMs), temperature, pH and ionic strength can tune the critical macromolecular concentration threshold (gray line) within different ranges (shaded green box) to drive the assembly or disassembly of membrane-less condensates. Image adapted from: (Mitrea and Kriwacki 2016).

The phase separation propensity of condensates is strongly influenced by the concentration of macromolecules and cellular conditions including pH, salt type, ATP levels and temperature (Franzmann et al., 2018; Jain et al., 2016; Kroschwald et al., 2015; Y. Lin et al., 2015; Mitrea & Kriwacki, 2016; Nott et al., 2015). Therefore, depending on the environmental conditions, phase separation can be used to buffer the concentration of protein and RNA molecules between the condensed and dilute phase (Figure 1.5).

The ability of RNP granules to rapidly respond to changing conditions is also strongly dependent on heterotypic inter- and intra-molecular interactions. Although granules contain thousands of different macromolecules, they were generally considered homogeneous in organisation. However, condensates have been recently shown to possess internal organisation on multiple scales. The nucleolus, for example, contains multiple coexisting liquid phases giving rise to a heterogeneous internal organisation (Feric et al. 2016). Such multi-phase organisation has also been reported in multiple RNP bodies such as stress granules, P bodies and P granules (Banerjee et al., 2017; Jain et al., 2016; Putnam et al., 2019; Weil et al., 2012). It is for this reason they are

best described as associative polymers that have a heterogeneous distribution of components held together by physical crosslinks. These crosslinks include protein-protein, RNA-protein and RNA-RNA interactions, which are predominantly weak electrostatic, hydrophobic and Van der Waals forces (Banani et al. 2017; Banerjee et al. 2017; Gomes and Shorter 2019).

RNP phase separation is regulated by multiple factors such as sequence composition, non-equilibrium features such as ATP driven processes and post translational modifications and multivalent interactions (Hofweber et al. 2018; Hofweber and Dormann 2019; Jain et al. 2016; Kim et al. 2019; Patel et al. 2017). Understanding the roles of each of these factors requires extensive manipulation in cells. However, fundamentally, it is extremely challenging to control all of the variables and factors that regulate condensates *in vivo*. Therefore, studying condensates *in vitro* under idealised conditions presented an alternative, yet powerful approach (Alberti et al. 2018). Strong support for this method was provided by Rosen and colleagues in 2012 when they purified protein components associated with actin and reconstituted them *in vitro* (Li et al. 2012). They showed that the reconstituted RNP components displayed liquid-like properties and promoted the nucleation of actin polymers *in vitro*. Following these discoveries, the phase separation propensity of several RNP components have been studied *in vitro* to understand several of the physicochemical properties of RNP granules, including the description of different material /biophysical states exhibited by condensates (Kato et al., 2012; Elbaum-Garfinkle et al., 2015; Lin et al., 2015; Patel et al., 2015).

1.5 Material states of condensates

When the discovery of P granules as liquid-like droplets emerged, it was widely assumed that all membrane-less compartments would exhibit similar material properties. However, several RNP condensates have been shown to exhibit material states other than liquids such as gels, glasses and solids (Boeynaems et al. 2018; Boke et al. 2016; Brangwynne et al. 2009; Hubstenberger et al. 2013, 2015; Putnam et al. 2019). The nature of a granule's material state is often influenced by the molecular composition and interaction strength, structural determinants of RNPs and external cellular conditions (Figure 1.6A). Some examples include the following: (a) Stress granules are liquid-like droplets that can reversibly assemble and disassemble

in response to stress (Wheeler et al. 2016); (b) P bodies in arrested *C. elegans* oocytes exist as semi-liquid condensates which allow sequestration of translationally repressed mRNAs (Hubstenberger et al. 2013); (c) Balbiani bodies found in primary oocytes depend on stable amyloid-like (solid) molecular interactions, serving as storage sites for organelles and macromolecules during dormancy (Boke et al. 2016). These examples illustrate how condensate material states translate to diverse biological functions across cell types and species.

Figure 1.6: Characteristics of protein phase separation. (A) Condensates can exhibit a wide range of material states which are majorly influenced by the nature of intra- and inter-molecular interaction strength and dynamics. Image adapted from (Boeynaems et al. 2018). **(B)** *In vitro* reconstituted FUS-GFP is shown to undergo maturation as it transitions from spherical liquid-like droplets to fibrous solid-like aggregates over time. Image adapted from: (Alberti and Hyman 2016).

In vitro reconstitution experiments have provided evidence that proteins undergo phase transitions from one material state to another (Figure 1.6B). *In vitro* reconstitution studies of the protein Fused in Sarcoma (FUS) showed that they initially form liquid-like droplets, which first ‘harden’ to form gels and later transform into solid fibrillar aggregates (Murakami et al. 2015; Murray et al. 2017; Patel et al. 2015). This

stepwise transition of material states is referred to as gelation or molecular aging or maturation and has been observed for a large fraction of *in vitro* reconstituted proteins. While the underlying structural features of this maturation process are not clear, such transitions are known to be accelerated by disease causing mutations (Lee et al. 2016; Molliex et al. 2015; Patel et al. 2015).

Phase transitions of condensates are primarily governed by transient multivalent interactions. *In vivo*, such interaction strengths can be modulated by changing macromolecular concentrations, salt, pH, or ATP levels, thereby allowing cells to reversibly control the assembly and disassembly of RNP condensates. Stress granules which form in response to cellular stress are examples of liquid-like droplets due to their ability to reversibly assemble and disassemble in the presence or absence of stress, respectively (Wheeler et al. 2016). However, stress granule proteins show varied behaviour *in vivo* and *in vitro*. FUS, for example, forms liquid-like droplets in cells without any signs of the molecular aging phenotypes observed *in vitro* (Patel et al. 2015). This suggests that cells contain inherent mechanisms, such as ATP-driven processes, which regulate intermolecular interactions, to prevent aging and maintain the liquid-like properties of FUS and other proteins. Supporting evidence for this comes from a study in the *C.elegans* embryo which showed the importance of an ATP dependent RNA helicase in maintaining the semi-liquid state of germ granule P bodies (Hubstenberger et al. 2013). Inactivation of the helicase caused an aberrant semi-liquid to solid phase transition, suggesting the importance of energy-driven processes in maintaining material states of RNP condensates *in vivo*.

Some condensates can also modify their material properties depending on varying physiological conditions. The centrosome, for example, is a compartment that organises microtubules, and alters between liquid-like and solid-like states depending on the cell cycle stage in the *C.elegans* embryo (Woodruff et al. 2017). This study indicates that different phase transitions, observed predominantly *in vitro*, could be physiologically relevant. Understanding the molecular determinants that regulate condensate material properties is, therefore, crucial.

1.6 Molecular determinants regulating phase separation

For phase separated condensates to form in cells, a collective network of several molecules and their accompanying interactions (protein-protein, RNA-RNA, and protein-RNA) must be established (Figure 1.7). This physical framework is emerging as the key organizing principle to understand the assembly, composition, material properties, and functions of biomolecular condensates. The importance of multivalent interactions, along with weak intermolecular forces, has been emphasised in recent work. Additionally, intrinsically disordered regions or low complexity domains identified within several RNA binding proteins (RBPs) have been proposed as a key driving force in condensate formation. Below is a brief overview of a few of the key molecular determinants regulating condensate phase separation.

1.6.1 Multivalency

Since several intracellular condensates contain RNA-protein complexes, it is not surprising that multivalent protein-protein and RNA-protein interactions have been shown to be important for their assembly (Banani et al. 2016; Molliex et al. 2015; Nakamura et al. 2018; Nott et al. 2015). Rosen and colleagues provided the initial evidence that multivalency is a key determinant of protein phase separation (Li et al. 2012). Valency refers to the actual number of modular motifs that facilitate specific or stochastic intra- and inter-molecular interactions. RBPs with multiple repeats of the same type of motif or different types of modular domains have been identified, with most interactions being of relatively weak affinity. The number of these modular domains, combined with the availability of binding partners, creates a saturation threshold above which phase separation is favoured. Therefore, an increase in modular interactions promotes the formation of larger complexes, which manifests as condensed droplets. Although cellular condensates vary greatly in their composition, the underlying principles governing their formation seem to stem from simple rules such as relative stoichiometry and valency of macromolecules.

1.6.2 Intrinsically disordered regions

Another key determinant that influences condensate assembly, material properties and diversity is the presence of intrinsically disordered proteins/regions (IDPs/IDRs) (Elbaum-Garfinkle et al. 2015; Nott et al. 2015; Smith et al. 2016; J. Wang et al. 2018). These proteins consist of small stretches of low sequence complexity, meaning they

have a biased amino acid composition. Many IDRs also have repetitive stretches of low complexity and hence subsets of these IDRs are also called low complexity domains (LCDs). It is important to note that the term IDP refers to two classes: (a) fully disordered proteins and (b) IDRs within an otherwise structured protein. Such IDRs, widely found in RBPs, are archetypally enriched in certain charged and polar amino acids such as arginine, lysine, glutamine, glycine, serine, proline, and glutamine. The term ‘intrinsically disordered’ also reflects the structural disorder of the protein due to the presence of these motifs, often leading to an inherent preference for conformational flexibility. This means IDRs can typically adopt multiple conformations, with each conformation associated with a probability of occurrence relative to the solution and the environmental conditions (Choi et al. 2019). According to the cellular conditions, the ability of IDPs to create an ensemble of structures by sampling multiple conformations supports the formation of complexes with different morphologies and dynamics. Distinct molecular interactions between proteins with IDRs or/and folded domains, and nucleic acids such as RNA can give rise to a wide range of assembly dynamics and properties. Especially within RBPs, the presence of IDRs and a multi-domain architecture facilitates the formation and regulation of diverse RNP condensates.

1.6.3 Structured domains

In addition to IDRs, evidence also points to the role of structured, well-folded domains in promoting phase separation through multi-domain interactions (Batty, Jensen, and Freemont 2012; Conicella et al. 2020; Hanazawa, Yonetani, and Sugimoto 2011). Any stably folded protein could be induced to form higher order structures given the right conditions. This has been practiced for years by crystallographers who induce protein crystallisation by placing proteins under different conditions such as varying concentrations of salts, crowding agents, and detergents. Therefore, it should not be assumed that the presence of IDRs is a prerequisite for inducing phase separation. Interestingly however, folded domains and IDRs can also interact in concert and this is key to inducing and regulating phase separation. In these proteins, folded domains tend to be interspersed by IDRs, thereby providing a multivalent domain network of interactions. A classic example is the phase separation of Nephrin-Nck-N-WASP condensates, both *in vitro* and *in vivo*, which induced F-actin polymerisation in the presence of Arp 2/3, a complex involved in actin regulation (Case et al. 2019). Phase

separation of the Nephrin-Nck-N-WASP complex is thought to be regulated by the interactive network of folded SH3 domains present on the Nck protein with the short IDR motifs interspersed between the SH3 domains. The IDR sequence containing highly-charged amino acids (a highly conserved positively charged N terminal motif and negatively charged C terminus) was shown to interact weakly with the negatively charged SH3 domains and the positively N terminal motif of the IDR itself. Taken together, the study demonstrated the essentiality of charged IDR motifs and the folded SH3 domains whose interactions with one another is essential for the phase separation of the complex, highlighting the role of folded domains in condensate formation.

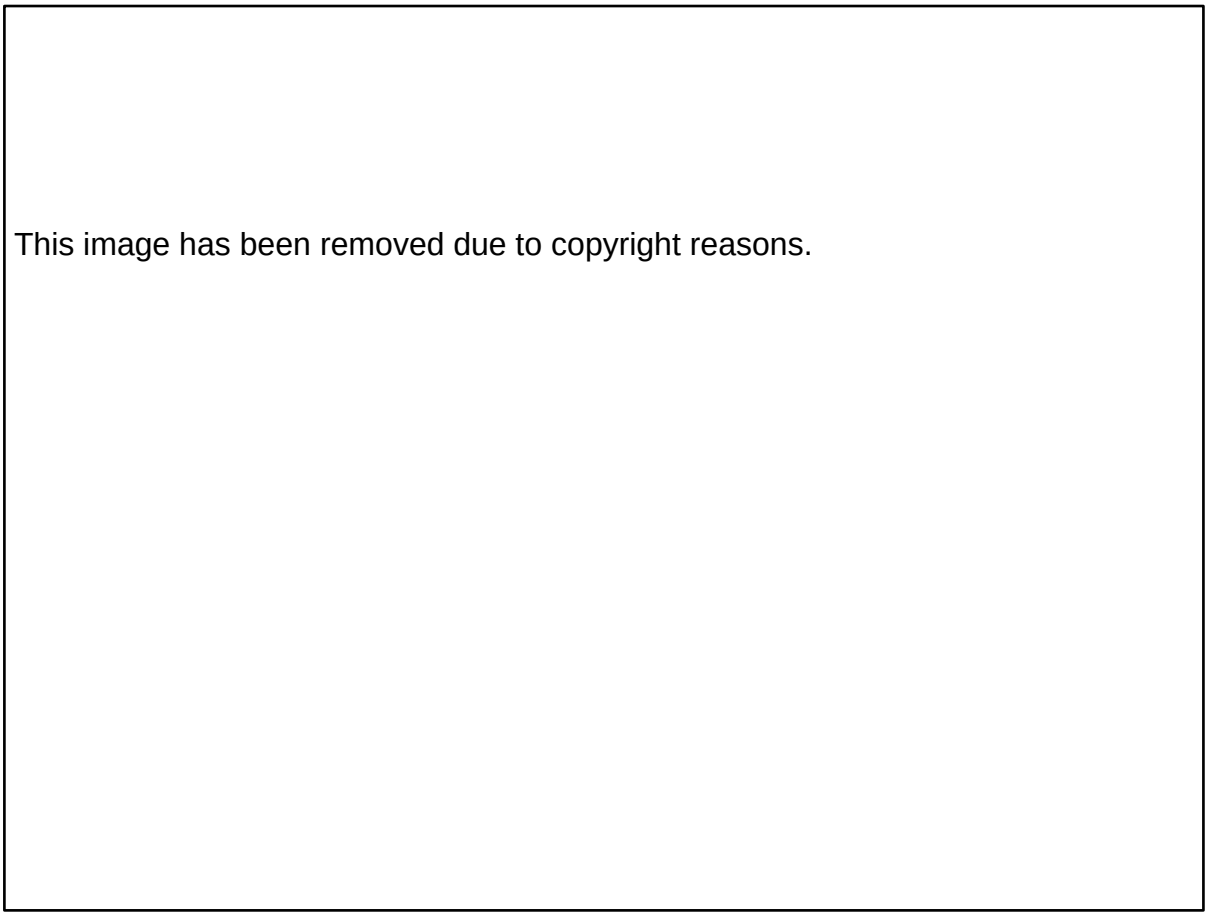

Figure 1.7: Schematic of the various interactions driving RNP granule phase separation. RNP granule assembly is regulated by a wide variety of specific and non-specific molecular interactions. Image adapted from (Van Treeck and Parker 2018).

1.6.4 RNA

RNP condensates not only contain proteins but also numerous RNAs, and recent work has only just begun to discover the role of RNA in condensate assembly and regulation. Given that RNA is a negatively charged molecule, an important source of multivalency can be derived from RNA sequences. Most proteins in RNP condensates contain RNA binding domains, in addition to IDRs, thereby creating a network of synergistic IDR-IDR, RNA-RNA and IDR-RNA interactions to induce phase separation (Banani et al. 2017; Boeynaems et al. 2019; Garcia-Jove Navarro et al. 2019; Langdon et al. 2018; Zhang et al. 2015). Generally, protein concentrations used for inducing phase separation *in vitro* are significantly higher than their physiological ranges. However, in the presence of RNA, the concentration of the protein required to promote phase separation could be titrated closer to physiological levels, thereby lowering the critical concentration. This effect has been observed with numerous RBPs, suggesting that RNA is sufficient to drive condensate assembly at physiological conditions (Burke et al. 2015; Elbaum-Garfinkle et al. 2015; Kroschwald et al. 2015; Lin et al. 2015a; Molliex et al. 2015; Saha et al. 2016; Schwartz et al. 2013; Smith et al. 2016; Zhang et al. 2015). RNA has also been shown to regulate the material properties of RNP condensates. Numerous *in vitro* studies have shown that the presence of RNA is critical for the maintenance of the liquidity of RNP condensates, as the absence of RNA leads to the formation of solid RNP aggregates (Elbaum-Garfinkle et al. 2015; Maharana et al. 2018; Zhang et al. 2015). Depending on the sequence length or concentration in the condensate, RNA can either increase or decrease the viscosity and/or morphology by altering surface tension of the resulting condensates (Elbaum-Garfinkle et al. 2015; Zhang et al. 2015). Interestingly, in ways that are only partially clear, RNA also appears to generate sub-compartmentalisation within RNP condensates (Feric et al. 2016; Gasior et al. 2019; Jain et al. 2016; Trcek et al. 2015). This has been observed in the nucleolus, where differences in the surface tension contributed by RNA-protein interactions create multiple phases within the same nucleolar assembly.

Taken together, condensate assembly and material properties can be regulated in several ways, some of which have been described above.

1.7 Physical basis for condensate phase separation and compositional control

1.7.1 Stickers and spacers model

The importance of multivalency, and inter- and intra-molecular interactions facilitated by IDRs and/or motifs within structured domains suggests that the molecular grammar underlying condensate phase separation is likely encoded in the protein sequence. Moreover, mutations in amino acid residues have been shown to tune and regulate the material states of condensates (Martin et al. 2016; Martin and Mittag 2018). The 'stickers and spacers' model is a useful amino acid-based framework to describe the physical origins of protein phase behaviour (Choi, Dar, and Pappu 2019). Stickers are thought to be motifs that drive phase separation while spacers are linkers interspersed between the stickers to tune material states and offer conformational flexibility. Stickers therefore drive inter-molecular interactions while spacers are more inert. This model can be explained using the Nephrin-Nck-N-WASP phase separation system which drives F actin polymerisation (Li et al. 2012). Nck protein, which contains modular domains such as SH3, can self-associate and phase separate. However, a short 50 residue IDR motif (linker/ spacer) between the first two SH3 domains readily enhanced Nck phase separation. SH3 domains are highly negatively charged and the short linkers have an overall positive charge, thereby creating a multi-domain network which enhances the phase separation. Additional studies also provide evidence for stickers in driving phase separation through various modes of interactions. For example, in the FUS family of proteins, arginine and tyrosine residues in the protein drive phase separation via cation- π and π- π stacking interactions (Wang et al. 2018). Proteins such as Pab1 use hydrophobic forces to drive phase separation (Riback et al. 2017), while others like TDP-43 and proteins with prion-like domains, are driven by aromatic residues (Martin et al. 2020; Schmidt, Barreau, and Rohatgi 2019).

Therefore, while the chemical basis of stickers which drive phase separation varies across proteins, the 'stickers and spacers' model is an attractive framework to describe linear multivalent proteins which contain folded domains connected by IDRs (Figure 1.8). The key takeaway from this model, backed by recent experiments, is a role for IDRs as modulators of material properties of phase separated droplets, even more so than driving their phase separation.

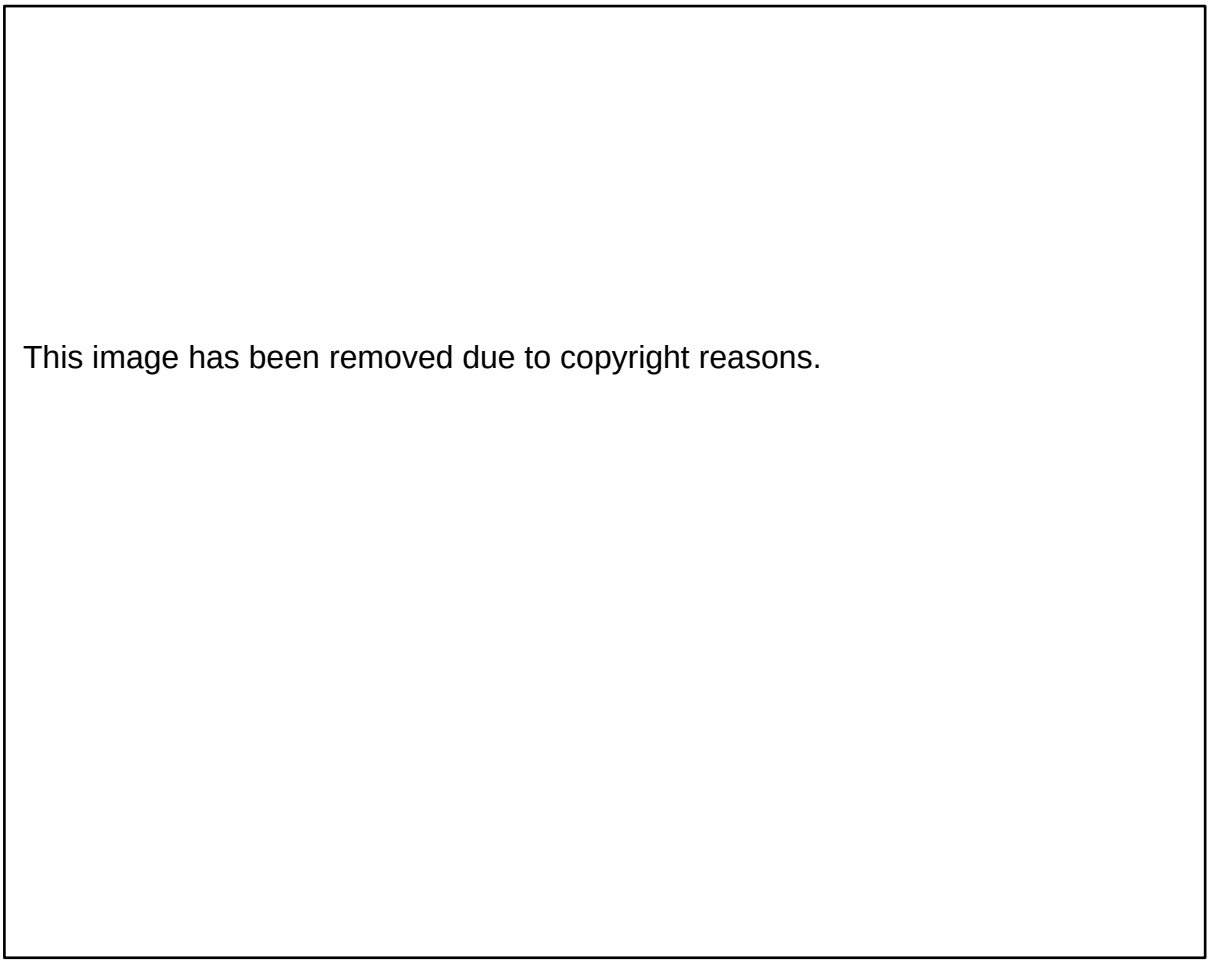

Figure 1.8: Schematic of stickers and spacers model for different systems. (A) For well-folded domains, spacers are regions which support stickers, which are the interaction areas. **(B)** For proteins with linear multivalent motifs, stickers could be mapped as binding domains. **(C)** For IDPs, stickers can be single amino acid residues, short motifs, or a combination of both. In both **(B)** and **(C)**, spacers act as flexible linkers that connect the stickers. Adapted from: (Choi et al. 2020).

1.7.2 Scaffold-client model

Individual cellular condensates can contain tens to hundreds of distinct molecular components. While some components are specific to individual condensates, several others are shared between several condensates, especially among RNP granules. In most, if not all condensates, the biochemical composition is highly dynamic at any given steady state and can be continuously altered under different cellular conditions. Interestingly, recent studies have shown that only a select number of components appear to be necessary for inducing condensate formation (Banani et al. 2016; Ditlev, Case, and Rosen 2018; Espinosa et al. 2020). Deletion or knock-down of these components results in a reduced size, number or even the ability to form condensates.

These molecules are classified as scaffolds. An example of a scaffold is the PML protein which is associated with the PML nuclear bodies (Banani et al. 2016). Deletion of PML protein completely abolishes PML body formation while PML overexpression results in increased PML bodies in the nucleus. On the other hand, several other components associated with these condensates, often by interactions with scaffolds, are dispensable for condensate formation. These components are classified as clients. Depletion of Sp100 and BLM, two proteins associated with PML nuclear bodies, does not affect PML body formation in the nucleus. Although client proteins do not participate in driving condensate assembly, they are thought to influence condensate material properties through distinct interactions with scaffolds. While condensates *in vivo* are highly complex, the scaffold-client distinction is a useful framework to understand the compositional control of minimally engineered condensates, *in vitro* (Figure 1.9). More recently, this model has proved useful to understand how the biochemical composition of P bodies, a conserved class of cytoplasmic RNP granules, is regulated in yeast (Xing et al. 2020).

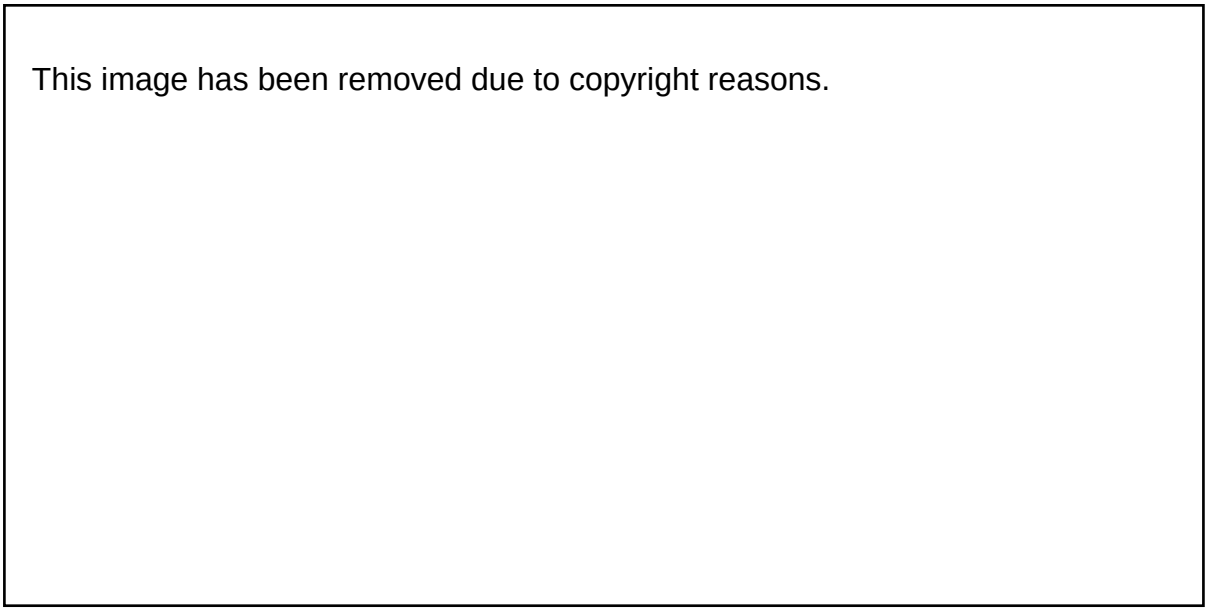

Figure 1.9: Simplified model for compositional control in condensates. (A) Multivalent scaffold proteins (dark blue molecules with homogeneous yellow domains) self-associate to promote granule assembly. **(B)** Client molecules with higher valency/ multivalent domains (dashed yellow domains) are more strongly recruited. **(C)** Partitioning of client proteins (light green molecules) into the condensed granules is regulated by interactions with scaffolds. **(D)** Finally, additional proteins (light blue trianguloid) that bind to different regions of the scaffolds may be recruited independent of client/scaffold stoichiometry. Image adapted and modified from: (Banani et al. 2016).

1.8 Overview of P bodies

P bodies are RNA-protein condensates that are evolutionarily conserved across eukaryotes (Eulalio, Behm-Ansmant, and Izaurralde 2007; Luo, Na, and Slavoff 2018; Standart and Weil 2018) and depend on multivalent RNA-protein network of interactions, presence of structurally distinct proteins, and LLPS for their assembly and regulation. Even though several protein components are shared between P bodies and other RNP condensates such as stress granules, P bodies are distinct in their molecular composition and function (Chantarachot and Bailey-Serres 2018; Decker and Parker 2012; Youn et al. 2019). A major class of proteins enriched in P bodies are involved in mRNA decay and mRNA deadenylation, including the 5'-3' exoribonuclease Xrn1, decapping enzymes DCP1/2 and activators EDC3, Pat1 and DDX6, and the conserved Ccr-Not and Lsm1-7 family of deadenylation complexes (Figure 1.10). Functionally, P bodies were thought to be sites of mRNA degradation due to the enrichment of mRNA decay and degradation factors (Chen and Shyu 2013; Parker and Sheth 2007). However, numerous studies have challenged this model by providing evidence that mRNA decay remains unaffected in the absence of P bodies (Decker, Teixeira, and Parker 2007; Eulalio, Behm-Ansmant, Schweizer, et al. 2007). Several observations, including mRNA localisation into P bodies during conditions such as nutrient stress, suggest that P bodies could act as RNA storage hubs. The effect of varying stresses on P body number, half-life and morphology support the hypothesis that untranslated mRNAs preferentially accumulate in P bodies during stress conditions, thereby promoting cell adaptation (Wang et al., 2018).

Figure 1.10: Outline of P bodies and their constituents. (A) P bodies visualised in COS7 kidney cells using Hedls (green), a decapping activator and Xrn1 (*red*), a 5'-3' exoribonuclease, both of which which localise to P bodies (merge). **(B)** Schematic representation of P body components assembled into an RNP complex. **(C)** P body proteins (yellow) bind to different regions of mRNA (red). Certain proteins recognise specific motifs on the RNA; Upf and Smg bind Premature Termination Codon (PTC) while GW182 and Ago bind AU-rich element (ARE), both of which target mRNAs to microRNA mediated silencing and degradation, respectively. Other protein complexes such as Dcp1/Dcp2, Rck, Edc3 and Hedls facilitate mRNA decapping while Not 1, Ccr4, Caf1, Pan2 complex facilitate mRNA deadenylation. Image adapted from: (Kulkarni, Ozgur, and Stoecklin 2010).

Separate studies involving P body purification from human epithelial cells (Hubstenberger et al. 2017) and ultra-structural analysis of *Drosophila* P bodies in mid-oogenesis have revealed that these condensates are devoid of ribosomes and contain several RNA transcripts, many of which are regulatory RNAs (Weil et al. 2012). Taken together, current evidence points to a more general role for P bodies in post-transcriptional regulation, such as storage and translational regulation, of RNAs.

1.9 Oocytes as a model system to study RNP condensation *in vivo*

Our current understanding of the physicochemical principles regulating condensates has been primarily informed through *in vitro* studies of purified RNP proteins under specific conditions (Elbaum-Garfinkle et al. 2015; Hofweber et al. 2018; Kato et al. 2012; Kim et al. 2019; Li et al. 2012; Lin et al. 2015; Patel et al. 2015). However, why cells need these compartments and what their biological functions are, remain largely unanswered.

RNP condensates such as P bodies typically form in response to an accumulation of untranslated mRNAs and the environment of the oocyte is one where RNP granules are more abundant than in any other cell type (Eulalio, Behm-Ansmant, Schweizer, et al. 2007; Patterson, Wood, and Schisa 2011; Schisa 2012; Voronina et al. 2011). Oocytes are highly organised cells which generally rely on RNP granules to localise key maternal transcripts for the patterning of the early embryo (Du, Schmid, and Jansen 2007; Jansova et al. 2018; Kloc and Etkin 2005; Medioni, Mowry, and Besse 2012). Oocytes, therefore, offer a unique opportunity to test the physicochemical principles of phase separation in a living system and further explore the biological role of RNP condensation.

When considering a model system for studying RNP condensation, *Drosophila melanogaster* could prove extremely valuable. *Drosophila* oocytes rely on maternal RNAs and proteins produced in the adjacent, supporting nurse cells which are subsequently deposited into the oocyte (Bastock and St Johnston 2008; Becalska and Gavis 2009; St. Johnston 2005; Kato and Nakamura 2012). To support egg development in the absence of transcription in the oocyte, many RNP granules are optimised to ensure long term storage and translational repression of maternal mRNAs until fertilisation (Derrick and Weil 2017; Kato and Nakamura 2012; Lasko 2012; Piccioni, Zappavigna, and Verrotti 2005; Wilhelm and Smibert 2005). Importantly, homologues and orthologues of *Drosophila* RNP proteins have been shown to phase separate in other systems, including yeast, *C.elegans* and zebrafish (Hondele et al. 2019; Hubstenberger et al. 2013; Roovers et al. 2018). Together with the many experimental advantages, *Drosophila* eggs offer a powerful system to investigate the

physical principles, developmental phase transitions and the biological role of RNP condensation in early development.

1.10 Overview of *Drosophila* oogenesis and early embryogenesis

Drosophila egg development proceeds in uniformly lined egg chambers composed of a cluster of 16 germ cells surrounded by somatic follicle cells (Avilés-Pagán and Orr-Weaver 2018; Bastock and St Johnston 2008; Spradling 1993). The 16 cells, interconnected with each other, originate from four rounds of synchronous and incomplete cell division of a germline daughter stem cell (cystoblast). The cells are connected by cytoplasmic bridges called ring canals, which are actin-rich. During the early stages of oogenesis, one out of the 16 cells is determined to become the future oocyte, while the remaining 15 cells develop into polyploid nurse cells. The nurse cells synthesise maternal mRNAs and several other factors which are actively transported to the oocyte via microtubules (Kato and Nakamura 2012; Trovisco et al. 2016). Several of the transported mRNAs are localised to specific regions in the oocyte (Hughes and Simmonds 2019; Lasko 2012; Weil 2014). While many mRNAs are translated at different stages of oogenesis, selective maternal transcripts are translationally repressed until egg activation (Cha, Koppetsch, and Theurkauf 2001; Eichhorn et al. 2016; Hara et al. 2018; Wang et al. 2017). Maternal mRNAs that are translationally repressed until egg activation are functionally required at a later time in development such as patterning in the embryo.

Egg activation, a universal mechanism conserved across species, is an important step to prepare the egg for fertilisation (Horner and Wolfner 2008; Runft, Jaffe, and Mehlmann 2002). While egg activation occurs during fertilisation in higher order vertebrates, in insects, including *Drosophila*, it occurs prior to fertilisation. Several changes at the molecular and cellular level happen at egg activation which are critical for the egg to progress through fertilisation and early embryogenesis (Krauchunas and Wolfner 2013; Sartain and Wolfner 2013; Weil et al. 2012; York-Andersen et al. 2015). Some of these include maternal mRNA translation and degradation, release from meiotic arrest, post translational modifications of RBPs, cytoskeletal remodelling, and cross linking of the vitelline membrane.

Post egg activation and fertilisation, early embryogenesis proceeds through a syncytial embryo containing ~6000 nuclei, as a result of rapid nuclear division without cell

membrane formation (Johnston and Nüsslein-Volhard 1992; Mahowald 1985). After 9 mitotic divisions, nuclei begin to migrate to the cortex, lining the plasma membrane of the embryo. During division 14, individual membranes surround each cortical nucleus and form a sheet of epithelial cells with apical and basal polarity, a stage of embryo development referred to as cellularisation. It is roughly around this stage that the maternal to zygotic transition occurs and the subsequent embryonic development is governed by the zygotic machinery. A schematic of the different stages in early *Drosophila* development is shown in Figure 1.11.

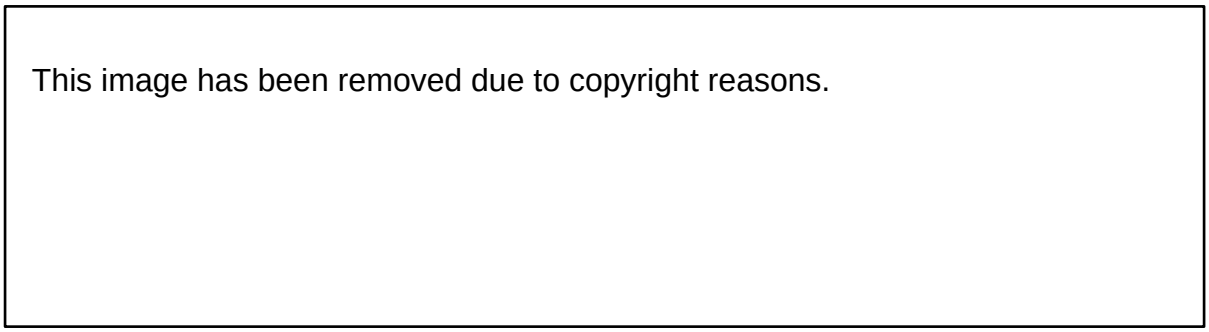

Figure 1.11: Overview of early *Drosophila* development. *Drosophila* females contain 2 ovaries which contain ~16 ovarioles. Each ovariole is a production line with different staged egg chambers consisting of one oocyte and 15 nurse cells (NC). The developing oocyte is surrounded by a layer of somatically derived follicle cells (FC) which participate in patterning in the early stages and eggshell deposition in the later stages. Around stage 10B, NCs begin to dump their contents into the oocyte and undergo apoptosis by the end of stage 13. Oocytes are stalled in prophase 1 until maturation. At maturation, this arrest is released and meiosis proceeds to a secondary arrest point in metaphase 1 in the mature oocyte (DNA in blue and spindle in green). As the mature oocyte descends into the oviduct upon ovulation, it undergoes egg activation by a combination of hydration and mechanical pressure. Fusion of the egg and sperm nuclei post fertilisation in the uterus initiates thirteen rounds of cell division in a common cytoplasm. Eggs which are activated but not fertilised are developmentally arrested after completion of meiosis. Image adapted from : (Avilés-Pagán and Orr-Weaver 2018).

1.11 The role of cytoskeleton in mRNA localisation

Transport of maternal mRNAs and proteins from the nurse cells to the oocyte is an active process that is dependent on the orientation and organisation of microtubule networks (Figure 1.12). The microtubule organising centre is positioned such that the microtubule minus end is pointed towards the oocyte and the dynein-dynactin complex, which is a minus-end directed motor, can facilitate the transport of materials from nurse cells to the oocyte (Figure 1.12A). Mid-oogenesis is marked by an

extensive re-arrangement of the microtubule cytoskeleton (Figure 1.12B), initiated by changes in the properties of the cortical actin. This re-arrangement within the oocyte helps in the localisation of specific maternal mRNAs such as *bcd* and *oskar* to the anterior and posterior poles, respectively. Once localised, these transcripts are anchored by the actin cytoskeleton until they undergo translation (Weil et al. 2008). Together, both the actin and microtubule networks facilitate the localisation and translational regulation of several maternal mRNAs which function in axes formation and development in the early embryo (Becalska and Gavis 2009; Kato and Nakamura 2012; Kloc and Etkin 2005; Saxton 2001).

Figure 1.12: Model for active mRNA localisation during early *Drosophila* development. **(A)** Cartoon depicting egg chambers during early oogenesis; maternal mRNAs (red, black filled circles) are transported from the nurse cells to oocyte via microtubules (green) through actin rich ring canals. Microtubule plus ends are marked in '+' to indicate their polarity. **(B)** Cartoon depicting a mid-staged egg chamber; mRNAs have mostly localised to the respective regions (anterior or posterior), microtubules undergo extensive rearrangement. Oocyte is in yellow; nurse cells and follicle cells are in gray. **(C)** Microtubule organisation in cellularised embryos; some mRNAs are actively localised to apical region via microtubules while others are localised to the basal side. Image adapted from: (Saxton 2001).

Microtubule associated proteins are thought to also influence RNP granule transport and properties during early embryogenesis (Figure 1.12C). For instance, in the stages preceding cellularisation, microtubules have been shown to actively transport embryonic RNAs to the apical region of the embryo (Wilkie and Davis 2001).

How cytoskeletal components regulate RNP granules is not clear, however, it is likely that RBPs interact with motor proteins to help sequester maternal mRNAs for post-transcriptional regulation. During early *Drosophila* development, such regulatory processes are thought to be controlled by P bodies.

1.12 The role of P bodies during *Drosophila* oogenesis

Mature *Drosophila* oocytes can be stored for multiple days without affecting RNA levels (Greenblatt et al. 2019). This efficient storage of RNAs is likely through RNP granules such as P bodies adopting a stable material state. Based on co-localisation studies of different P body proteins, P bodies in the nurse cells and oocytes are thought to have distinct molecular compositions (Lin et al. 2008). Ultra-structural analysis of *Drosophila* P bodies revealed that maternal mRNAs stored inside P bodies are dynamically partitioned according to their translational status (Weil et al. 2012). For instance, *gurken* (*grk*) mRNA enriched on the P body periphery is translated during mid-oogenesis while *bicoid* (*bcd*) mRNA is concentrated in the P body core and translationally repressed until egg activation (Figure 1.13). How P bodies change their material states to differentially regulate maternal mRNA translation is key to understanding their role in *Drosophila* development.

Figure 1.13: Differential partitioning of *bcd* and *grk* within P bodies. Ultrastructural immuno-electron microscopy of P bodies during mid-oogenesis reveals dynamic association of maternal mRNAs *bcd* (*green circles*) and *grk* (*red circles*) according to their translational status. While *bcd* is concentrated within the core, *grk* is dispersed along the edge of P bodies. Image adapted from: (Weil et al. 2012).

At egg activation, P body proteins Maternal expression at 31B (Me31B) and Trailer hitch (Tral) in the mature oocyte were shown to undergo dispersion (Figure 1.14). The significance of this dispersal is not clear; however, current models suggest that P body dispersal upon egg activation allows release of stored mRNAs such as *bcd* for translation. Whether P bodies re-form post activation and fertilisation has not been explored. Although there is not much information on the role of P bodies in embryogenesis, recent studies suggest that P body functions may switch from translational regulation to degradation of maternal RNAs in the early embryo (Patel, Barbee, and Blankenship 2016; Wang et al. 2017).

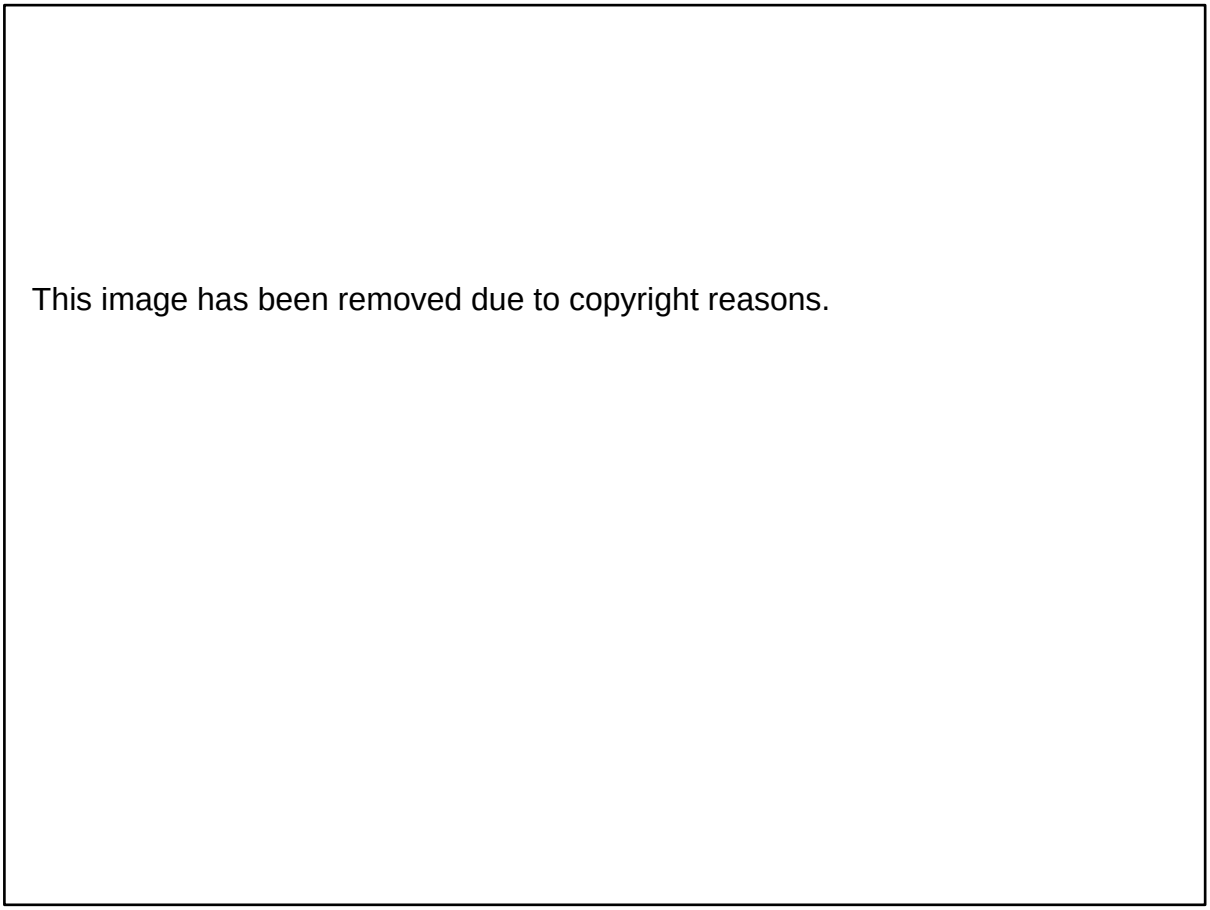

Figure 1.14: P bodies undergo dispersion at egg activation. Two conserved P body proteins Me31B::GFP **(A)** and Tral::YFP **(B)** before and after egg activation. Me31B and Tral are present as large punctate particles prior to activation. Following activation by the addition of activation buffer, Me31B or Tral labelled P bodies disperse into smaller sized, cytoplasmic particles. Image adapted from: (Weil et al. 2012).

1.13 Investigating *Drosophila* P bodies

To visualise and study P bodies during early *Drosophila* development, I utilised two different proteins, Me31B and Tral, as markers. Me31B is an RBP which belongs to the conserved class of ATP dependent DEAD-box RNA helicases that regulate major steps of cellular RNA metabolism. Me31B and its orthologs in humans (DDX6/ RCK/p54), *Xenopus laevis* (Xp54), *C.elegans* (CGH-1) and *Saccharomyces cerevisiae* (Dhh1p) act as global post-transcriptional regulators by mediating mRNA decapping and translational repression (Hondele et al. 2019; Weston and Sommerville 2006). In *Drosophila*, Me31B is thought to repress mRNA translation and stimulate decay. During early embryogenesis, Me31B is shown to repress translation through another P body protein called Cup, which interacts with Me31B through Tral, which

acts as an adaptor protein. Since Cup is known to bind the translational initiation factors eIF4E and eIF4G at the same sites, the Cup-Me31B-Tral complex is thought to disrupt the interactions of eIF4E and eIF4G to inhibit translational initiation (Wilhelm et al., 2003; Nakamura et al., 2004; Nelson et al., 2004; Kinkelin et al., 2012). Me31B also regulates microRNA-mediated decay where it is recruited by CNOT1 protein, which a major component of the CCR4-NOT deadenylase complex (Hillebrand, Barbee, and Ramaswami 2007; McCann et al. 2011; Nishihara et al. 2013). Once bound, Me31B recruits other decapping and deadenylation factors through additional adaptor proteins such as Enhancer of decapping 3 (EDC3) and HPat (or Pat1). Throughout oogenesis, Me31B localises to diverse cytoplasmic maternal RNP granules including nuage, P bodies, sponge bodies and polar granules, indicating that Me31B is a prominent maternal granule protein (DeHaan et al. 2017). In fact, knockdown of Me31B results in the disruption of egg chamber development beyond mid-oogenesis, in addition to the premature translation of certain maternal mRNAs. Whether Me31B mutants affect RNP granule formation was not explored, however, it is likely that Me31B knockdown disrupted granule formation thereby resulting in premature release of stored mRNAs. Me31B, therefore, is a key RBP involved in the translational regulation of mRNAs during oogenesis.

Tral, also a prominent P body protein and interacts with Me31B, is a highly conserved member of the LSm protein family (RAP55 in vertebrates, CAR-1 in *C-elegans*) and a key component of *Drosophila* P bodies (Bouveret 2000; Decker and Parker 2006; Götze et al. 2017; Monzo et al. 2006; Tanaka et al. 2006; Wilhelm, Buszczak, and Sayles 2005). Tral has been implicated in multiple functions during *Drosophila* oogenesis which include: (a) secretion of gurken protein, key dorso-ventral patterning factor and yolkless, the vitellogenin receptor (Herpers and Rabouille 2004; Wilhelm et al. 2005); (b) translational repression of maternal mRNAs as part of the P body complex (Bouveret 2000; Hara et al. 2018) and; (c) normal endoplasmic reticulum exit site formation. Tral expression is not just confined to the germ line but is also found in cultured *Drosophila* S2 cells and neurons (as a component of neuronal transport granules), suggesting a more general role for Tral in RNA metabolism (Tritschler et al. 2007, 2008, 2009). Given their importance in regulating mRNAs during *Drosophila* early development, I utilised both Me31B and Tral to investigate P bodies.

1.14 Thesis objectives

The morphology, localisation, and function of P bodies in *Drosophila* have only been moderately explored. Despite their importance in RNA regulation, the underlying biophysical properties that regulate P body function in the mature oocyte remains unclear. Furthermore, P bodies have been shown to disperse at egg activation. Whether or not P bodies reform post egg activation and if so, what their roles are in the embryo remains less understood. The overall objective of my thesis is to investigate the properties of P bodies and their impact on mRNA regulation during early *Drosophila* development. To this extent, I have presented my findings in the following chapters:

Chapter 2. Materials and Methods

Chapter 3. Investigating Me31B granule properties and function in the mature oocyte

Chapter 4. Investigating Me31B granule properties and function in the early embryo.

Chapter 5. Investigating recombinant Me31B phase separation and material properties *in vitro*.

Chapter 6. Investigating Trailer hitch granule properties and function in the mature oocyte.

Chapter 7. Summary and Conclusion

Chapter 8. References

Chapter 2

Materials and Methods

2.1 Fly husbandry

Fly stocks were maintained at 25ºC on Iberian recipe fly food and stocks were flipped every 3-4 weeks. For dissection of mature oocytes, female flies were 'fattened' on yeast for two days at 25ºC.

2.2 Fly strains

The following fly strains were used for this project:

Table 2.1: The list of *Drosophila* fly stocks used in this project.

Fly line	Genotype	Source
Me31B::GFP	y[1] w[*]; P{w[+mC]=PTT-GB}me31B[CB05282]	Fly Trap CB05282 Bloomington stock number: 51530
ftz^{w20}		Gift from Dr. Erik Clark, Akam lab, University of Cambridge
Trail::GFP	w*; P{w^{+mC}=PTT-un1}G00089	Fly Trap G00089, Kyoto stock DGGR stock number: 110584
Trail^{1} mutant	y[1]; P{y[+mDint2] w[BR.E.BR]=SUPor-P}tral[KG08052] ry[506]/TM3, Sb[1] Ser[1]	Bloomington stock number: 14933
Deficiency (Df(3L)ED4483)	w[1118]; Df(3L)ED4483, P{w[+mW.Scer\FRT.hs3]=3'.RS5+3.3'}ED4483/TM6C, cu[1] Sb[1]	Bloomington stock number: 8070
bcd-RFP	y,w, *bcd* MS2-6-RFP(18)	Gift from Gavis lab (Princeton university)

2.3 Sample preparation

2.3.1 Preparing oocytes: Mature oocytes from fattened female flies were dissected into halocarbon oil on a 22mm by 40mm cover slip for live imaging. For extrusion assays, membranes of dissected mature oocytes were poked and ruptured using sharp forceps to extrude the oocyte contents into the oil. Extruded material was then subjected to live imaging.

2.3.2 Preparing embryos: For embryo collection, 50-100 flies were placed in a plastic cage sealed with an apple juice agar plate containing yeast. Fertilised embryos deposited on the agar plate were collected at different time points depending on the experiment. To remove the hard-outer eggshell (chorion), embryos were

dechorionated in 50% bleach, then were washed with distilled water. Embryos were then placed directly into a drop of halocarbon oil on a 22mm by 40mm coverslip for live imaging.

2.4 Live imaging

Live imaging, including all Fluorescent Recovery After Photobleaching experiments (FRAP), were performed on the Olympus FV3000 microscope using the 1.35 NA, 60X silicone objective. Low magnification images to include whole mature oocytes or embryos were captured using the 1.05 NA, 30X silicone objective. FRAP experiments of Me31B granules at different temperatures were performed on Andor STORM spinning disk confocal microscope using the 1.45 NA, 100X objective. Temperature gradients were controlled using an in-house temperature controller stage built by Dr. Anatol Fritsch (Hyman lab, MPI-CBG, Dresden). Live imaging of recombinant Me31B condensates, induced on 35mm glass bottom MatTek dishes, was performed on the DeltaVision Core widefield microscope (Alberti lab, MPI-CBG, Dresden) using a 1.42 NA, 60X oil immersion objective.

2.5 Temperature assays

To test the effect of temperature on Me31B granules, two independent approaches were used. In the first approach, a temperature-controlled stage was used on which mature oocytes were mounted in a drop of oil. Temperature was rapidly shifted between 20ºC and 35ºC manually, using a temperature controller software.

Since it was difficult to keep mature oocytes alive due to lack of circulating air in the mounting set up, a second approach was also utilised. Here, dissected oocytes mounted in oil on a 22mm by 40mm coverslip were placed in a heat bath set to the temperature of interest. Although temperature was monitored using a mercury thermometer, it is important to acknowledge that the temperature experienced by the oocyte would be a few degrees of magnitude lesser.

2.6 Pharmacological treatments

Mature oocytes mounted in oil on a 22 by 40mm coverslip and set up under the microscope were treated with one or two drops of 10 µg/ml cytochalasin-D or 50 µg/ml colchicine or 5% 1,6 hexanediol [all mixed in 1X Dulbecco’s Phosphate-buffered saline

solution without $MgCl_2$ (Sigma-Aldrich)], or home-made activation buffer (3.3mM NaH_2PO_4, 16.6mM KH_2PO_4, 10mM NaCl, 50mM KCl, 5% PEG 8000, 2mM $CaCl_2$, pH 6.4) using a glass pipette. Me31B or Trailer hitch (Tral) granules before and after treatment were then imaged. In the case of excessive movement of the oocytes during addition of solutions, the focal plane of interest was adjusted accordingly, and imaging was performed.

Table 2.2: The list of pharmacological agents used in this project.

Pharmacological agent	Function	Final concentration	Source
Cytochalasin-D	Depolymerize actin	50 µg/ml	Sigma-Aldrich
Colchicine	Depolymerize microtubules	10 µg/ml	Sigma-Aldrich
1,6 Hexanediol	Disrupt hydrophobic forces	5% w/v	Sigma-Aldrich

2.7 Biochemistry

2.7.1 Lysate preparation: Ovaries from three-day fattened Me31B::GFP or Tral::GFP flies were dissected into Schneider's insect medium and washed with 1x PBS. 0-3 hr old Me31B::GFP or Tral::GFP embryos were collected from a cage, dechorionated in 50% bleach and washed with distilled water. For SDD-AGE, samples (ovary or embryonic extracts) were resuspended in lysis buffer A (150 mM KCl; 20 mM HEPES-KOH; 1mM $MgCl_2$; 1x complete Mini EDTA-free protease inhibitor (Roche); 1x PhosSTOP (Roche)). For SDS-PAGE, samples were resuspended in lysis buffer B (10 mM Tris-Cl pH 7.5; 150 mM NaCl; 0.5 mM EDTA; 0.5% Triton X-100; 1x complete Mini EDTA-free protease inhibitor (Roche); 1x PhosSTOP (Roche). In both cases, addition of lysis buffer was followed by mechanical lysis. Supernatant was collected by centrifugation at 14,000 rcf at 4 °C for 10 min. Protein concentration was measured by Bio-Rad Protein Assay.

2.7.2 SDD-AGE: Aliquots of denatured lysates corresponding to 15 µg of total protein were subjected to SDD-AGE as described in: (Halfmann & Lindquist, 2008), except samples were separated on a 1.8% agarose gel and run at 50V, 4°C.

2.7.3 Sucrose gradient: Lysed extracts (~ 60µl) were layered on top of a 0.6ml linear 15-40% (w/v) sucrose gradient in PBS. The gradient was then centrifuged at 34000 rpm for 20 hours at 4ºC on a Beckman bench ultracentrifuge, followed by fractionation into 60µl fractions. Finally, the pellet was resuspended in 40% sucrose solution and SDS PAGE analysis and western blot analysis were performed.

2.7.4 SDS-PAGE: Aliquots of denatured lysates corresponding to 15 µg of total protein were subjected to SDS-PAGE on a 4-12% Bis-Tris gel (Invitrogen) and blotted by wet transfer to a nitrocellulose membrane.

2.7.5 Western blot: After blocking overnight, membranes were probed with the indicated primary antibody followed by an appropriate horseradish peroxidase-conjugated secondary antibody. α-GFP antibody (Abcam, ab6673) was used at a dilution of 1:2000, α-Me31B antibody (gift from Akira Nakamura) was used at a dilution of 1:200.

2.8 *In situ* HCR

Fertilised embryos were collected at different time points (post deposition) to capture specific stages of development (2 hours for pre-cellularisation, 3 hours for cellularisation and 4 hours for post cellularisation). After dechorionation, embryos were washed and fixed with 4% paraformaldehyde in Phosphate-buffered saline (PBS) for 20 minutes, followed by washing using 1% PBS-tween20 (PBST). *In situ* hybrid chain reaction (*in situ* HCR v3), coupled to immunostaining was carried out in 3 steps:

2.8.1 Hybridisation

200 µl of probe hybridisation buffer (30%) was added to the fixed embryos for pre-incubation at 37ºC for 30 minutes. Following this, probe hybridisation buffer (1:10 dilution) containing the probe of interest (*hairy* or *fushi tarazu*) was added to the embryos and incubated at 37ºC overnight.

2.8.2 Amplification

Post hybridisation, embryos were washed with probe wash buffer 5 times (5X) before pre-incubation in amplification buffer at room temperature for 30 minutes. Simultaneously, a hairpin solution was prepared by heating fluorescently labelled

hairpins at 95ºC for 90 seconds and cooling down to room temperature by placing them in a dark environment for 30 minutes to prevent phototoxicity. Following this, the hairpin solution was mixed with amplification buffer and was added to the embryos and incubated in a dark environment for 2 hours. Post incubation, excess hairpins were removed by washing with 500 µl 5X SSCT buffer at room temperature (5X), followed by washing with 1% PBST (3X). Probes and hairpins were a gift from Dr. Erik Clark, Akam lab, University of Cambridge.

2.8.3 Immunostaining

Post *in situ* hybridisation, embryos were blocked with 5% BSA in 0.2% PBST for 45 minutes, following which embryos were incubated with primary antibody (1:500 goat-αGFP, Abcam; or 1:200 mouse-αMe31B/ 1:200 rabbit-αPat-1, gifts from Akira Nakamura) mixed in 0.2% PBST overnight at 4ºC. Embryos were washed well with 1% PBST (5X) and incubated with secondary antibody (donkey-αgoat-488 or goat-αmouse 488 or goat-αrabbit 561: all at 1:400 dilution) mixed in 1% PBST for 2 hours at room temperature; followed by washing with 1% PBST (5X). Embryos were mounted in ProLong Diamond (ThermoFisher scientific) before imaging.

2.9 Protein purification

Recombinant Me31B-GFP-MBP, both wild-type (WT) and Me31BΔNC mutants, were expressed in and purified from insect cells using the baculovirus expression system (Designing plasmids and viral vectors for expression in insect cells were performed by colleagues at the Alberti lab/protein purification facility at the MPI-CBG, Dresden). Cells were lysed using a microfluidiser in lysis buffer containing 50mM Tris/HCl pH 7.6, 2mM EDTA-containing protease inhibitor cocktail (Roche), 1M KCl, 5% glycerol and 10mM imidazole. The soluble lysate fraction was collected after centrifugation for 1 hour at 16000 rpm at 4ºC. MBP-tagged protein was captured using amylose resin (New England Biolabs), following which the protein from the amylose column was eluted with lysis buffer containing 20mM maltose. The eluted protein was incubated with GST 3C- precision protease (1:50) at room temperature for 2 hours to cleave off the MBP tag. Samples were finally applied to size exclusion chromatography followed by concentrating using an Amicon Ultra centrifugal-500-30K filter at 400 rpm. Aliquots were flash frozen and stored at -80ºC.

2.10 Formation of recombinant condensates and RNA visualisation

To induce phase separation of Me31B condensates (WT and mutants), 7.5 µM Me31B protein was added to the buffer containing 50mM KCl, 20mM PIPES, pH 7, 1% PEG-3K. To induce condensates in the presence of different RNAs (*polyA*, *grk*, etc..), 7.5 µM Me31B protein was added to the buffer containing 50mM KCl, 20mM PIPES, pH 7, 1% PEG and the RNA of interest. To detect RNA, one or two drops of diluted (1:1000) F22 dye (gift from Dr. Shovamayee Maharana, Alberti lab) were added to induced condensates at different time points of interest.

2.11 Optical tweezer experiments

Droplet fusions for WT Me31B, Me31B+*polyA* RNA or Me31B+$MgCl_2$ condensates were quantified using a custom built dual-trap optical tweezer instrument (Jahnel et al., 2011). Condensates were freshly formed in the phase separation buffer containing 50mM KCl and 5% PEG at the following concentrations protein and/or RNA concentrations: a) For WT Me31B, 20 µM Me31B; b) For Me31B+*polyA* RNA, 20 µM Me31B and 75ng/µl *polyA*; c) For Me31B+$MgCl_2$, 20 µM Me31B, 5mM $MgCl_2$. Post condensation, two droplets were trapped using two separate optical traps and brought into close contact to induce fusion. Fusion experiments were carried out by Dr. Marcus Jahnel (MPI-CBG, Dresden).

2.12 Image analyses

2.12.1 Fluorescence Recovery After Photobleaching (FRAP)

For whole particle FRAP of P bodies in the mature oocyte and whole particle FRAP of recombinant Me31B condensates, Me31B/Tral granules or recombinant Me31B condensates were entirely photobleached for 10 seconds using 40% laser intensity from the 405nm laser channel. For internal FRAP, a small region within Me31B granules or recombinant Me31B condensates was photobleached for 5 seconds using 40% laser intensity from the 405nm laser channel. Time lapse series of granule recovery was recorded every 30 seconds (for Me31B or Tral granules) or 10 seconds (recombinant condensates) using the pre-bleach imaging parameters (minimal laser intensity using the 488nm laser channel, 2 Airy unit pinhole, 2048*2048 pixels). Mean fluorescence intensities were calculated using the Fiji ImageJ software. For all FRAP series, except for whole particle FRAP analyses of untreated Me31B granules (Figure 3.8) and hexanediol treated Me31B granules (Figure 3.16), background correction was

performed by subtracting the fluorescent intensities of unbleached, cytoplasmic area from fluorescent intensities of bleached regions. For figures 3.8 and 3.16, it was difficult to get reliable and reproducible background intensity due to the presence of several smaller sized granules, therefore, analyses were performed without background correction. Post background subtraction, fluorescence intensity at each time point was normalised to the pre-bleach condition.

For all FRAP series, statistical analysis, curve fitting and plotting was performed using Rstudio/R software. Data for each condition was averaged and standard deviation was calculated where applicable. Recovery fitting of the normalised mean intensity as function of time was fitted by the least square analysis to determine fit to:

Single exponential: Normalised intensity = $P\times(1-e(-t/\tau))$ or
Double exponential: Normalised intensity= $P1(1-e(-t/\tau^1)) + P2(1-e(-t/\tau^2))$
where P is the recovery plateau, t is time, τ is the time constant. The half maximum ($t_{1/2}$) was calculated from the equation, $t_{1/2}=\tau\times\ln(2)$

To infer the spatiotemporal pattern of fluorescence recovery, kymographs were produced using the ImageJ plugin 'reslice' by measuring fluorescence across of a region of interest over time.

2.12.2 Apparent viscosity estimations

Protocol was adapted from: (Hubstenberger et al., 2013). To determine Me31B granule viscosity in the mature oocytes, two independent approaches were employed. In the first approach, apparent viscosities were estimated from analyses of relaxation times post granule fusions. To quantify relaxation kinetics, granule aspect ratios (A.R), which represents the ratio of major and minor axes length along the granule, was calculated over time (t) using the particle analysis function on the Fiji ImageJ software. The data was fitted by least square analysis:
$a=(a(t0)-P)\times e-t/\tau+Pa=(a(t0)-P)\times e^{-t/\tau+P}$
where a=A.R, t=time, a(t0)=aspect ratio at time zero, P=plateau reached at infinite time, τ=relaxation time constant.

Lengths (L) of fusing granules, $L=[(Major(t0)-Minor(t0))\times Minor(t0)]^{1/2}$), were calculated manually at t=0 and plotted against τ to determine the capillary velocity from the slope, the inverse of which is ~ η/γ, where η and γ are the viscosities and surface tensions of the granules, respectively. Surface tension γ was determined to be ~ $4.06e^{-5}$ using the following approximations:

$\gamma \approx KbT/d^2$, where Kb is the Boltzmann constant, T is temperature in Kelvin and d is the length size of the particle. The average length of RNPs is assumed to be 10 nm from: (Brangwynne et al., 2011). From this, the apparent viscosity η was estimated.

In the second method, granule viscosity was estimated from internal FRAP analysis of Me31B granules shortly post dissection (0-2 hours). Apparent diffusion of ~ 0.00071 $\mu m^2/s$ was estimated from the calculated half-maximum (62.79s) using the equation: $D \approx 0.224\omega^2/ t^{1/2}$, where ω is the radius of the bleach region, t is the time. Using the equation $\eta=(KbT)6\pi RhD$, where Rh is the hydrodynamic radius, assumed to be 2.4nm from: (Hubstenberger et al., 2013) and T is the temperature at which experiments were conducted (21ºC), the apparent viscosity was estimated.

2.12.3 Total fluorescence intensity measurements

To calculate the proportion of total florescence intensity of Me31B that was within granules and the cytoplasm, images were manually segmented based on an arbitrary threshold to extract as much detail as possible. Segmentation resulted in three groups of fluorescence clusters: Me31B granules, cytoplasm, and the background. For each condition, individual clusters were masked onto to the original image to calculate the total fluorescence intensity of the cluster of interest. The proportion of granule-cytoplasmic Me31B fluorescence was calculated by dividing the respective individual total fluorescence intensities. To generate a density plot, similar steps of segmentation and clustering was performed. After masking the clusters onto the original image, using a labelling algorithm in R, Me31B granules per cytoplasmic area were counted and plotted.

2.12.4 Quantifying Me31B granule/condensate morphology and area

Me31B granule morphology was quantified using the ‘shape descriptors’ function on the Fiji ImageJ software. Me31B granule or recombinant Me31B condensate particle area was quantified using the ‘area’ function on the Fiji ImageJ software.

2.12.5 Quantifying Me31B granule and pair-rule mRNA association

Associations between Me31B granules and the pair-rule RNAs *hairy* and *fushi tarazu* were analysed manually using the Fiji ImageJ software. Me31B granules and RNA particles exhibiting complete overlap or 50% overlap were considered as 'associated' whereas those touching each other on the edge or not overlapping were considered 'non-associated'.

2.12.6 Particle tracking

Time lapse images of Me31B granule dynamics before and after pharmacological treatment with 10 µg/ml cytochalasin-D and 50 µg/ml colchicine were collected. A max projection across the Z-stack was generated and opened using the TrackMate plugin on the Fiji ImageJ software. Spots were detected using the Laplacian of Gaussian detection algorithm (Me31B granule analysis: estimated spot size = 0.7 microns, threshold = 250). Tracks were connected using the Simple Linear Assignment Tracker algorithm (Me31B analysis: max linking distance = 0.3 microns, gap closing distance = 0.3 microns, max frame gap = 2). Data was exported and analysed in R.

2.12.7 Scaled fusion time using optical tweezers

For quantifying the scaled fusion time for WT Me31B, Me31B+*polyA* RNA and Me31B+$MgCl_2$ condensates, firstly, a relaxation time constant was derived from the fusion process over time. The scaled fusion time was then calculated by dividing the time constant by condensate radii to express the fusion time as a function independent of condensate size. For Me31BΔNC condensates, due to their rapid aggregation post condensation, fusion was not quantifiable.

2.12.8 Statistical analyses

Quantification and statistical tests were conducted using R software. To compare Me31B granule circularity before and after extrusion or before and after hexanediol treatment, Wilcoxon signed-rank test was performed. To compare granule dynamics using TrackMate before and after treatment with colchicine, cytochalasin-D, one-way analysis of variance (ANOVA) was used. To compare Me31B granule circularity and particle area between the mature oocyte and early embryo, Wilcoxon signed-rank test was performed. To compare the percentage of *fushi tarazu*-Me31B granule or *hairy*-

Me31B granule association between different stages (stage1, stage2 and stage3) of the early embryo, Fisher's exact test with Bonferroni corrections were performed. To compare droplet area at different time points for WT Me31B, Me31B+*polyA* RNA or Me31B+*grk* RNA condensates, Kruskal-Wallis test was performed. For all statistical tests, asterisks represent the following: ** $p<0.05$ and *** $p<0.0001$.

Chapter 3

Investigating Me31B granule properties and function in the mature oocyte

3.1 Introduction

Drosophila oogenesis can be divided into 14 morphologically different staged egg chambers. The female possesses two ovaries made up of 16-18 ovarioles, each of which is effectively an egg production line. As the egg chambers pass down the ovariole, they bud off and reach the posterior as mature oocytes, competent for fertilisation. Establishing polarity in egg chambers during early development is key to maintaining a defined and polarised oocyte and this will determine the future embryonic axes. The localisation and translational regulation of key maternal transcripts during oogenesis is critical to the progress of the initial stages of development, and pattern formation later in the embryo. Localisation of maternal mRNAs allows targeting of proteins to regions of the cell where they are required. This is usually coupled to translational repression to prevent ectopic or premature synthesis of the encoded protein. In *Drosophila*, several key maternal transcripts need to be stored and translationally repressed for long periods of oogenesis. For example, *bicoid* (*bcd*), a key axis determining maternal transcript, is localised to the anterior region of the oocyte during mid-oogenesis but is translationally repressed until the mature oocyte undergoes egg activation. How maternal mRNAs such as *bcd* are faithfully stored and translationally regulated during oogenesis is poorly understood.

P bodies, a conserved class of cytoplasmic biomolecular condensates, have been proposed to be sites of RNA storage and translational regulation across eukaryotes. P bodies have also been shown to differentially regulate stored maternal mRNAs in *Drosophila* oocytes, suggesting a universal role for P bodies in the storage and regulation of mRNAs, especially during *Drosophila* oogenesis.

The localisation, morphology and role of P bodies have been moderately studied during early and mid-oogenesis. However, a mechanistic understanding of their material properties, stability, internal organisation, and function during late oogenesis is completely lacking. The mature oocyte provides an ideal stage to investigate P bodies since regulatory processes, including the storage, translational repression, and translational activation of maternal RNAs, are tightly controlled and co-ordinated by P bodies.

3.2 Chapter objectives

In this chapter, I have studied the material properties and role of Me31B labelled P bodies (referred to as Me31B granules in the results section) in the mature oocyte. The specific questions addressed are as follows:

1. Do Me31B granules adopt a specific material state?
2. What factors (eg. proteins, RNA, cellular structures such as the cytoskeleton) maintain the integrity of Me31B granules?
3. How do Me31B granules facilitate storage of *bcd* mRNA?

3.2.1 Author contributions

Experimental strategy, design and execution, and image analyses in this chapter were performed by me except for the following contributions from:

1. Evvia Gonzalez: performed particle tracking analysis (Figures 3.13D and 3.14D)
2. Matt Wayland: generated graphical plots using ‘R’ software. Assisted with data analyses.

3.3 Me31B granules are multi-layered viscoelastic condensates

Studies from yeast and mammalian systems have shown that P bodies display liquid-like properties (Kroschwald et al. 2015). A primary characteristic of a liquid droplet is the spherical morphology it possesses due to surface tension. Surface tension is a mechanical stress that exists at the boundary between two phases and tends to reduce the surface area of this interface until it reaches a minimum. The minimal surface area of a liquid droplet corresponds to a spherical shape, therefore, surface tension drives liquid-like compartments to be spherical.

To visualise Me31B granules, an Me31B::GFP protein trap line (Buszczak et al. 2007), where the fusion protein is expressed from its endogenous locus, was utilised (Figure 3.1A). Live imaging revealed that Me31B granules are present as cytoplasmic compartments in large numbers throughout the mature oocyte (Figure 3.1B).

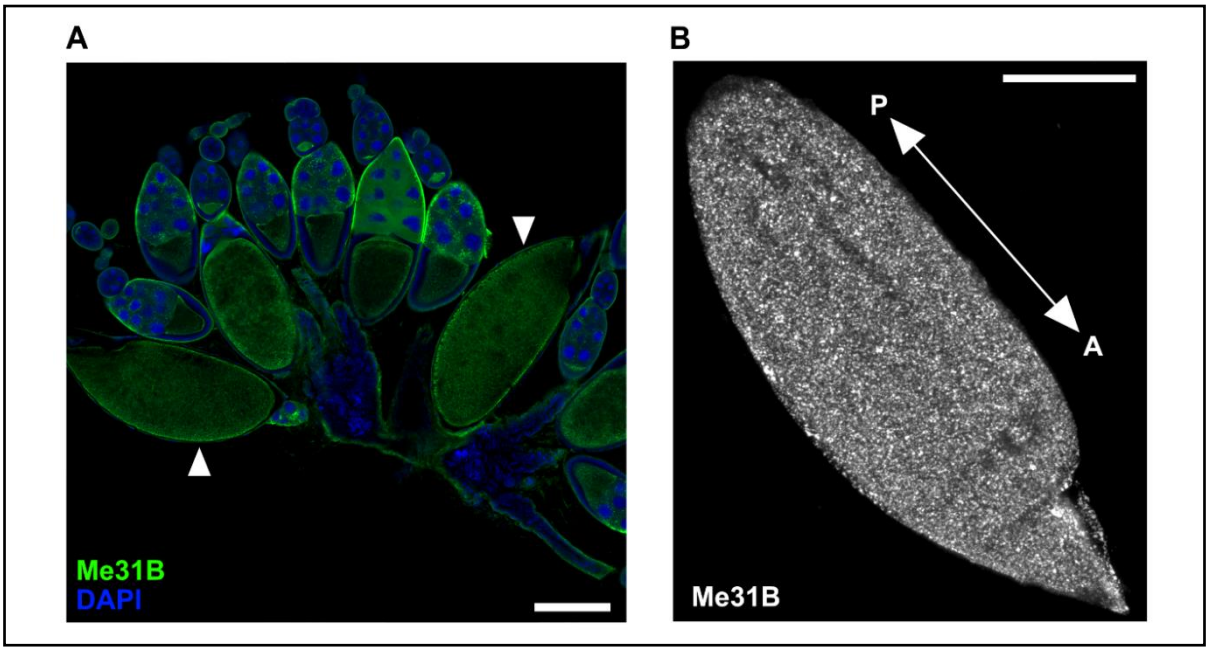

Figure 3.1: Me31B granule distribution in the mature oocyte. (A) Fixed *Drosophila* ovarioles consisting of different staged egg chambers expressing Me31B::GFP stained for Me31B (green) and DNA (DAPI in blue); white arrowheads point to mature oocytes. **(B)** Me31B granules are distributed throughout the mature oocyte. A-P refers to the anterior-posterior axis. Scale bar: 100 µm (A, B).

High resolution imaging revealed that while most granules tend to display morphologies similar to liquid-like droplets, several granules also exhibited amorphous shapes (Figure 3.2A). Analysis of aspect ratios (A.R) revealed that Me31B granules

generally inclined between 1-2 (A.R of liquid=1), suggesting that Me31B granules may exist in a material state deviating from liquids (Figure 3.2B). Condensates formed by liquid-liquid demixing normally exhibit a broad size distribution. Differential morphologies and sizes exhibited by Me31B granules (Figure 3.2A) indicate that Me31B granules likely form by liquid-liquid condensation. Interestingly, most, if not all, granules exhibited multiple internal sub-domains, indicating that Me31B granules are heterogeneously organised condensates (Figure 3.2C).

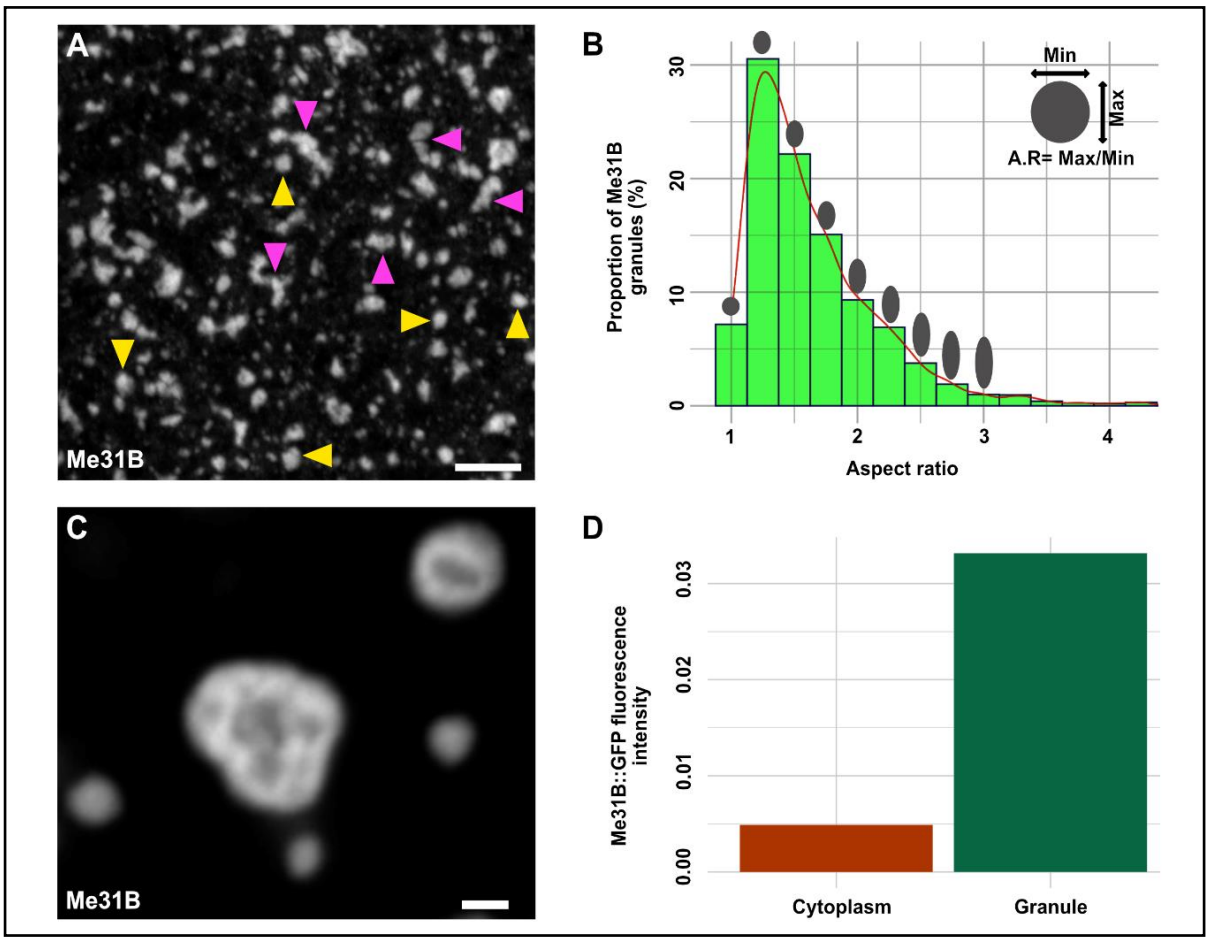

Figure 3.2: Me31B granules are heterogeneous phase separated condensates. (A-D) Mature oocytes expressing Me31B::GFP. **(A)** Differential morphologies, spherical (yellow arrowheads) and amorphous (magenta arrowheads), exhibited by Me31B granules in the mature oocyte; scale bar: 10 µm. **(B)** Me31B granules (>1 µm) converged towards a spherical aspect ratio (A.R) of 1, as predicted for liquids. **(C)** Me31B granules exhibiting multiple sub-domains indicative of heterogeneous internal organisation; scale bar: 10 µm. **(D)** Quantification of total Me31B::GFP fluorescence intensity between the granule and cytoplasmic pool (N=3 oocytes).

Analysis of relative Me31B concentrations between the granule and cytoplasm revealed that Me31B is highly partitioned inside granules (Figure 3.2D). This indicates that Me31B may function as a scaffold protein for P body assembly during oogenesis, due to its increased local enrichment within granules.

Time lapse imaging revealed that Me31B granules exhibited constant expansion and contraction, reflective of elastic properties (Figure 3.3A-C). Analysis of A.R of granules over time revealed that elastic recovery from amorphous to spherical shape was approximately 30 minutes (Figure 3.3D). The timescale of recovery significantly diverges from conventional liquid droplets which are thought to have relaxation times in the order of milliseconds. This suggests that Me31B granules are highly viscous structures with elastic behaviour, which partly explains the amorphous morphology.

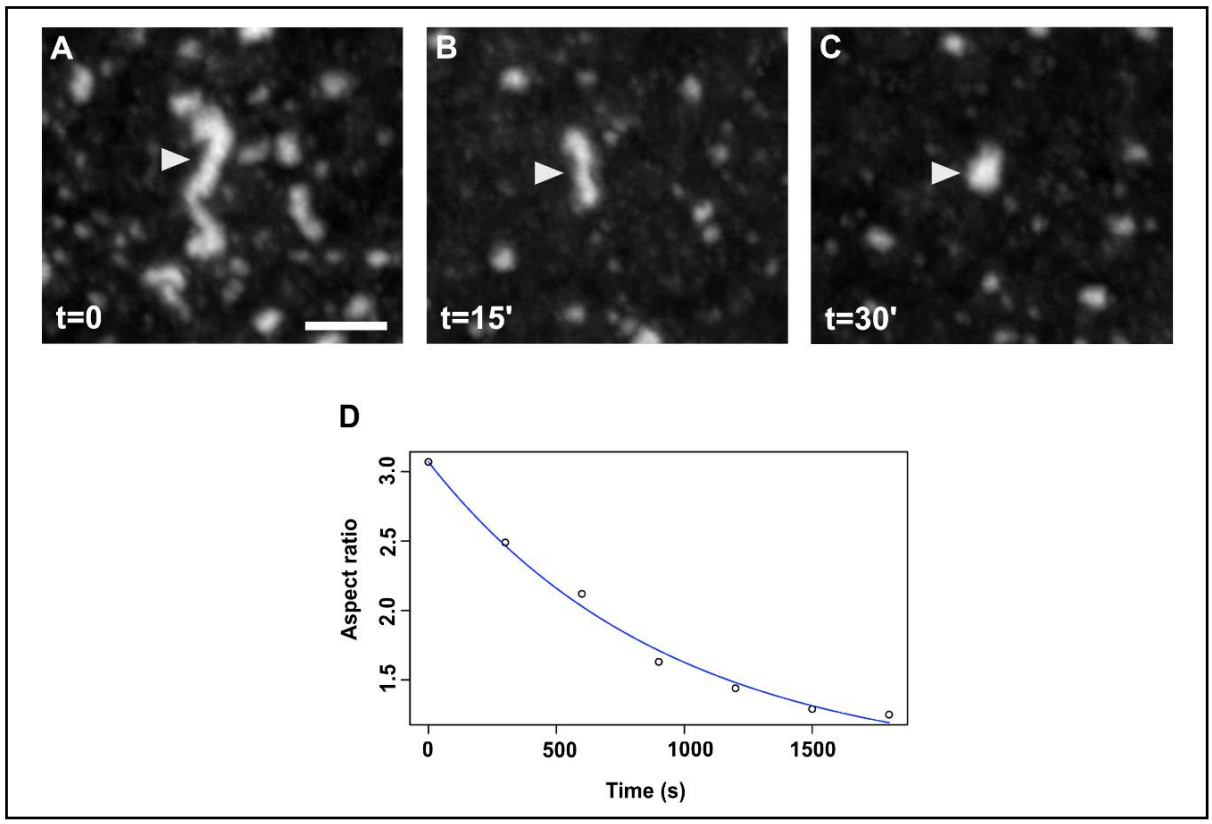

Figure 3.3: Me31B granules exhibit elastic behaviour. (A-C) Mature oocytes expressing Me31B::GFP; representative image sequence of Me31B granule elastic recovery over a time course of 30 minutes (white arrowheads). **(D)** Plot of Me31B granule A.R over time showing granule relaxation from elastic (A.R~3) to spherical shape (A.R~1); scale bar: 10 µm.

Live imaging of Me31B granules also revealed frequent fusion events whereby two granules coalesced with each other (Figure 3.4A-C). Additionally, granules exhibit fission events as well, whereby one granule splits into two or more smaller granules (Figure 3.4D-F). Granule fusion and fission may, therefore, provide a mechanism for controlling Me31B granule size and number in the mature oocyte.

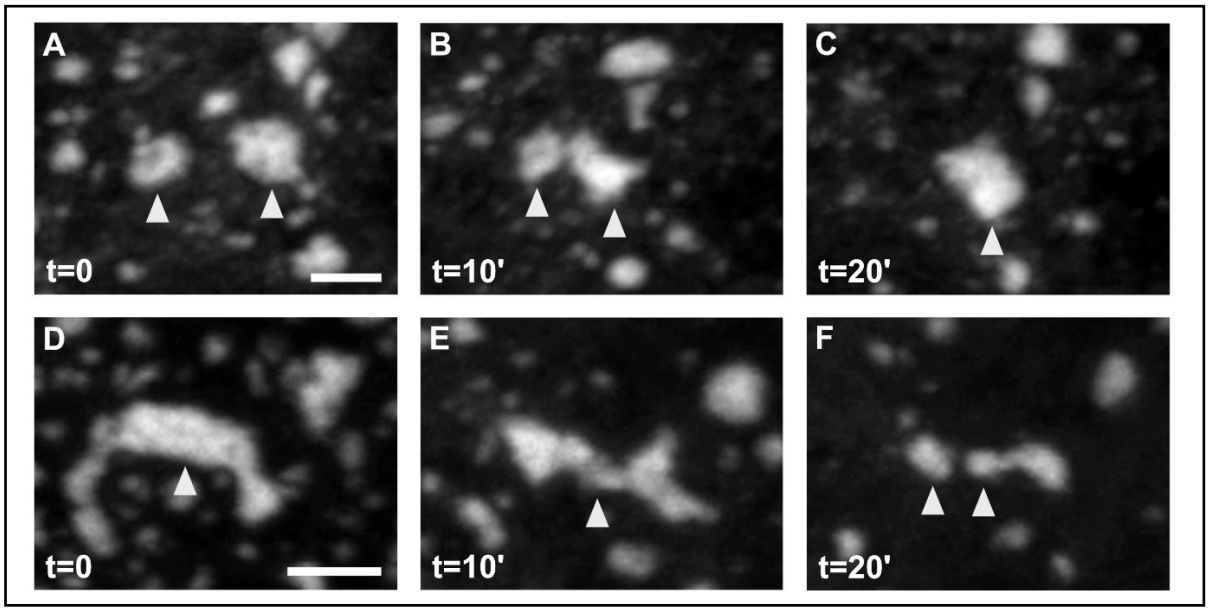

Figure 3.4: Me31B granules exhibit fusion and fission behaviour. (A-C) Mature oocytes expressing Me31B::GFP; representative image sequence of Me31B granules exhibiting coalescence over time (white arrowheads); scale bar: 10 µm. **(D-F)** Representative image sequence of Me31B granule fission over time (white arrowheads); scale bar: 10 µm.

Conclusions: Me31B in the mature oocyte exists as micron sized cytoplasmic granules distributed uniformly across the oocyte cytoplasm and exhibits both viscous and elastic (viscoelastic) properties.

3.4 Me31B granule properties are partly tuned by cytoplasmic crowding

The ability of ribonucleoproteins (RNPs) to phase separate into condensed compartments largely depends on the local concentration of specific proteins and RNAs. In both *in vivo* and *in vitro* systems, cytoplasmic crowding has been shown to increase partitioning of RNPs into the condensed phase and regulate their function (Delarue et al. 2018). The presence of external crowding agents such as polyethylene glycol (PEG) and dextran have also been shown to affect condensate material properties *in vitro* (Kaur et al. 2019). Crowding, therefore, can tune the viscosity of the

cytoplasm, which in turn affects the local concentration of RNPs and their material states.

Since the oocyte is a compact and relatively crowded environment (eg. presence of yolk granules), I wanted to examine if Me31B granule properties are influenced by crowding. To test this, an extrusion assay was developed whereby the oocyte membrane was physically punctured to release its cellular contents into oil (Figure 3.5A). Extrusion into oil, in part, assumes that while the overall Me31B concentration remains constant, the local Me31B concentration may be altered thereby simulating an environment with decreased crowding.

Upon exerting mechanical stress over the extruded contents using a cover slip, granules exhibited elastic morphologies lasting long periods of time, characteristic of both elastic and viscous properties (Figure 3.5B).

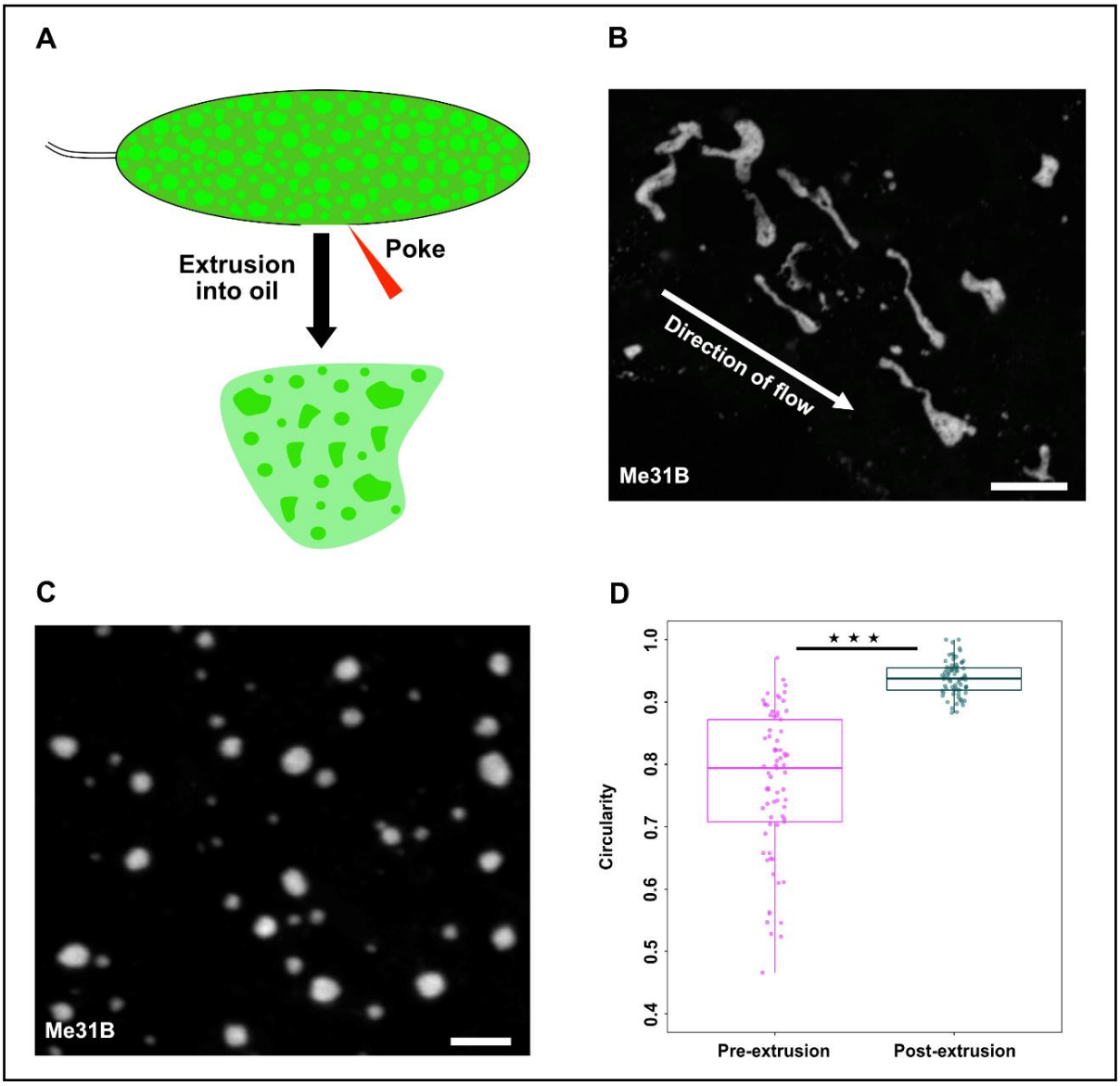

Figure 3.5: Me31B granules exhibit elastic properties and spherical morphology post extrusion. (A) Schematic showing granule extrusion into oil induced by poking part of the oocyte membrane. **(B)** Application of moderate stress using a coverslip induced Me31B granules to form stretched, elastic morphologies; scale bar: 20 µm. **(C)** Extruded Me31B granules exhibiting spherical morphology; scale bar: 10 µm. **(D)** Quantification of Me31B::GFP granule circularity before and after extrusion; n=78 Me31B granules, p<0.0001).

Time lapse imaging showed that over a time course of 30 minutes post extrusion, granules exhibited highly spherical morphology (Figure 3.5C,D). Liquid droplets have a circularity of 1 and since the majority of the extruded granules tend toward 1, extruded Me31B granules converge towards liquid-like states. Live imaging also revealed the following features of Me31B granules across several extruded oocytes:

Fusion

Constant fusion events were detected whereby Me31B granules in close proximity fused and relaxed toward a larger spherical body (Figure 3.6A). Analysis of A.R of granules over time revealed that, in contrast to the slow elastic recovery observed *in vivo*, droplet fusion relaxation of tens of minutes was significantly faster (Figure 3.6B). However, relaxation kinetics quantified for several fusion events estimated an apparent viscosity of ~16000 Pascal second (Pa.s) for Me31B granules (Figure 3.6C), which is several orders of magnitude more viscous than previously reported liquid-like condensates such as P granules (Elbaum-Garfinkle et al. 2015). Since Me31B granule sizes vary greatly (which likely affects the resulting surface tension), the actual viscosity estimates could broadly range between 10^3-10^4 Pa.s. Furthermore, relaxation time for fusion recovery was significantly faster than elastic recovery (Figure 3.6D). Since *in vivo* fusion events were hard to capture, I have compared *in vivo* elastic recovery to *ex vivo* fusion recovery based on the observation that both *in vivo* and *ex vivo* fusion recovery have similar relaxation times. Taken together, these results further support the idea that Me31B granules in the mature oocyte are highly viscous, elastic condensates driven by LLPS.

Interestingly, over time, the fusion dynamics decreased, resulting in granules that fail to undergo fusion (Figure 3.6E). This indicates that Me31B has an intrinsic property to undergo maturation/ aging-like behaviour under certain conditions.

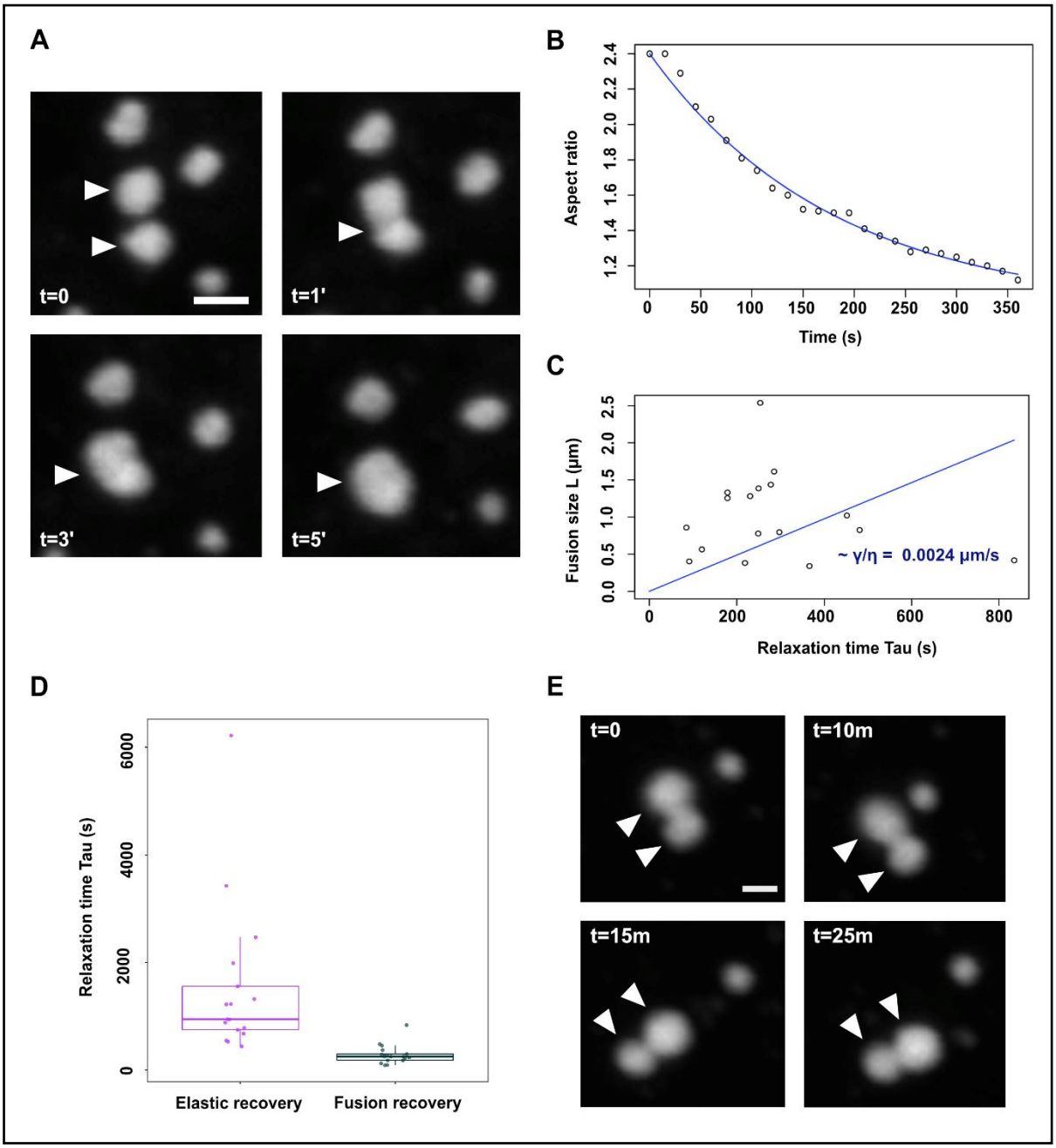

Figure 3.6: Extruded Me31B granules display viscoelastic properties. (A) Representative image sequence of extruded Me31B granules undergoing coalescence (white arrowheads); scale bar: 10 µm. **(B)** Plot of A.R of fusing granules over time yielded an average relaxation time (Tau) of ~ 350s. **(C)** Plot of length scales of granule fusion (L) versus Tau yielded an apparent capillary velocity/slope (γ/η) of ~ 0.0024 µm/s, where γ is the apparent surface tension and η is the apparent viscosity. **(D)** Quantification of granule fusion and granule elastic relaxation kinetics; n=20 extruded granules. **(E)** Representative image sequence of 'aged' extruded Me31B granules failing to exhibit fusion (white arrowheads); scale bar: 2 µm.

Fission

On a few occasions, fission events whereby individual granules emerged from a larger Me31B granule were detected, similar to those observed *in vivo*. This suggests that granule fission is an intrinsic property of Me31B (Figure 3.7).

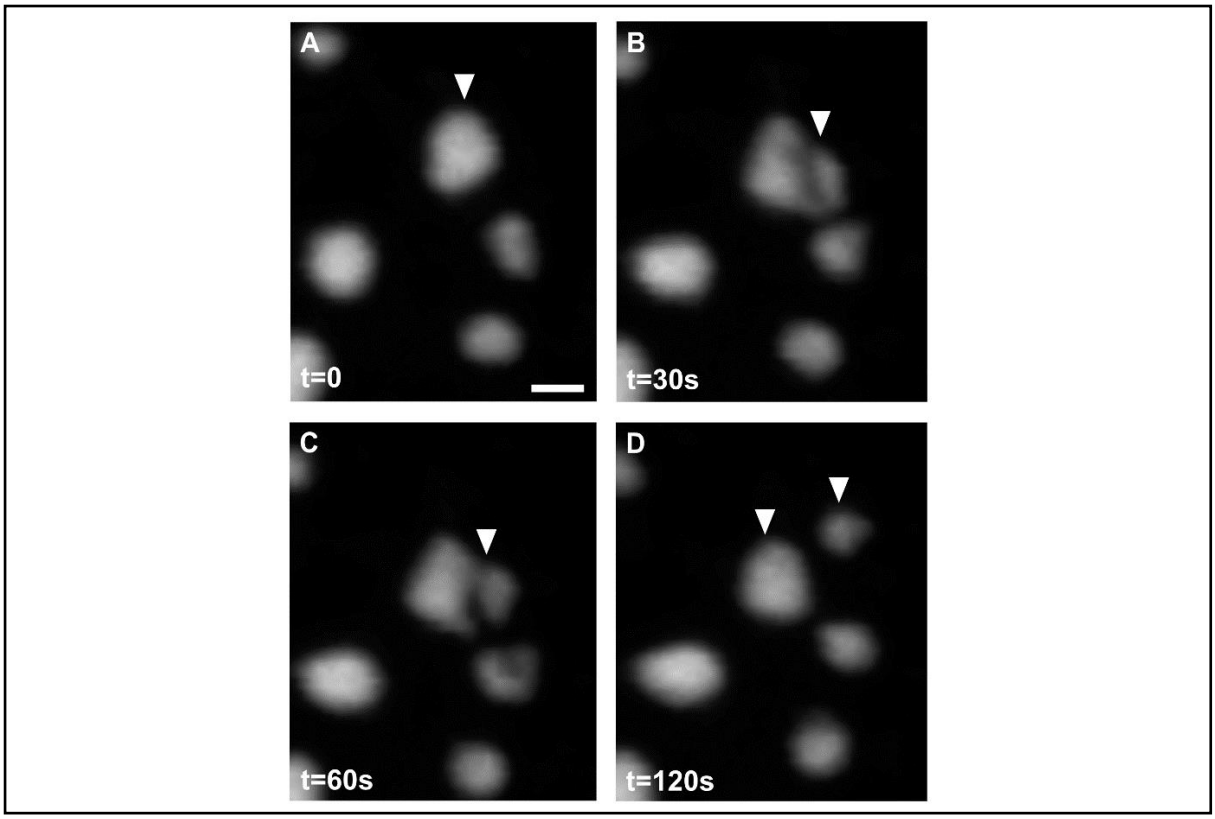

Figure 3.7: Extruded Me31B granules exhibit fission behaviour. (A-D) Representative image sequence of extruded Me31B granules exhibiting fission behaviour (white arrowheads). Scale bar: 5 µm.

Liquid-rupture

Sometimes, two granules that are already fused, subsequently pulled apart from each other. In such cases, pinch-off behaviour was observed in which a slender 'bridge' links the two granules (Figure 3.8A,B); this 'bridge' is a classic feature of viscous fluids observed in condensates such as the nucleolus (Brangwynne, Mitchison, and Hyman 2011). As soon as the bridge ruptures, the two threads retract and resorb into the resulting individual granules (Figure 3.8C,D).

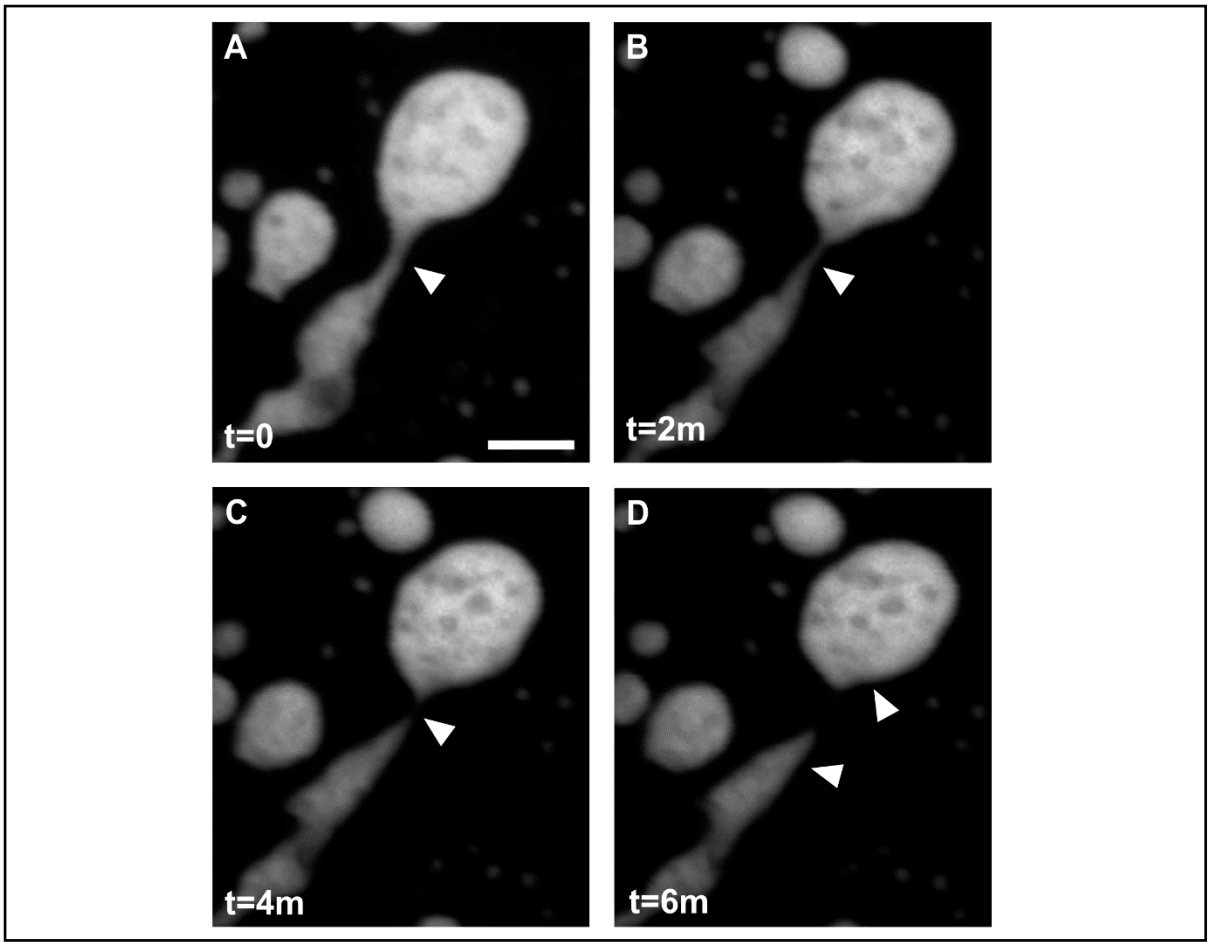

Figure 3.8: Extruded Me31B granules exhibit 'pinch-off' behaviour. (A) Representative image of extruded Me31B granules which have already fused held together by a 'bridge'. **(B, C)** Image sequence displaying 'pinching off' of the unstable bridge. White arrowheads point to the region of liquid rupture in (A,B,C). **(D)** The two granules resorb within a minute of bridge rupturing. Scale bar: 10 µm.

Conclusions: Extrusion of oocyte cytoplasmic contents into oil does not dramatically alter Me31B granule properties. However, additional properties of Me31B granules such as highly spherical morphologies and granule maturation were observed, suggesting that the *in vivo* crowded environment likely regulates granule morphology and prevents such aging-like behaviour. While extruded P bodies display classic liquid-like behaviour, the longer timescale at which these events occur, compared to well-characterised liquid-like droplets, indicate that they are highly viscous in nature. Application of stress-induced elongation of Me31B granules also revealed their elastic property. Since most of the observed properties were consistent with *in vivo* results, viscoelasticity and liquid-like properties are likely an intrinsic property of Me31B granules.

3.5 Me31B granules do not exhibit exchange of molecules with the cytoplasm

Cytoplasmic RNP granules nucleate and assemble into condensed compartments acting as hubs for various cellular processes. A key characteristic of such hubs is to facilitate exchange of molecules between the soluble and the granular fraction to facilitate reactions in a controlled manner. To determine the flux of Me31B molecules entering and exiting the granules, I performed the Fluorescence Recovery after Photobleaching (FRAP) experiment. FRAP is a widely used technique to probe the material state of phase separated condensates which allows for quantification of exchange dynamics and mobility of molecules. Measuring the fluorescence recovery rate allows estimation of the speed and mobility of the components of the membrane-less granule. Incomplete fluorescence recovery, or a minimal mobile fraction indicates immobile molecules that are not free to exchange and could point to a divergence from a liquid-like material state.

To test if Me31B granules in the mature oocyte exchange components between the oocyte cytoplasm and the granule, I performed FRAP on whole Me31B granules (whole particle FRAP). Over time, granules displayed very little fluorescence recovery post photobleaching (Figure 3.9A). The fraction of mobile particles was very minimal, suggesting that there is little exchange of Me31B molecules between the granule and cytoplasm in the mature oocyte (Figure 3.9B,C).

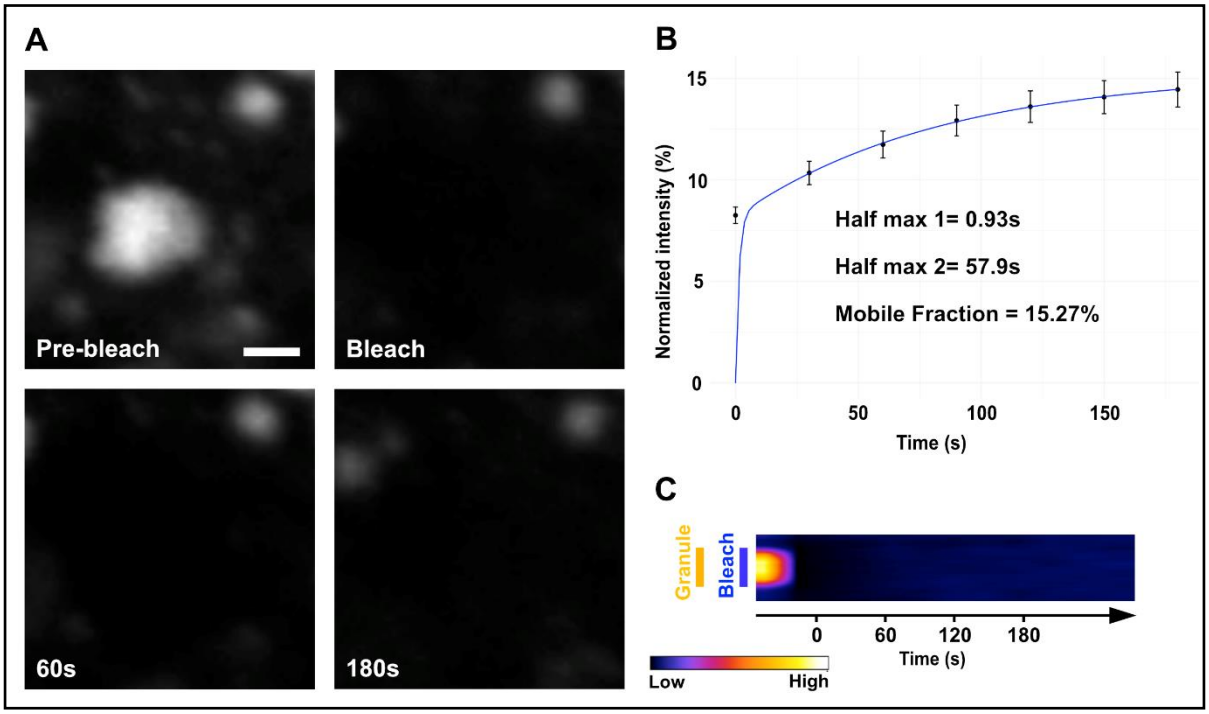

Figure 3.9: Me31B granules do not exhibit exchange of molecules with the cytoplasm. **(A)** Time lapse images of Me31B granule before and after photobleaching whole Me31B granule; scale bar: 3 µm. **(B)** Analysis of whole particle FRAP of Me31B granules. Standard deviation/data (black), fit (blue), n=20 Me31B granules, N=5 oocytes. Double exponentials fit the FRAP curve, suggesting biphasic response. **(C)** Kymograph of whole particle FRAP shows very minimal (homogeneous) recovery, suggesting that exchange of Me31B molecules between the granule and cytoplasm is rate limiting.

Conclusion: Me31B granules in the mature oocyte exist in an 'arrested' state by exhibiting minimal exchange of molecules between the granule and cytoplasm.

3.6 Me31B granules have a semi-liquid internal core

RNP granules are best described as complex structures with a heterogeneous internal composition and arrangement of macromolecules. Stress granules, for example, are thought to be partitioned into a solid internal core and a dynamic outer shell (Jain et al. 2016). Such multi-layered structuring has been observed in other RNP granules, including P bodies. In fact, during mid-oogenesis, maternal mRNAs such as *bcd* and *gurken* have been shown to differentially partition within P bodies (Weil et al. 2012). Whether Me31B granules in the mature oocyte exhibit a reversible internal core to allow dynamic partitioning of components is not known.

To test the internal dynamics of Me31B, I performed FRAP by photobleaching a small region (~0.5 µm) within the granule (internal FRAP). Fluorescent Me31B molecules within the granule exhibited significant recovery post photobleaching (Figure 3.10A,B). Interestingly, the spatiotemporal pattern showed that recovery appeared to progress from the periphery to the centre of the particle, indicating diffusion mediated mobility (Figure 3.10C).

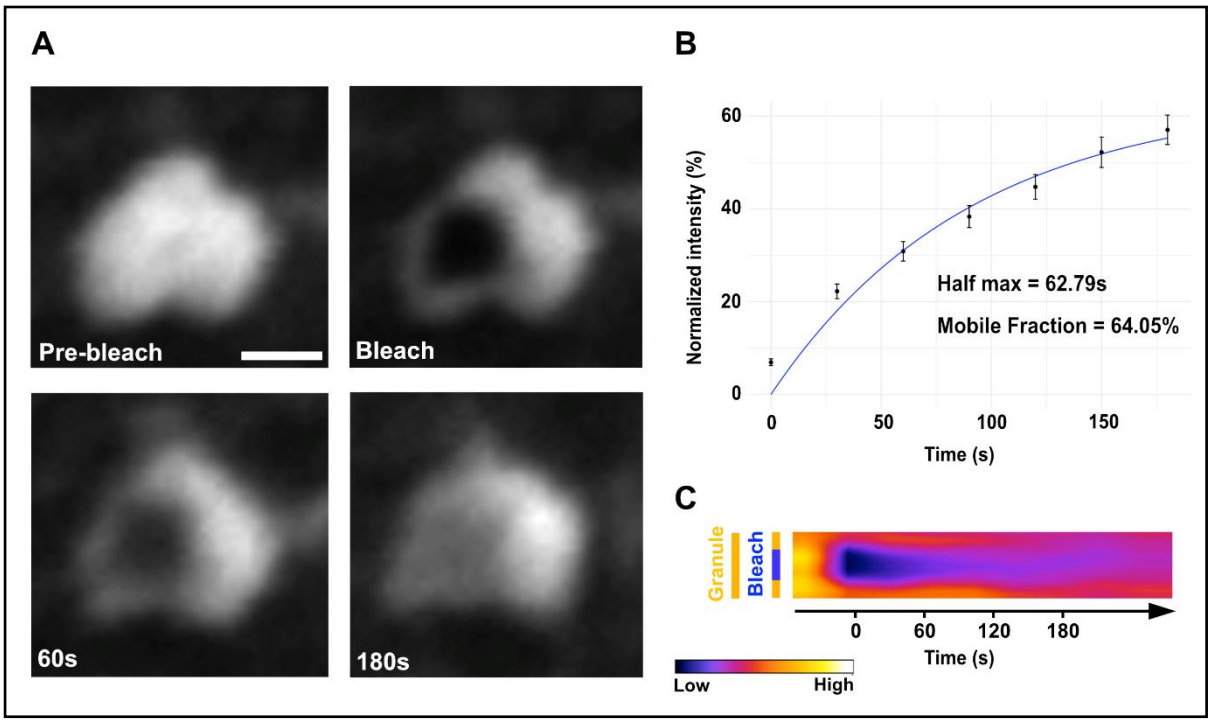

Figure 3.10: Me31B granule core exhibits internal re-arrangement. (A) Time lapse images of Me31B granule before and after photobleaching a small region (~0.5 µm) within the granule; scale bar: 3 µm. **(B)** Analysis of internal particle FRAP of Me31B granules. Standard deviation/data (black), fit (blue), n=24 Me31B granules, N=5 oocytes. Single exponential fits the FRAP curve. **(C)** Kymograph shows spatiotemporal recovery of Me31B fluorescence from periphery to centre, suggesting diffusion mediated mobility.

Although complete recovery was not achieved, the percentage of mobile Me31B molecules within the granules was ~ 64%, significantly higher than the mobility of Me31B between the granule and cytoplasm (Figure 3.9B). Additionally, the half-maximum ($t^{1/2}$) of ~63 seconds indicates that recovery kinetics of Me31B molecules is relatively slower compared to the well-characterised liquid-like P granules (Brangwynne et al. 2009). The apparent viscosity estimated from the FRAP rates (~126.25 Pa.s) suggest that despite displaying a higher percentage of mobile Me31B molecules, the internal core of Me31B granules is relatively viscous. Taken together

with results from the whole particle FRAP, Me31B granules exist in an arrested gel-like biophysical state which prevents exchange of components with the surrounding cytoplasm but allows internal mixing within the granule.

Conclusion: Me31B granules contain a semi-liquid internal core, likely to maintain regulated mobility of components within the granule.

3.7 Me31B granule internal core matures with time

Molecules in RNP granules that exhibit liquid-like properties are free to diffuse rapidly within the droplets and undergo constant exchange between the condensed phase and the soluble bulk solution to maintain the system in thermodynamic equilibrium. Purified RNP components, such as FUS, have been shown to phase separate into liquid-like droplets *in vitro* (Gui et al. 2019; Molliex et al. 2015; Patel et al. 2015). However, these liquid-like compartments have also been shown to transition into a more solid, and less dynamic state over time. This concept is referred to as maturation or aging, a common phenomenon observed in several reconstituted RBPs. Interestingly though, FUS condensates expressed in cultured cells do not appear to display maturation behaviour. Thus, it is unclear whether similar maturations occur in RBPs under physiological conditions *in vivo*.

Contrary to *in vitro* reconstituted droplets, Me31B granules *in vivo* are multi-component systems with diverse macromolecules regulating their material properties. Moreover, Me31B granules have been shown to undergo aging-like behaviour under extruded conditions (Figure 3.6E). To test if Me31B granules in the mature oocyte show any signs of aging/maturation, mature oocytes were dissected into and incubated in oil for a duration (4 hours) longer than normal (~ 0-1 hour). Post 4 hours incubation, internal FRAP was performed on Me31B granules and the percentage of mobile Me31B molecules within the granule core was used as a metric to construe the maturation event (Figure 3.11A). Interestingly, over a time course of 4 hours, the internal mobility of Me31B molecules was close to ~41% (Figure 3.11B,C), significantly lesser than those observed with Me31B granules examined shortly after dissection (Figure 3.10).

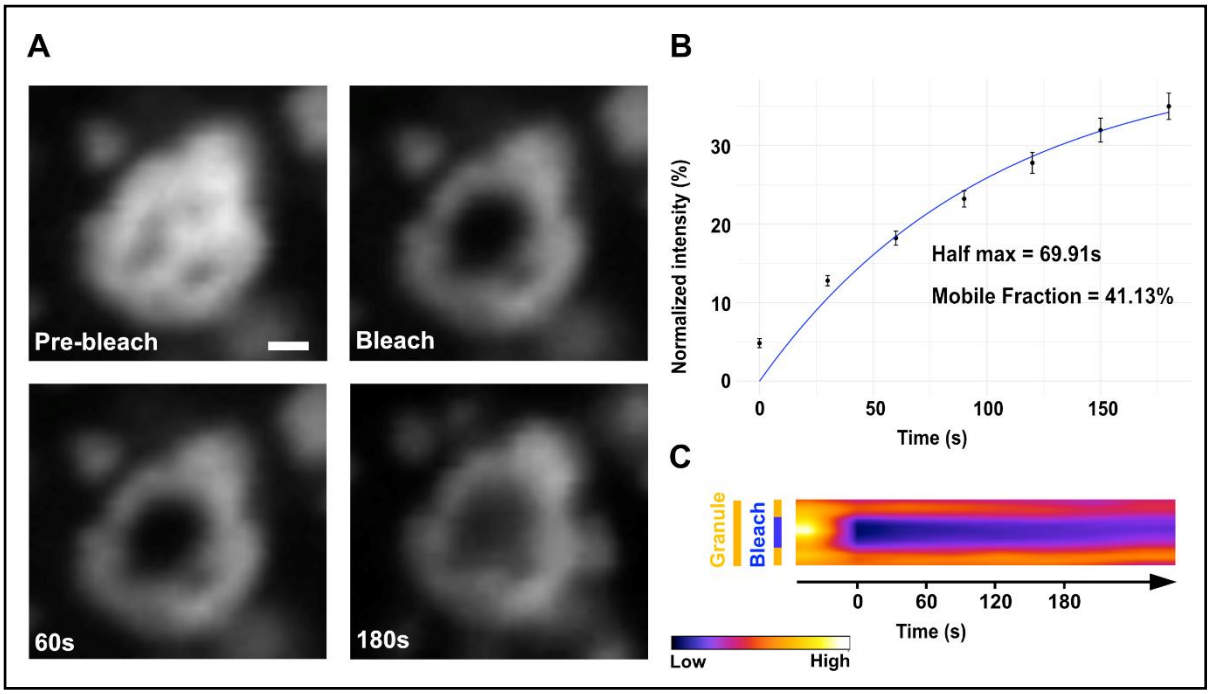

Figure 3.11: Me31B granules, over time, exhibit decreased internal mobility. (A) Time lapse images of Me31B granule before and after photobleaching of a small region within the granule; scale bar: 3 µm. **(B)** Analysis of internal particle FRAP of Me31B granules. Standard deviation/data (black), fit (blue), n=25 Me31B granules, N=5 oocytes. Single exponential fits the FRAP curve. **(C)** Kymograph shows very slow spatiotemporal recovery of Me31B fluorescence, indicating decreased dynamics.

Interestingly, while the extent of recovery post photobleaching was also significantly lesser in the 4-hour incubated Me31B granules, $t^{1/2}$ of Me31B recovery remained fairly similar. This suggests that the kinetics of exchange within Me31B granules remain unaffected despite a significant decrease in the percentage of mobile Me31B molecules in the Me31B granules examined after a 4-hour incubation.

Conclusion: Prolonged incubation of mature oocytes in oil causes Me31B granule core to mature over time and exhibit decreased internal mobility of Me31B molecules, likely because of stronger inter- and intra-molecular interactions.

3.8 ATP-dependent activity is essential to maintain the semi-liquid Me31B granule core

ATP dependent kinases and RNA helicases have been implicated in driving RNP assembly and/or disassembly. Several recent lines of evidence suggest a model where the dynamics of phase separated RNP granules are, in part, modulated by ATP

dependent processes. This has been studied for stress granules where impairment of ATP production halts granule dynamics (Jain et al. 2016). Moreover, ATP depletion also impairs exchange of stress granule proteins with the cytoplasmic pool.

Since oocyte Me31B granules have a semi-liquid internal core and Me31B is an ATP dependent RNA helicase, I examined whether ATP dependent processes (such as helicase activity) are essential to maintain the semi-dynamic internal core of Me31B granules. To test this, I used sodium orthovanadate, a commonly used ATPase inhibitor. Shortly after pharmacological treatment with sodium orthovanadate, Me31B granule dynamics were severely affected. To test if the treatment affected the internal granule dynamics, I performed internal FRAP within Me31B granules five minutes post treatment. Contrary to the semi-liquid nature of the Me31B granule core, sodium orthovanadate treated Me31B granules exhibited no internal recovery post photobleaching (Figure 3.12A). The percentage of mobile Me31B molecules was negligible, giving rise to non-dynamic Me31B granules (Figure 3.12B).

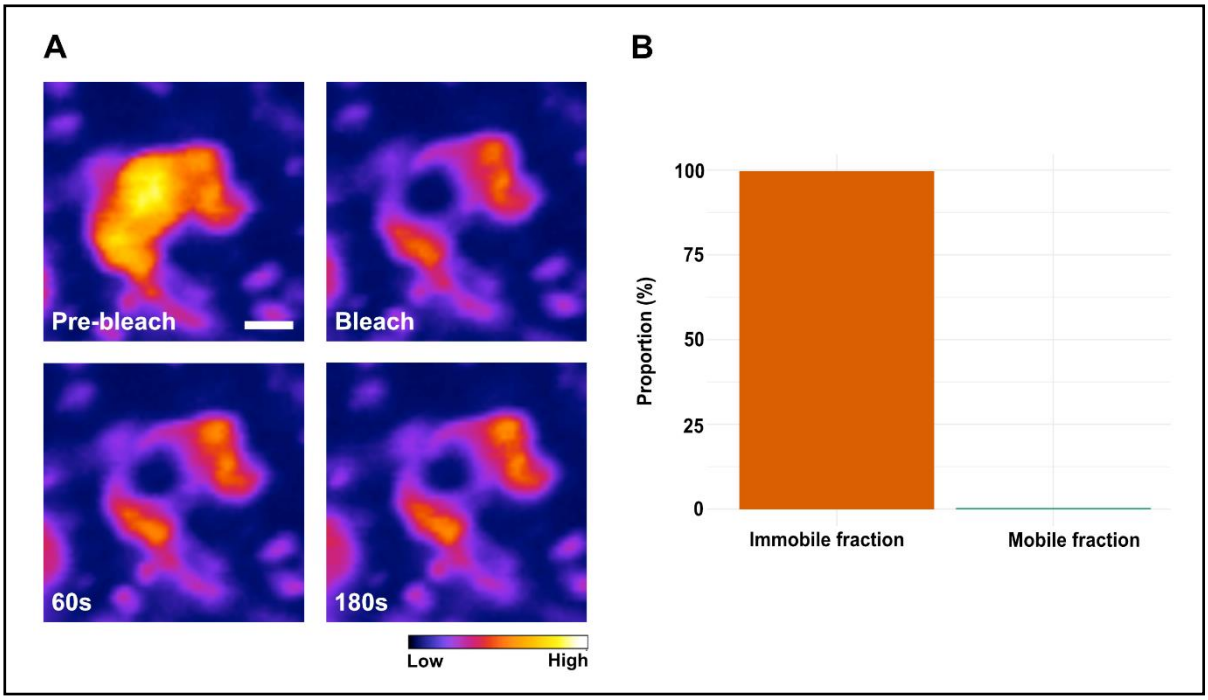

Figure 3.12: Sodium orthovanadate inhibits internal re-arrangement of molecules within Me31B granules. (A) Time lapse images of Me31B granule before and after photobleaching a small region within the granule; scale bar: 3 µm. **(B)** Quantification of Me31B immobile and mobile fractions post photobleaching; n=5 Me31B granules, N= 3 oocytes.

Conclusion: ATP dependent processes are likely required to maintain the semi-liquid state of Me31B granule core. Caveat: Sodium orthovanadate is non-specific and also inhibits phosphatase activity. Therefore, usage of relatively more specific inhibitors such as apyrase would be essential to test the role of ATP dependent activity to regulate Me31B properties.

3.9 Actin and microtubule cytoskeletal networks are required to maintain Me31B granule size and dynamics

Me31B granules in the mature oocyte exhibit very limited dynamics across space. Since the actin and microtubule cytoskeleton are thought to be distributed throughout the oocyte, it is possible that the granules are tethered to the cytoskeleton which prevents large scale movements. This idea is supported by the relatively regular spacing of granules in the oocyte. Association of P bodies with actin cytoskeleton has also been observed and reported across several other systems (Aizer et al. 2008).

To determine if the actin cytoskeleton is required to maintain Me31B granule integrity, mature oocytes were treated with cytochalasin-D (cyto-D), a commonly used depolymerizing drug that causes partial depolymerisation of the actin cytoskeleton, but that does not affect oocyte viability. Cyto-D treatment resulted in the dissociation of Me31B granules (Figure 3.13A-C). This dissociation not only resulted in the breaking of granules into smaller particles, but also was accompanied by an increase in the cytoplasmic partitioning of Me31B (Figure 3.13D). To test if actin depolymerisation caused changes in the spatial dynamics of the dissociated granules, Me31B granule dynamics were recorded before and after treatment. Particle dynamics were quantified using TrackMate, an algorithm used for single particle detection and tracking in live cells. Particle tracking analysis revealed that actin depolymerisation caused an increase in the spatial dynamics of Me31B granules (Figure 3.13E). This result suggests that the actin cytoskeleton could act as an anchor, stabilizing oocyte Me31B granules.

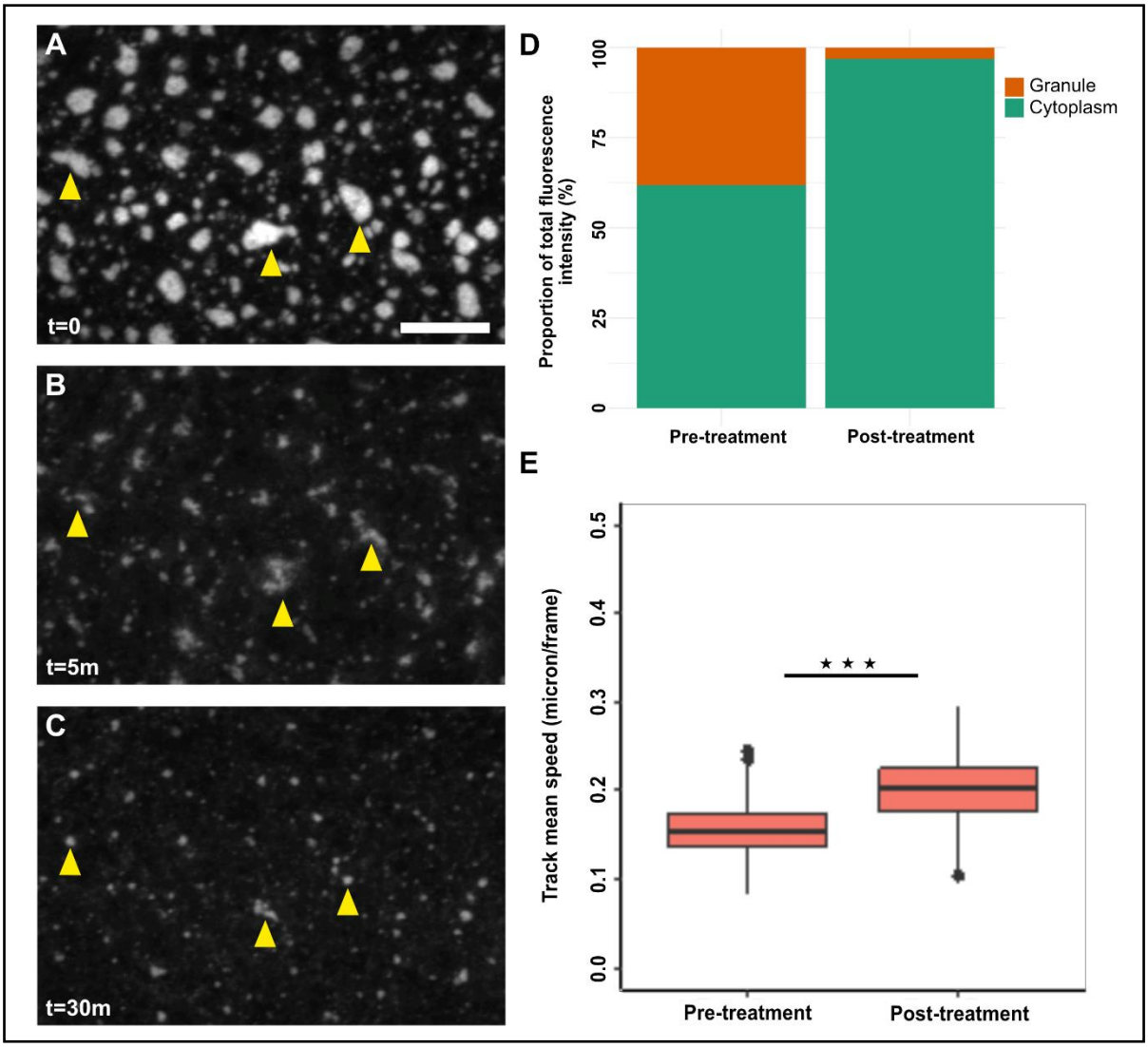

Figure 3.13: Cyto-D treatment results in the dissociation and increased spatial dynamics of Me31B granules. (A-C) Mature oocytes expressing Me31B::GFP; image sequence of Me31B granule dissociation post treatment with 10 µg/µl cyto-D. Representative granules undergoing dissociation are highlighted by yellow arrowheads; scale bar: 10 µm. **(D)** Analysis of total Me31B::GFP fluorescence quantified from granules and the cytoplasm showing a decrease in Me31B partitioning within granules post cyto-D treatment (N=3 oocytes). **(E)** Quantification using TrackMate showing an increase in granule dynamics post treatment; (n=668 Me31B granules; $p<0.001$)

To test if microtubules influence Me31B granule integrity and dynamics, mature oocytes were treated with colchicine, a commonly used microtubule depolymerizing drug. Colchicine treatment resulted in the dissociation of Me31B granules into smaller particles (Figure 3.14A-C), similar to cyto-D treated oocytes. This dissociation not only resulted in the breaking of granules into smaller particles, but also was accompanied

by an increase in the cytoplasmic partitioning of Me31B (Figure 3.14D). While P bodies have been shown to increase in numbers upon microtubule depolymerisation in mammalian cells, I did not observe a considerable change in Me31B granule numbers in the oocyte.

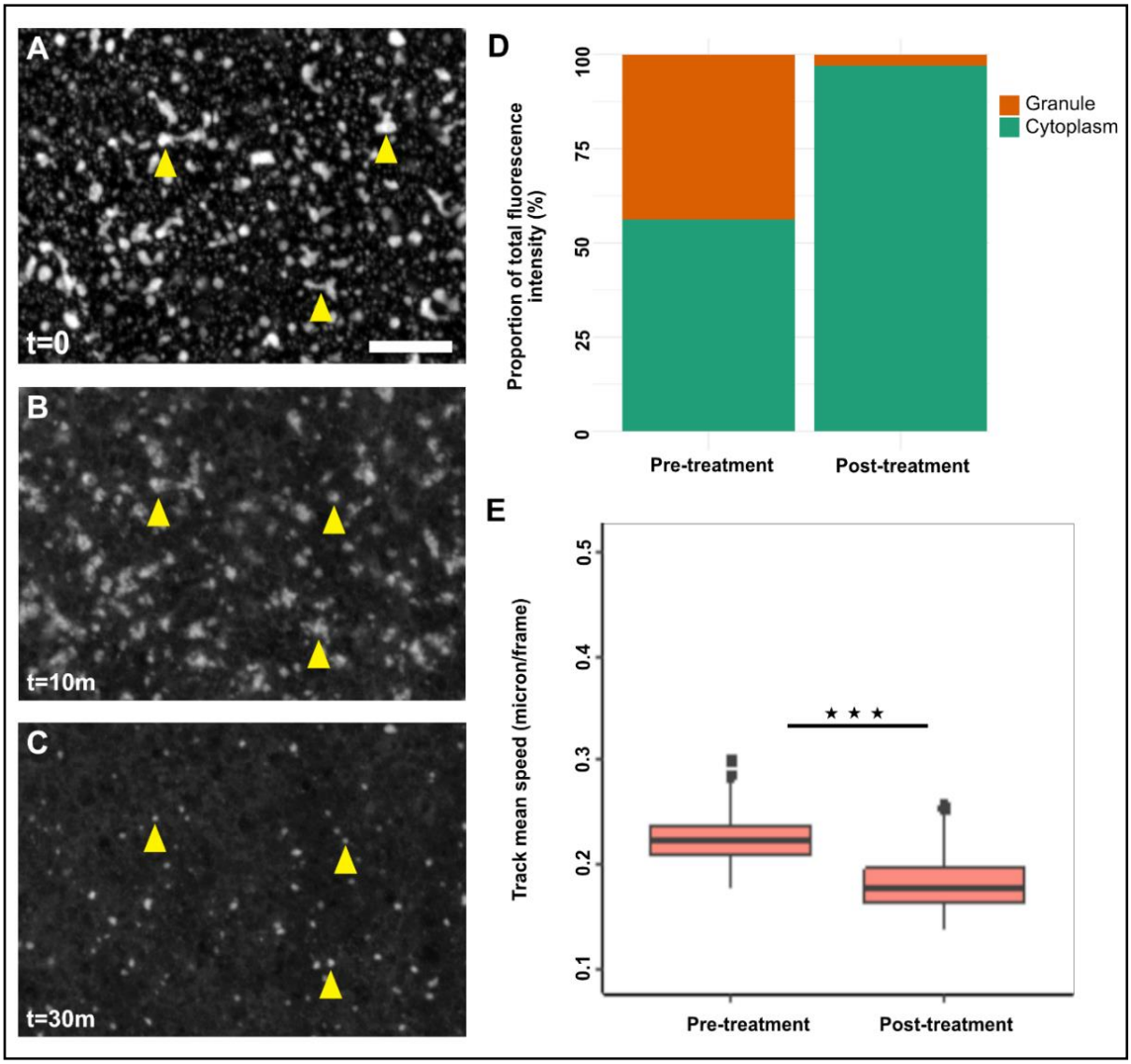

Figure 3.14: Colchicine treatment results in the dissociation and decreased dynamics of Me31B granules. (A-C) Mature oocytes expressing Me31B::GFP; image sequence of Me31B granule dissociation post treatment with 50 µg/µl colchicine. Representative granules undergoing dissociation are highlighted by yellow arrowheads; scale bar: 10 µm. **(D)** Analysis of total Me31B::GFP fluorescence quantified from granules and cytoplasm showing a decrease in Me31B partitioning in granules post colchicine treatment (N=3 oocytes). **(E)** Quantification using TrackMate showing a decrease in granule dynamics post colchicine treatment; (n=1102 Me31B granules, $p < 0.0001$).

To test if the dissociated Me31B granules exhibited a change in the spatial dynamics, granule movements before and after treatment were quantified. Contrary to cyto-D treatment, particle tracking analysis showed that colchicine treated Me31B granules appear to have decreased dynamics compared to untreated granules (Figure 3.14E). This result suggests that the microtubule cytoskeleton provides a framework for controlled dynamics of Me31B granules in the mature oocyte.

Conclusions: Actin and microtubule cytoskeletal network in the mature oocyte are crucial to maintaining Me31B granule integrity and dynamics. Additionally, estimated spatial dynamics of dissociated granules indicate that the actin network appears to stabilise the Me31B granules, while the microtubule network likely controls the dynamics of Me31B granules in the mature oocyte.

3.10 RNA degradation causes dissociation of Me31B granules

Numerous studies have shown the importance and requirement of RNA for the assembly and integrity of P bodies. Several reports have also highlighted the importance of the DDX6 family of helicases in P body formation, suggesting that the rearrangement of RNA is critical for P body assembly (Ayache et al. 2015). While Me31B granules contain several maternal mRNAs, whether RNA is necessary for the structural integrity and maintenance of Me31B granules in the mature oocyte is not known.

To test whether RNA regulates the integrity of Me31B granules, mature oocytes were treated with RNase A to digest RNAs. Shortly after treatment, granules broke down into smaller sized particles (Figure 3.15A-C). Interestingly, over a time course of 60 minutes post treatment, several small granules nucleated and formed in the mature oocyte (Figure 3.15D). These observations are supported by Me31B granule density quantitation which reveals the high number of Me31B granules at 60 minutes post treatment (Figure 3.15E). A likely explanation for the de-novo formation of Me31B granules is that individual RNA transcripts may facilitate granule assembly by recruiting Me31B and its associated proteins.

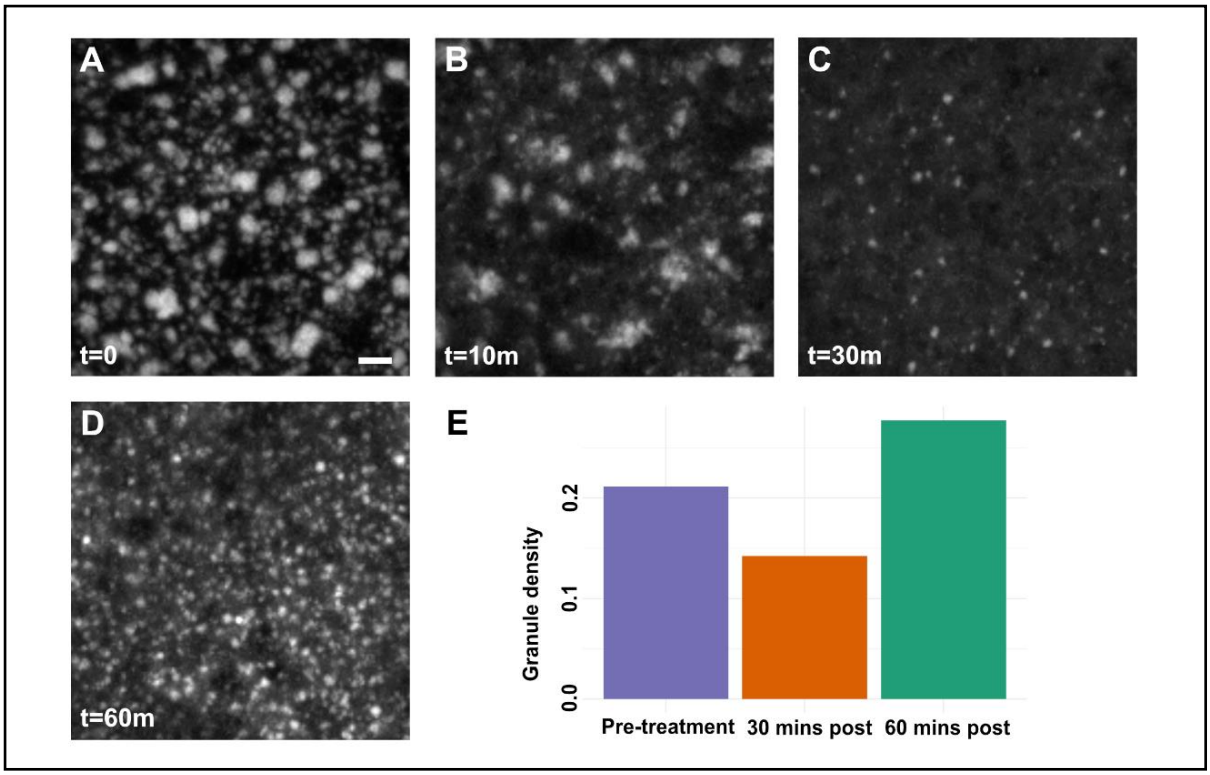

Figure 3.15: RNase A treatment causes Me31B granule dissociation. (A-D) Mature oocytes expressing Me31B::GFP. **(A-C)** Image sequence of Me31B granule dissociation post treatment with 50ng/µl RNase A. **(D)** Several Me31B granules reform at 60 minutes post treatment. Scale bar: 20 µm (A-D). **(E)** Quantification of Me31B granule density per unit cytoplasmic area at different time points. N=3 oocytes.

Conclusion: RNA is critical for regulating Me31B granule integrity and stability. Nucleation and formation of new Me31B granules post RNase A treatment suggests a role for RNA in the assembly of Me31B granules in the mature oocyte.

3.11 1,6 Hexanediol causes Me31B granules to transition from gel-like to liquid-like material state

Both under native and mutant conditions, RNP condensates have been shown to exhibit diverse material states, ranging from liquid, gel or solid. Several techniques have been used to probe and distinguish between the different material states. 1,6 hexanediol, an aliphatic alcohol, has been frequently used to test the material properties of phase separated granules *in vitro* and *in vivo*. Several studies have collectively demonstrated the ability of hexanediol to perturb weak hydrophobic interactions that are required to maintain the native material states of RNP condensates (Kroschwald et al. 2015). Hexanediol dissolves liquid-like compartments

but not solid condensates in yeast and mammalian cells, thereby allowing identification of liquid like states from solid states.

Since Me31B granules exhibit several liquid-like properties, I hypothesised that treatment with hexanediol would dissolve the granules. To test this, mature oocytes were treated with 5% 1,6 hexanediol solution. Surprisingly, Me31B granules underwent a dramatic shape change from irregular to spherical morphology post hexanediol treatment, as quantified by their circularity (Figure 3.16). Several fusion events of individual granules were also observed shortly post hexanediol treatment (data not shown). This suggests that Me31B transitions into a liquid-like material state post hexanediol treatment.

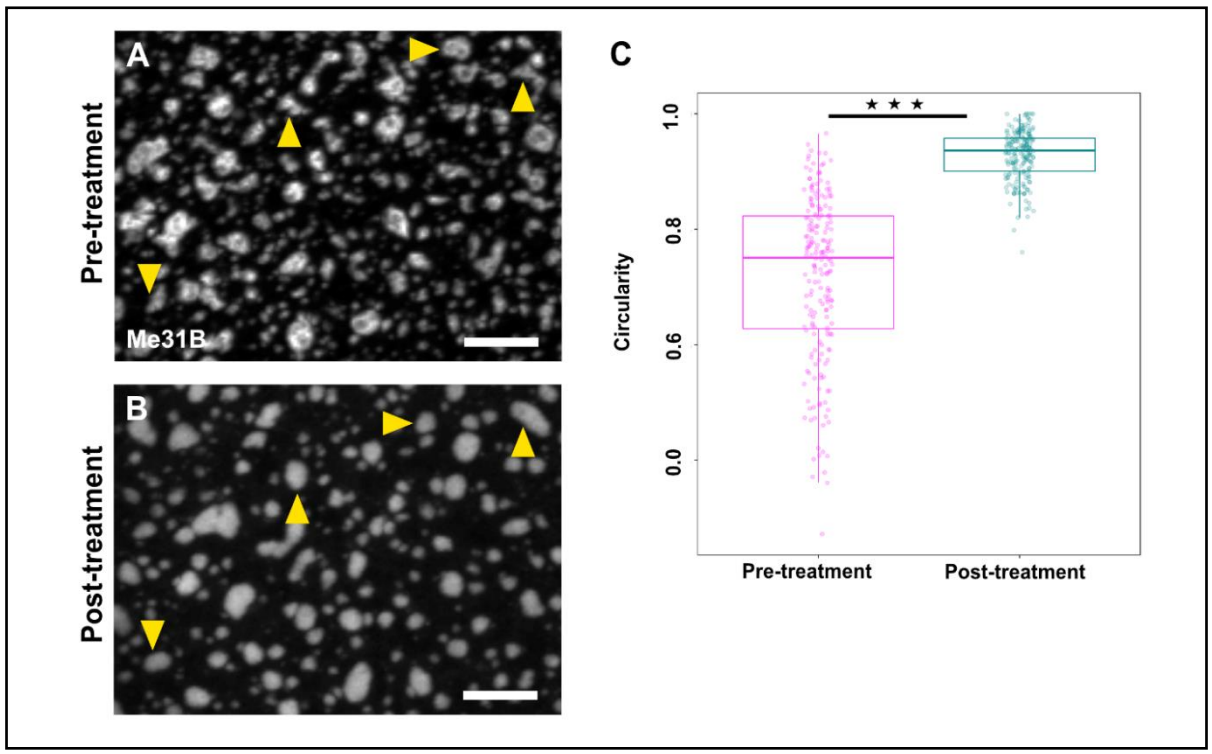

Figure 3.16: Me31B granules exhibit highly spherical morphology post hexanediol treatment. (A) Representative image of Me31B granules in mature oocytes expressing Me31B::GFP. Several granules exhibit internal sub-domains. **(B)** Representative image of Me31B granules exhibiting increased spherical morphology post 5% 1,6 hexanediol treatment compared to pre-treated granules (yellow arrowheads). Me31B granules display homogeneous fluorescence distribution, indicating loss of internal structuring post hexanediol treatment. Scale bar: 10 µm. **(C)** Quantification of Me31B granule circularity pre- and post-hexanediol treatment; n=200 Me31B granules, $p<0.0001$.

To confirm the liquid-like material state, I performed whole particle FRAP on hexanediol treated Me31B granules to test their exchange kinetics. Contrary to previous observations (Figure 3.9), hexanediol treated granules displayed rapid exchange of Me31B molecules with the cytoplasm with a significantly high proportion of mobile Me31B molecules post photobleaching (Figure 3.17). Additionally, biphasic response of Me31B recovery as indicated by two different $t^{1/2}$ indicates the following possibilities: (a) there exists two populations of Me31B molecules with different dynamics or (b) diffusion of a fraction of Me31B molecules is partially hindered, likely due to their binding to immobile cytoplasmic structures such as the cytoskeleton. Nonetheless, the faster $t^{1/2}$ of ~7.7 seconds indicates rapid exchange kinetics exhibited by Me31B molecules, converging towards a liquid-like material state.

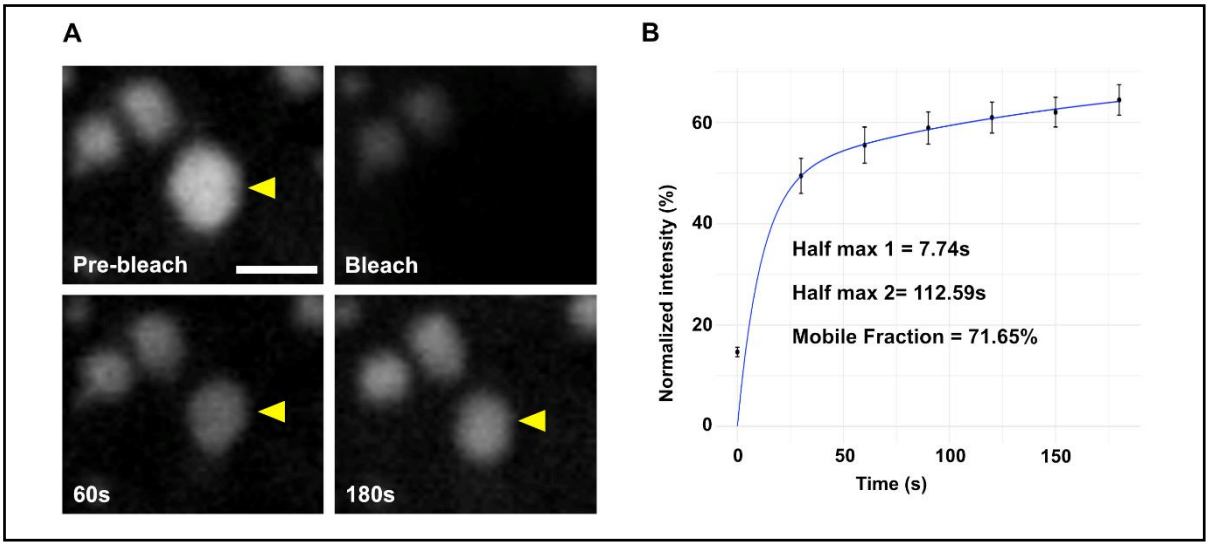

Figure 3.17: Hexanediol treated Me31B granules exhibit exchange of molecules with the cytoplasm. (A) Time lapse images of Me31B granules before and after photobleaching of whole granules (yellow arrowheads); scale bar: 3 µm. **(B)** Analysis of whole particle FRAP of Me31B granules. Standard deviation/data (black), fit (blue), n=12 Me31B granules, N=4 oocytes. Double exponentials fit the FRAP curve, indicating a biphasic response.

To test if the Me31B granule core exhibited faster dynamics, internal FRAP was performed on hexanediol treated Me31B granules. Indeed, Me31B molecules were highly dynamic and recovered as fast as 30s post photobleaching (Figure 3.18), confirming the phase transition of Me31B granules to a liquid-like state post treatment with hexanediol.

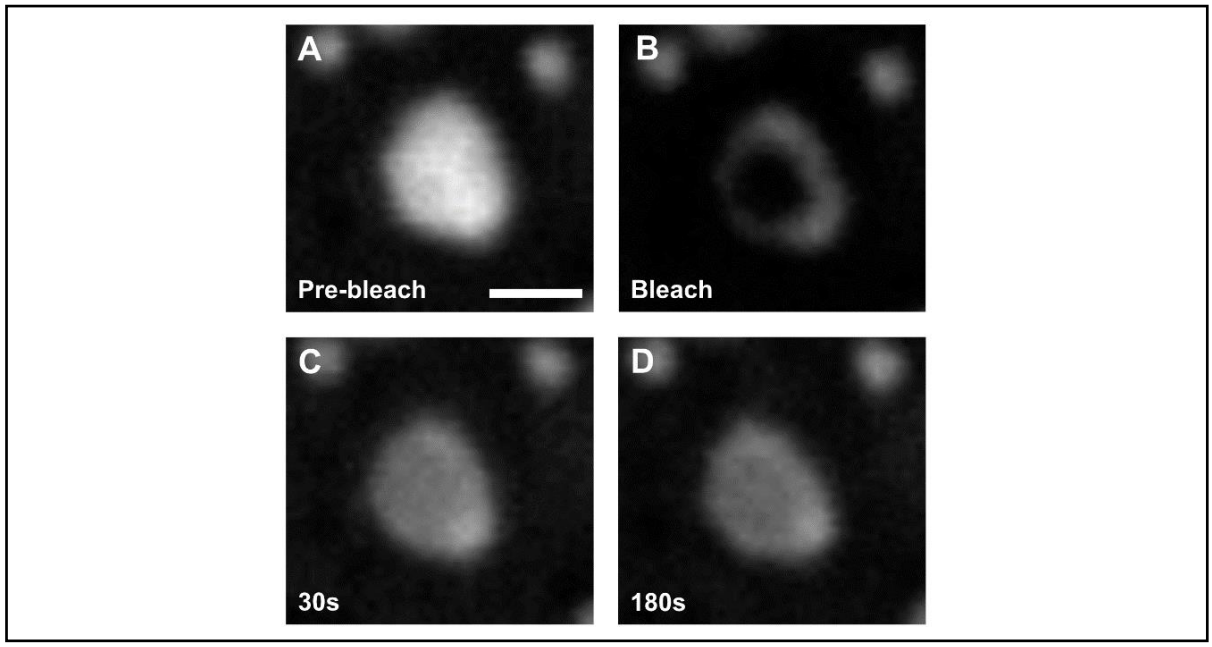

Figure 3.18: Hexanediol treated Me31B granule core exhibits rapid internal mobility. (A-D) Time lapse images of Me31B granule before and after photobleaching of a small region within Me31B granule; scale bar: 3 µm.

Longer exposure to hexanediol resulted in the dissolution of granules (Figure 3.19). This indicates that Me31B granules are more stable in the native gel-like state compared to the altered liquid-like state post hexanediol treatment. Moreover, the amino acid composition of Me31B contains about 48% hydrophobic residues. Therefore, it is likely that the hydrophobic interactions arising between different P body proteins may form the underlying core for the native gel-like material state.

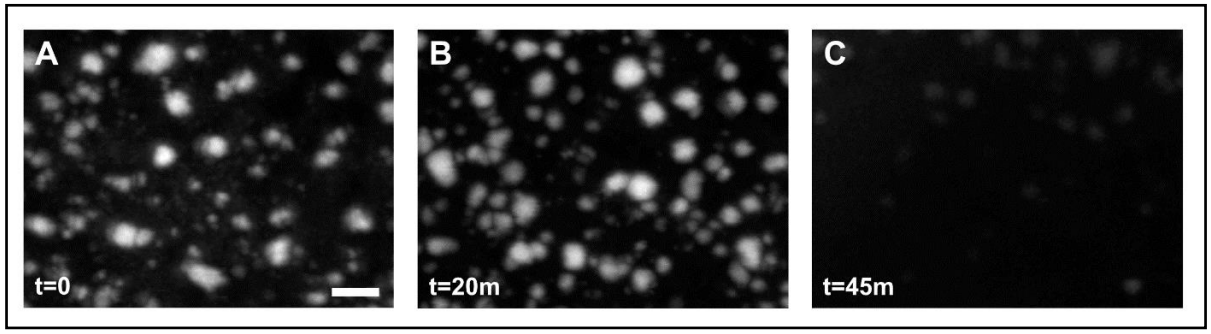

Figure 3.19: Prolonged exposure to hexanediol causes Me31B granule dissolution. (A-C) Representative image sequence shows Me31B granules treated with 5% 1, 6 hexanediol treatment undergo dissolution over time; scale bar: 10 µm.

Conclusions: Hexanediol treatment induces an abnormal gel to liquid-like phase transition which renders Me31B granules highly unstable, eventually causing them to dissolve. These results indicate the role of hydrophobic forces in maintaining the native gel-like state of Me31B.

3.12 High temperature causes Me31B granules to transition into a less-stable, highly dynamic state

Phase separation is a highly sensitive process whereby minute changes in cellular temperature, ionic or nucleic acid concentrations or pH can lead to changes in the conformation and properties of phase separated compartments. A key determinant regulating the physicochemical and conformational properties of a protein is the identity and patterning of hydrophobic residues within that protein. The previous section highlighted the importance of hydrophobic interactions in maintaining the gel-like material state of Me31B granules. However, hexanediol is not a physiological condition which oocytes encounter. This prompted me to test an alternative, yet natural condition which oocytes are exposed to. One such condition which modulates phase separation of several RNP granules *in vivo* and *in vitro* is temperature. For instance, stress granules assemble when cells are exposed to high temperatures, and later dissolve when relieved from the stress, thus dynamically and reversibly responding to changes in temperature (Wheeler et al. 2016). Temperatures well below physiological range have also been used to induce phase separation of several recombinant RBPs *in vitro* (Molliex et al. 2015).

To test if temperature affects the gel-like material state of Me31B granules, mature oocytes were imaged live while subjecting them to rapid temperature shifts using a temperature-controlled stage. Firstly, to check if Me31B granules exhibited distinct exchange kinetics at different temperatures, whole particle FRAP of Me31B granules before and after temperature shifts was performed. At 20ºC, Me31B molecules displayed very minimal exchange between the granule and cytoplasm, with an extremely low percentage of mobile Me31B molecules (Figure 3.20A,B). At 35ºC, however, Me31B granules displayed an increased percentage of mobile Me31B molecules between the granular and cytoplasmic pool, indicating a phase transition to a highly dynamic state upon exposure to higher temperatures (Figure 3.20C,D). Interestingly, although the percentage of mobile Me31B molecules differed between

20ºC and 35ºC, exchange kinetics of Me31B between the granule and cytoplasm remained similar as indicated by their $t^{1/2}$ estimates (Figure 3.20B,D). This suggests that while higher temperature results in an increased mobile fraction of Me31B, the viscosity of Me31B granules likely remain the same. Perhaps, this may also explain why Me31B granules require extremely high temperatures to undergo complete dissolution (Figure 3.22C), contrary to liquid-like P granules (Putnam et al. 2019).

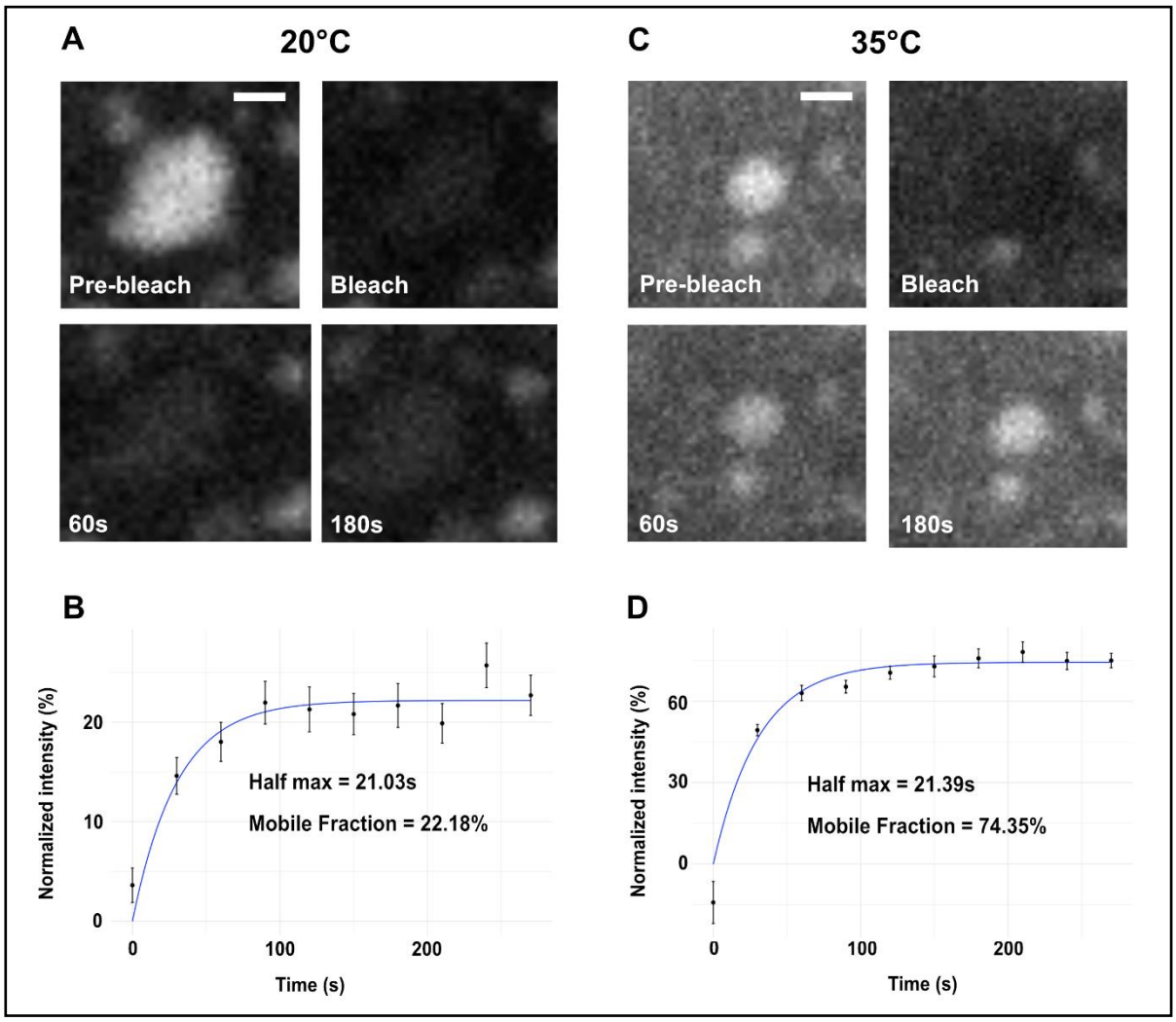

Figure 3.20: Me31B mobility between the granule and cytoplasm increases at higher temperatures. (A-D) Mature oocytes expressing Me31B::GFP. **(A)** Time lapse images of Me31B granule before and after photobleaching of whole granules subjected to a temperature of 20ºC. **(B)** Analysis of whole particle FRAP of Me31B granules. Standard deviation/data (black), fit (blue), n=10 Me31B granules, N=2 oocytes. Single exponential fits the FRAP curve. **(C)** Time lapse images of Me31B granule before and after photobleaching of whole granules subjected to a temperature of 35ºC. **(D)** Analysis of whole particle FRAP of Me31B granules. Standard deviation/data (black), fit (blue), n=10 Me31B granules, N=2 oocytes. Single exponential fits the FRAP curve. Scale bar: 10 µm (A, C).

Additionally, I observed increased cytoplasmic Me31B::GFP fluorescence at higher temperatures (Figure 3.21A-C). Quantification of the ratio of Me31B fluorescence intensity between the granular and cytoplasmic pool further confirmed this observation (Figure 3.21D). This decrease in granular Me31B intensity is likely due to the release of Me31B into the cytoplasm due to continuous exchange between the granule and the cytoplasm at higher temperatures.

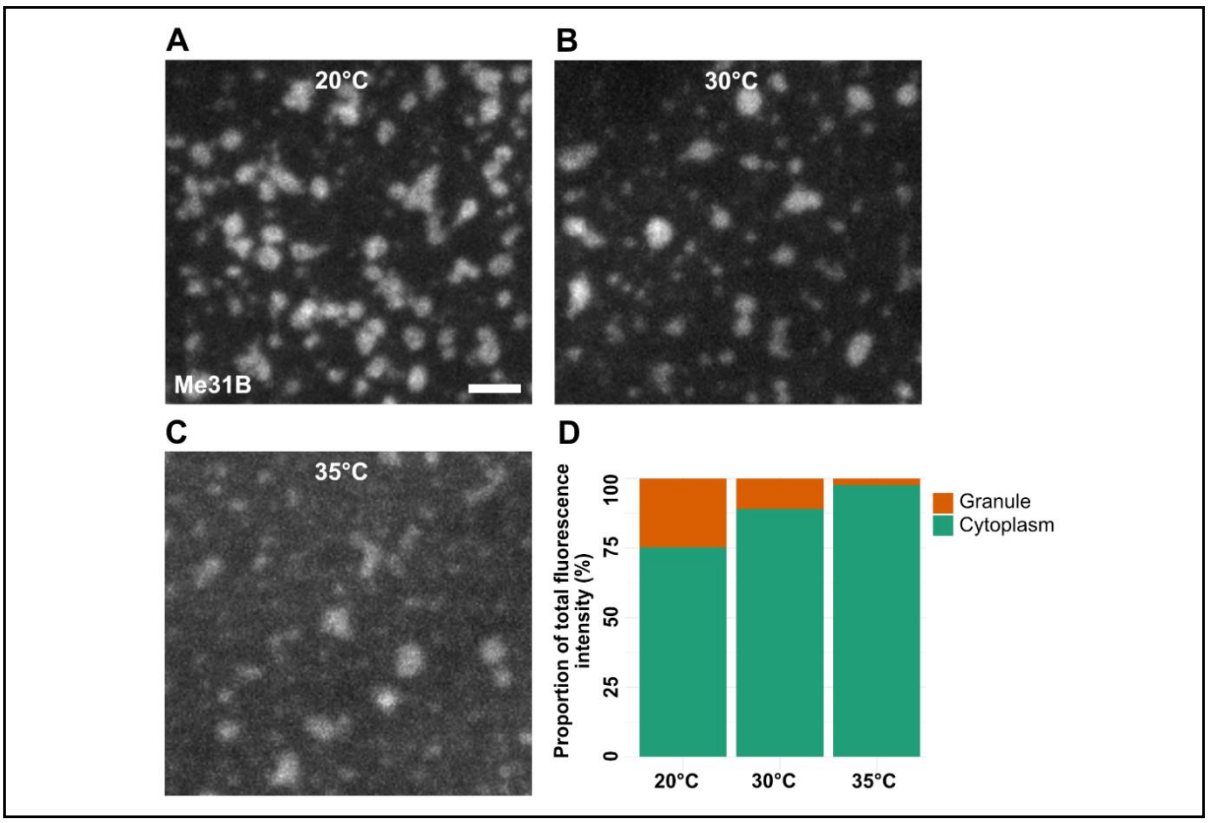

Figure 3.21: Partitioning of Me31B molecules inside the granule decreases with increase in temperature. (A-C) Mature oocytes expressing Me31B::GFP. Image sequence of Me31B granules at 20ºC (A), 30ºC (B) and 35ºC (C). **(D)** Analysis of total Me31B::GFP fluorescence quantified from granules and cytoplasm showing a decrease in Me31B partitioning in granules at temperatures 30ºC and 35ºC compared to 20ºC (N=3 oocytes).

An interesting observation was recorded when oocytes were transiently exposed to 40ºC; the Me31B granule core displayed numerous tiny Me31B particles, suggestive of internal dissociation (Figure 3.22B; B',B''). At 50ºC, granules appeared less condensed and more diffuse (Figure 3.22C). This suggests that transition from particulate to diffuse state likely involves an intermediate dissociation phase, as observed at 40ºC. Furthermore, this demonstrates a plausible stepwise dissociation

mechanism of Me31B granule dissociation in response to different developmental or environmental cues.

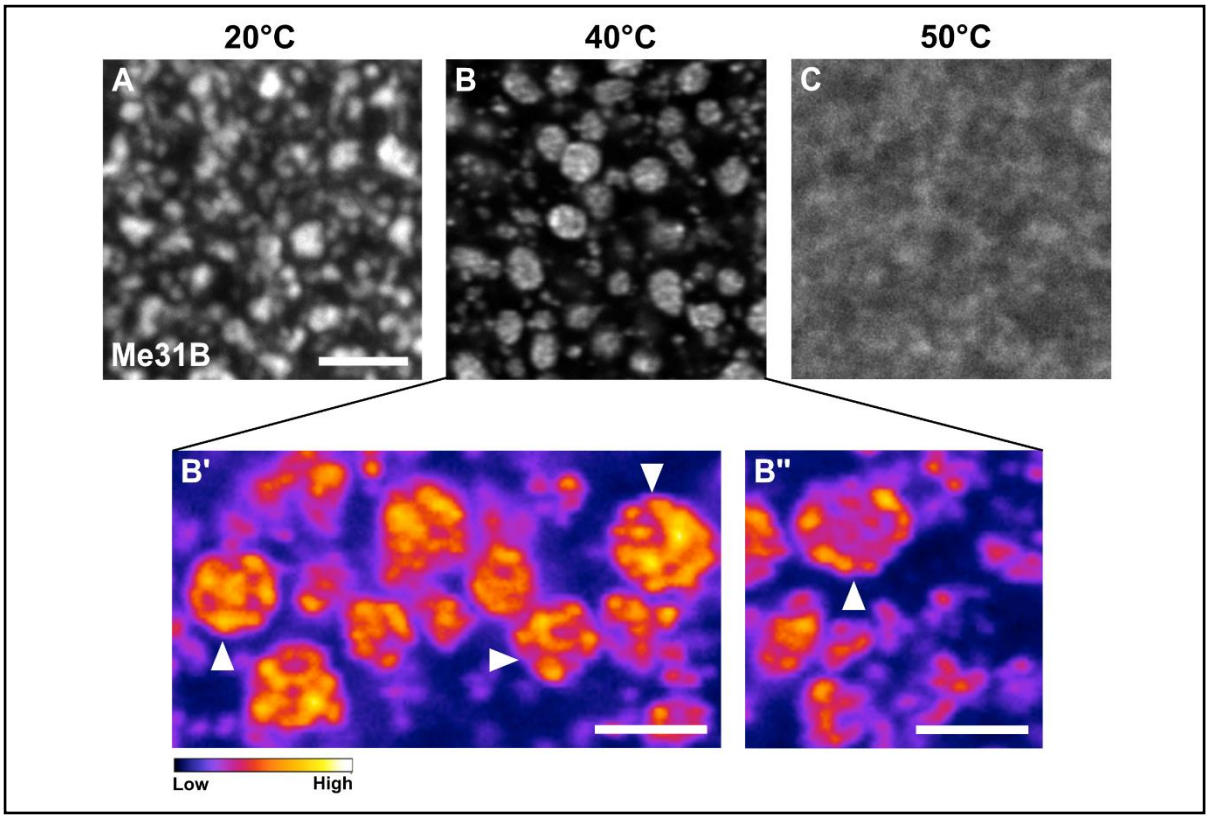

Figure 3.22: Me31B granules exhibit internal dissociation before dissolving at higher temperature. (A-C) Mature oocytes expressing Me31B::GFP. (A) Representative image of Me31B granules subjected to 20ºC temperature reveal homogeneity within granules. **(B)** Representative image of Me31B granules subjected to 40ºC reveals the formation of multiple small granules internally within the granules; Inset **(B'-B'')** shows representative high-resolution images of Me31B granules at 40ºC revealing internal dissociation (white arrowheads). **(C)** Representative image of Me31B granules subjected to 50ºC shows complete dissolution. Scale bar: 10 µm.

Conclusions: Me31B granules exhibit upper critical solution temperature (UCST) properties where phase separation occurs only at temperatures below a critical temperature, above which, the system is in the solution state. Higher temperatures also increase the fraction of mobile Me31B molecules, resulting in faster exchange kinetics between the granule and cytoplasm. Furthermore, Me31B granules exhibited internal dissociation at 40ºC indicative of stepwise granule disassembly. Complete granule dissolution was only observed at 50ºC demonstrating that Me31B granules are inherently more stable than conventional liquid-like condensates.

3.13 *bcd* mRNA is dynamically partitioned inside Me31B granules

RNA localisation is a conserved and widespread mechanism to regulate localised protein production. To generate precise protein synthesis and prevent ectopic expression, mRNA localisation is often coupled to translational regulation. This is particularly important in *Drosophila* oocytes where key maternal mRNAs such as *bcd* are localised to the anterior pole, to provide primary patterning signals for axis formation. *bcd* is transcribed in the adjacent nurse cell nuclei, actively transported to the anterior region of the oocyte during mid-oogenesis and translationally repressed until egg activation. Several studies have shown that *bcd* is associated with P bodies at the anterior region of the oocyte during mid-oogenesis. Using ultrastructural analysis and super resolution microscopy, Weil et.al showed that during mid-oogenesis, *bcd* is enriched within the core of P bodies, whereas post egg activation, *bcd* is on the edge or outside the P bodies (Weil et al. 2012). This study also demonstrated that P bodies, much like stress granules, appear to have sub-regions within the granule where RNP components could be differentially localised and regulated.

Since the temporal regulation of *bcd* translational regulation is relatively well understood, I wanted to examine if the gel-like material state of Me31B granules contributed to *bcd* storage in the mature oocyte. To determine this, *bcd* mRNA and Me31B granules were visualised simultaneously in the mature oocyte. For live imaging of *bcd*, I used the MS2 system, a commonly used method to follow transcripts in live cells. mRNA tagging is achieved by multiple MS2 sequence repeats that form stem loop structures integrated in the 3' UTR of the mRNA of interest. The MS2 stem loops are then coated by the MS2 coat protein fused to a fluorophore, thereby providing distinct staining of *bcd*.

Live imaging of oocytes expressing Me31B::GFP and *bcd*-RFP revealed that *bcd* significantly overlaps with Me31B granules at the anterior region of the mature oocyte (Figure 3.23A), consistent with previous observations. Sometimes, Me31B granules in the mature oocyte display sub domains internally indicative of multi-layered organisation. When co-visualised with *bcd*-RFP, *bcd* was preferentially localised to these domains (Figure 3.23B), suggesting dynamic partitioning of *bcd* within Me31B granules. Physiologically, under what conditions such multi-layered organisation is

induced is not clear. However, these observations show the ability of *bcd* to differentially segregate within Me31B granules in response to certain conditions.

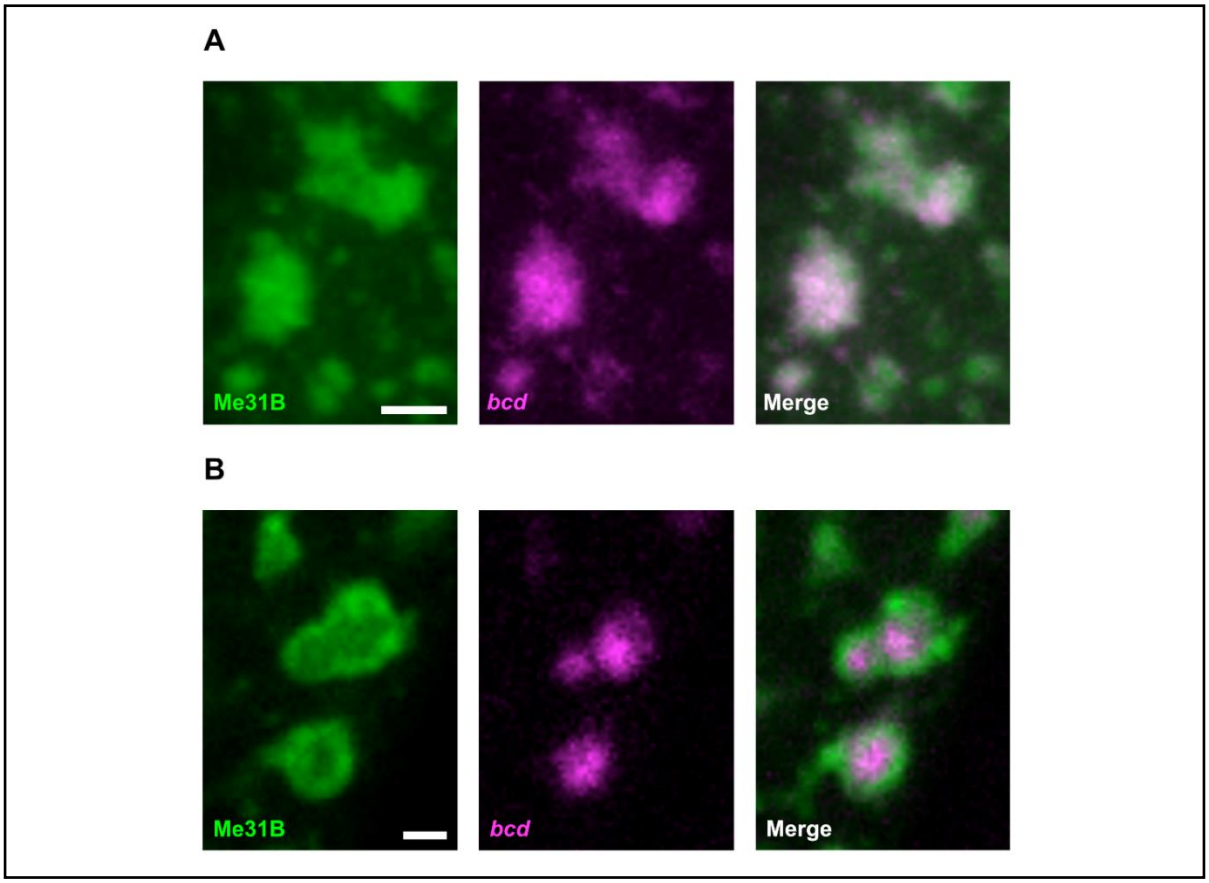

Figure 3.23: *bcd* dynamically partitions inside Me31B granules. (A) Representative image of mature oocytes expressing Me31B::GFP and *bcd*-RFP shows *bcd* mRNAs significantly overlap with Me31B granules. **(B)** Representative image of Me31B granules exhibiting sub-domains to which *bcd* is localised. Scale bar: 5 µm (A,B).

Since *bcd* transcripts display dynamic partitioning within Me31B granules, it is likely that *bcd* molecules are mobile. To test this, I performed whole particle FRAP on *bcd* particles in the anterior region of the oocyte. Contrary to whole particle Me31B dynamics, *bcd* exhibited moderate fluorescence recovery post photobleaching, albeit at a significantly slower exchange rate (Figure 3.24A). However, the percentage of mobile *bcd* particles was approximately 35%, significantly higher than Me31B molecules (Figure 3.24B).

Previous studies had ruled out the possibility of free *bcd* mRNA in the oocyte anterior (Weil et.al, 2008). However, these results show that while the majority of *bcd* is concentrated in the granules, there appear to be residual levels in the cytoplasm.

Alternatively, recovery could also have been from the pool of *bcd* particles within Me31B granules.

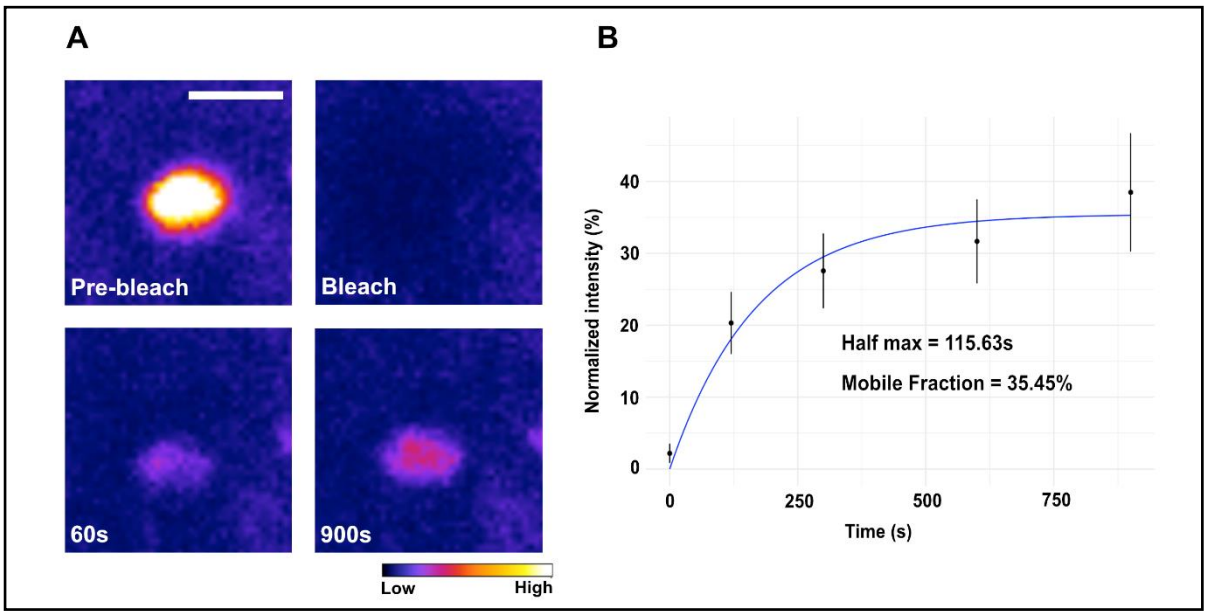

Figure 3.24: *bcd* exhibits slow exchange kinetics between the granule and cytoplasm. **(A)** Time lapse images of *bcd*-RFP before and after photobleaching of whole *bcd* particles; scale bar: 5 µm. **(B)** Analysis of whole particle FRAP of *bcd* particles. Standard deviation/data (black), fit (blue), n=7 *bcd* particles, N=3 oocytes. Single exponential fits the FRAP curve.

Conclusions: *bcd* is associated with Me31B granules at the anterior region of the mature oocyte and can dynamically partition in sub-domains within the granules under specific conditions. Furthermore, *bcd* exhibits a dynamic, semi-liquid material state, likely contributing to the viscous nature of the Me31B granule core.

3.14 1,6 Hexanediol treatment causes premature release of *bcd* from Me31B granules

Many proteins have been shown to exhibit diverse material properties, but how these material states directly translate to biological functions in living cells remains elusive. In an earlier section, I demonstrated the importance of hydrophobic interactions in maintaining the gel-like material state of Me31B granules, disruption of which resulted in an aberrant phase transition to a liquid-like state. This transition also caused Me31B to rapidly exchange between the granule and the cytoplasm. Since *bcd* transcripts are stored in Me31B granules throughout mid- to late oogenesis, I wanted to examine whether the gel state of Me31B granules is necessary for the storage of *bcd*.

To test this, mature oocytes expressing Me31B::GFP and *bcd*-RFP were treated with 5% 1,6 hexanediol solution. As observed earlier, upon hexanediol treatment, Me31B granule morphology changed from an irregular to spherical shape (Figure 3.25 A,C). Surprisingly, similar to Me31B, *bcd* also underwent a morphological change from an amorphous to a more spherical shape (Figure 3.25 B,D). This suggests that *bcd* molecules are present in an inter-connected matrix with Me31B.

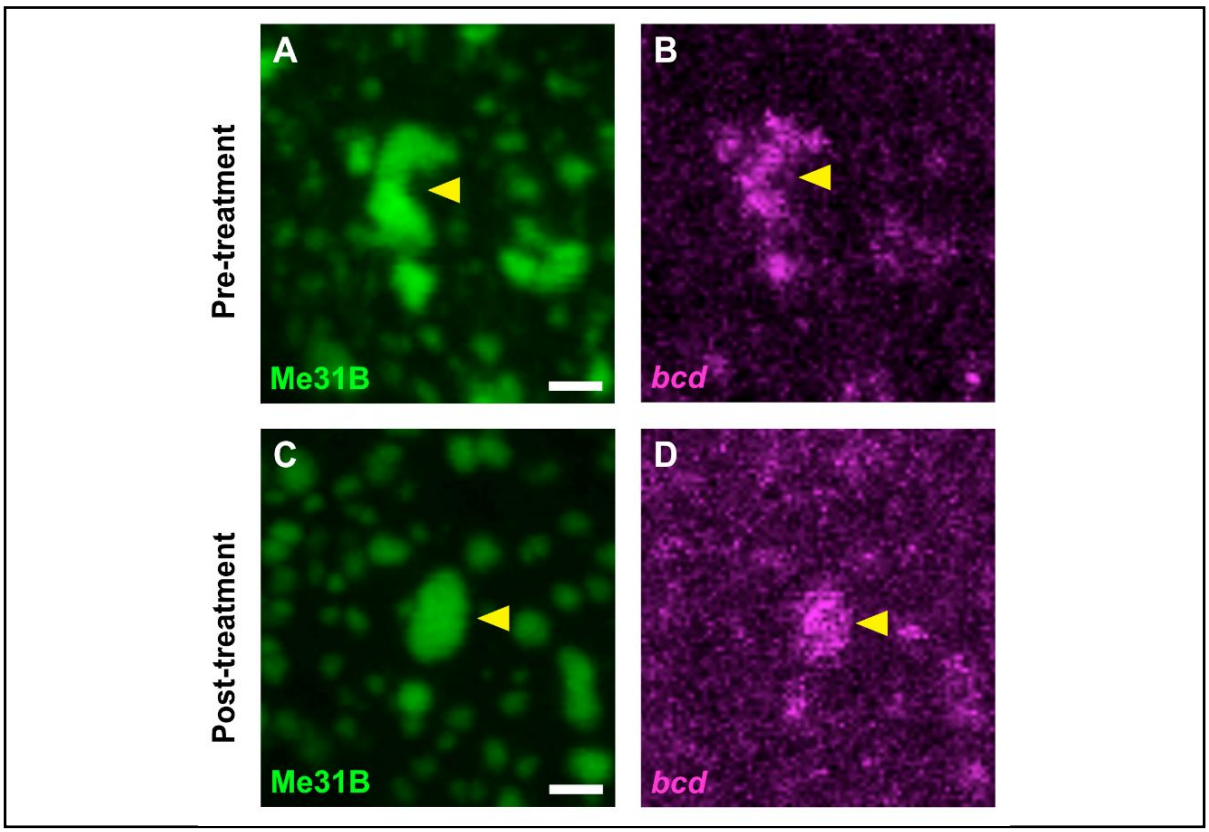

Figure 3.25: *bcd*, like Me31B granule, exhibits spherical morphology post hexanediol treatment. (A-D) Mature oocytes expressing Me31B::GFP and *bcd*-RFP. **(A,B)** Representative images of Me31B granule and *bcd* particle exhibiting amorphous morphology respectively (yellow arrowheads). **(C,D)** Representative images of Me31B granule and *bcd* particle exhibiting spherical morphology post hexanediol treatment, respectively (yellow arrowheads). Scale bar (A-D): 10 µm.

Interestingly, hexanediol treatment resulted in a rapid loss of *bcd*-RFP fluorescence intensity (Figure 3.26B,D,F) compared to untreated *bcd*-RFP particles (Figure 3.26H,J,L). Me31B granules, despite displaying a gradual loss of fluorescence (Figure 3.26 G,I,K) compared to untreated granules (Figure 3.26A,C,E), remained mostly particulate at 20 minutes post treatment (Figure 3.26K).

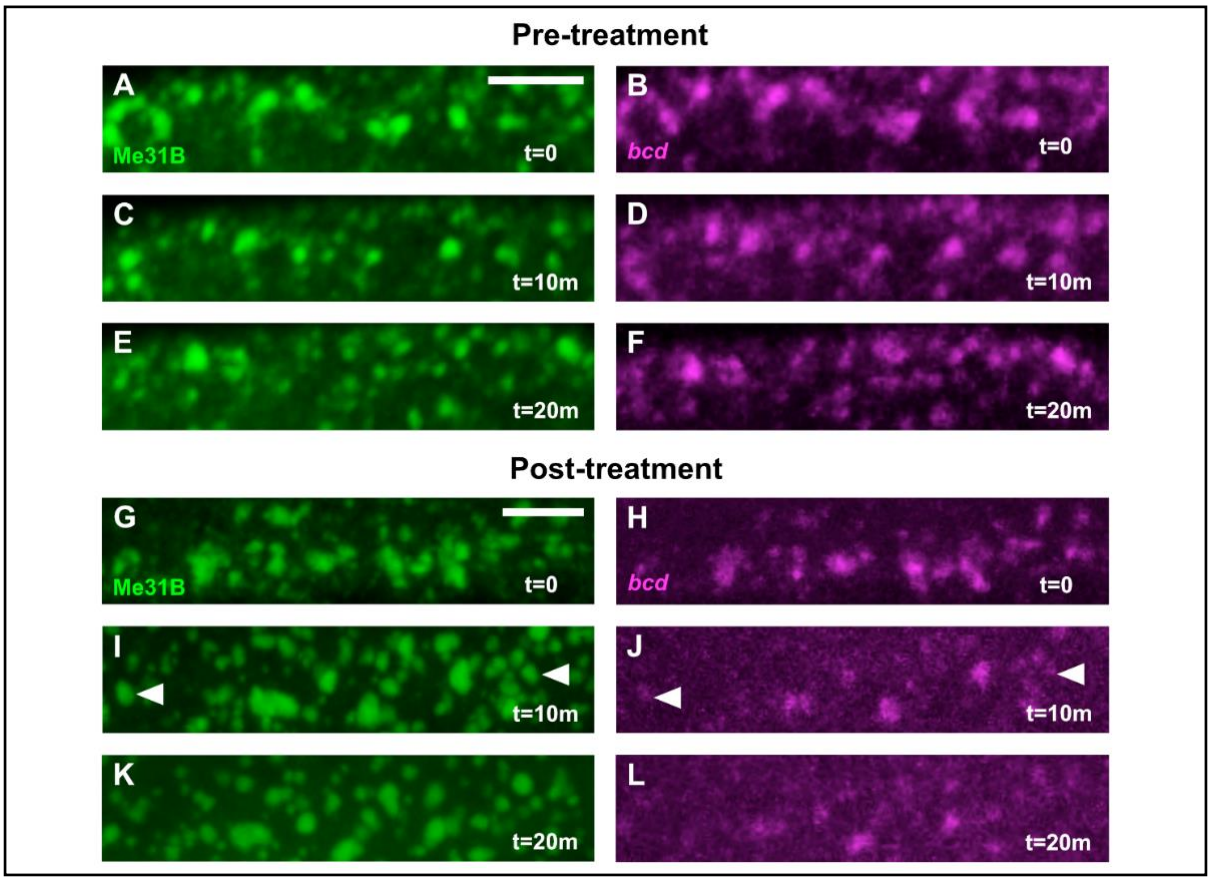

Figure 3.26: Hexanediol treatment causes premature dispersion of *bcd*. (A-L) Mature oocytes expressing Me31B::GFP and *bcd*-RFP. **(A-F)** Representative images of Me31B granules and *bcd* particles at different time points prior to hexanediol treatment. Both Me31B and *bcd* remain particulate throughout the imaging sequence; scale bar 10 µm. **(G-L)** Representative images of Me31B granules and *bcd* particles at different time points post hexanediol treatment. While Me31B particles, despite exhibiting decrease in fluorescence, remained particulate, significant percentage of *bcd* particle fluorescence appeared diffuse as early as 10 mins post treatment (white arrowheads); scale bar: 10 µm.

To confirm that the loss of intensity was a consequence of the hexanediol treatment, *bcd* fluorescence intensity was measured at different time points with addition of PBS (control solution). As determined from the intensity plot (Figure 3.27), while control measurements did show a decrease in *bcd* fluorescence intensity (likely due to photobleaching the RFP fluorophore), hexanediol induced a significantly dramatic reduction in the *bcd* fluorescence as early as 5 minutes post treatment. These results show that hexanediol treatment causes premature release of *bcd* mRNA.

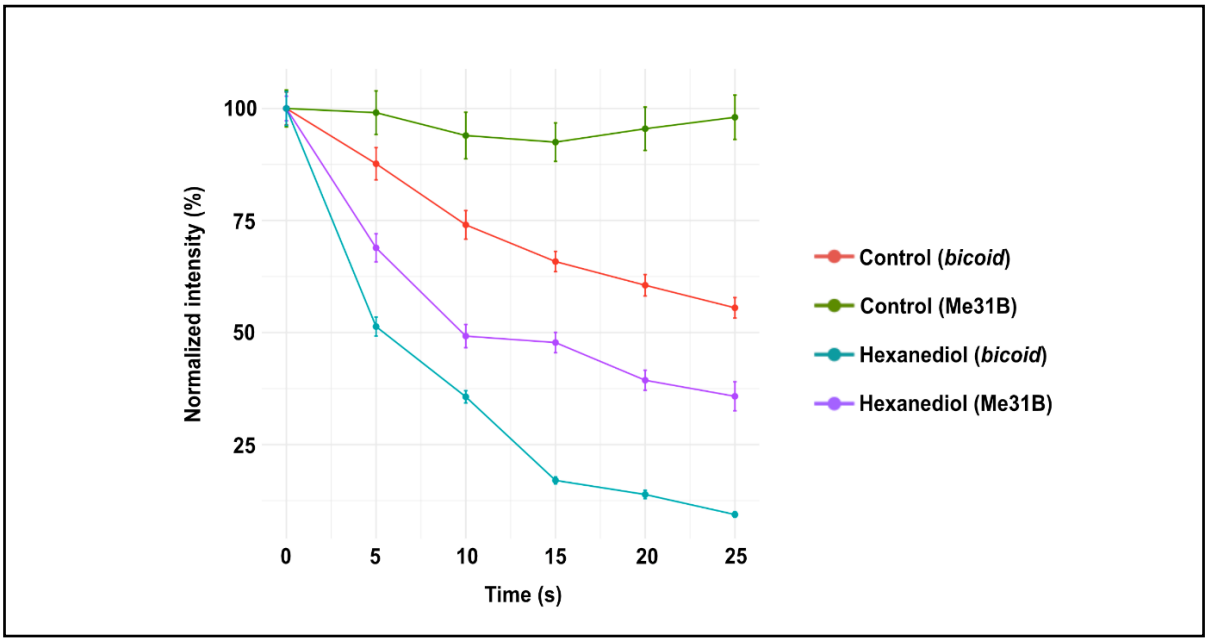

Figure 3.27: Loss of *bcd* fluorescence is a consequence of hexanediol treatment. Quantification of Me31B::GFP and *bcd*-RFP fluorescence post PBS and hexanediol treatment; n=37 Me31B and *bcd* particles (PBS treatment), n=71 Me31B and *bcd* particles (hexanediol treatment); N=5 oocytes.

Conclusions: Hexanediol treatment results in a morphological change of *bcd* from an amorphous to a more spherical shape, similar to Me31B. Additionally, hexanediol also results in the premature release of *bcd* from Me31B granules, indicating the importance of the gel-like material state in the storage of *bcd*.

3.15 Summary of results

How P bodies regulate mRNA storage in the mature oocyte is less well understood. To address this question, I used the conserved P body protein Me31B to visualise and characterise Me31B granules (representative of P body properties) in the mature oocyte. Using a combination of extrusion assays and *in vivo* live imaging, my data demonstrates the viscoelastic properties of P bodies in the mature oocyte. Whole particle and internal FRAP assays revealed the arrested (minimal exchange of components between the granule and cytoplasm) and reversible (increased mobility of Me31B molecules inside the granule) gel-like material state of P bodies. Using a combination of pharmacological treatment and internal FRAP assay, my data describes the role of ATP activity to maintain the semi-liquid state of the P body internal core. Pharmacological treatment using cytoskeletal depolymerizing drugs revealed the role of actin and microtubule cytoskeleton in maintaining the morphology, integrity, and spatial dynamics of P bodies in the mature oocyte. Using RNase A pharmacological treatment, my data indicates a role for RNA in maintaining P body assembly and integrity. Using multiple approaches, namely 1,6 hexanediol pharmacological treatment and temperature gradient assays, my data describes the role of weak intermolecular forces in regulating the gel-like state of P bodies. Finally, my data demonstrates the importance of the gel state of P bodies in the storage of *bcd*, a key axis patterning maternal mRNA.

3.16 Discussion

3.16.1 P body internal compartmentalisation

Recent studies have reported that RNP condensates, such as stress granules and the nucleolus, exhibit internal compartmentalisation (Feric et al. 2016; Jain et al. 2016). Live imaging in the mature oocyte revealed that P bodies are not homogeneous structures but rather contain distinct subdomains, characteristic of internal structuring. In fact, whole particle and internal FRAP results of Me31B granules lead to a P body model of a semi-dynamic inner core surrounded by a hard-outer shell.

P bodies exhibiting sub-domains also revealed heterogeneous partitioning of *bcd* mRNA, which otherwise displays a homogeneous distribution. Although only partially understood, RNAs can generate significant compartmentalisation within RNP complexes. Therefore, internal structuring induced within P bodies likely promotes dynamic partitioning of stored RNP components in response to specific developmental and cellular cues.

A role for ATP in maintaining the internal dynamics of granules was reported for the nucleolus when ATP depletion caused the apparent viscosity within the condensate to increase by 10-fold and exhibited a state of “freezing” (Brangwynne et al. 2011). I observe similar behaviour for P bodies in the presence of an ATPase inhibitor, indicating that energy driven dissipative processes, such as helicase activity, play a role in modulating the internal organisation and dynamics of RNP granules.

3.16.2 Cytoskeleton and P body regulation

P body assembly, maintenance and disassembly is regulated based on cellular cues. In the mature *Drosophila* oocyte, P bodies are distributed throughout the cytoplasm, contrary to certain maternal mRNAs such as *bcd* which are localised and anchored to specific regions in the oocyte. Therefore, due to their distribution pattern, one would expect P bodies to diffuse around freely in the cytoplasm. However, my results suggest that P bodies appear anchored and confined to regions with minimal spatial dynamics across the cytoplasm as if tethered to the cytoskeleton. While P body dissociation is a common consequence of both actin and microtubule depolymerisation, differences in the dynamics of dissociated P bodies were quite interesting. P body movements were decreased post microtubule depolymerisation, while actin depolymerisation caused P

bodies to exhibit increased movements. In fact, colchicine has been shown to activate actin polymerisation by depolymerizing microtubules (Jung et al. 1997). Therefore, stimulation of actin polymerisation could lead to increased stabilisation and anchoring of P bodies, explaining their decreased dynamics post colchicine treatment.

A key feature of phase separated compartments is the spherical morphology of the condensates. Oocyte P bodies, however, largely possess an amorphous morphology, possibly dictated by their dynamic elastic property and interactions with cytoplasmic structures. What promotes the irregular morphology is not very well understood. Recent studies have suggested a role for polyanions, such as microtubules, in influencing the irregular morphology of condensates reconstituted *in vitro* (Boeynaems et al. 2019). In the mature *Drosophila* oocyte, microtubule, or actin depolymerisation not only results in the breakdown of P bodies into smaller particles but stimulates the formation of spherical particles. These results suggest that interactions with the cytoskeletal network likely maintain the amorphous shape of P bodies in the mature oocyte. Moreover, extrusion of oocyte cytoplasm into oil caused P bodies to become more spherical. The act of puncturing the oocyte membrane for extrusion most likely destroyed the intact cytoskeleton. Therefore, it is possible that the loss of cytoskeletal interaction contributed to the spherical morphology of extruded P bodies.

Several studies have shown the importance of RNP granule association with cytoskeletal proteins, namely kinesin and dynein, to maintain the structural integrity of granules (Clark, Meignin, and Davis 2007; Delanoue et al. 2007). While it remains less clear as to why/how these molecular motors have a dramatic effect on granule integrity, one possible explanation is that the antagonistic activities of motor proteins is key to maintaining the influx of RNPs and preventing aberrant disassembly.

3.16.3 The gel-like material state of P bodies and its importance

While many membrane-less organelles exhibit highly dynamic, liquid-like material states, biological condensates can also be present in higher order polymeric states for its normal physiological function. P bodies in the mature *Drosophila* oocyte exist in an arrested, gel-like material state which promotes active internal rearrangement but prevents any exchange between the granule and the cytoplasm. However, disrupting weak interactions between P body components, either by increasing temperature or

treatment with hexanediol (which disrupts hydrophobic forces), cause P bodies to undergo an aberrant phase transition from a stable gel-like to dynamic liquid-like state, and eventually dissolve, indicating that weak multivalent interactions are key to holding RNP together.

In the mature oocyte, it is likely that the gel-like state of P bodies ensures long term storage of maternal mRNAs and strongly inhibits access of the stored mRNAs to the cytosolic environment where translation and degradation are known to be active. Similar properties have been observed in the P bodies of arrested *C.elegans* oocytes (Hubstenberger et al. 2013), suggesting that such biophysical states could be a conserved mechanism to protect mRNAs during development. To ensure stored mRNAs are protected, it is critical that molecules entering and exiting the P bodies are tightly controlled. Large and irregular shaped granules with minimal dynamics effectively inhibit exchange of components between the granular and cytoplasmic P bodies. Therefore, conditions that lead to changes in the native material state and cause premature release of stored mRNAs could potentially lead to abnormalities during development. It is plausible that such properties may also be prevalent in polarised cells such as neurons which exhibit long-term storage and translational repression of several mRNAs at the pre-synapse.

3.17 Future directions

3.17.1 Super-resolution imaging of P bodies in the mature oocyte

While multi-layered organisation has been reported in RNP bodies such as stress granules and P granules, their biological significance remains less clear. Since P bodies are multi-layered condensates, whether sub-domains within P bodies exhibit different material states is not known. While most P body proteins observed during early oogenesis appear to be co-localised, live imaging of distinct proteins using light sheet microscopy could elucidate their sub-organelle organisation and dynamics, as demonstrated for P granule components in the *C.elegans* embryo (Putnam et al. 2019). Additionally, quantitative assays such as FRAP and single molecule assays of different P body components to determine molecular dynamics could provide insights into their biophysical states. Differential material states of proteins present in distinct sub-domains have been shown in the maternal granule, nuage, during *Drosophila* oogenesis (Webster et al. 2015). Therefore, super resolution imaging to reveal finer

structure and localisation of molecules, combined with quantitative single molecule assays to discern material states, could inform whether P body components within distinct internal domains exhibit differential material states. Additionally, they also would inform how diverse RNP components contribute to the overall material state and function of P bodies.

3.17.2 Quantifying *bcd* mRNA translation post hexanediol treatment

Hexanediol treatment of mature oocytes not only induced a phase transition of P bodies from gel-like to liquid-like state, but also led to the premature release of stored *bcd* transcripts. Whether or not *bcd* gets translated is not known, however, it is generally assumed that once in the cytoplasm, RNAs undergo translation. Multiple groups have demonstrated this idea primarily via biochemical approaches (Eichhorn et al. 2016).

To confirm if *bcd* undergoes premature translation post hexanediol treatment, Bicoid:GFP transgenic line could be used to monitor bicoid protein synthesis, either by live imaging or western blotting of lysates from mature oocytes, before and after treatment. While visualizing Bicoid protein in the mature oocyte might be technically challenging due to excessive background fluorescence, western blot analysis could provide detection of Bicoid protein. Alternatively, polysome profiling of lysates obtained from mature oocytes prior to and post hexanediol treatment could also demonstrate the degree of *bcd* mRNA translation. Confirming whether *bcd* mRNA is translated post hexanediol treatment could help attribute an additional function for the gel-like material state of P bodies in regulating the translational repression of mRNAs.

3.17.3 Characterising different populations of P bodies in the mature oocyte

P bodies in the mature oocyte are present in different sizes. While larger P bodies were predominantly distributed along the surface, smaller sized P bodies can be observed, primarily, in shallower regions of the oocyte. Preliminary observations indicate that the smaller P bodies are highly dynamic compared to the surface anchored, larger P bodies. Additionally, dynamics of smaller P bodies appear highly directional, indicating their movement along short microtubule tracks. While my results have implicated a function for the larger P bodies in mRNA storage and translational regulation, it will be crucial to understand the role of these smaller bodies in the mature

oocyte. It is highly probable that two different pools of P bodies exist serving distinct functions: while larger P bodies function in the storage of maternal transcripts, smaller P bodies, may serve as transport granules to carry key factors, including protein and RNA molecules, around the mature oocyte.

Chapter 4

Investigating Me31B granule properties and function in the early embryo

4.1 Introduction

The transition from an oocyte to embryo is a fundamental and universal event in developmental biology. The mature oocyte that is poised to begin embryogenesis is very different from a fertilised egg. Egg activation is a fundamental step in priming eggs for embryogenesis, often accompanied by fertilisation in vertebrates and marine invertebrates (Horner and Wolfner 2008). Fusion of the egg and sperm triggers a downstream cascade of signalling events, the most prominent being calcium transients, that promote a myriad of vital cellular processes. However, in some species, egg activation is not accompanied by fertilisation. Rather, it is triggered by osmotic or mechanical pressure as the egg passes through the oviduct, which activates downstream events. This feature is pertinent to *Drosophila* species which reproduce parthenogenetically, suggesting that egg activation alone may be sufficient for development. Some key molecular changes at *Drosophila* egg activation include the following: (a) A rapid calcium wave that propagates from the posterior to the anterior pole of the oocyte; (b) Release from meiotic arrest to allow formation of haploid female pronucleus that can combine with the male pronucleus to form the embryo; (c) Large-scale cytoskeletal rearrangement believed to support zygotic development and growth; (d) Alterations in maternal RNA expression and protein levels through controlled translation, degradation, and post translational modifications.

Post egg activation and fertilisation, early *Drosophila* embryogenesis proceeds through a syncytial embryo containing ~6000 nuclei as a result of rapid nuclear divisions without cell membrane formation. After 9 mitotic divisions, the nuclei begin to migrate to the periphery, lining the plasma membrane of the embryo. During cell cycle 14, individual membranes surround each cortical nucleus forming a sheet of epithelial cells with apical and basal polarity (Figure 4.1). This stage of development, called cellularisation, is roughly when the maternal to zygotic transition occurs, from which point embryo development is governed by the zygotic machinery.

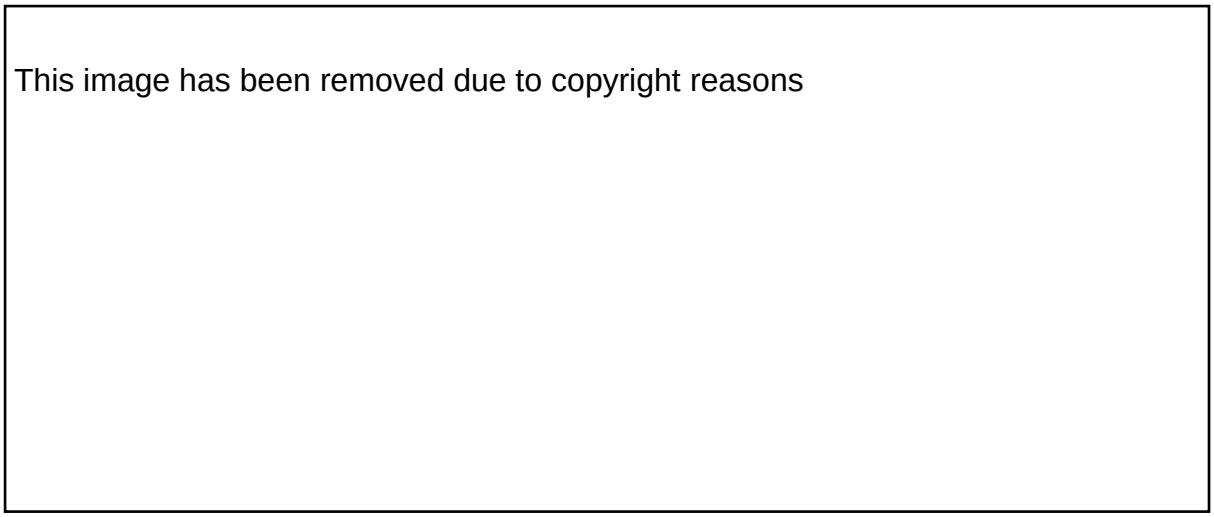

Figure 4.1: Overview of early stages during *Drosophila* embryogenesis. Schematic of the different stages during early embryogenesis which begins with the pre-blastoderm embryo consisting of the fused male and female pronuclei. 13 rounds of synchronous cell division give rise to a blastoderm embryo consisting of ~6000 nuclei. During cellularisation, nuclei migrate to the periphery where each nucleus is enclosed by a membrane; inset shows a more detailed view of the cellularisation process. Completion of cellularisation then leads to the onset of gastrulation. Note: While the depicted embryo at gastrulation is a surface view with the ventral side up, all others are displayed as mid-sections of the embryo with the ventral side to the right. Figure adapted from: (Farrell and O'Farrell 2014).

Early embryogenesis is also characterised by active transcriptional and post-transcriptional regulation of a cascade of segmentation genes (Figure 4.2):
Gap genes: Maternal determinants present in the early embryo are responsible for the transcriptional initiation of gap genes. These gap genes are transcribed in partially overlapping domains spatially organised across the embryo. Gap genes encode transcription factors that regulate the expression of the pair-rule genes.

Pair-rule genes: Combinatorial expression of gap genes initiates the periodic output of pair-rule gene expression. There are 7 canonical pair-rule genes that are expressed in evenly spaced stripes establishing pairs of segments. At this point, the anterior-posterior axis of the embryo is subdivided into individual para-segments, by both gap and pair-rule genes. Pair-rule genes encode transcriptional factors that regulate the expression of segment polarity genes.

Segment-polarity genes: Segment polarity genes expressed following gap and pair-rule genes, are primarily active from gastrulation. Their expression sets the anterior-posterior axis for each segment.

This complex chain of events involves tightly regulated transcriptional control and crosstalk between the different segmentation genes (Figure 4.2). However, expression of each of these genes and their subsequent RNA products are temporally distinct. While past work has extensively focused on understanding mechanisms underlying transcriptional regulation of segmentation genes (Scott and Carroll 1987), post-transcriptional and spatio-temporal regulation of embryonic mRNAs is a relatively under explored topic.

Figure 4.2: Overview of gene regulation during early embryogenesis. Schematic highlighting the localisation pattern and role of different genes during early embryogenesis. *Gap*, *pair-rule*, and *segment polarity* genes, collectively known as segmentation genes are induced by maternal effect genes, resulting in the regulation of embryonic pattern formation. Image adapted from S. Carroll and S. Paddock.

In the previous chapter, I described the material properties of P bodies and their role in maternal RNA storage and translational repression in the mature oocyte. In subsequent stages of development, the mature oocyte undergoes egg activation which makes the egg competent for fertilisation. Translational control of maternal RNAs is integral to the oocyte to embryo transition. Previous work from our lab showed

that activation of the mature oocyte causes P body dispersal (York-Andersen et al. 2015). How P body dispersion occurs and what its physiological significance is, remains less clear. Additionally, whether P bodies re-assemble post activation is relatively unexplored. In the early embryo, recent biochemical studies of conserved P body proteins such as Me31B and Trailer hitch showed that the ability of these complexes to efficiently repress translation of mRNA transcripts is reduced dramatically while their roles in facilitating RNA degradation are increased (Wang et al. 2017). This suggests that P bodies likely switch their roles from translational regulation to degradation post egg activation. However, at a cellular level, P body material properties in the embryo and whether they associate with embryonic mRNAs remains to be explored. Furthermore, the possibility of P bodies modifying their material properties post egg activation to facilitate diverse functions specific to the early embryo is an exciting model to test.

4.2 Chapter objectives

In this chapter, I have studied the properties and potential function of Me31B granules post egg activation. The specific questions addressed are:

1. What happens to Me31B granules during and post egg activation?
2. Do Me31B granules in the early embryo display similar or different material properties compared to the mature oocyte?
3. Do P bodies regulate embryonic mRNAs?

4.2.1 Author contributions

Experimental strategy, design and execution and image analyses in this chapter were performed by me except for the following contributions from:

1. Christo.P. Christov: performed the sucrose gradient assay (Figure 4.14).
2. Liza Sarde: assisted with colocalization analysis (Figures 4.21, 4.22 and 4.23).
3. Mathew Peacy: performed the SDD-AGE assay (Figure 4.15)
4. Dr. Matt Wayland: generated graphical plots using ‘R’ software. Assisted with data analyses.

4.3 *In vivo* activated oocytes display a diffuse distribution of Me31B granules.

The mature oocyte at the end of oogenesis, ready to be activated and fertilised is usually in a dehydrated state, presumably due to its relatively small size and large surface area to volume ratio. As it passes through the oviduct, the oocyte gets hydrated and activated (Figure 4.3A), thereby triggering downstream signalling cascades.

To test if *in vivo* egg activation affects Me31B granules, activated eggs expressing Me31B::GFP were dissected from the oviduct of a female fly and observed under the microscope. Dissected oocytes were swollen/hydrated, confirming that they were activated. Interestingly, Me31B granules displayed a diffuse distribution throughout the egg (Figure 4.3B). This suggests that the molecular changes that occur at egg activation prevent condensation of Me31B granules.

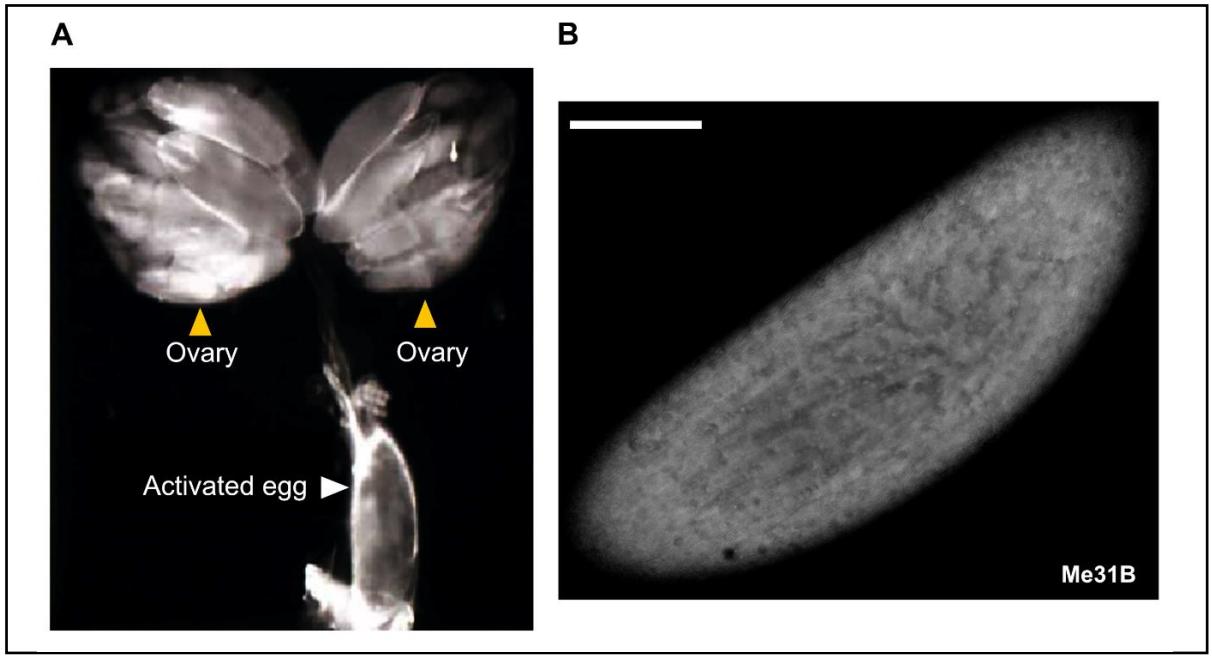

Figure 4.3: Me31B granules exist in a diffuse state in activated eggs. (A) A *Drosophila* female reproductive tract consisting of two ovaries (yellow arrowheads) with different staged egg chambers; an activated egg in the common oviduct is highlighted by a white arrowhead. Image adapted from: (Heifetz, Yu, and Wolfner 2001). **(B)** A hydrated and activated egg expressing Me31B::GFP dissected from the common oviduct shows a diffuse distribution of Me31B; scale bar: 50 µm.

Conclusion: Me31B granules exist in a diffuse, cytoplasmic phase in activated eggs.

4.4 *Ex vivo* activation of mature oocytes causes Me31B granule dispersion

Since the *Drosophila* abdomen and the tissues surrounding egg chambers impede visualisation of events preceding and during activation *in vivo*, an artificial *in vitro* system to trigger egg activation of dissected oocytes (*ex vivo*) was developed by Anthony Mahowald (Mahowald, Goralski, and Caulton 1983). By placing dissected oocytes in 'activation buffer', a solution that is hypotonic to the oocyte and contains the appropriate ionic makeup, e*x vivo* activation causes the oocyte to swell upon intake of the fluid, mimicking the hydration that occurs in the oviduct. These *ex vivo* activated eggs also display signs of normal cellular processes post activation including, progression through meiosis, large-scale translation of stored mRNAs, and changes in cytoskeletal dynamics.

Previous work from the lab had shown that upon *ex vivo* egg activation, Me31B granules underwent dispersion (Weil et al. 2012; York-Andersen et al. 2015). However, this dispersion was not imaged and recorded in high resolution. To confirm this observation, mature oocytes expressing Me31B::GFP were dissected into oil and activation buffer was added. Upon activation, Me31B granules underwent rapid dispersion (Figure 4.4). The observed dispersion was significantly faster than previously recorded (~20 minutes). Moreover, distribution of Me31B in *ex vivo* activated eggs mirrored the *in vivo* diffuse state of Me31B, suggesting that *ex vivo* pharmacological treatments on mature oocytes can be used reliably to understand Me31B granule properties at activation.

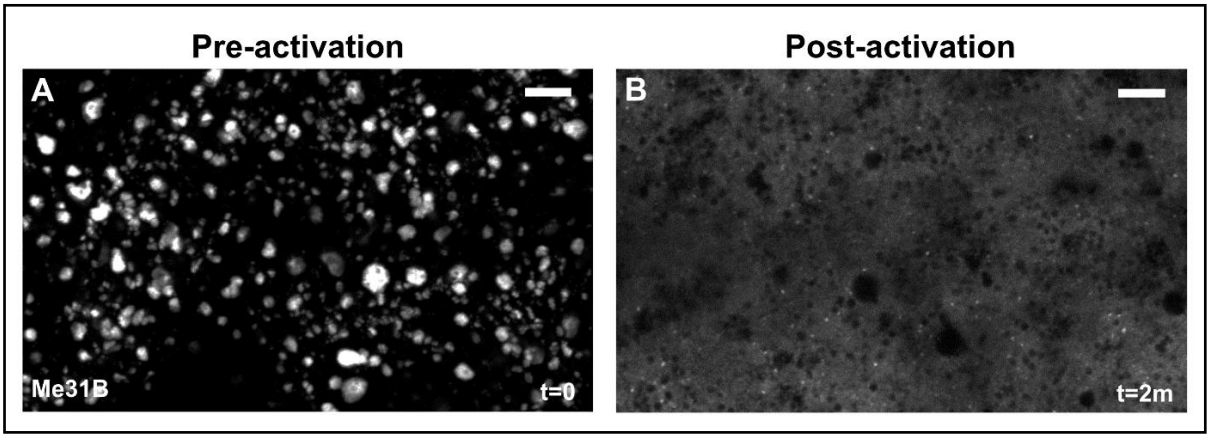

Figure 4.4: Me31B granules disperse upon *ex vivo* activation of the mature oocyte. (A-B) Mature oocytes expressing Me31B::GFP. **(A)** Me31B granules exhibit a granular distribution in the mature oocyte. **(B)** Addition of activation buffer causes Me31B granule dissociation, leading to a diffuse distribution of Me31B. Scale bar: 10 µm.

A classic hallmark of egg activation is the presence of a calcium wave that passes through the mature oocyte (Kaneuchi et al. 2015; Krauchunas and Wolfner 2013; York-Andersen et al. 2015). It was proposed that granule dispersion could be a downstream event of the calcium wave. From my results, Me31B granule dispersion was observed uniformly across the oocyte and almost immediately upon activation suggesting that it is unlikely to be a consequence of the calcium wave, which occurs over a time course of 20 minutes from the posterior to anterior pole from the time of activation.

Conclusion: *Ex-vivo* activation of mature oocytes causes rapid dispersion of Me31B granules, resulting in a soluble phase of Me31B similar to *in vivo* activated eggs.

4.5 Factors causing Me31B granule dispersion at egg activation

A key feature of egg activation is swelling, which is thought to induce mechanical changes to the egg. A consequence of such mechanical changes results in large scale cytoplasmic modifications. Below, I describe potential factors that facilitate Me31B granule dispersal at egg activation:

4.5.1 Swelling

As the mature egg passes through the oviduct, fluid uptake by osmosis is thought to cause swelling of the egg. This hypo-osmotic swelling has been proposed to be sufficient to initiate the calcium wave, an essential process for egg development post activation. Since Me31B granules are distributed uniformly across the oocyte and the larger granules appear selectively anchored at the surface, any changes to the oocyte volume is likely to have an effect on Me31B granule integrity.

To test if swelling is sufficient for Me31B granule dispersion, mature oocytes were incubated in Phosphate-buffered saline (PBS) solution for 30 minutes. PBS has been used as a control solution to incubate drugs used for pharmacological treatments on mature oocytes. Incubation in PBS did not result in the swelling of the oocytes. More importantly, Me31B granules retained their granularity and remained unaffected by incubation in PBS (Figure 4.5A). However, incubation of mature oocytes in the activation buffer resulted in swelling of the egg, and Me31B distribution was largely diffuse (Figure 4.5B). These results strongly suggest that swelling of the egg is sufficient to initiate Me31B granule dispersal at egg activation.

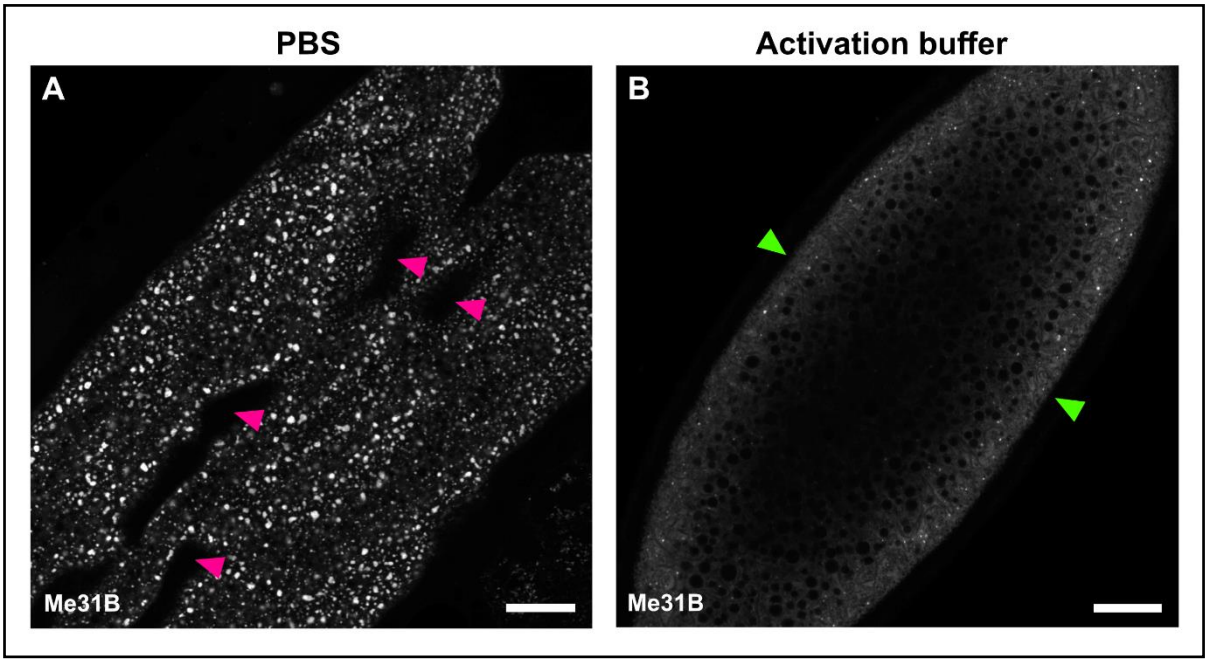

Figure 4.5: Swelling is sufficient to cause Me31B granule dispersion. (A,B) Mature oocytes expressing Me31B::GFP. **(A)** Mature oocyte displaying punctate distribution of Me31B granules post incubation in PBS for 30 minutes. Wrinkles observed indicate dehydrated state of the oocyte (magenta arrow heads). **(B)** Mature oocyte displaying diffuse distribution of Me31B post incubation in activation buffer in 30 minutes. Oocytes display uniformly rounded surface area, indicating hydrated state (green arrow heads). Scale bar: 30 µm (A,B).

4.5.2 Ionic concentration

At activation, swelling of the egg is thought to open mechano-sensitive ion channels on the oocyte membrane, which leads to changes in the ionic concentrations of the oocyte cytoplasm (Hu and Wolfner 2019; Sartain and Wolfner 2013). For instance, increases in the influx of divalent salts such as calcium chloride ($CaCl_2$) and magnesium chloride ($MgCl_2$) as well as monovalent salts as sodium chloride (NaCl) and potassium chloride (KCl) are thought to contribute to changes in ionic levels at egg activation. Since oocyte P bodies are held together by weak inter-molecular interactions such as electrostatic forces, changes in ionic concentrations in the cytoplasm are likely to have an effect on Me31B granule integrity and material properties.

To test the effect of salt on Me31B granules, I utilised the extrusion assay since treating mature oocytes with salt solutions caused swelling of the egg (data not shown) and therefore would render it impossible to distinguish the effect of salt from swelling. Extrusion assay allowed the release of contents of the oocyte cytoplasm into oil, following which different salt solutions were added.

To examine if divalent ions affected Me31B granule integrity, different concentrations of $MgCl_2$ were added to the extruded sample. While lower concentrations of $MgCl_2$ did not appear to affect granule integrity (Figure 4.6A), concentrations upwards of 50mM $MgCl_2$ resulted in the breakdown of Me31B granules (Figure 4.6B,C). These results show that influx of divalent ions at activation likely contribute to Me31B granule dispersion.

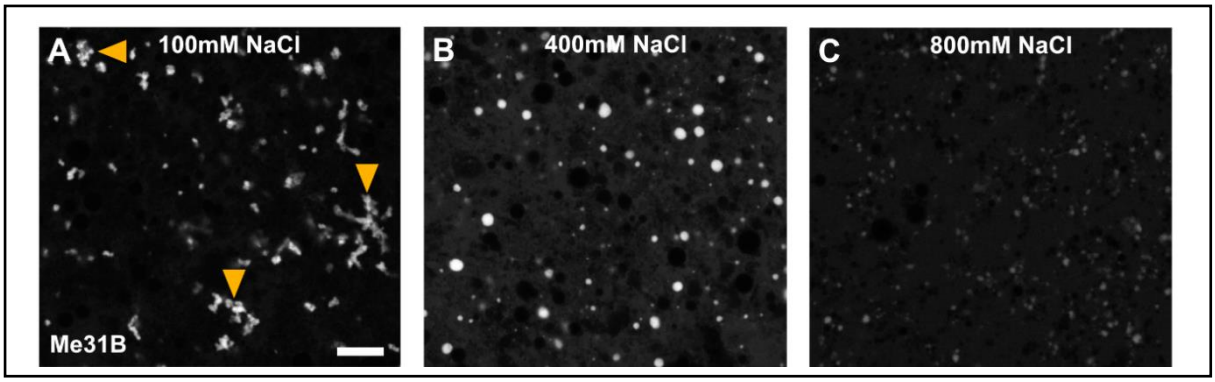

Figure 4.6: Addition of NaCl causes differential effects on extruded Me31B granules. **(A-C)** Representative images of extruded Me31B::GFP granules at different concentrations of NaCl. **(A)** Addition of 100mM NaCl causes granules to aggregate (yellow arrow heads), while 400mM NaCl results in the formation of highly spherical granules **(B)**. **(C)** Higher concentrations of NaCl (800mM) causes dissolution of extruded granules. Scale bar: 10 µm.

To test if monovalent ions also had a similar effect to divalent ions, different concentrations of NaCl were added to the extruded sample. Lower concentrations of NaCl (100mM) resulted in granules sticking to each other, forming a network of aggregates (Figure 4.7A). However, at 400mM NaCl concentration, a dramatic phase transition was observed, whereby Me31B granules began to fuse and drip like liquid droplets (data not shown), in addition to adopting fully spherical morphologies (Figure 4.7B). This liquid-like property was observed up until 600mM NaCl concentrations, beyond which the granules began to dissolve (Figure 4.7C). These results show that although higher concentrations of monovalent ions (800mM) are required to

completely dissolve Me31B granules compared to divalent ions, at certain concentrations (100mM-300mM and 400mM-600mM), monovalent ions can efficiently modulate Me31B phase behaviour between sticky and liquid-like states.

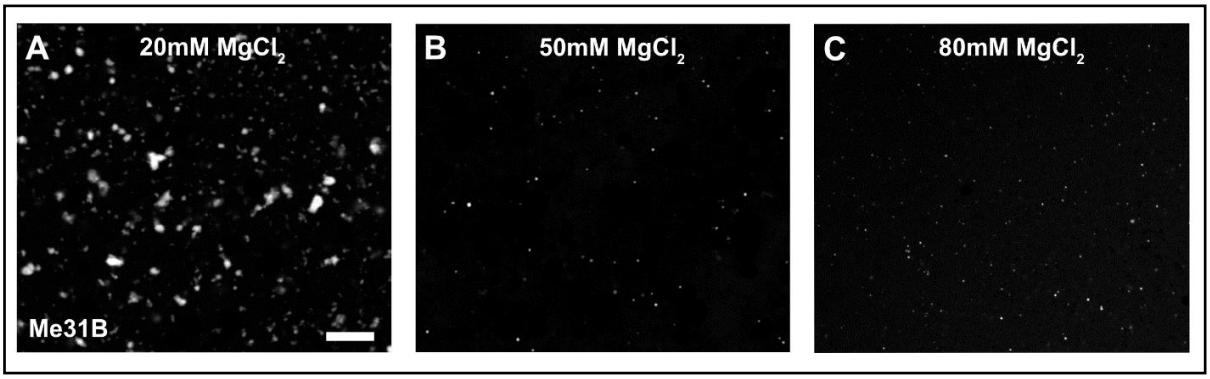

Figure 4.7: Addition of $MgCl_2$ causes breakdown of extruded Me31B granules. (A-C) Representative images of extruded Me31B::GFP granules at different concentrations of $MgCl_2$. While extruded Me31B granules appear particulate at 20mM $MgCl_2$ **(A)**, they break down into smaller particles at concentrations greater than 50mM **(B,C)**. Scale bar: 10 µm.

4.5.3 Cytoskeletal rearrangement

Previous studies have shown that swelling causes large-scale cytoplasmic changes, which includes cytoskeletal rearrangement. In the previous chapter, using drugs that depolymerise actin (cyto-D) and microtubules (colchicine), my data showed that affecting either of the two results in the dissociation of Me31B granules into smaller particles. Here, I demonstrate that simultaneously depolymerizing both actin and microtubules results in the complete dissolution of Me31B granules (Figure 4.8), indicating a role for the cytoskeleton in maintaining Me31B granule integrity. Therefore, rapid rearrangement of actin and microtubule networks induced by swelling of the egg could combinatorially cause Me31B granule dispersal at activation.

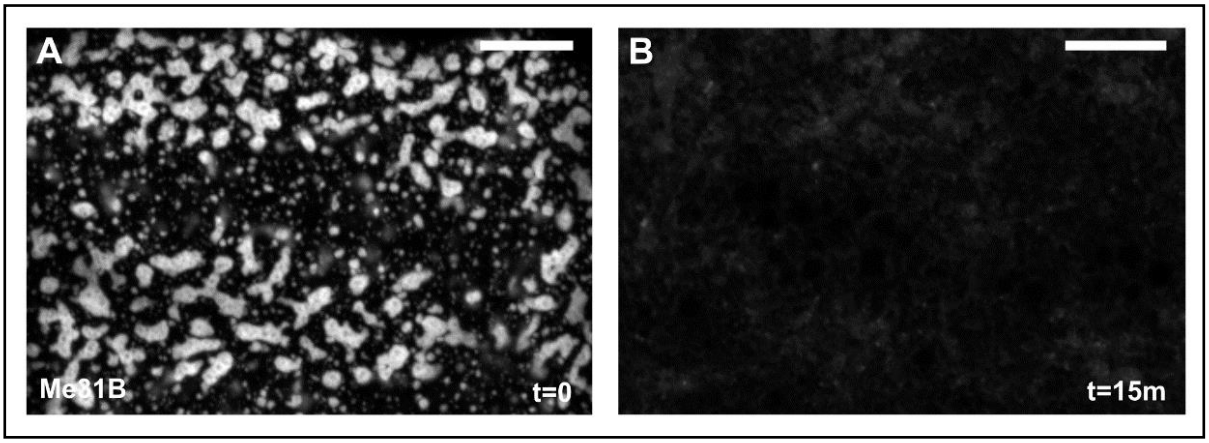

Figure 4.8: Depolymerisation of actin and microtubule causes Me31B granule dispersion in the mature oocyte. (A) Me31B::GFP granules exhibit a granular distribution in the mature oocyte. **(B)** Depolymerisation of actin and microtubule, by the addition of cyto-D and colchicine respectively, causes Me31B granule dissociation, leading to a diffuse distribution of Me31B. Scale bar: 20 µm.

4.5.4 Release of stored mRNAs

bicoid (bcd), a key axis patterning maternal transcript, is associated with Me31B granules in the anterior region of mature oocyte (Figure 4.9A-C). It is generally assumed that P body dispersal triggered at egg activation leads to the release of stored mRNAs, including *bcd* (Weil et al. 2012).

To test this, mature oocytes expressing Me31B::GFP and *bcd*-RFP (Figure 4.9A-C) were treated with an activation buffer. Shortly after activation, the dispersion of Me31B granules coincided with the dissociation of *bcd* particles (Figure 4.9D-F), providing strong evidence to the dispersion model. Alternatively, a likely possibility is that release of stored RNAs such as *bcd* may trigger the dispersion of P bodies.

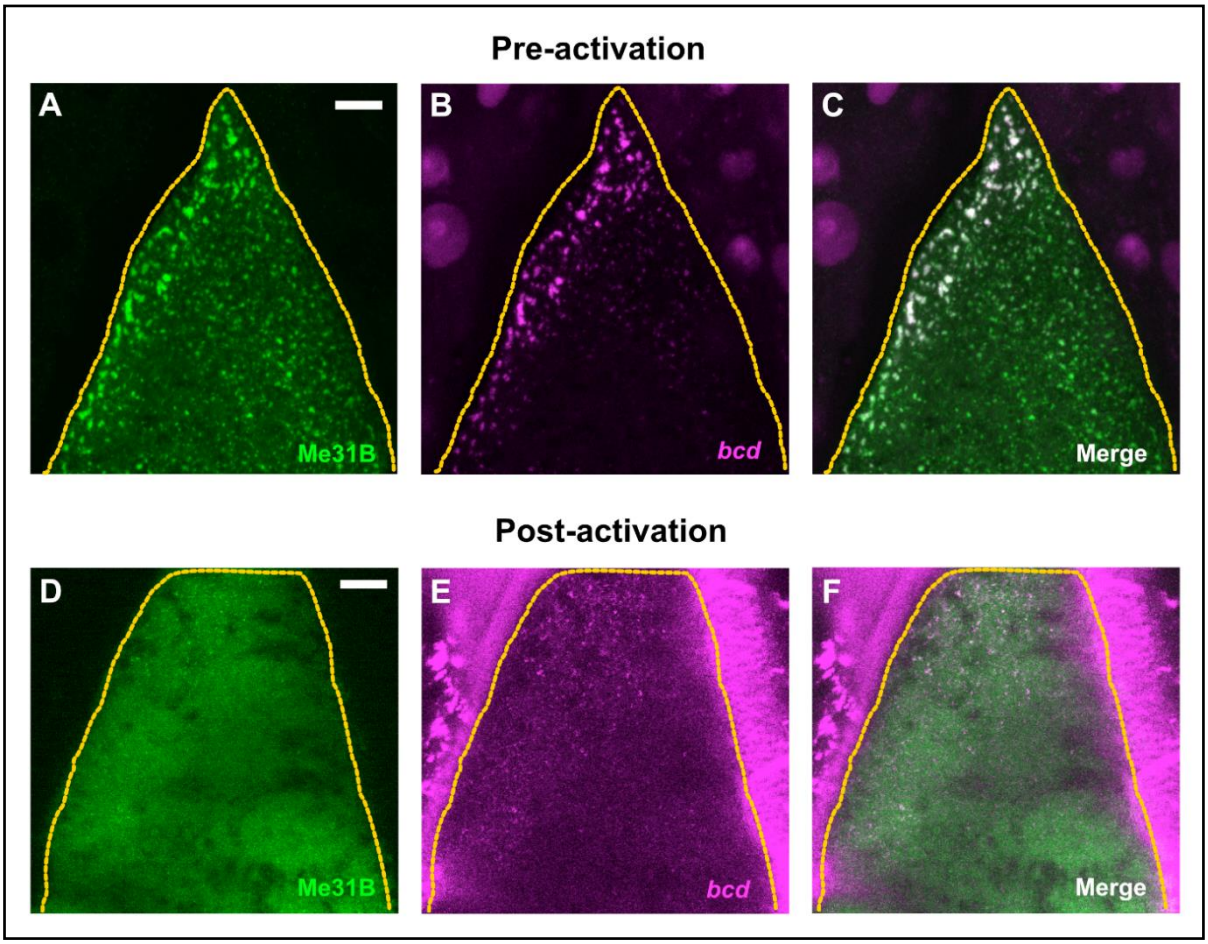

Figure 4.9: Me31B granules and *bcd* rapidly disperse upon *ex vivo* activation of the mature oocyte. (A-F) Mature oocytes expressing Me31B::GFP and *bcd*-RFP. **(A-C)** Me31B granules and *bcd* particles colocalise at the anterior region of the mature oocyte; scale bar: 10 µm. **(D-F)** Addition of activation buffer causes simultaneous dispersion of Me31B granules and *bcd* particles from the anterior region of the mature oocyte; scale bar: 10 µm. Excessive background signal observed in **(E)** and **(F)** panels are from the follicle cells and fat tissues surrounding the oocyte, which display autofluorescence upon activation. Yellow dotted lines outline the mature oocyte.

Furthermore, time lapse imaging of Me31B and *bcd* particles post dissociation revealed an interesting observation. Shortly after activation, the dispersed Me31B and *bcd* particles could still be detected (Figure 4.10A-C). However, over time, Me31B reformed into several smaller sized granules (Figure 4.10D) likely resembling embryonic P bodies, but *bcd* particles remained diffuse (Figure 4.10E). This suggests that Me31B granules that reform post activation may be devoid of RNAs.

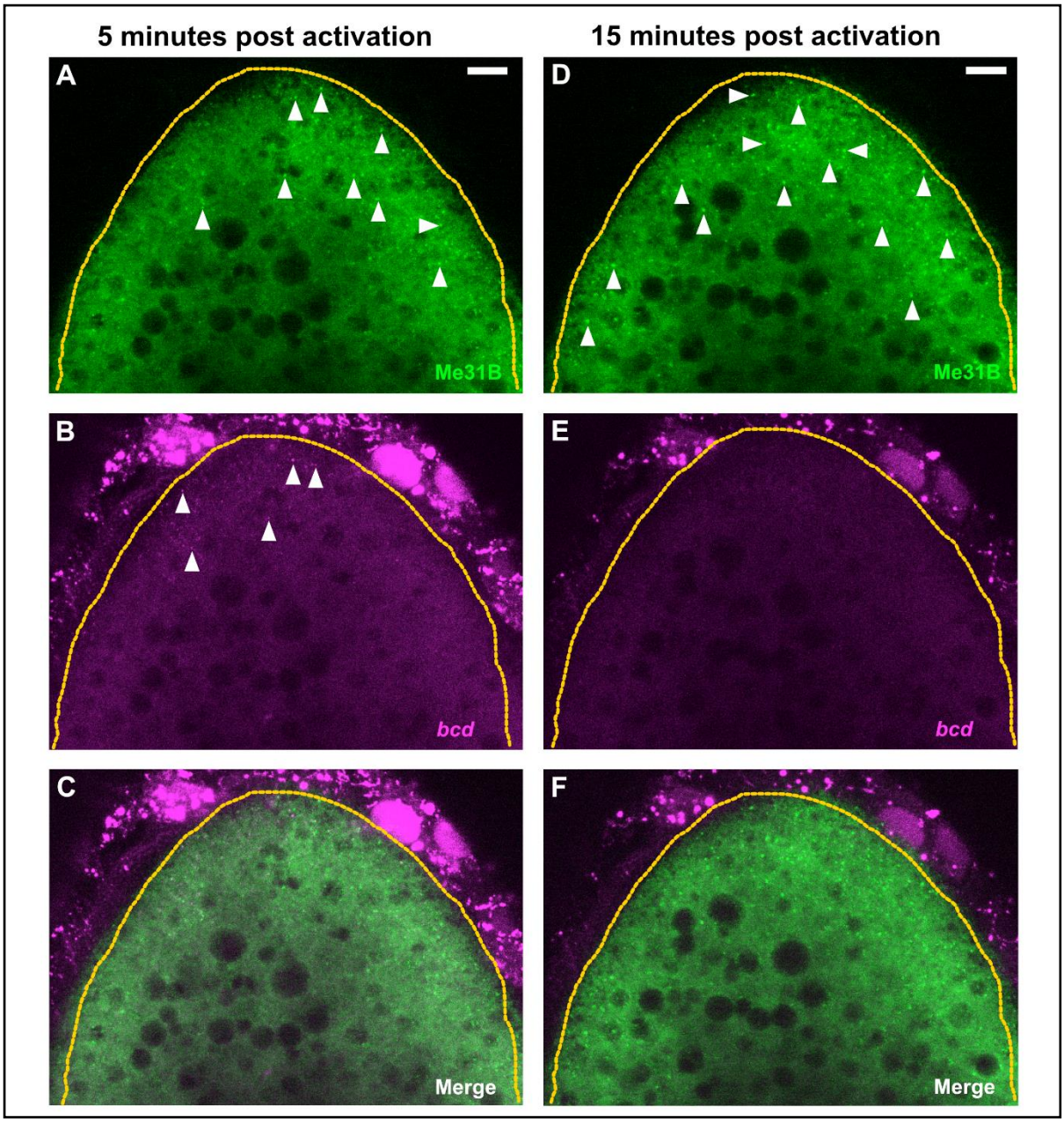

Figure 4.10: Me31B, not *bcd*, re-forms into condensed granules post activation. (A-F) Mature oocytes expressing Me31B::GFP and *bcd*-RFP. **(A-C)** Although Me31B and *bcd* appear mostly dispersed 5 minutes post activation, few numbers of granular Me31B and *bcd* particles can be observed (white arrowheads); Scale bar: 10 µm. **(D-F)** 15 minutes post activation, Me31B reforms into several smaller sized granules (white arrowheads), while *bcd* remains diffuse. Scale bar: 10 µm. Yellow dotted lines outline the mature oocyte.

Conclusion: Taken together, based on the above results, a combination of egg swelling, changes in ionic concentrations, cytoskeletal reorganisation, and release of RNAs cause Me31B granule dispersion at egg activation.

4.6 Me31B exists as smaller sized, spherical condensates in the early embryo

Me31B granules transition from micron-sized granular distribution to a soluble cytoplasmic state at egg activation. The natural follow-up question was whether Me31B granules re-form in the early embryo. There are few studies pertaining to P body proteins in the early embryo suggesting that P bodies could possibly reform post activation (Lin et al. 2008; Patel, Barbee, and Blankenship 2016). Additionally, results from the previous section (Figure 4.10) indicate that Me31B likely form smaller sized granules post activation.

To visualise if Me31B reforms into condensed granules post-activation, I imaged 0-2 hours old embryos (hereafter referred to as 'early embryo') expressing Me31B::GFP. Live imaging revealed that Me31B exists as condensed particles in the early embryo (Figure 4.11A).

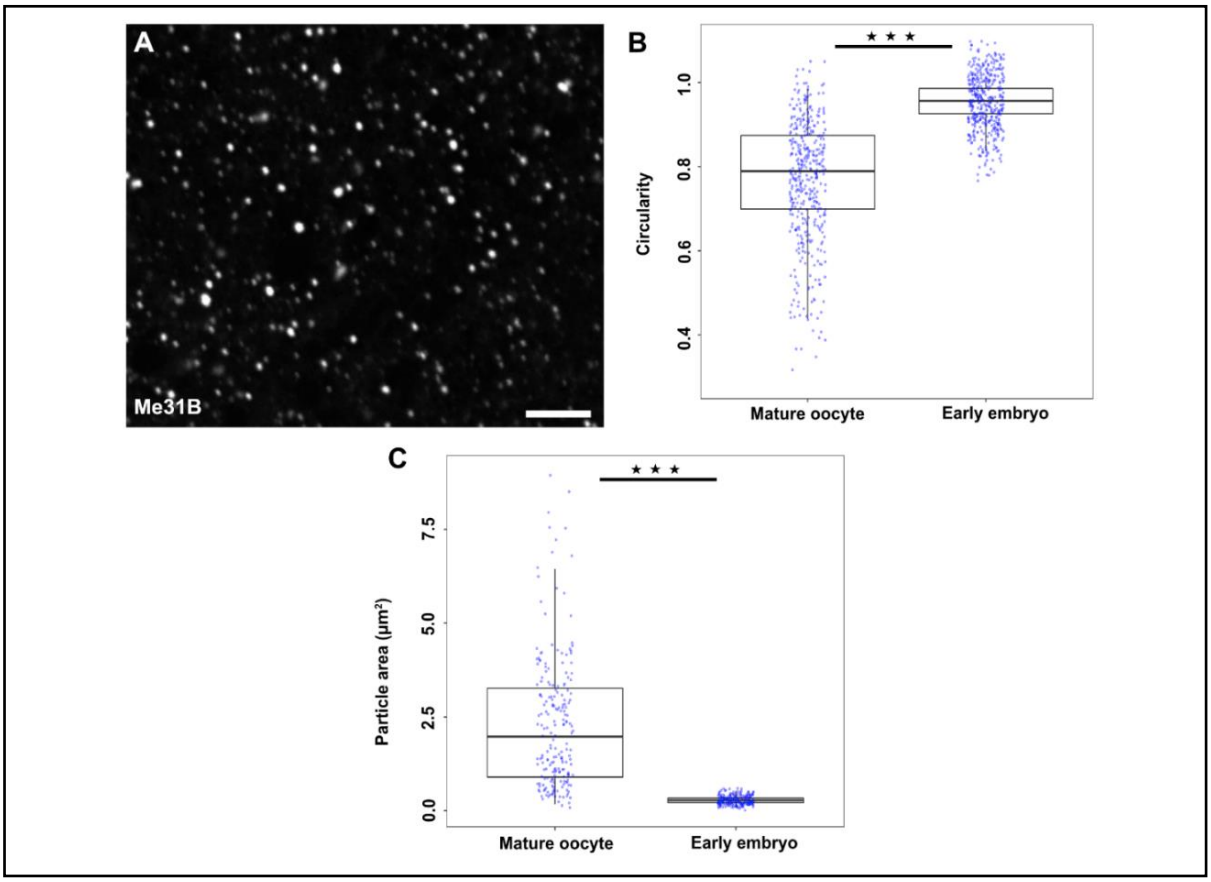

Figure 4.11: Me31B granules in the early embryo are smaller and more spherical than granules in the mature oocyte. (A) Representative image of Me31B::GFP granules in the early embryo; scale bar: 3µm. **(B)** Quantification of Me31B granule morphology between the mature oocyte and early embryo; $p<0.0001$. C) Quantification of Me31B particle area between the mature oocyte and early embryo; $p<0.0001$.

However, these granules appeared significantly smaller in size (Figure 4.11B) and exhibited a highly spherical morphology (Figure 4.11C), compared to granules in the mature oocyte. Due to their highly dynamic nature, it was challenging to record whether embryonic Me31B exhibited liquid-like properties such as fission and fusion. Occasionally, however, I did observe fusion events (data not shown), suggesting that embryonic P bodies possess liquid-like features.

Conclusion: Me31B in the early embryo exists as smaller-sized, morphologically spherical, and highly dynamic cytoplasmic granules.

4.7 Me31B granules display moderate exchange kinetics between the granule and cytoplasm

Since Me31B granules in the early embryo displayed properties converging towards a liquid-like state, I next checked if they exchanged components with the cytoplasm. If the granules are liquid-like, there would be a higher flux of Me31B molecules between the granule and the cytoplasmic pool. To test this, I performed whole particle FRAP on Me31B granules in the early embryo. Whole particle FRAP showed that Me31B molecules were mobile and exchanged between the cytoplasm and the granule (Figure 4.12A). Quantification also revealed that, post photobleaching, Me31B molecules recovered up to ~35% and showed relatively slow exchange kinetics ($t_{1/2}$ = 161.2s). However, a significant fraction (~47%) of Me31B molecules were mobile (Figure 4.12B), indicating that while Me31B in the early embryo is not highly liquid-like, they are significantly more mobile and dynamic than Me31B granules prior to activation.

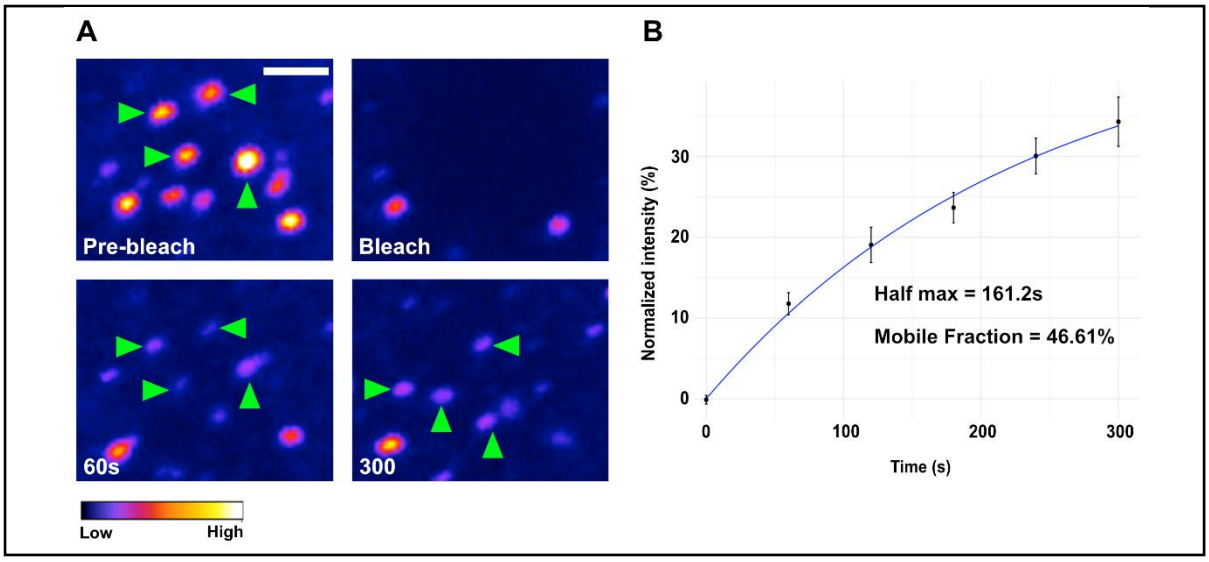

Figure 4.12: Me31B granules exhibit slow exchange kinetics with the cytoplasm. (A) Time lapse images of Me31B::GFP granules before and after photobleaching (green arrowheads); scale bar: 3 µm. **(B)** Analysis of the whole particle FRAP of Me31B::GFP granules. Standard deviation/data (black), fit (blue), n=13 Me31B granules, N=4 embryos. Single exponential fits the FRAP curve.

Conclusion: Slow exchange kinetics and a high proportion of mobile Me31B molecules indicate that Me31B granules in the early embryo regulate exchange of components in a controlled manner.

4.8 Me31B shows differential biochemical properties between the mature oocyte and early embryo

Results in previous sections have demonstrated that Me31B granules in the mature oocyte and early embryo have distinct material properties. P bodies are ribonucleoprotein (RNP) complexes containing different sized protein-RNA macromolecules. Therefore, to test if Me31B associated complexes were biochemically different between the mature oocyte and early embryo, firstly, western blot analysis of lysates obtained from mature oocytes and early embryos expressing Me31B::GFP were performed to test the relative levels of Me31B protein. Lysates from both samples displayed similar amounts of the protein, indicating that Me31B protein levels do not vary significantly before and after egg activation (Figure 4.13). Since standard loading controls, including actin and GAPDH, were not reliable and reproducible, ponceau staining of gels post SDS-PAGE was performed to confirm protein amounts from the two samples (Figure 4.13C,D).

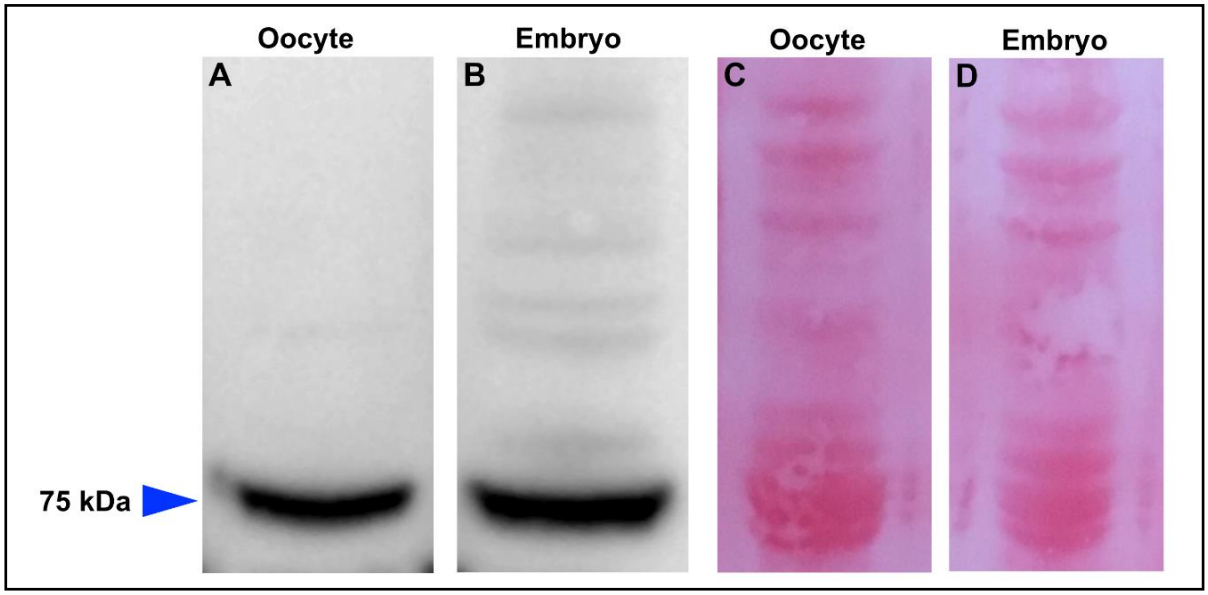

Figure 4.13: Me31B protein levels remain similar between the mature oocyte and early embryo. (A,B) Lysates from mature oocytes and 0-3-hour old embryos expressing Me31B::GFP were subjected to SDS-PAGE. Me31B::GFP (75 kDa) was detected by western blot against GFP. (B,D) Ponceau staining of lysates from mature oocytes and 0-3-hour old embryos after SDS-PAGE used as a proxy for loading controls.

To further investigate the density of Me31B complexes, lysates from both stages were subjected through a continuous sucrose gradient followed by western blotting analysis. While monomeric and low molecular weight complexes would pass through the dense sucrose fractions due to their smaller size and mass, high molecular weight complexes will be enriched in the initial sucrose fractions. Remarkably, Me31B from the mature oocyte sedimented through the sucrose gradient as low and high molecular weight entities (Figure 4.14A), whereas the embryonic Me31B was restricted predominantly to high molecular weight fractions (Figure 4.14B). Results from the embryonic lysates are interesting since Me31B in the embryo, due to their smaller sizes, were expected to be mostly in low molecular weight complexes. However, this indicates there is no obvious correlation between granule size and density of protein complexes within the granules.

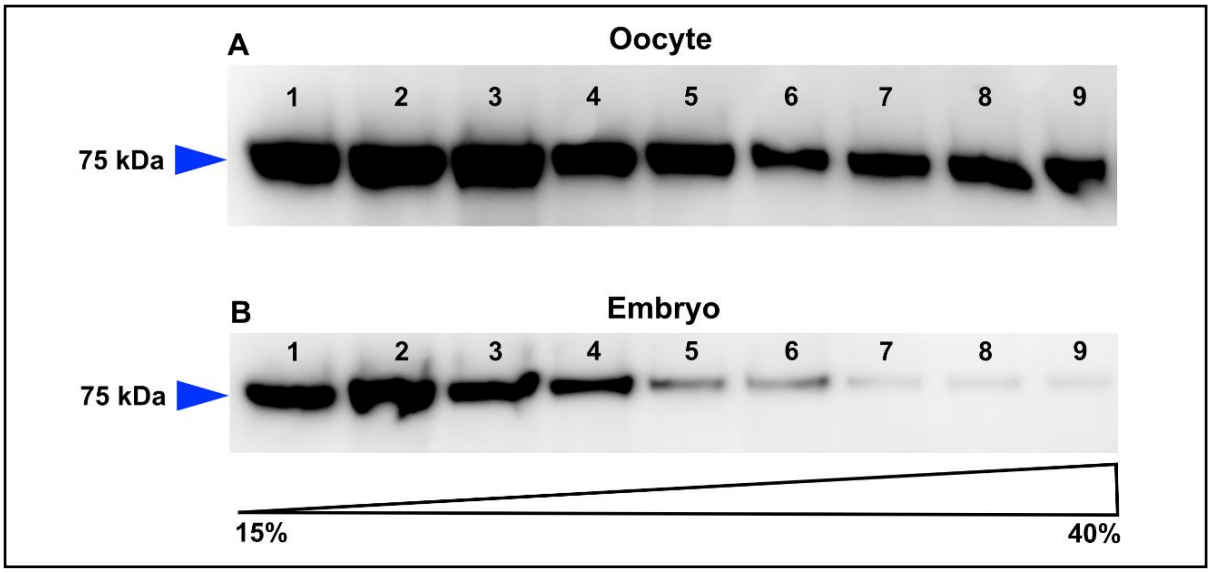

Figure 4.14: Me31B is present in distinct molecular weight complexes in the mature oocyte and early embryo. Lysates obtained from mature oocytes **(A)** and 0-3-hour old embryos **(B)** expressing Me31B::GFP were subjected to a 15-40% continuous sucrose gradient. Me31B::GFP in different lanes was detected by western blot against GFP.

Conclusions: Me31B protein levels do not vary significantly between the mature oocyte and early embryo. However, Me31B in the early embryo is present largely in high molecular weight complexes while Me31B in the mature oocyte exists both in low and high molecular weight complexes.

4.9 Me31B complexes are not held by amyloid-like interactions

High-molecular weight fractions of oocyte and embryonic Me31B detected by sucrose gradient prompted the question about the nature of interactions holding the complex together. Although *in vivo* analysis of Me31B in the mature oocyte and early embryo was reflective of a gel-like and semi-liquid state respectively, the possibility of higher order amyloid-like interactions maintaining the integrity of the larger Me31B complexes cannot be ignored. To test if Me31B complexes in the mature oocyte and early embryo are amyloid-like, semi-denaturing detergent agarose gel electrophoresis (SDD-AGE) was utilised, a method that allows the separation of high molecular weight SDS-resistant polymers which are held together by stable amyloid-like interactions (Alberti 2009; Boke et al. 2016; Halfmann and Lindquist 2008). The yeast prion protein Rnq-1, for example, which forms high molecular weight aggregates, displays as a smear on the SDD-AGE, which is indicative of amyloid properties (Figure 4.15A). Additionally, proteins with amyloid features are naturally resistant to detergents such as sodium

dodecyl sulphate (SDS). Therefore, Me31B lysates from mature oocytes separated by SDD-AGE were subjected to varying concentrations of SDS. Even at low SDS concentrations (0.2%), no high molecular-weight complexes or smears of Me31B were detected (Figure 4.15B).

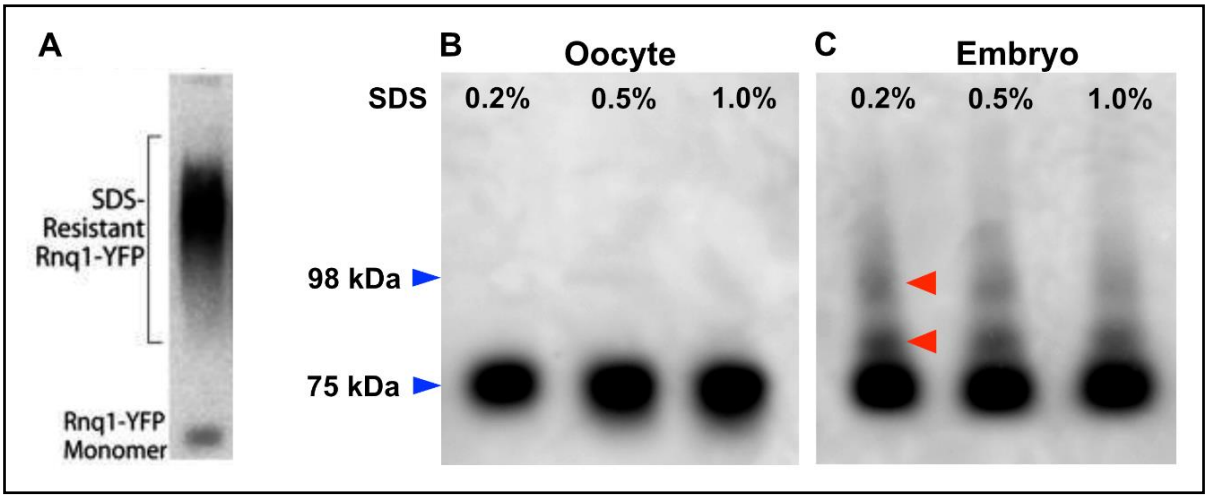

Figure 4.15: Me31B complexes are non-resistant to SDS treatment. (A) SDD-AGE analysis of the yeast prion protein Rnq-1. Presence of SDS-resistant smear indicates amyloid-like property; image adapted from: (Douglas et al. 2008). **(B,C)** Lysates from mature oocytes or 0-3-hour old embryos expressing Me31B::GFP were subjected to SDD-AGE, using sample buffers of varying SDS concentration. Me31B::GFP (75 kDa) was detected by western blot against GFP. **(C)** Multiple high molecular weight bands were detected in lysate samples from the embryo (red arrowheads).

This suggests that, in contrast to static pathological amyloid aggregates or physiological amyloid-like compartments (such as the Balbiani body), high-molecular weight complexes associated with oocyte Me31B are sensitive to SDS treatment and therefore, are less stable than amyloids. This is consistent with their ability to change properties after egg activation and their proposed gel-like state.

Lysates from early embryos separated by SDD-AGE revealed an interesting observation. In addition to the monomeric protein at 75kDa, they also displayed supplemental high molecular weight bands (Figure 4.15C). These are unlikely to correspond to SDS-resistant polymers, since they are present relatively closer to the monomeric protein and display as discrete bands rather than ‘smears’, which are typical of amyloid assemblies. Instead, these additional bands may represent

phosphorylated forms of Me31B that migrate at a higher molecular weight on account of their additional negative charge.

Conclusions: Me31B present in high molecular weight complexes in mature oocytes is less stable than amyloid-like polymers. Additionally, Me31B in the early embryos represent post-translationally modified P bodies.

4.10 Me31B is phosphorylated in the early embryo but not in the mature oocyte

Condensation of RNP granules such as P bodies is highly dependent on weak promiscuous interactions among proteins or/and RNAs, thereby creating a dense multivalent network of macromolecules. Post translational modifications (PTMs) of RNA binding proteins (RBP) such as phosphorylation, acetylation and methylation have emerged as important regulators of condensate properties. These modifications can directly weaken or enhance the strength of multivalent interactions and influence their composition, material states and dynamics (Hofweber and Dormann 2019; Owen and Shewmaker 2019; Snead and Gladfelter 2019; Söding et al. 2020).

Among the well-studied PTMs, phosphorylation has been shown to both positively and negatively regulate condensate formation and function. In fact, during *Drosophila* egg activation, several proteins have been shown to undergo massive phosphorylation events (Krauchunas and Wolfner 2013). A key molecule involved in regulating phosphorylation at egg activation is Pan-Gu, a serine/threonine kinase. In a recent study, the Pan-Gu complex was shown to phosphorylate two P body proteins *in vitro*, one of them being Me31B (Hara et al. 2018; Hara, Petrova, and Orr-Weaver 2017). Therefore, it is plausible that phosphorylation of Me31B may help regulate granule dynamics and properties post activation.

To test if Me31B is phosphorylated *in vivo*, mature oocytes and early embryos expressing Me31B::GFP were lysed in the presence of phosphatase inhibitors to prevent degradation by phosphatase enzymes. Post lysis, samples were run on an SDS-PAGE under denaturing conditions and western blot analysis was performed. Interestingly, multiple additional bands were detected in lysates from the embryo (Figure 4.16A,C) but none in the oocyte (Figure 4.16B,D). These are unlikely to result

from non-specific antibody binding since they could be detected with both anti-GFP and anti-Me31B antibodies.

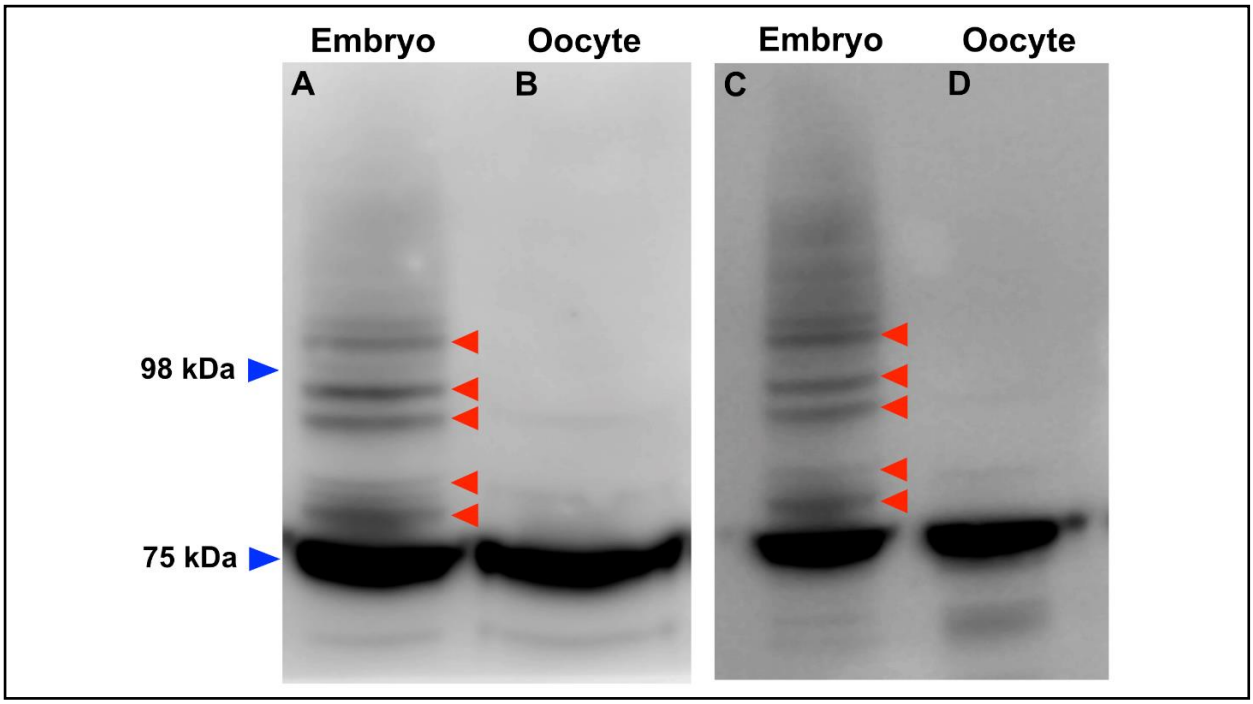

Figure 4.16: Me31B exhibits multiple high molecular weight bands in the early embryo but not in the mature oocyte. Lysates from mature oocytes **(B,D)** and 0-3-hour old embryos **(A,C)** expressing Me31B::GFP were subjected to SDS-PAGE. Me31B::GFP (75 kDa) was detected by western blot against GFP **(A,B)** or Me31B **(C,D)**. Multiple high molecular weight bands were detected in lysates from the early embryo (red arrowheads), but not in the oocyte.

To confirm if the multiple bands observed were a result of phosphorylation, lysates from early embryos and mature oocytes treated with or without phosphatase inhibitors were subjected to western blot analysis. Indeed, samples without a phosphatase inhibitor in the lysate did not display the observed high molecular weight bands (Figure 4.17). The presence of multiple bands, therefore, suggest that Me31B is present in multiple phosphorylated forms the early embryo.

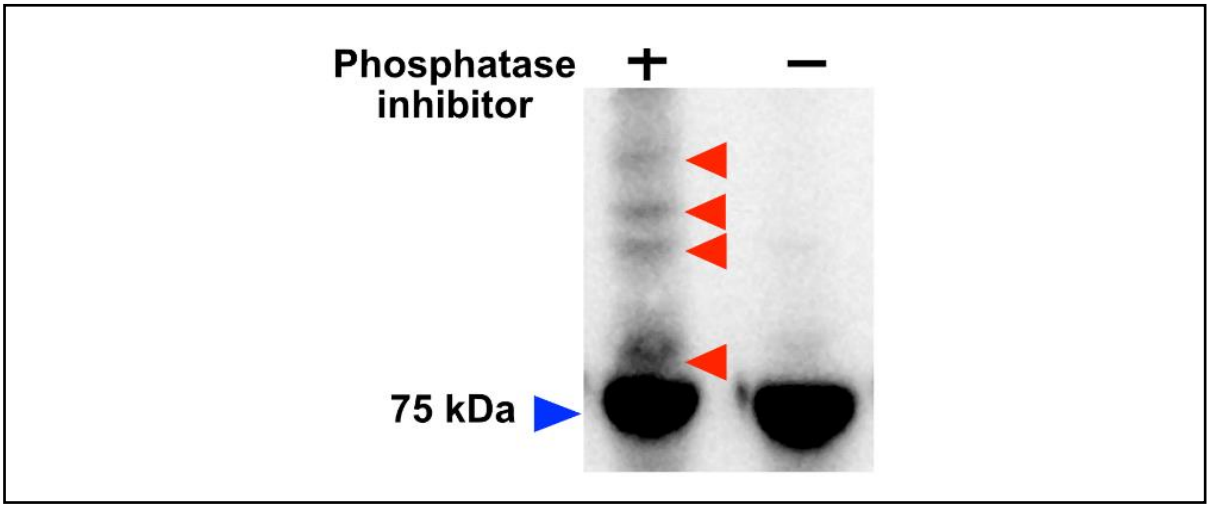

Figure 4.17: Me31B in the early embryo displays multiple phosphorylated bands. Lysates from 0-3hr old embryos expressing Me31B::GFP were subjected to SDS PAGE, using sample buffers with or without phosphatase inhibitors. Samples treated with inhibitors displayed multiple high molecular weight bands (red arrowheads). Me31B::GFP (75 kDa) was detected by western blot against GFP.

Conclusion: Me31B is highly phosphorylated in the early embryo but not in the mature oocyte.

4.11 The role of P bodies in the early embryo

Through live imaging and biochemistry, my results have demonstrated that post egg activation, Me31B labelled P bodies reform into punctate cytoplasmic granules, albeit with modified properties from the mature oocyte. However, the overriding question is the role of P bodies in the early embryo; are they associated with the storage, translational regulation, or degradation of embryonic mRNAs? As a first step towards addressing this question, I have documented the localisation pattern of Me31B granules in the early embryo and attempted to provide evidence of their association with key pair-rule mRNAs, *hairy* and *fushi tarazu (ftz).*

4.11.1 Me31B granules are enriched on the apical region of the cellularised embryo

The early embryo is a syncytium consisting of ~6000 nuclei. As the embryo develops, nuclei migrate to the periphery, membranes enclose each nuclei and form cells with apical-basal polarity. This is a cellularised embryo when segmentation of the embryo occurs.

Live imaging of embryos expressing Me31B::GFP showed that in early cycle 14 embryos, granules are distributed throughout the embryo, with a higher proportion on the basal region (Figure 4.18A). However, at cellularisation (late cycle 14), Me31B granules are more enriched in the apical region of the embryo, while also present in low proportion on the basal side (Figure 4.18B,C). These results demonstrate the changes in Me31B granule localisation during early embryogenesis.

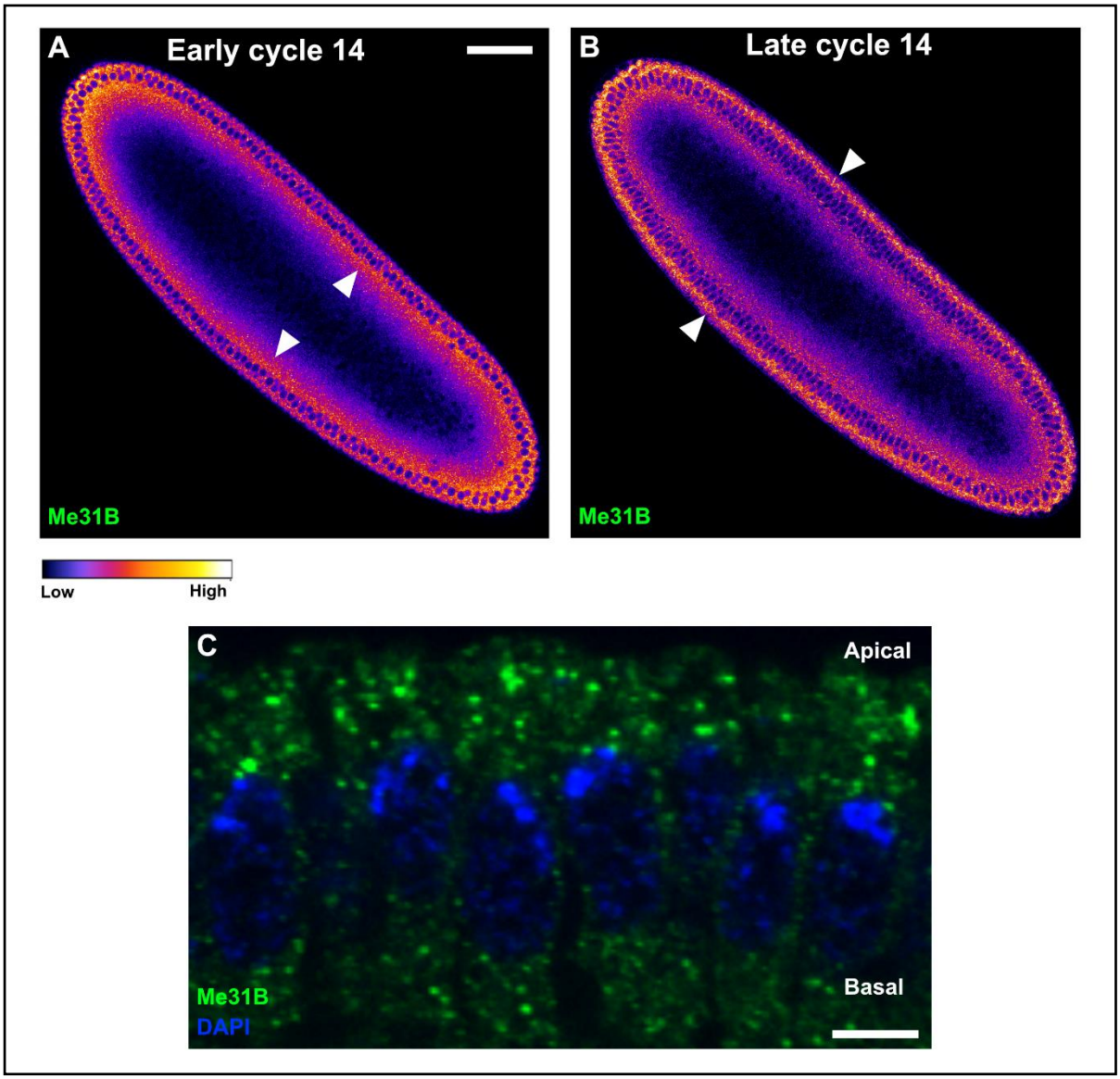

Figure 4.18: Me31B granules are apically enriched at cellularisation. (A-C) Embryos expressing Me31B::GFP. **(A)** Heat map of Me31B granules in early cycle 14 embryos displaying a more basally enriched distribution (white arrowheads). **(B)** Heat map of Me31B granules in late cycle 14 embryos displaying a more apically enriched distribution (white arrowheads). Scale bar: 50 µm (A,B). **(C)** High magnification image of cellularised embryos stained for Me31B (green) and nucleus (DAPI; blue) displaying apical enrichment of Me31B granules. Scale bar: 10 µm.

To determine whether apically enriched Me31B granules are representative of P bodies, fixed embryos expressing Me31B::GFP were stained for Me31B and a second P body protein, Pat1. Me31B and Pat1 colocalised both apically and basally, confirming that Me31B granules present in the early embryo were indeed P bodies.

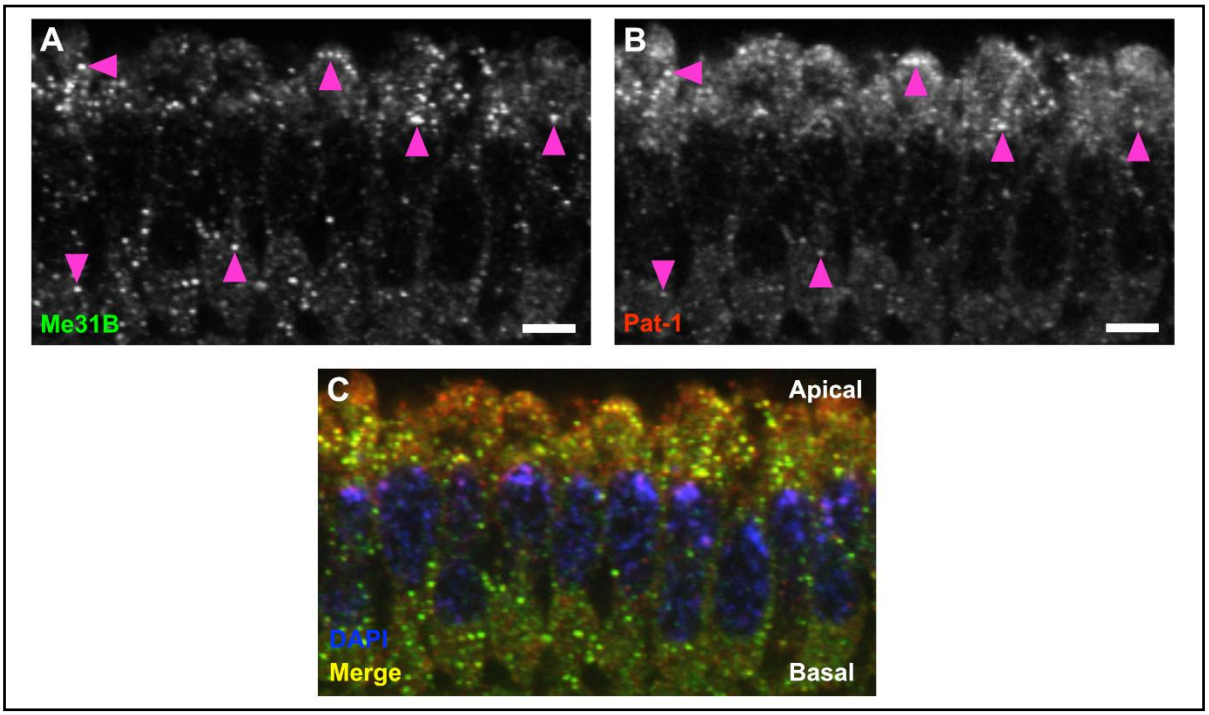

Figure 4.19: Me31B granules apically enriched at cellularisation are representative of P bodies. (A-C) Embryos expressing Me31B::GFP. **(A, B)** Cellularised embryos stained for Me31B **(A)** and Pat-1 **(B)**. Scale bar: 10 µm (A,B). **(C)** Merge shows colocalisation of Me31B and Pat-1 granules; DNA is stained by DAPI (blue). Magenta arrow heads in **(A,B)** highlight representative Me31B and Pat-1 granule colocalisation.

Conclusion: Me31B granules exhibit differential localisation pattern during early embryogenesis, changing from uniform distribution in the blastoderm stage to apical enrichment at cellularisation. Co-localisation with a second P body protein, Pat-1, confirmed that Me31B granules in the early embryo are representative of P bodies.

4.11.2 *hairy* and *ftz* mRNAs overlap with Me31B granules on the apical region of the cellularised embryo

Of the three segment cascade gene products expressed during early embryogenesis, pair-rule mRNAs specifically localise to the apical region of the cellularised embryo (Bullock and Ish-Horowicz 2001; Bullock, Zicha, and Ish-Horowicz 2003; Gagnon and Mowry 2011; Johnston and Nüsslein-Volhard 1992; Lall et al. 1999; Wilkie and Davis

2001). There are seven established pair-genes: *fushi tarazu*, *hairy*, *runt*, *even-skipped*, *odd-skipped*, *paired* and *sloppy-paired*, all expressed in evenly spaced transverse stripes encircling the cellular blastoderm (Clark 2017). Several pair-rule mRNAs, including *hairy*, *ftz* and *runt*, are thought to have a very brief half-life of ~6.5 minutes, which is significantly shorter than other cytoplasmic mRNAs present during this period (Edgar et al. 1986; Edgar, Odell, and Schubiger 1989). This suggests that these mRNAs may be specifically targeted for rapid translation and degradation in a spatio-temporal manner. Since P bodies are also apically enriched during cellularisation, I hypothesised that pair-rule mRNAs could be associated with and, thereby, regulated by P bodies.

To overcome the challenges posed by traditional whole mount fluorescent *in situ* hybridisation such as lack of sensitivity, specificity, larger size of detected RNA due to lack of control over amplification and high background noise, I utilised used the *in situ* hybrid chain reaction (HCR) assay to follow pair-rule mRNAs. This method employs multiple small length probes which bind to the RNA of interest. The fluorescent hairpins binding to the probe amplifies only up to a certain point beyond which steric hindrance of the hairpin loops prevents excess amplification. This way the *in situ* HCR provides increased specificity, sensitivity, and signal to noise ratio (Choi et al. 2018; Choi, Beck, and Pierce 2014).

To examine the association between Me31B granules and pair-rule mRNAs, I performed third generation *in situ* HCR of the well-studied pair-rule transcripts *ftz* and *hairy*, coupled with immunostaining for the Me31B protein. In cellularised embryos, several *hairy* (Figure 4.20A-D) and *ftz* (Figure 20E-H) transcripts overlapped with Me31B granules on the apical side. The relative numbers of overlap observed for both *ftz* and *hairy* with P bodies appear significant considering the following points: (a) mRNAs are, likely, only transiently associated with Me31B granules (b) the observed overlap is recorded at a particular steady state when embryos were subjected to fixation. Their association, therefore, could mean that Me31B granules are involved in the regulation of pair-rule mRNAs. Since *hairy* and *ftz* transcripts have very short half-lives and require rapid turnover, Me31B granules may act as sites of degradation of these mRNAs due to their spatial proximity and enrichment of degradation machinery. This interpretation, however, needs to be investigated in detail.

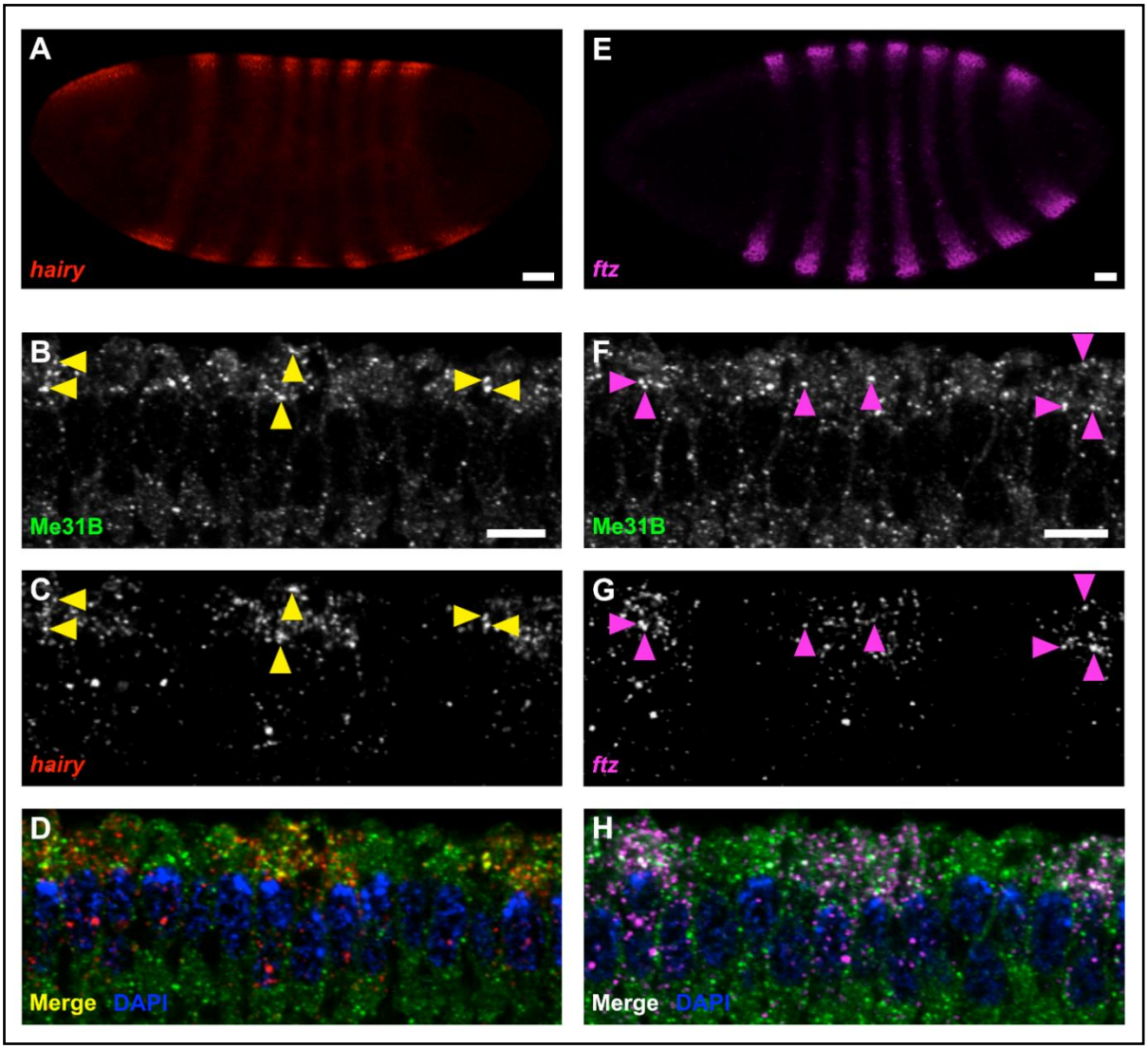

Figure 4.20: *hairy* and *ftz* mRNAs overlap with apical Me31B granules in cellularised embryos. (B-D, F-H) Embryos expressing Me31B::GFP. **(A)** Low magnification image of *hairy* RNA distribution in cellularised embryo; scale bar: 30µm. **(B,C)** High resolution images of cellularised embryo stained for *hairy* and Me31B, respectively. Arrowheads (yellow) highlight representative Me31B and *hairy* overlap. **(D)** Merge shows overlap of *hairy* and Me31B particles; DNA is stained by DAPI (blue); scale bar: 10µm. **(E)** Low magnification image of *ftz* RNA distribution in cellularised embryo; scale bar: 30µm. **(F,G)** High resolution images of cellularised embryo stained for *ftz* and Me31B, respectively. Arrowheads (magenta) highlight representative Me31B and *ftz* overlap. **(H)** Merge shows overlap of *ftz* and Me31B particles; DNA is stained by DAPI (blue); scale bar: 10µm.

Conclusion: *hairy* and *ftz* mRNAs overlap with Me31B granules in the apical region of the cellularised embryo.

4.11.3 *hairy* and *ftz* mRNAs exhibit varying levels of overlap with Me31B granules at different stages of the early embryo

Since both Me31B granules and the pair-rule mRNA particles (*hairy* and *ftz*) are enriched apically, a key challenge was to decipher if the observed overlaps were functional or merely a result of spatial proximity. To partly address this issue, the following approaches were adopted: (a) associations at different stages of the early embryo development were analysed to decipher patterns in the overlap of Me31B granules with *ftz* and *hairy* transcripts and (b) analysis by image randomisation (whereby Me31B granules and mRNA particles from different images are scrambled together) to score the degree of random overlap.

The resolution limit of the confocal microscope may not allow resolving the absolute sizes of Me31B and mRNA particles and therefore, the degree of colocalisation may not be fully resolved. In order to overcome this, I have simplified the classification of association as follows: mRNA particles exhibiting 100% overlap, or 50% overlap are classified as ‘association’ (Figure 4.21A).

Analysis of pair-rule mRNA (*hairy* and *ftz*) and Me31B granule overlap at different stages of the early embryo development revealed an interesting pattern. For *ftz* transcripts, about 21% of the mRNAs overlap with Me31B granules prior to cellularisation and this significantly increases to around 48% during cellularisation. Post cellularisation, the percentage of overlap significantly drops to almost 33%. For *hairy* transcripts, initially 24% of the mRNAs overlap with Me31B granules before cellularisation and this number significantly increases to 36% at cellularisation. Post cellularisation however, less than 23% of the mRNAs remain together, this is significantly lower than those observed at cellularisation. Taken together, *ftz* and *hairy* mRNA overlap with Me31B granules are maximum at cellularisation (Figure 4.21B).

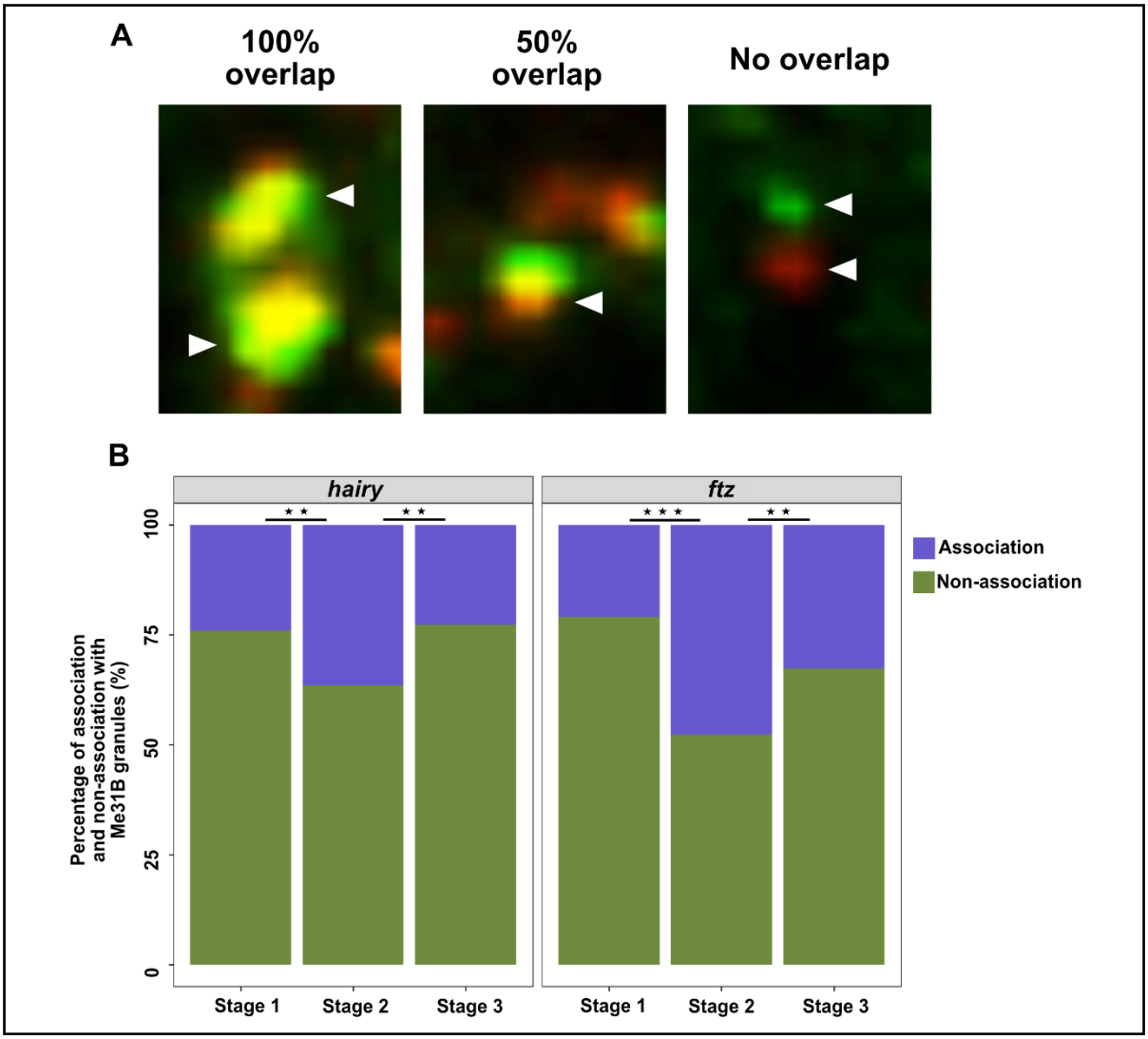

Figure 4.21: *hairy* and *ftz* mRNA overlap with apical Me31B granules is highest at cellularisation. (A) Representative images displaying differential levels of *hairy* RNA-Me31B colocalisation (white arrowheads). 100% and 50% overlap classify as association while no overlap classifies as non-association. This classification has also been followed for *ftz* RNA-Me31B colocalisation. **(B)** Quantification of *hairy* (n=350 particles) and *ftz* RNA (n=265 particles) association with Me31B granules at different stages of embryos expressing Me31B::GFP displaying significant overlap at cellularisation. Stage 1: pre-cellularisation, Stage 2: cellularisation and Stage 3: post-cellularisation. $p<0.05$ between stage 1 and stage 2; $p<0.005$ between stage 2 and stage 3 (*hairy*). $p<0.0001$ between stage 1 and stage 2; $p<0.05$ between stage 2 and stage 3 (*ftz*).

Moreover, image randomisation analyses performed during these three different stages revealed a very minimal percentage of random associations (Figure 4.22). Taken together, these results indicate that the association of pair-rule mRNAs *hairy* and *ftz* observed with Me31B granules during cellularisation could be physiologically functional.

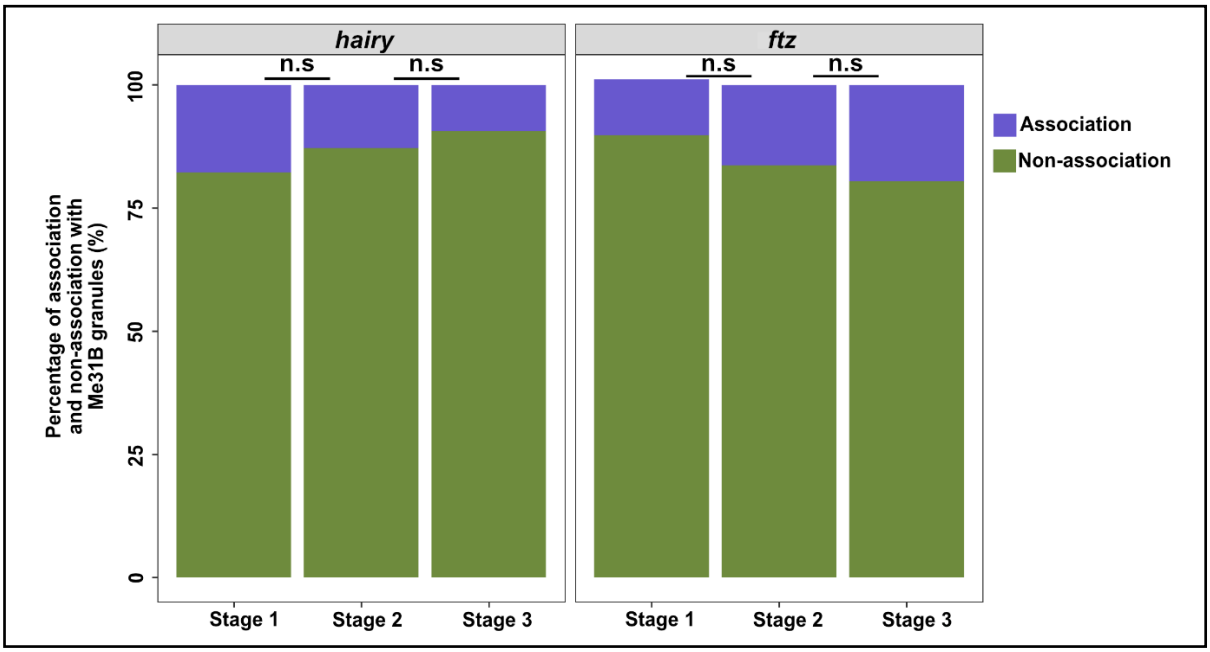

Figure 4.22: *ftz* and *hairy* overlap with Me31B granules is significantly lesser in scrambled images. Quantification of *hairy* (n=968 particles) and *ftz* RNA (n=541 particles) association with Me31B::GFP granules at different stages in scrambled images displaying minimal association; stage 1: pre-cellularisation, stage 2: cellularisation and stage 3: post-cellularisation; n.s - non-significant.

A high percentage of association of Me31B granules with pair-rule transcripts was observed on the apical side compared to the basal region of the cellularised embryo (Figure 4.20). Analysis of *hairy* and *ftz* association with Me31B granules on the basal side showed that the proportion of association on the basal region is practically non-existent (Figure 4.23). This suggests that association of pair-rule mRNAs and Me31B granules is specific to the apical region of the cellularised embryo.

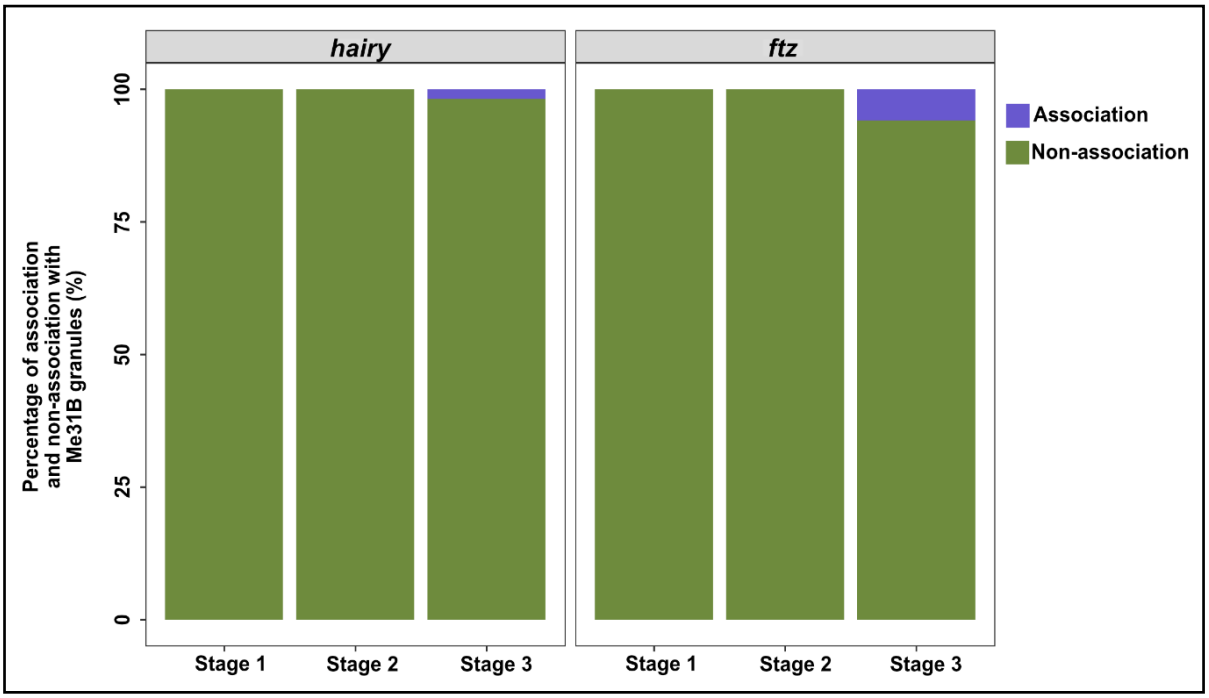

Figure 4.23: *hairy* and *ftz* association with Me31B granules is negligible in the basal region of cellularised embryo. Quantification of *hairy* (n=208 particles) and *ftz* RNA (n=267 particles) association with Me31B::GFP granules in the basal region of the embryo at different stages displaying little or no association; stage 1: pre-cellularisation, stage 2: cellularisation and stage 3: post-cellularisation.

Furthermore, in pre-cellularised embryos, pair-rule transcripts have been shown to be actively transported from basal to apical region on microtubules (Bullock and Ish-Horowicz 2001; Wilkie and Davis 2001). However, I do not observe any association of Me31B granules and the pair-rule mRNAs during the basal to apical transport. Based on these results, it is likely that association with Me31B granules may only occur at the final intracellular location (apical side) where pair-rule mRNAs are likely subjected to translational activation or degradation.

Conclusions: *ftz* and *hairy* association with Me31B granules is maximum at cellularisation compared to earlier and later stages. Additionally, this association is specific to the apical region of the cellularised embryos.

4.11.4 *hunchback* mRNA does not associate with Me31B granules

To test if association with Me31B granules was specific to pair-rule transcripts, *in situ* hybridisation was performed on *hunchback* (*hb*) mRNA, a gap gene transcript which is expressed during the first two hours of embryogenesis (Figure 4.24A) and not intracellularly localised, coupled with immunostaining for the Me31B protein.

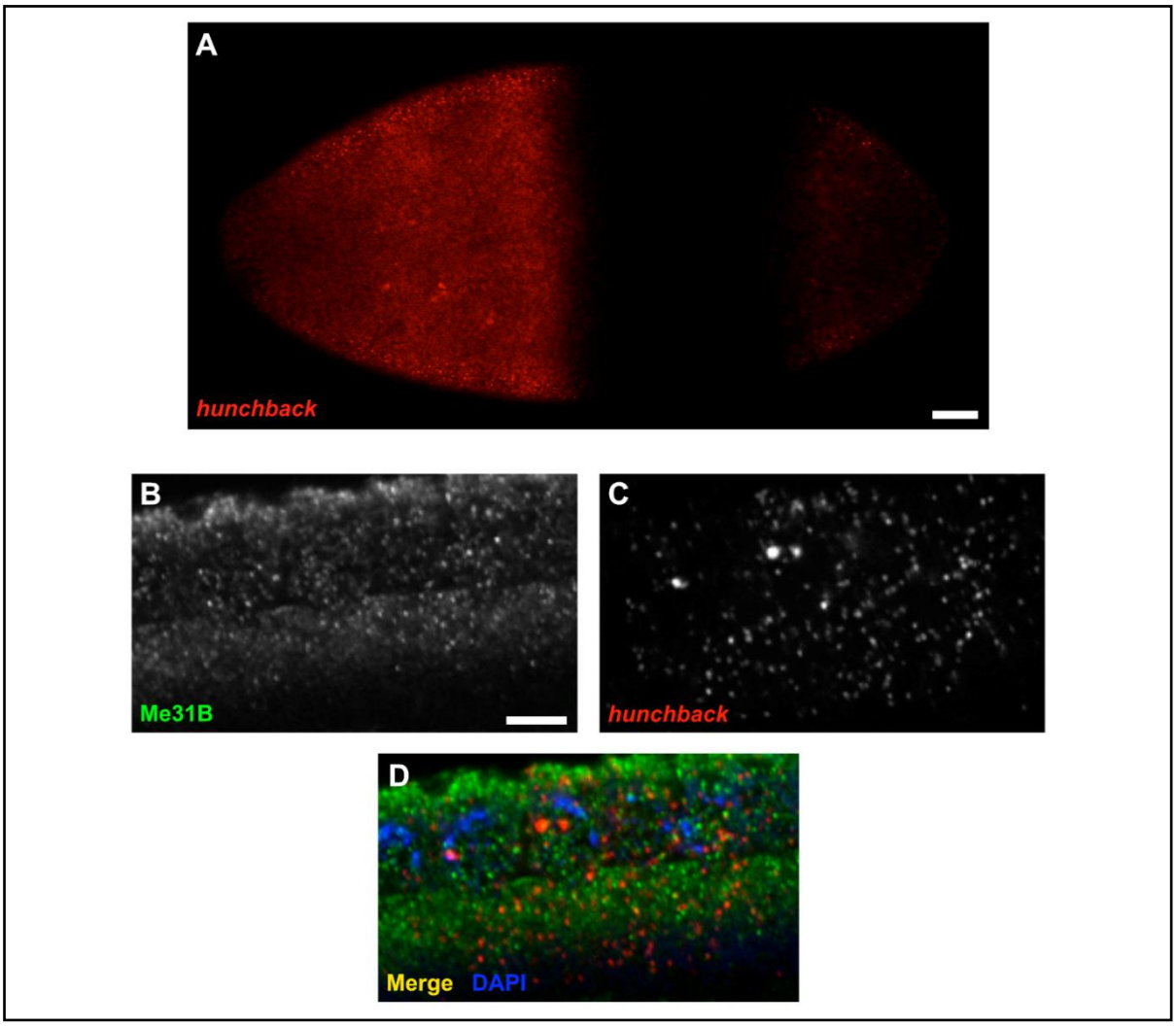

Figure 4.24: *hunchback* does not associate with apical or basal Me31B granules. (A) Low magnification image of *hunchback* RNA distribution in cellularised embryo; scale bar: 50µm. **(B-D)** Embryos expressing Me31B::GFP. **(B,C)** 0-2-hour old embryos stained for Me31B **(B)** and *hunchback* **(C)**. Scale bar: 10 µm. **(D)** Merge shows no association of Me31B granules and *hunchback*; DNA is stained by DAPI (blue).

Most *hb* mRNA particles are present in the basal region (Figure 4.24C) since they are not apically localised like *hairy* and *ftz*. In the basal region of the embryo, *hb* transcript association with Me31B granules were practically non-existent (Figure 4.24B-D), suggesting that association of pair-rule mRNAs with Me31B granules is specific and localised to the apical region of the cellularised embryo.

Conclusion: *hb* mRNA does not associate with Me31B granules in the early embryo.

4.11.5 Apical localisation of *ftz* is important for Me31B granule condensation

As discussed in the previous chapter, a key factor that regulates the integrity of Me31B granules is RNA. Since pair-rule mRNAs are associated with Me31B granules apically, I hypothesised that the interaction of the pair-rule mRNAs with key P body proteins such as Me31B would be essential for granule formation on the apical region.

Since association of *ftz* with Me31B granules was the highest among the pair-rule RNAs tested, I decided to test this hypothesis by utilizing ftz^{w20} embryos, in which a mutation in the *ftz* localisation sequence disrupts their targeting to the apical region of the embryo (Weiner et.al, 1984). *In situ* hybridisation showed that while *ftz* was present in alternate stripe patterns in Me31B::GFP embryos (Figure 4.25B), it was uniformly distributed across the embryos in $ftzw^{w20}$ mutants (Figure 4.25E) contrary to its apical localisation. Interestingly, P bodies in the ftz^{w20} embryos, appeared less particulate and more diffuse in the absence of apical *ftz* mRNA (Figure 4.25D), compared to the Me31B::GFP embryos (Figure 4.25A). However, the diffuse distribution of Me31B granules along all segments of the embryo was slightly puzzling. Since normal *ftz* mRNA distribution is limited to the seven individual stripes along the embryo, the diffuse distribution of Me31B would only have been expected along these stripes. *ftz* is regulated by several other segmentation factors, therefore, loss of apical localisation of *ftz* most likely affects Me31B granule formation in the embryo indirectly. An alternate possibility is the presence of an additional mutation on the chromosome and this could be tested using independent *ftz* alleles.

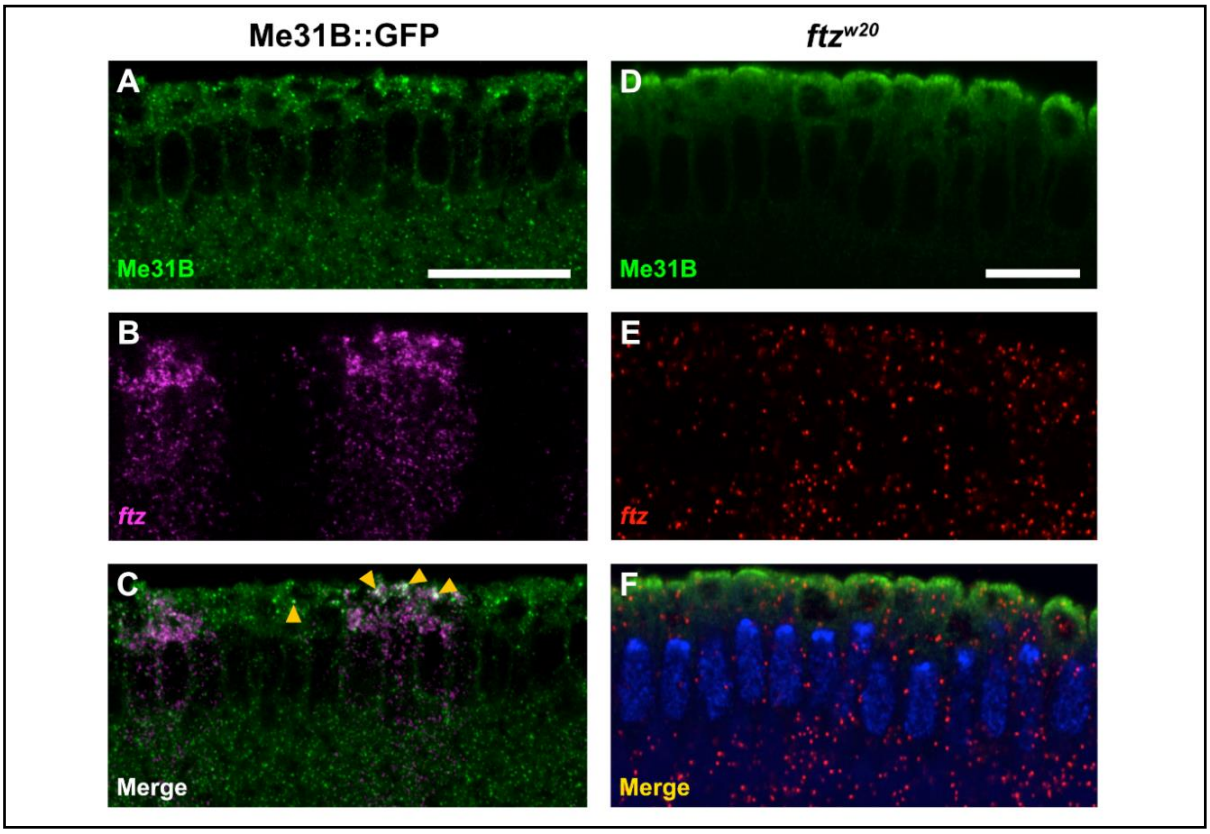

Figure 4.25: Mis-localisation of *ftz* mRNA affects Me31B granule formation on the apical region of cellularised embryos. (A-C) Embryos expressing Me31B::GFP**. (A,B)** High resolution images of cellularised embryo stained for *ftz* and Me31B, respectively. **(C)** Merge shows association of *ftz* and Me31B particles (yellow arrowheads). **(D-F)** Embryos expressing ftz^{w20} mutation. **(D)** Cellularised embryos stained for Me31B displaying a largely diffuse distribution of Me31B granules in the apical region. **(E)** Cellularised embryos stained for *ftz* displaying mis-localised *ftz* throughout the embryo. **(F)** Merge shows no association of *ftz* and Me31B in cellularised embryos. Scale bar: 10 µm (A-F).

To verify if the diffuse nature of Me31B granules was due to the absence of apically localised *ftz* and not due to reduced Me31B protein levels in the embryo itself, I performed western blot analysis of lysates obtained from Me31B::GFP and ftz^{w20} embryos. Analysis revealed that there was little or no difference in the relative levels of Me31B protein between the two embryos (Figure 4.26).

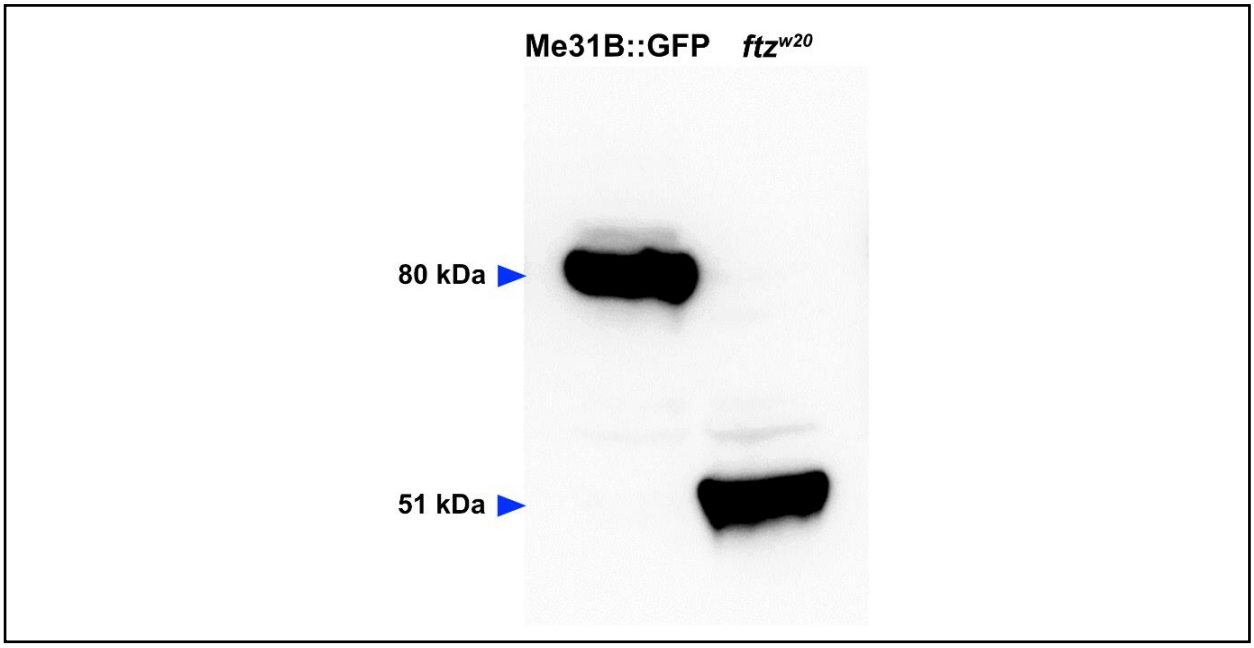

Figure 4.26: Me31B protein levels do not appear to be decreased in the *ftz*^{w20} embryos. Lysates from 0-3-hour old embryos expressing Me31B::GFP and *ftz*^{w20} were subjected to SDS-PAGE. Me31B in Me31B::GFP (80 kDa) and *ftz*^{w20} (51 kDa) lysates was detected by western blot against Me31B.

Conclusion: Mis-localisation of *ftz* RNA appears to affect apical Me31B granule condensation. This data raises the possibility that association of pair-rule mRNAs with Me31B promotes granule assembly.

4.12 Summary of results

Previous work from the lab showed that upon *ex vivo* activation of the mature oocyte, P bodies underwent dispersion. Whether this dispersal was physiological and if so, what happens to P bodies post activation, was unknown. Using a combination of *in vivo* live imaging and pharmacological treatment, my data demonstrates the potential factors (swelling, ionic strength, cytoskeletal re-arrangement, and release of RNA) which lead to the diffuse state of P bodies in the activated egg. My data also shows that Me31B and *bcd* mRNA particles disperse simultaneously upon *ex vivo* activation. However, while Me31B reforms into smaller sized granules shortly after dispersion, *bcd* particles appear dispersed, indicating that P bodies in the embryo may likely be devoid of RNA. Furthermore, using live imaging and biochemical assays, my data demonstrates differences in the biochemical properties of Me31B between the mature oocyte and early embryo. Finally, using immunofluorescence and *in situ* hybridisation assays, my data shows that P bodies specifically associate with apically localised pair-rule mRNAs during cellularisation, indicating a regulatory role for P bodies in early embryogenesis.

4.13 Discussion

4.13.1 Embryogenesis modulates P body properties

The onset of embryogenesis post oocyte to embryo transition occurs in the presence of maternal determinants and thus, requires reorganisation of RNA regulation by altering the proteome. In *Drosophila*, the early embryo is a developmentally vital stage since residual maternal mRNAs need to be degraded and cleared to allow initiation of zygotic transcription (Hamm and Harrison 2018; Tadros and Lipshitz 2009). While the maternal to zygotic transition takes place around cellularisation (3 hours post fertilisation), clearance of maternal products begin post egg activation itself. Recent reports suggest that most of the mRNAs stored inside P bodies code for degradation enzymes (Hubstenberger et al. 2017). Therefore, to ensure that mRNAs in the cytoplasm are readily degraded and cleared, P bodies must possess an important characteristic of exchanging contents between the granule and the cytoplasm. My data shows that although P bodies in the early embryo exhibit relatively slow exchange kinetics with the cytoplasmic pool, they exhibit a high percentage of mobile Me31B molecules. This suggests that the semi-liquid nature of embryonic P bodies could allow for controlled release of degradation enzymes for maternal mRNA degradation.

The smaller size of embryonic P bodies is intriguing. Results from the previous chapter showed that upon RNase A treatment, P bodies dissociated into multiple smaller condensates, suggesting a role for RNA in dictating P body size and integrity. Since early embryogenesis involves large scale maternal RNA degradation, embryonic P bodies might be devoid of mRNAs, likely explaining their smaller size compared to the oocyte P bodies.

Differences in the density of Me31B complexes before and after activation suggest that the biochemical composition of P bodies undergo large scale remodelling at egg activation, likely contributing to the modified properties of embryonic P bodies. Taken together, the biophysical properties of P bodies and their resulting functions are tuned in response to specific developmental signals. While P bodies in the oocyte help regulate maternal RNA storage and translational repression, P bodies in the early likely facilitate maternal RNA degradation. Therefore, P bodies are not merely mediators of translational repression but have specific regulatory functions that change during development.

4.13.2 The role of phosphorylation in modulating P body properties at egg activation

A key difference observed in P bodies between the mature oocyte and the early embryo was the increased phosphorylation of the Me31B protein, leading to the idea that phosphorylation at egg activation likely modulates P body properties in the early embryo. A key kinase called PNG has been shown to phosphorylate a myriad of proteins during the oocyte to embryo transition. PNG kinase is thought to be activated by mechanical stress as the egg is activated and its phosphorylation activity is restricted to the first half hour post activation (Hara et al. 2017). Reformation of P bodies is also observed within the first half hour of activation, suggesting that phosphorylation and P body reformation post activation could be mutually inclusive. *In vitro* studies of several RBPs have shown that post-translational modifications such as phosphorylation can influence the formation, maintenance, and material properties of condensates (Hofweber and Dormann 2019; Söding et al. 2020). Therefore, based on my results and data from recent studies, the following models for P body regulation at egg activation could be derived:

1. Phosphorylation of P body proteins triggered by mechanical stress during activation causes P body dispersal. To restore equilibrium, the soluble P body proteins condense and form smaller sized compartments during early embryogenesis.

2. Swelling at egg activation leads to P body dispersal. At the same time, large-scale phosphorylation of multiple proteins leads to reformation of P bodies with dramatically altered material properties due to post-translational modifications of associated proteins.

4.13.3 Pair-rule mRNA regulation by P bodies

To date, a comprehensive analysis on the role of P bodies in the developing embryo has been lacking. While the translational regulation of pair-rule mRNAs is poorly understood, in-silico modelling studies revealed that pair-rule mRNA translation is highest during cycle 14 of nuclear division (Becker et al. 2013). Interestingly, this cycle coincides with the completion of cellularisation. Based on the percentage and timing of association of *ftz* and *hairy* with P bodies, it is likely that they are targeted to P bodies for rapid translation or degradation (primarily due to their extraordinarily short half-lives) at cellularisation. A role for P bodies in the storage or translational

repression of pair-rule mRNAs is unlikely due to the following reasons: (a) The smaller size and increased dynamics of P bodies in the early embryo make it less likely to store pair rule mRNAs until cellularisation; (b) association of pair-rule transcripts and P bodies in embryos of roughly the same stage varies with every fixation suggesting that pair-rule mRNAs only transiently associate with P bodies. While further studies are essential to confirm the above described model (see section 4.15.3; Future Directions), preliminary evidence suggests that P bodies in the embryo could serve as micro-compartments to allow controlled regulation of mRNAs in the early embryo.

4.14 Future directions

4.14.1 Investigating factors affecting embryonic P body integrity and properties

Since the early embryo is hydrated and has a hard-outer shell that is extensively cross-linked post egg activation, pharmacological treatments proved difficult to test embryonic P body properties. An alternate approach to studying P body properties in the early embryo is micro-injection. Injecting fluorescent molecules, especially *in vitro* transcribed RNAs, into the syncytial blastoderm embryos is a well-established assay, historically used for studying RNA localisation in *Drosophila* development (Bullock and Ish-Horowicz 2001; Bullock et al. 2003; Lall et al. 1999).

How P bodies remain anchored apically in the cellularised embryo is not known. Microinjection of cytochalasin-D (to depolymerise actin) and colchicine (to depolymerise microtubules) could elucidate if cytoskeletal networks play a role in regulating the transport and anchoring of embryonic P bodies.

A likely reason for the smaller size and lower viscosity of embryonic P bodies is the absence of stored RNAs. Injecting fluorescently labelled RNA could help monitor changes in P body size and dynamics and examine whether injected RNAs get incorporated into these P bodies. Furthermore, microinjecting solutions with hexanediol or different salts (monovalent and divalent) could give insights into the nature of inter-molecular interactions that regulate P bodies in the early embryo.

4.14.2 Characterising Me31B PTMs in the mature oocyte and early embryo

To better understand the changes that accompany P bodies before and after egg activation, mass spectrometry analysis of purified Me31B::GFP from the mature oocyte and early embryo could provide information regarding the putative PTMs of Me31B between the two developmental stages. Identification and positioning of amino acid residues prone to such modifications could inform whether Me31B contains distinct domains with residues which could act as stickers or spacers to control their phase behaviour.

4.14.3 Examining the role of P bodies in pair-rule mRNA regulation

Imaging associations of pair-rule mRNA particles and P bodies using optical nanoscopy techniques including 3D Structured Illumination microscopy (3D-SIM) or Stimulated Emission Depletion microscopy (STED) could help overcome the limitation posed by the diffraction-limited resolution of the confocal microscope.

To further ascertain the ‘authenticity’ of association, quantitation using colocalisation algorithms such as Pearson correlation coefficient (PCC) and PCC (Costes) analyses could be adopted (Trcek et al. 2015). These methods are insensitive to object shape and analyse the spatial association between two fluorescent particles rather than the frequency of their co-occurrence.

Pair-rule mRNA stability could be measured by inhibiting *in vivo* transcription at different stages using inhibitors such as actinomycin-D followed by quantitative polymerase chain reaction or northern blot analysis. If the dwell time of mRNA association with P bodies and mRNA half-life at different stages reveal a pattern, functional roles can be deduced.

Finally, in situ hybridization of embryos expressing fluorescently labelled xRNA (5’-3’ exoribonuclease reporter to monitor RNA decay intermediates) genetically engineered into flies expressing fluorescently labelled Me31B, could be used to perform *in situ* hybridisation of the pair-rule RNA of interest. Employing spot detection and colocalisation analyses could then inform whether P bodies act as sites of pair-rule RNA degradation.

Chapter 5
Investigating recombinant Me31B phase separation and material properties *in vitro*

5.1 Introduction

In vitro reconstitution and phase separation studies of diverse RNP components has led to the acceptance of the model which states that RNP assembly is seeded by LLPS, driven by both specific and promiscuous multivalent interactions, primarily between IDRs. IDRs can typically create an ensemble of structures by sampling multiple conformations that support condensate assembly with different morphologies and dynamics. However, the initial nucleation step for the assembly of several membrane-less organelles is thought to be mediated by protein and/or RNA scaffolds. Protein molecules as scaffolds are the most commonly observed, and drive phase separation in a concentration dependent manner. Such scaffold proteins often contain IDRs, however, client proteins that interact with scaffolds and partition inside the condensates also contain IDRs. Therefore, while some IDRs participate in driving phase separation of RNP granules, in some others, IDR roles are limited to regulating the material properties of phase separated condensates. In the latter case, the role of structured domains in contributing to the assembly of condensates becomes important.

Results from the previous chapters have demonstrated the ability of P bodies to transition between different material states during development. While cytoplasmic factors such as RNA, ionic strength, cytoskeletal network and osmolarity play a key role in controlling P body integrity and material state, the intrinsic role of core P body proteins has not been considered thus far. The maternal protein Me31B used as a marker to study P body properties, belongs to a highly conserved family of ATP dependent DEAD-box RNA helicases. Human DEAD-box protein DDX6 and its orthologues in *Xenopus laevis* (Xp54), *C.elegans* (CGH-1), *Saccharomyces cerevisiae* (Dhh1p) and *Drosophila* (Me31B), all play a critical role in post-transcriptional regulation by mediating both translational regulation and mRNA decapping. Additionally, some of these proteins, including DDX6 and Dhh1 have been shown to contain IDRs. Although IDR sequences present in DDX6 and Dhh1 are considerably different, recombinant versions of both proteins have been shown to phase separate *in vitro* (Hondele et al. 2019). While IDRs of Dhh1 are not essential for driving their assembly, they have been shown to enhance their propensity to phase separate through promiscuous interactions with other proteins (Protter et al. 2018). These results led to the hypothesis that Me31B may contain IDRs that promote P body

condensation or regulate their material properties in the mature oocyte and early embryo.

A major proportion of our understanding of condensate phase separation and material properties has been driven primarily by studying the associated RNP components in a minimally engineered *in vitro* system. This approach has been instrumental in describing the role of non-equilibrium features of living cells. Experimentally, it is fairly difficult to control the relative contributions of the various factors that regulate P body condensation and material properties *in vivo*. Additionally, previous studies have shown that knockdown of Me31B prevents progress of egg development beyond mid-oogenesis (Nakamura et al. 2001), rendering any mutation studies on *in vivo* Me31B impossible. Therefore, testing the underlying sequence determinants that regulate phase separation and material properties of minimally reconstituted Me31B condensates, *in vitro*, provided an alternative approach. Testing the influence of factors such as RNA and salt in this minimal system could inform how Me31B condensate properties such as size and viscosity are influenced, and lead to a better interpretation of how these condensates might operate *in vivo*.

5.2 Chapter objectives

In this chapter, I have studied the phase separation and material properties of *in vitro* reconstituted/recombinant Me31B condensates. The specific questions addressed are as follows:

1. Does recombinant Me31B form phase separated condensates *in vitro*? What factors are required to drive recombinant Me31B condensation?
2. Do Me31B condensates exhibit liquid-like or gel-like material state? How do factors such as RNA and salt influence recombinant Me31B material properties?
3. Does Me31B contain IDRs? If so, what are their roles?

5.2.1 Author contributions

Experimental strategy, design and execution and image analyses in this chapter were performed by me except for the following contributions from:

1. Irmela Trussina (Alberti lab, Biotec, TU Dresden): assisted with protein purification.
2. Marcus Jahnel (Grill lab, MPI-CBG, Dresden): performed optical tweezer experiments.

5.3 Me31B, on its own, does not undergo condensation

Numerous RNPs have been shown to undergo condensation on their own or when bound to RNA. To determine whether the material states of Me31B granules observed *in vivo* are influenced by the intrinsic properties of the protein itself, I studied the material properties of purified recombinant Me31B protein fused to a GFP fluorophore (GFP-Me31B). Firstly, to examine the phase separation propensity of recombinant Me31B, a standard phase separation assay was performed by mixing the purified protein in a 'phase separation' buffer (hereby referred to as 'protein buffer') that mostly recapitulates physiological salt conditions. Although the estimated concentration of Me31B is ~ 7.5 µM *in vivo* (Götze et al. 2017), I tested varying concentrations of Me31B to see if a concentration-dependent condensation pattern could be observed.

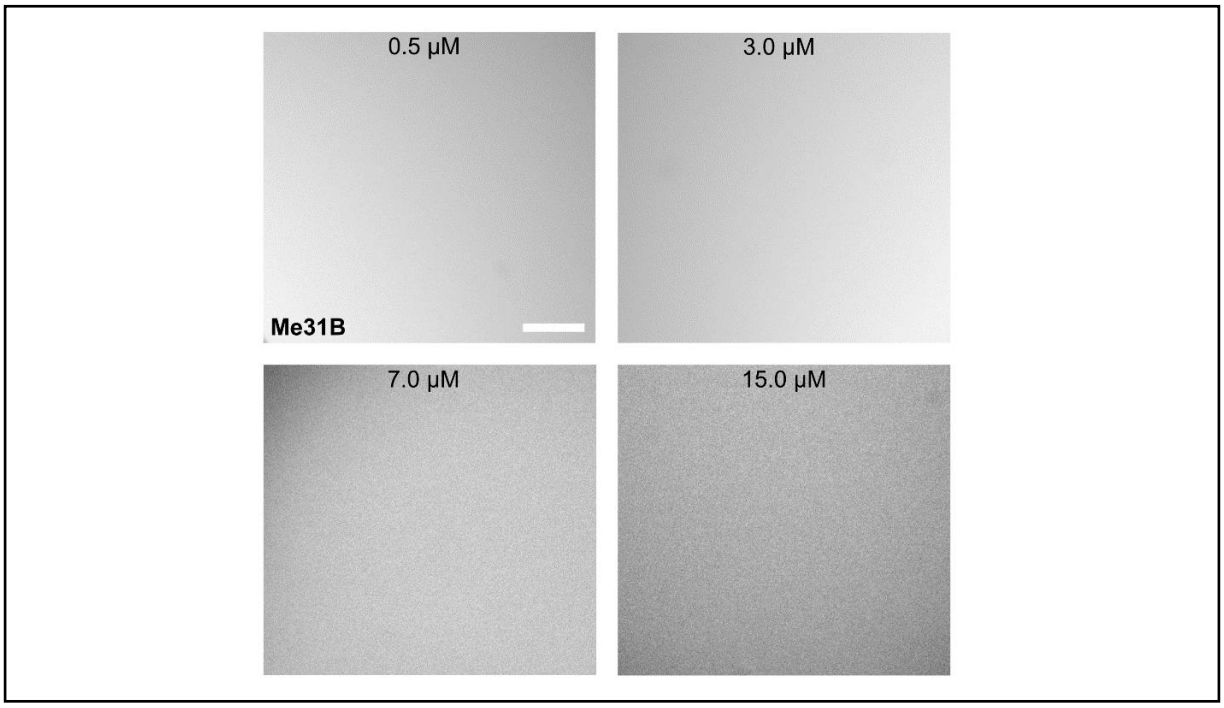

Figure 5.1: Recombinant Me31B does not phase separate on its own. Purified GFP-Me31B at different concentrations does not undergo condensation. Scale bar: 5 µm.

Live imaging revealed that Me31B failed to form phase separated droplets and appeared diffuse at all concentrations (Figure 5.1). This is possibly due to the absence of factors such as RNA, cytoskeleton and other interacting proteins which would otherwise be present *in vivo*.

Conclusion: Me31B does not phase separate on its own and requires additional factors to drive its condensation *in vitro*.

5.4 Presence of RNA is not sufficient to promote Me31B condensation

Multivalency is a key determinant in driving phase separation. RNA, being a multivalent ligand, not only regulates condensate material properties, but also drives their phase separation. Multiple studies have shown that RNA alone is sufficient to drive RNP droplet formation in physiological concentrations. Since Me31B in the *Drosophila* mature oocyte is associated with multiple mRNAs, one hypothesis was that the addition of RNA may promote Me31B condensation. To test this, commercially synthesised short homopolymeric *polyA* RNA (~360 nucleotides) was added to the protein buffer. Live imaging revealed that Me31B failed to form phase separated condensates in the presence of short *polyA* RNA (Figure 5.2A). Since the length of the RNA can also influence phase separation, a longer *polyA* RNA that could provide multiple interaction domains to promote Me31B condensation was utilised. The addition of long *polyA* RNA, consisting of ~3000 nucleotides (referred to as *polyA* RNA for the rest of the chapter), also failed to promote Me31B phase separation (Figure 5.2B).

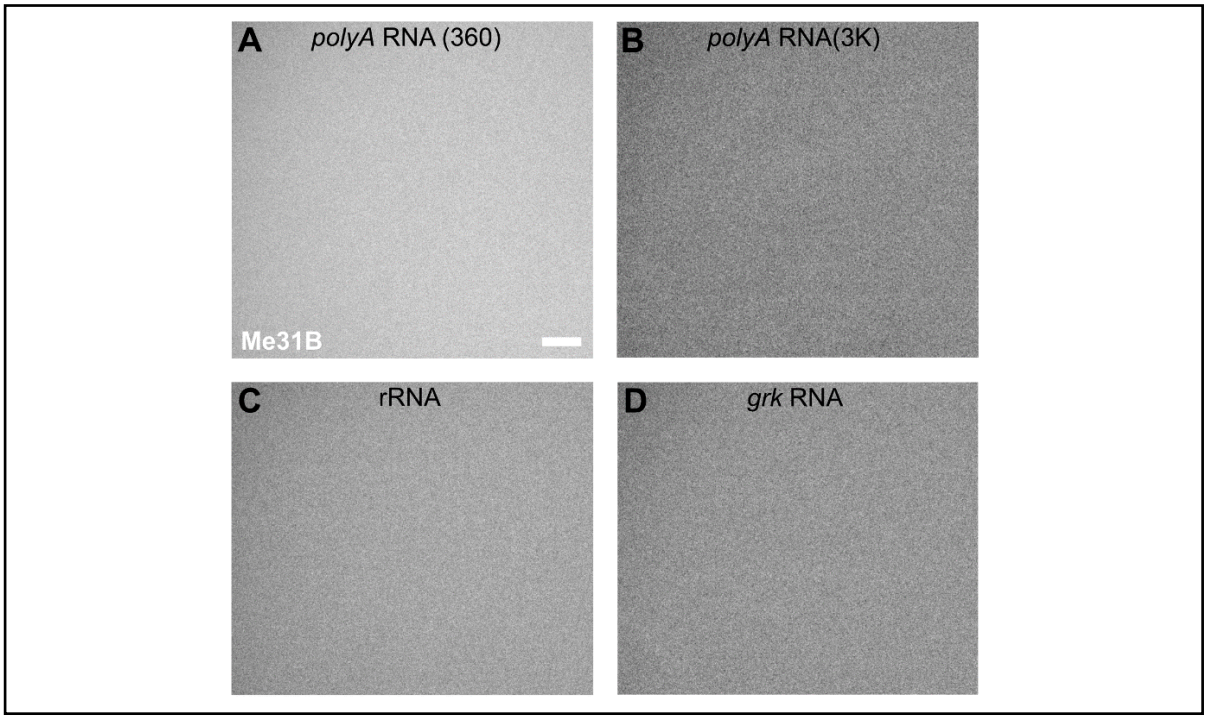

Figure 5.2: Presence of RNA does not induce Me31B condensation. (A-D) 7.5 µm purified GFP-Me31B in the presence of different types of RNA does not form condensed droplets. Scale bar: 5 µm.

Since homopolymeric *polyA* RNA is highly unstructured, I reasoned that structured RNAs might drive Me31B condensation. To test this, ribosomal RNA (rRNA), which is highly structured, was added to the protein buffer. Live imaging revealed that rRNAs also failed to induce Me31B condensation (Figure 5.2C). Me31B is associated with multiple maternal mRNAs *in vivo* and therefore its condensation might be specifically induced by maternal RNA-Me31B interactions. To determine if synthesised maternal transcripts could induce Me31B condensation, I added *in vitro* transcribed *gurken (grk)* RNA, a key maternal transcript associated with P bodies during mid-oogenesis in *Drosophila* (Weil et al. 2012), to the protein buffer. However, live imaging revealed that Me31B failed to phase separate in the presence of *grk* RNA (Figure 5.2D), indicating that additional factors are required to drive Me31B phase separation.

Conclusion: Me31B does not undergo phase separation in the presence of unstructured *polyA* RNA, structured rRNA or structured *grk* RNA.

5.5 Me31B forms liquid-like condensates in the presence of crowders

A key feature of *in vivo* oocytes that is absent in the *in vitro* system is macromolecular crowding. Since phase separation propensity is influenced by increased local concentration of macromolecules, the addition of crowding agents to the protein buffer could mimic *in vivo* crowding. In fact, several RBPs which do not form condensates on their own have been shown to undergo phase separation upon the addition of crowding agents such as polyethylene glycol (PEG) and Ficoll, *in vitro*. To test if crowding influences Me31B phase separation *in vitro*, 1% PEG, a frequently used crowder, was added to the protein buffer. Immediately upon addition of PEG, Me31B condensed into spherical liquid-like droplets (hereafter referred to as ‘condensates’), suggesting that crowding promotes Me31B phase separation (Figure 5.3A).

To find the minimum concentration of PEG required for Me31B condensation, I added lower concentrations of PEG to the protein buffer. Me31B failed to condense at concentrations of PEG less than 1%, irrespective of Me31B concentration (Figure 5.3B-E).

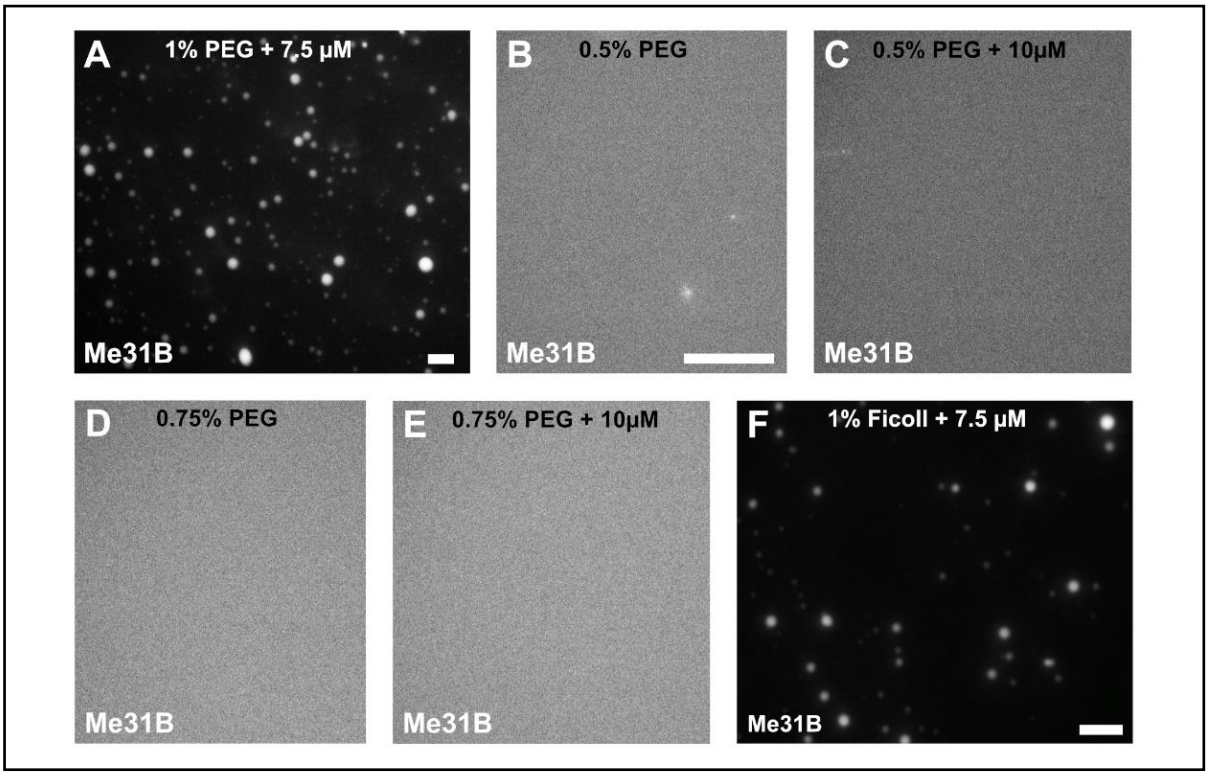

Figure 5.3: Presence of crowders induces Me31B condensation. (A) 7.5 µm purified GFP-Me31B in the presence of 1% PEG readily forms phase separated condensates. **(B-E)** Different concentrations of purified Me31B at PEG concentrations below 1% do not form phase separated condensates. **(F)** 7.5 µm purified Me31B in the presence of 1% Ficoll readily forms phase separated condensates. Scale bar: 5 µm (A-F).

Although PEG is the most frequently used crowding agent, some studies have also reported indirect effects of PEG on protein phase separation and their material properties (Kaur et al. 2019). Therefore, to confirm that Me31B phase separation was due to the crowding effect and not an artifact caused by PEG, 1% Ficoll was added to the buffer and the phase separation assay was performed. Similar to PEG, the addition of Ficoll also induced Me31B to form phase separated condensates (Figure 5.3F), confirming the role of crowding in inducing Me31B condensation. For the rest of the chapter, Me31B condensates are induced with 1% PEG.

Conclusion: Crowding is sufficient and necessary to induce condensation of recombinant Me31B.

5.6 Me31B condensates mature over time

Purified RNP components which form liquid-like droplets have been shown to transition into a less dynamic, solid-like state over time. This concept is referred to as maturation or gelation. Gelation is a common phenomenon observed with several phase separated components reconstituted *in vitro* (Lin et al. 2015; Molliex et al. 2015; Murakami et al. 2015; Patel et al. 2015; Riback et al. 2017). How gelation occurs is not fully understand, however, it is generally assumed that the strength of molecular interactions increases over time in the absence of factors such as ATP and RNA which help regulate 'liquidity', thereby causing the phase transition.

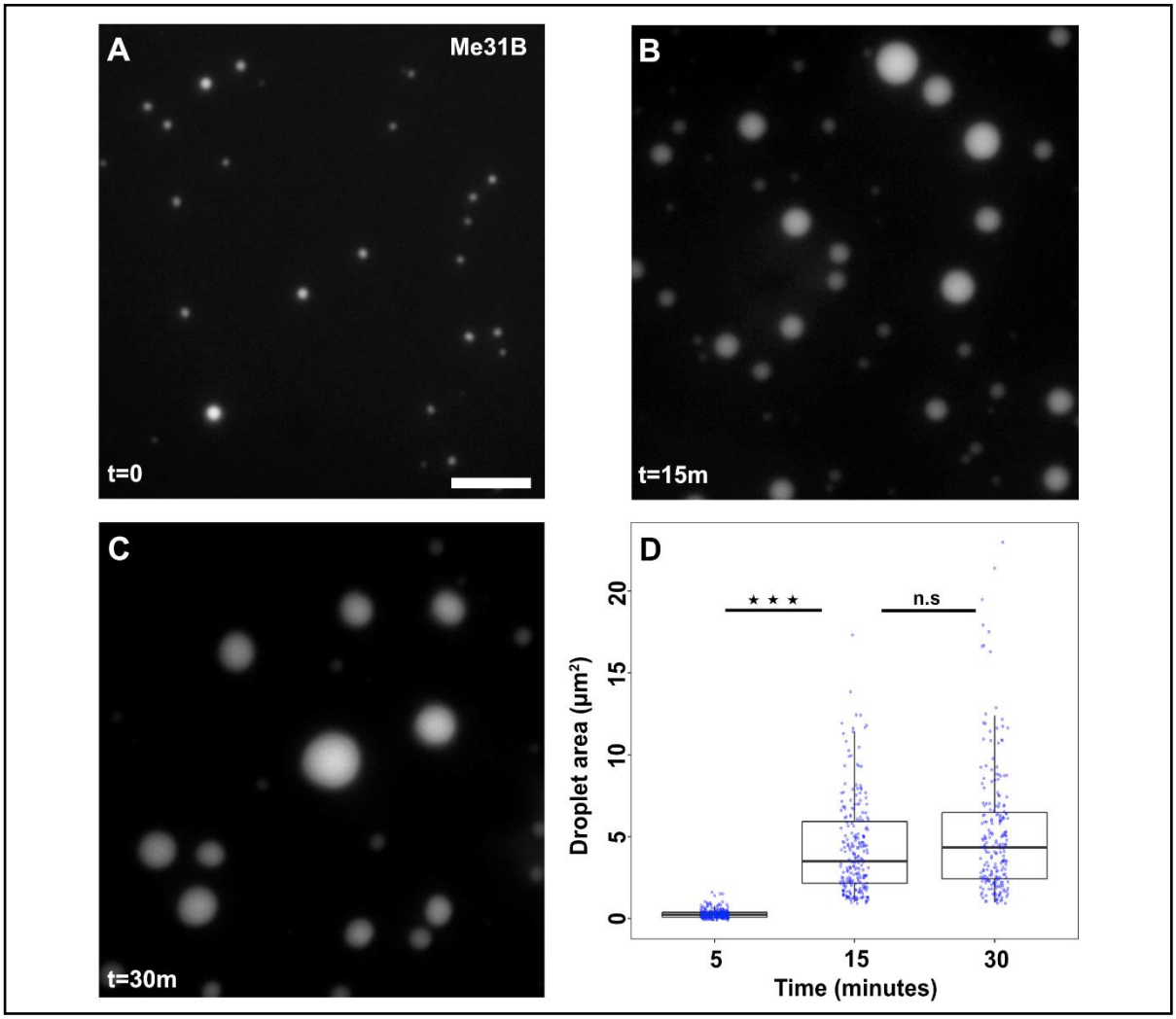

Figure 5.4: Me31B condensates, over time, exhibit signs of gelation. (A-C) Image sequence of purified GFP-Me31B (7.5 µm) at different time points post condensation; scale bar: 5 µm. **(D)** Quantification of Me31B condensate droplet area at different points post condensation. $p<0.0001$ between 5 and 15 minutes; non-significant (n.s) between 15 and 30 minutes.

To test if gelation occurs, induced Me31B condensates were imaged over a time course of 30 minutes. Time lapse imaging revealed two properties of Me31B condensates: (a) condensates exhibited continuous fusion and coalescence initially, giving rise to larger sized condensates over time (Figure 5.4A-C); (b) about 15 minutes post condensation, condensates failed to undergo fusion (Figure 5.4D, 5.5), which are signs of gelation.

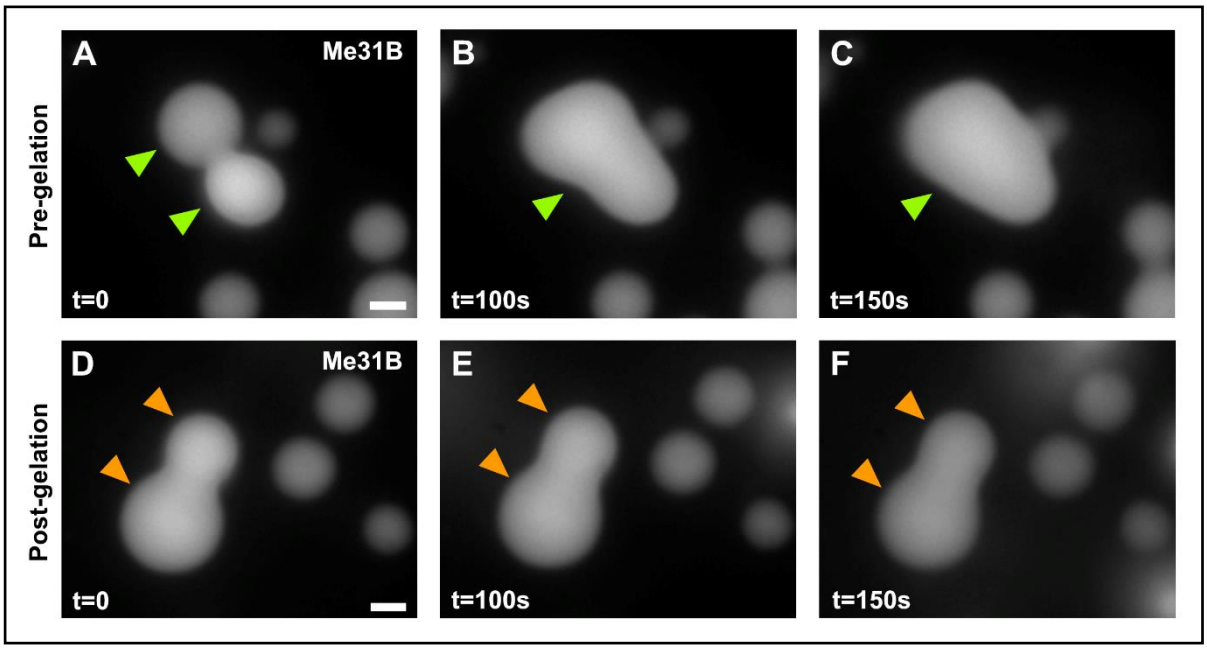

Figure 5.5: Me31B condensates exhibit slow fusion dynamics post gelation. (A-C) Image sequence of purified GFP-Me31B condensates (7.5 µm) undergoing fusion (green arrowheads) pre-gelation. **(D-F)** Image sequence of purified Me31B condensates (7.5 µm) failing to fuse (orange arrowheads) post-gelation. Scale bar: 5µm (A-F).

While condensate coalescence observed by live imaging provided clues about changes in Me31B material properties, it was not quantitative. To gain further insights into the altered physical properties over time, quantitative droplet fusion experiments using a dual trap optical tweezer were performed (Guillén-Boixet et al. 2020; Jahnel et al. 2011; Patel et al. 2015; Wang et al. 2018). Using optical tweezers, droplet behaviour can be monitored over time by using one laser beam to hold an Me31B droplet at a fixed position while another Me31B droplet trapped by a second laser beam is moved towards the first droplet at constant velocity (Figure 5.6A).

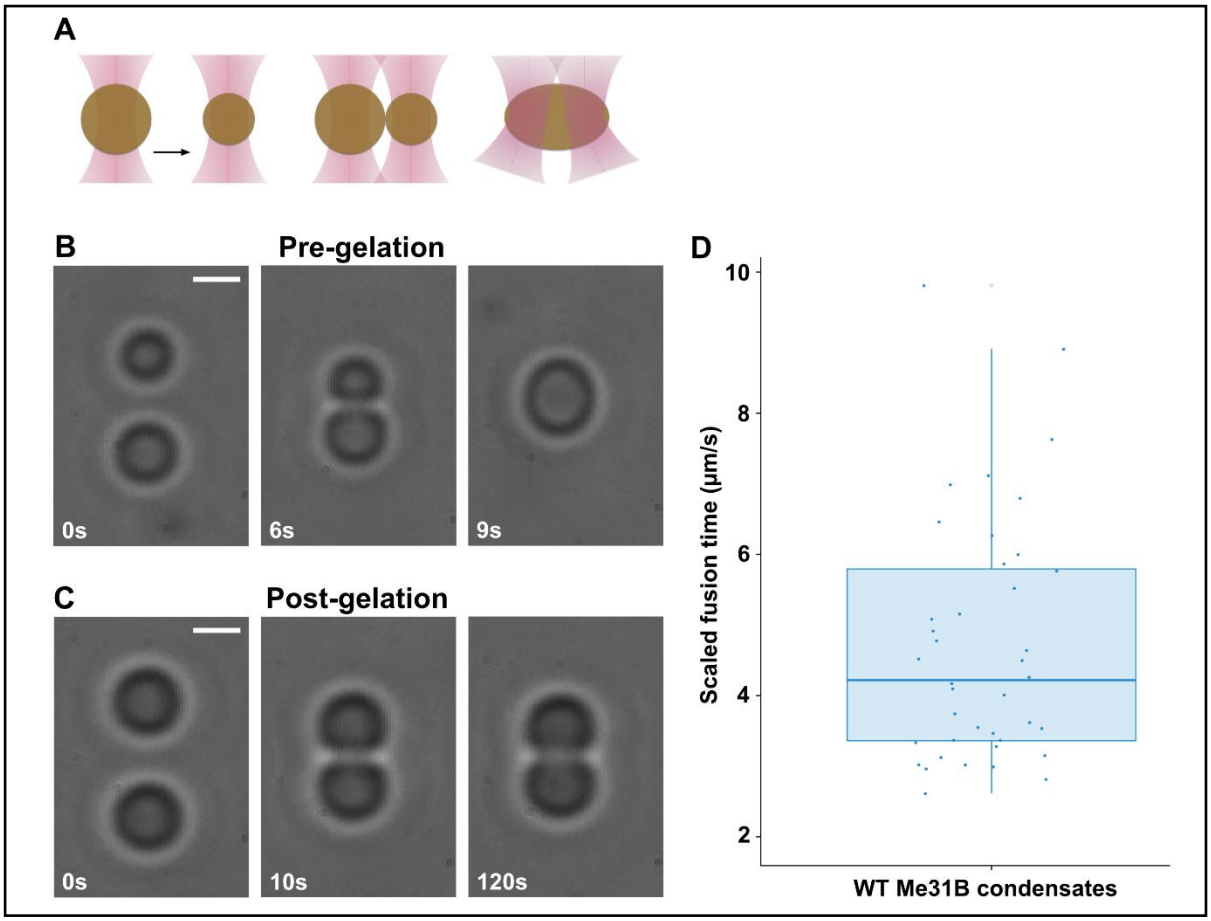

Figure 5.6: Optical tweezer assay confirms Me31B condensate gelation over time. (A) Schematic of controlled coalescence of two droplets using dual optical traps. **(B)** Image sequence of GFP-Me31B condensate coalescence using optical traps displaying rapid fusion prior to gelation. **(C)** Image sequence of Me31B condensate coalescence recorded over a time course of 45 minutes using optical traps displaying decreased fusion post gelation. Scale bar: 1.5 µm (B,C). **(D)** Quantification of scaled fusion time of multiple Me31B condensate fusions over time.

Between 0-30 minutes (pre-gelation) after condensate formation, Me31B condensates fused very quickly, often within 5s (Figure 5.6B). However, as the condensates aged (post-gelation), the relaxation time was significantly longer, with some condensates failing to fuse, similar to those observed using live imaging (Figure 5.6C). Additionally, the scaled fusion time of Me31B condensates, which measures the relaxation time constant over time (independent of condensate size), was quantified. Purified RNPs such as FUS and LAF-1, which are classified as liquid-like droplets, have been shown to exhibit a characteristic relaxation time of ~0.12s and 0.093s respectively (Elbaum-Garfinkle et al. 2015; Wang et al. 2018). However, the average scaled fusion time for

Me31B condensates was ~3.5s, confirming gelation of Me31B condensates over time (Figure 5.6D). Longer scaled fusion kinetics also suggests that Me31B condensates are intrinsically more viscous.

Conclusion: Me31B condensates, while liquid-like initially, undergo a phase transition to a more stable, gel-like state over time.

5.7 Me31B exhibits high internal viscosity

Phase separated polymers can exhibit a wide range of material states, from dynamic liquids to highly stable solids. *In vitro* reconstituted Me31B condensates display classic liquid-like behaviours including spherical morphology and frequent fusions. To test if Me31B molecules are dynamic and mobile, I first performed whole particle FRAP on newly induced condensates to test the exchange dynamics of Me31B between the condensate and bulk solution before gelation occurs. Post photobleaching, Me31B condensates exhibited significant fluorescence recovery (Figure 5.7A-D). Although the extent of recovery was only up to ~50%, the recovery kinetics and proportion of mobile fraction indicate that Me31B molecules constantly exchange between the condensate and bulk solution (Figure 5.7E). Interestingly, a higher degree of recovery along the edges and regions away from the core (Figure 5.7C). This suggests that the core of the condensate is highly viscous, likely preventing rapid diffusion of molecules. A plausible reason for condensates achieving only up to ~50% recovery could also be due to the lack of free Me31B molecules in the bulk solution.

Interestingly, whole particle FRAP of condensates post gelation decreased the amount of fluorescence recovery, suggesting that exchange between the condensate and bulk solution was reduced (Figure 5.7F-I). This is also exemplified by the decrease in the exchange kinetics and mobile fraction of Me31B molecules (Figure 5.7J). This shows that post gelation, when condensates likely are more viscous, exchange of molecules is rate limiting.

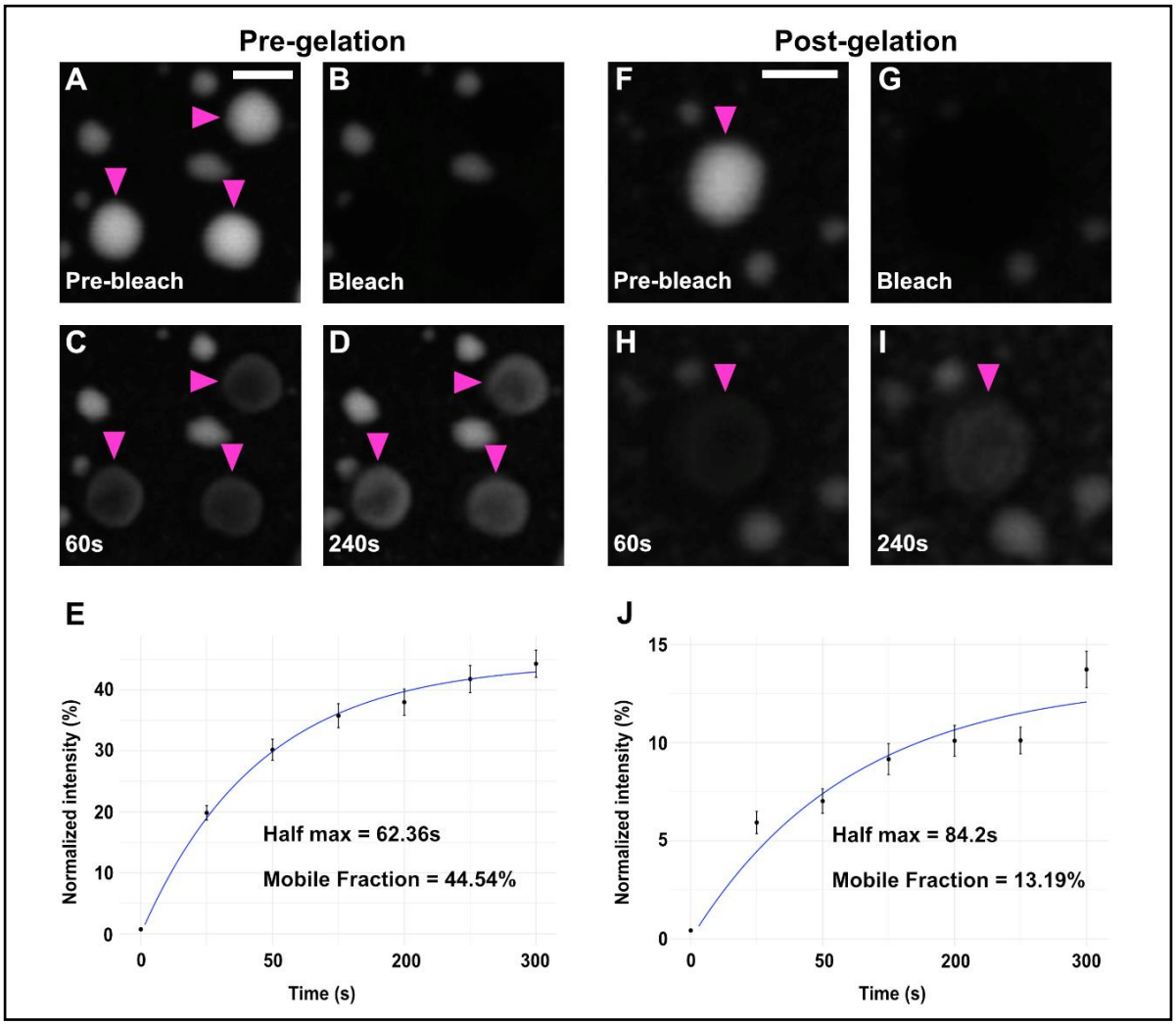

Figure 5.7: Gelation decreases the fraction of mobile Me31B between the condensate and bulk solution. (A-J) Purified GFP-Me31B condensates (7.5 µm) in the presence of 1% PEG. **(A-D)** Time lapse images of Me31B condensate fluorescence recovery before and after photobleaching whole condensate pre-gelation. Scale bar: 3 µm. **(E)** Analysis of whole particle FRAP of Me31B condensates. Standard deviation/data (black), fit (blue), n=17 condensates. Single exponential fits the FRAP curve. **(F-I)** Image sequence of Me31B condensate fluorescence recovery before and after photobleaching whole condensate post-gelation. Scale bar: 3 µm. **(J)** Analysis of whole particle FRAP of Me31B condensates. Standard deviation/data (black), fit (blue), n=15 condensates. Single exponential fits the FRAP curve.

If the initial condensates formed by Me31B are liquid-like, they would be expected to exhibit rapid internal rearrangement of molecules. To test if Me31B molecules inside condensates are freely diffusing, I performed internal FRAP on the newly induced Me31B condensates. Surprisingly, there was no recovery of Me31B molecules post

internal photobleaching (Figure 5.8). This was unexpected since the Me31B condensates exhibited several characteristics of liquid-like droplets.

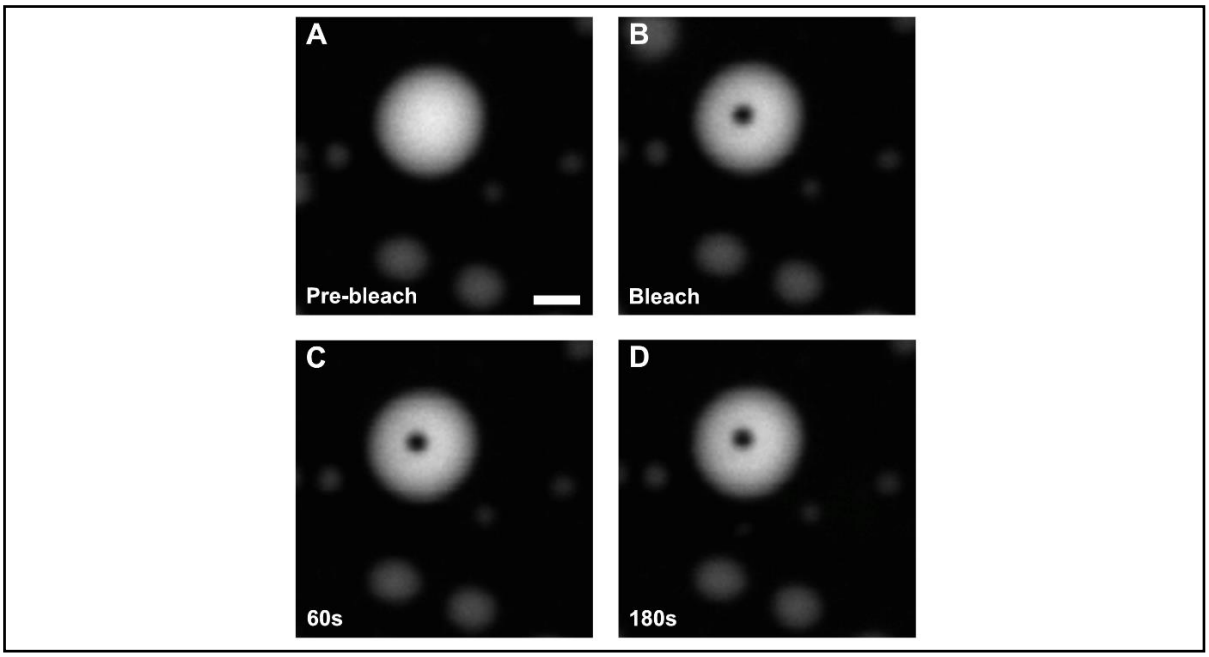

Figure 5.8: Me31B condensates do not exhibit internal re-arrangement of molecules. (A-D) Purified GFP-Me31B condensates (7.5 µm) in the presence of 1% PEG; time lapse images of Me31B condensate before and after photobleaching of a small region inside the condensate. Scale bar: 3 µm.

Simultaneously imaging fusion events and fluorescence recovery post internal photobleaching revealed that while condensate size increased over time, internal mixing was much slower (Figure 5.9). Similar properties have been observed with chromatin condensates *in vitro* (Gibson et al. 2019). These results indicate that Me31B condensates have high surface tension and high internal viscosity.

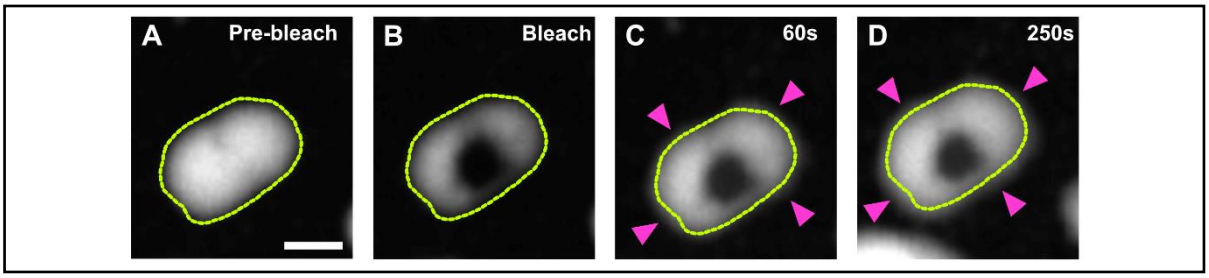

Figure 5.9: Me31B condensates exhibit an increase in size post internal photobleaching. (A-D) Time lapse images of GFP-Me31B condensate before and after internal photobleaching reveal negligible fluorescence recovery. Magenta arrowheads point to excess condensate fluorescence over time, indicating increase in condensate size. Scale bar: 3 µm.

Conclusions: Me31B condensates exhibit exchange of molecules between the condensate and bulk solution until gelation. Condensates, however, display minimal internal rearrangement indicating high internal viscosity.

5.8 *polyA* RNA delays gelation but increases condensate viscosity

Previously, I demonstrated that the presence of *polyA* RNA alone was not sufficient to promote Me31B condensation. However, RNA often regulates the material properties of RNP complexes. RNA has been shown to either increase or decrease the surface tension and/or viscosity of condensates depending on the concentration, sequence, or structure of RNA. To test the effect of unstructured homopolymeric RNA on Me31B condensates, *polyA* RNA was added to the protein buffer. Time lapse imaging of Me31B condensates in the presence of *polyA* RNA revealed that condensates continued to fuse over a time course significantly longer than wild-type (WT) Me31B condensates without RNA (Figure 5.10A-C).

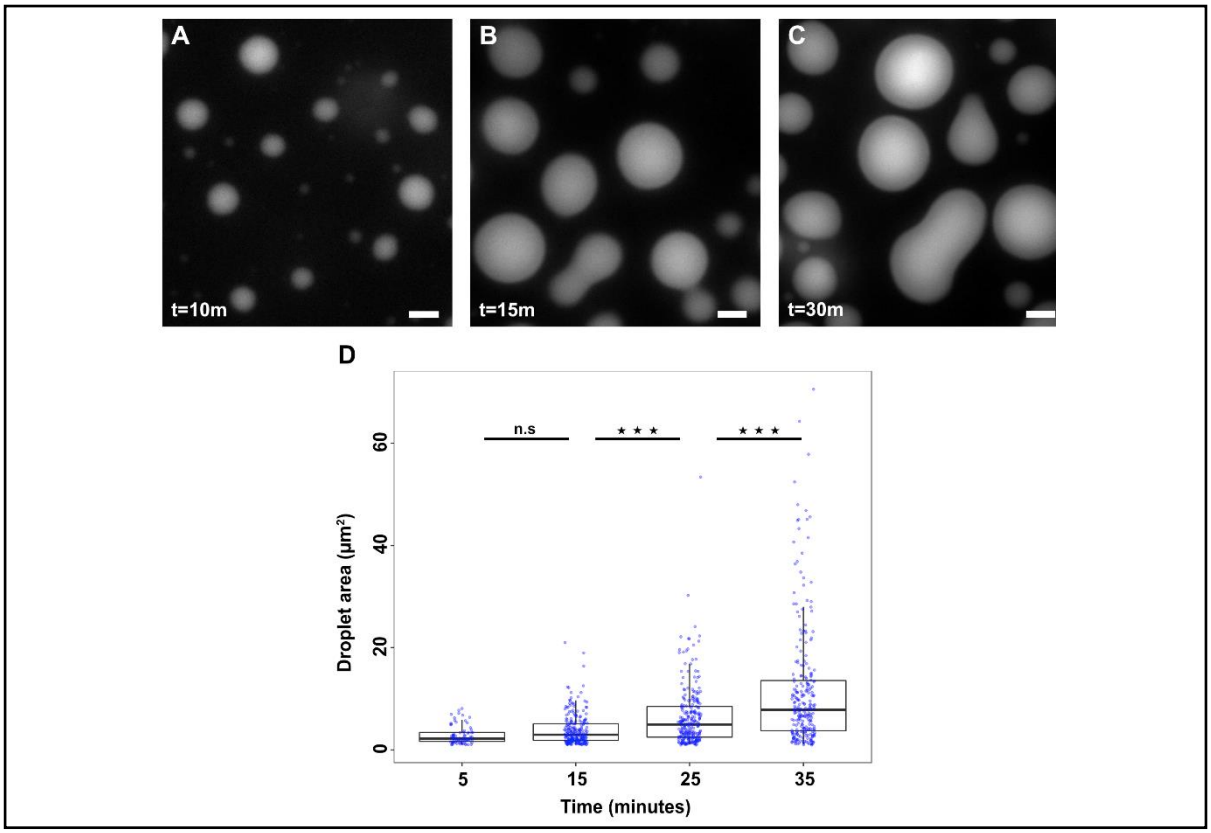

Figure 5.10: *polyA* RNA increases Me31B condensate surface tension. (A-C) Image sequence of purified GFP-Me31B condensates (7.5 µm) in the presence of *polyA* RNA (75ng/µl) at different time points. **(D)** Quantification of Me31B condensate droplet area at different time points post condensation. Non-significant (n.s) between 5 and 15 minutes; $p<0.0001$ between 15 and 25 mins, 25 and 35 minutes. Scale bar: 5µm (A-C).

This was quantified by comparing condensate droplet area at different time points between the two conditions (Figure 5.10D). These results suggest that *polyA* RNA increases surface tension of Me31B condensates.

Me31B condensate fusions in the presence of *polyA* RNA was also recorded using optical tweezers. Fusion events were observed even at 60 minutes post condensation, demonstrating the high surface tension of Me31B condensates in the presence of *polyA* RNA (Figure 5.11).

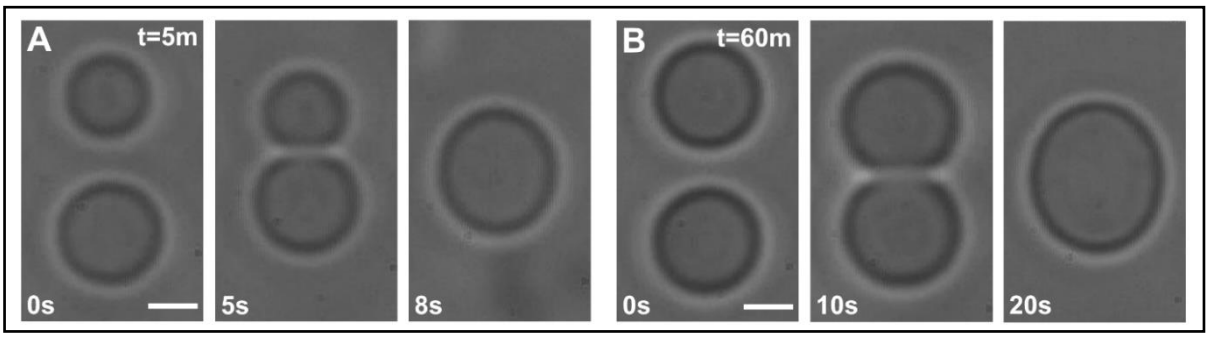

Figure 5.11: Me31B condensates do not display signs of gelation in the presence of *polyA* RNA. (A, B) Image sequence of GFP-Me31B condensate coalescence in the presence of *polyA* RNA (75 ng/µl) using optical traps which display rapid fusion shortly after condensation **(A)**, continue to exhibit relatively faster fusion dynamics at 60 minutes post condensation **(B)**.

The presence of an additional component such as RNA is normally thought to increase condensate viscosity in a two-component system of RNA and protein. To test if *polyA* RNA affects Me31B condensate viscosity, I first performed whole particle FRAP to examine the exchange kinetics between the condensate and bulk solution. Interestingly, there was very minimal fluorescence recovery post photobleaching for newly induced condensates (Figure 5.12A-D). This is supported by the slow exchange kinetics and negligible proportion of mobile Me31B molecules (Figure 5.12E). This indicates that the presence of RNA increases condensate viscosity which prevents or slows down the exchange of molecules between the condensate and bulk solution.

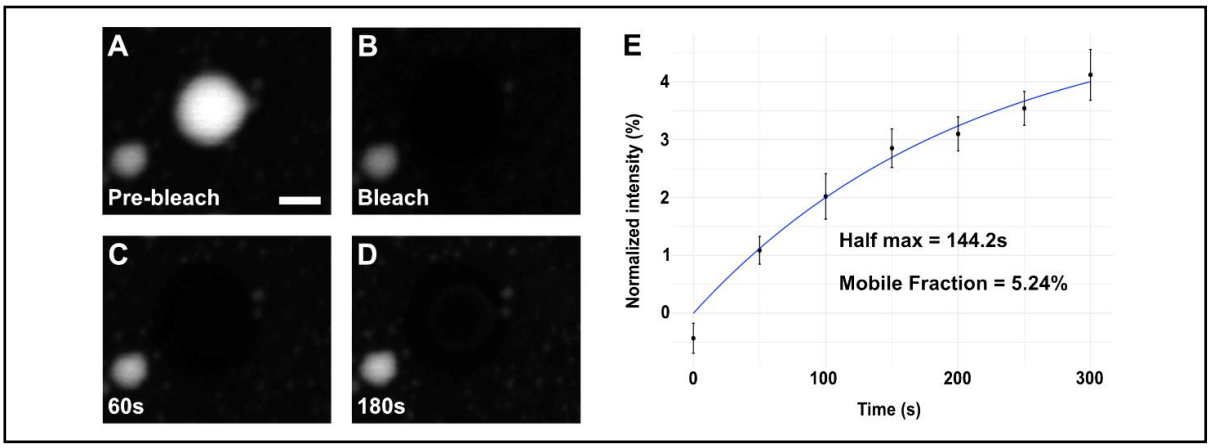

Figure 5.12: Me31B condensates exhibit no exchange of molecules between the condensate and bulk solution in the presence of *polyA* RNA. (A-E) Purified GFP-Me31B condensates (7.5 µm) in the presence of 1% PEG and *polyA* RNA (75ng/ µl). **(A-D)** Time lapse images of Me31B condensate fluorescence recovery before and after photobleaching whole condensate. Scale bar: 10 µm. **(E)** Analysis of whole particle FRAP of Me31B condensates. Standard deviation/data (black), fit (blue), n=8 condensates. Single exponential fits the FRAP curve.

RNA has been shown to increase the internal liquidity of several RNP condensates, therefore, I performed internal FRAP on Me31B condensates post addition of *polyA* RNA. Remarkably, there was no recovery of Me31B molecules post photobleaching (Figure 5.13).

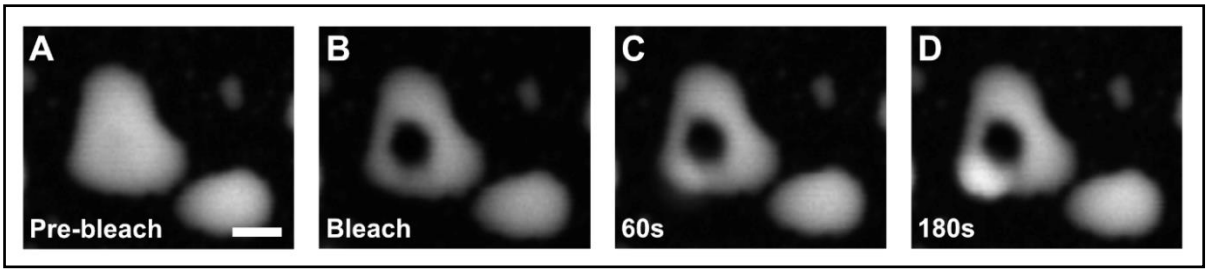

Figure 5.13: Me31B condensates do not exhibit internal re-arrangement of molecules in the presence of *polyA* RNA. (A-D) Purified GFP-Me31B condensates (7.5 µm) in the presence of 1% PEG and *polyA* RNA (75ng/µl); time lapse images of Me31B condensate before and after photobleaching of a small region inside the condensate; scale bar: 10 µm.

Conclusions: *polyA* RNA increases surface tension and viscosity of Me31B condensates.

5.9 *polyA* RNA promotes reentrant phase transition of Me31B condensates over time

In addition to increased fusion and condensate size observed in the previous section, prolonged imaging of Me31B condensates in the presence of *polyA* RNA revealed an additional interesting phenotype. 60 minutes post condensation, condensates displayed large vacuoles, originating primarily from the centre, which were devoid of Me31B (Figure 5.14A). However, longer incubation of Me31B condensates in the presence of *polyA* RNA resulted in complete dissolution of Me31B condensates (Figure 5.14B).

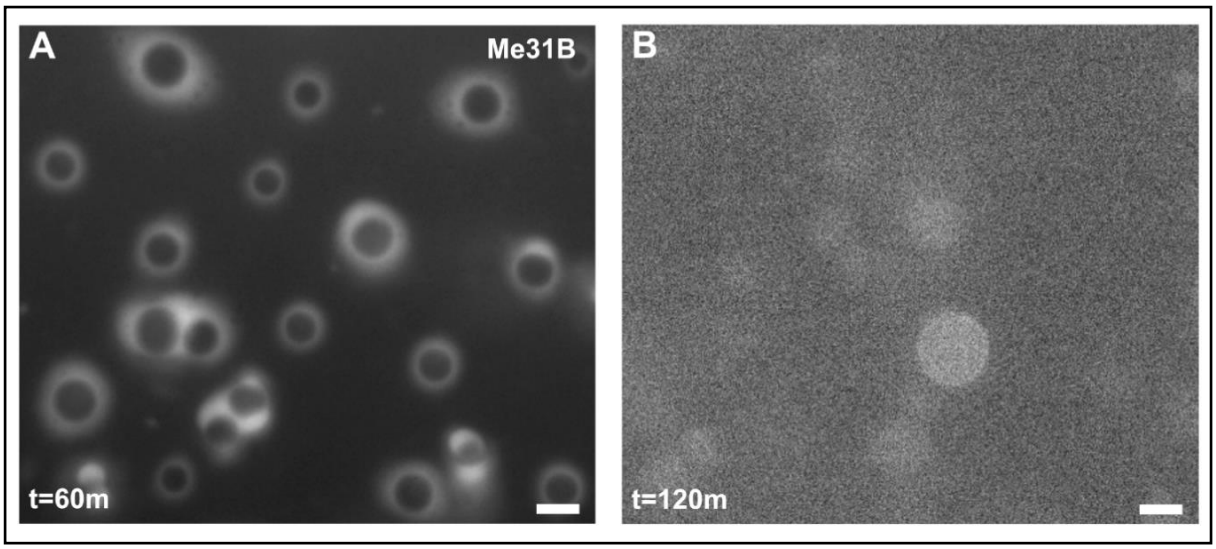

Figure 5.14: Me31B condensates, in the presence of *polyA* RNA, undergo dissolution over time. (A,B) Purified GFP-Me31B condensates (7.5 µm) in the presence of *polyA* RNA (75ng/µl). **(A)** Representative image of Me31B condensates exhibiting giant vacuoles at 60 minutes post condensation, while longer incubation leads to condensate dissolution **(B)**. Scale bar: 5µm (A,B).

These results prompted me to test whether these vacuoles were devoid of RNA as well. To visualise *polyA* RNA distribution, I utilised the F22 RNA binding dye (Li and Chang 2006). Me31B condensates containing *polyA* RNA were treated with the F22 dye and visualised at different time points. For a brief period after condensation, both *polyA* and Me31B co-existed in the condensates, as revealed by their colocalisation (Figure 5.15A-C). However, over time, Me31B condensates began forming vacuoles which preferentially stained for *polyA*. In fact, several condensates exhibited multiple vacuoles in which *polyA* RNA was enriched and these same vacuoles were devoid of Me31B (Figure 5.15D-I).

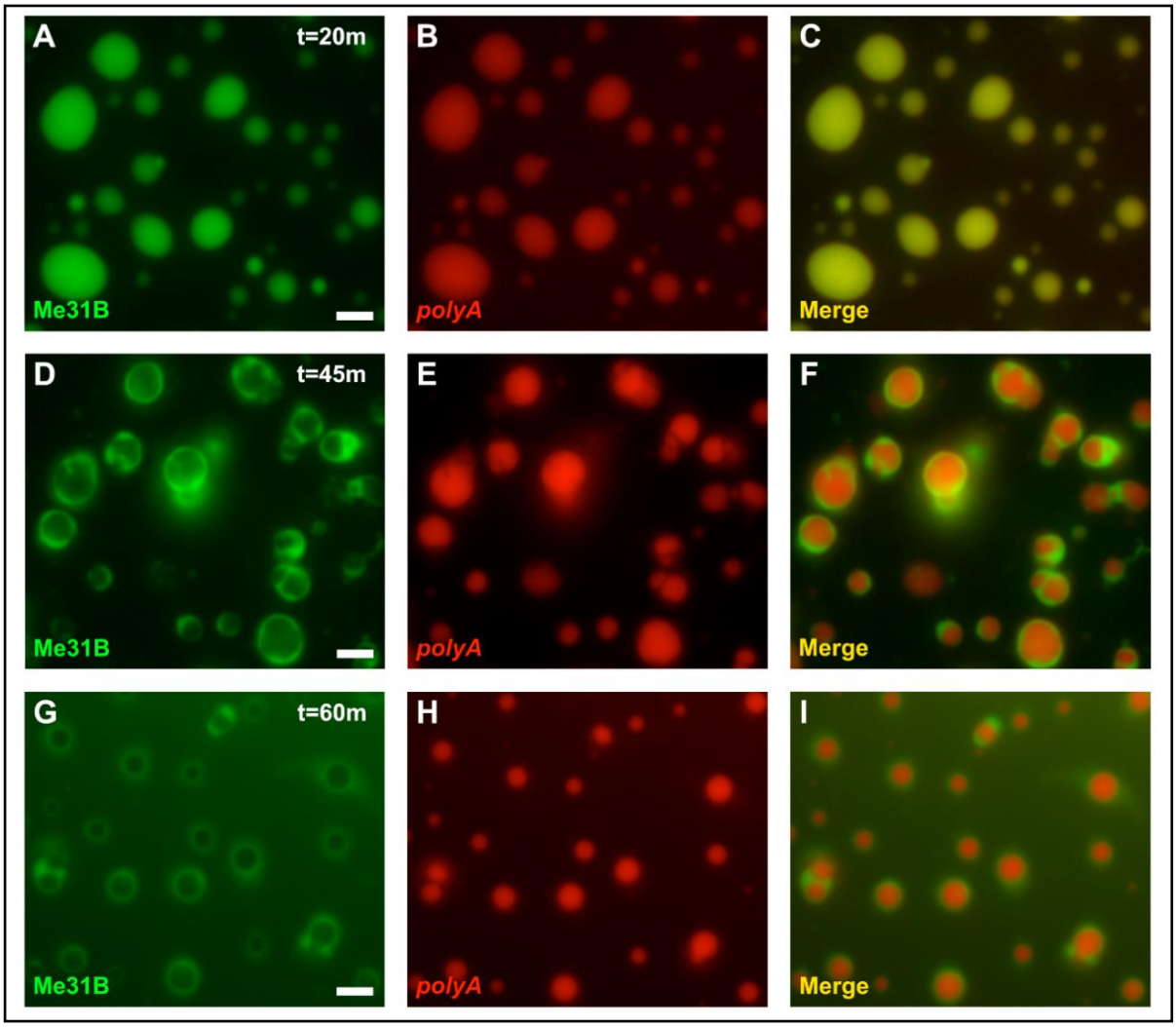

Figure 5.15: *polyA* RNA preferentially partitions into regions of the condensates that are devoid of Me31B. (A-I) Purified GFP-Me31B condensates (7.5 µm) in the presence of *polyA* RNA (75ng/µl) imaged at different time points; *polyA* RNA is detected by F22 RNA binding dye. **(A-C)** Representative images of *polyA* RNA and Me31B partitioned at similar levels inside condensates at 20 mins post condensation, as revealed by the colocalisation **(C)**. **(D-F)** Representative images of condensates exhibiting vacuoles **(D)** and *polyA* RNA preferentially partitioned into regions of condensates devoid of Me31B **(F)** at 45 minutes post condensation. **(G-I)** Representative images of condensates exhibiting vacuoles devoid of Me31B **(G)** and enriched for *polyA* RNA **(I)** at 60 minutes post condensation. Scale bar: 5 µm (A-I).

This type of vacuolisation has been previously demonstrated in RNP coacervates *in vitro*. This phenomenon, called reentrant phase transition, is thought to allow the creation of dynamic internal sub-compartments inside RNP coacervates, primarily driven by RNA concentration and the strength of multivalent interactions promoted by

RNA (Alshareedah et al. 2020; Banerjee et al. 2017; Milin and Deniz 2018). It is likely that initially, the addition of *polyA* RNA leads to the assembly of Me31B condensates in which *polyA* RNA is homogenously partitioned. Over time, as a consequence of multiple fusion events, the concentration of *polyA* RNA, and therefore RNA-RNA interactions inside individual condensates is more favourable than Me31B-RNA and Me31B-Me31B interactions, thereby resulting in Me31B dissolution from, and enrichment of *polyA,* inside the condensates.

Conclusion: Presence of *polyA* RNA induces a reentrant phase transition of Me31B condensates by selective dissolution of Me31B and preferential enrichment of *polyA* RNA.

5.10 *grk* RNA promotes faster gelation but does not induce reentrant phase transition of Me31B condensates

The *polyA* RNA used in previous sections is representative of an unstructured homopolymeric RNA with multiple interaction domains due its long tail of adenine nucleotides. Therefore, increased surface tension of Me31B condensates observed in the presence of *polyA* RNA is likely due to the several weak interactions formed between Me31B and *polyA* RNA. By this logic, addition of a structured RNA would promote less interactions with Me31B due to the availability of less free binding domains. To test this, I used *grk*, a highly structured RNA with multiple secondary structure loops (dos Santos, Simmonds, and Krause 2008). Time lapse imaging of Me31B condensates in the presence of *grk* revealed that within 15 minutes of condensate formation, condensates exhibited signs of gelation (Figure 16A,B). This observation is supported by the quantification of Me31B droplet area over time which shows that the majority of the condensates formed over time do not display a significant increase in size post 15 minutes (Figure 5.16C,D). Additionally, condensate droplet area observed at 15 minutes (~1.5 μm^2) was significantly smaller than WT Me31B condensates in the absence of RNA (~ 4.3 μm^2) quantified at the same time point (Figure 5.4D).

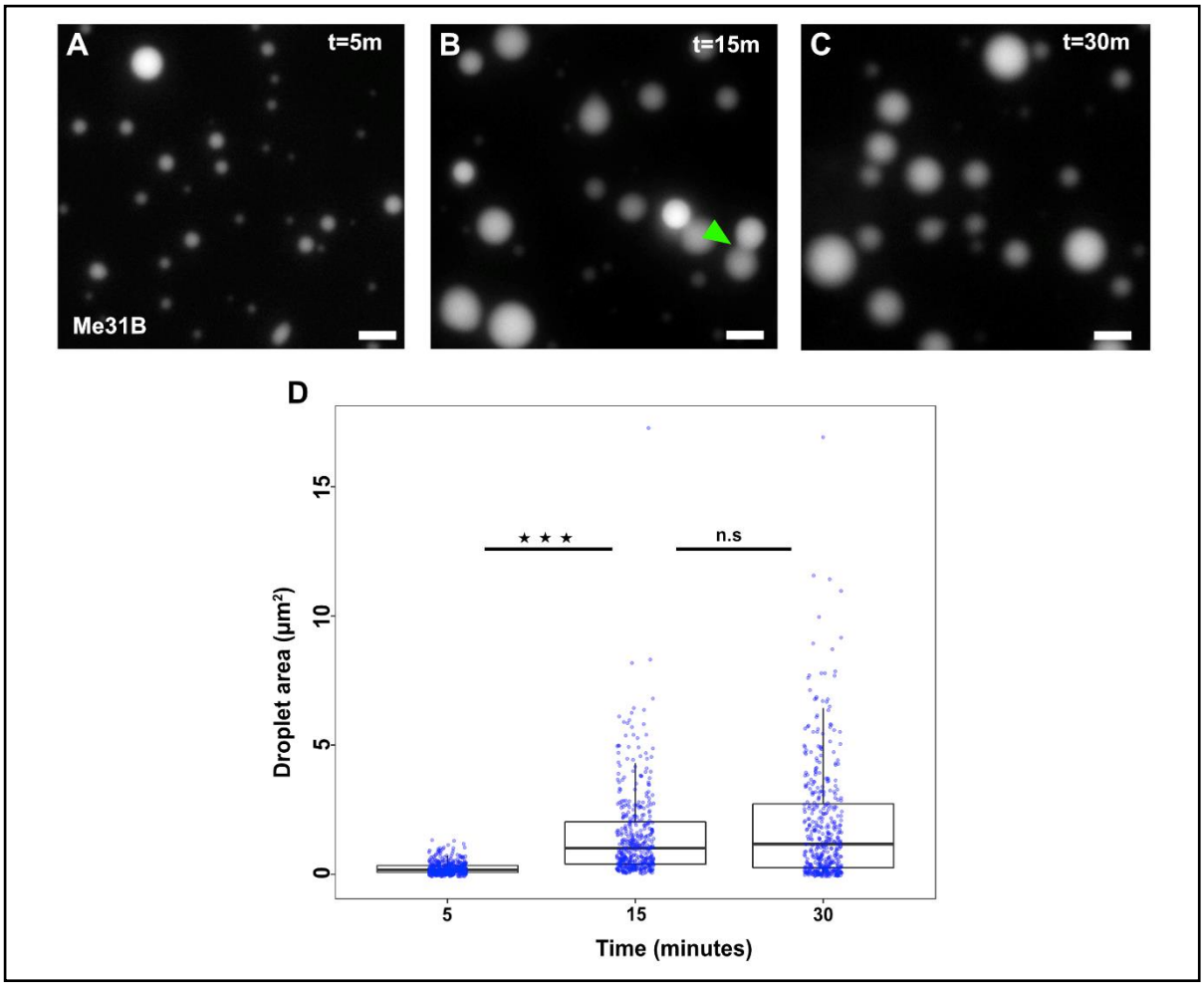

Figure 5.16: *grk* RNA induces faster gelation of Me31B condensates. (A-C) Purified GFP-Me31B condensates (7.5 µm) in the presence of *grk* RNA (75ng/µl) imaged at different time points; granules exhibit gelation behaviour as early as 15 minutes **(B)**. Scale bar: 5 µm. **(D)** Quantification of Me31B condensate droplet area in the presence of *grk* RNA over time.

The faster gelation observed with Me31B condensates in the presence of *grk* RNA was also confirmed by optical tweezer experiments which revealed slow/-incomplete fusion of condensates observed shortly post condensation (Figure 5.17A). Moreover, analysis of scaled fusion kinetics revealed that Me31B condensates continue to exhibit coalescence in the presence of *polyA* but not *grk* RNA, over a time course of 2 hours post condensation (Figure 5.17B).

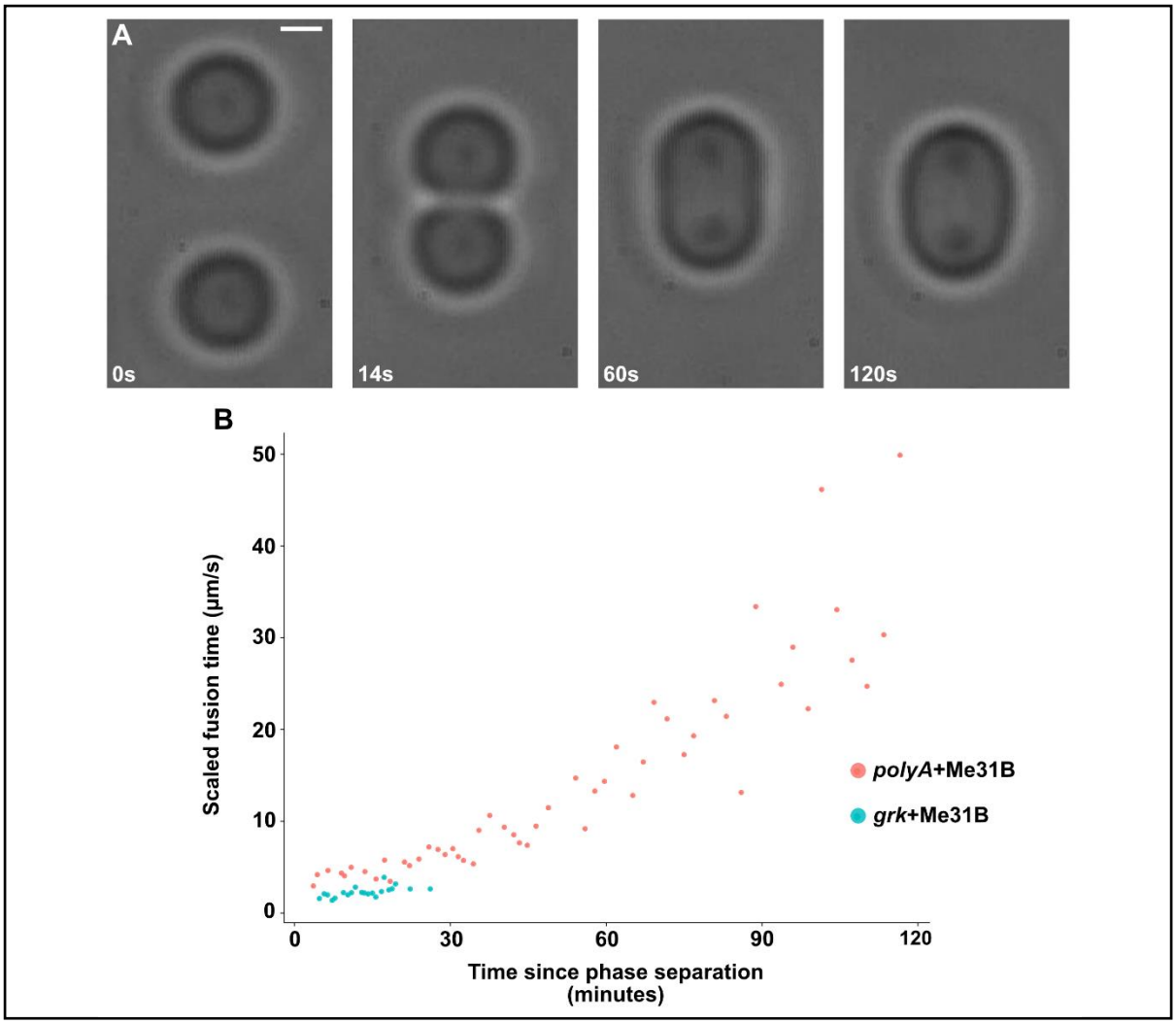

Figure 5.17: Me31B condensates exhibit slower fusion dynamics in the presence of *grk* RNA. (A) Image sequence of GFP-Me31B condensate coalescence in the presence of *grk* RNA (75ng/µl) using optical traps displaying slow fusion dynamics shortly after condensation. Note that even at 120s, the fused condensate has not completely relaxed to a sphere. Scale bar: 1.5 µm. **(B)** Quantification of scaled fusion time for Me31B condensates in the presence of *grk* (green) or *polyA* RNA (orange).

However, it must also be noted that even though condensates in the presence of *polyA* RNA continue to fuse for longer durations, with time, the scaled fusion time also increases, indicating that the transition to a stable gel-state is an intrinsic property of Me31B which can be modulated by specific RNAs.

To test if *grk* also induces a reentrant phase transition of Me31B condensates like *polyA* RNA, condensates containing *grk* RNA were incubated for 45 minutes before being treated with F22 dye. Contrary to *polyA* RNA, Me31B condensates did not

exhibit vacuolisation or differential partitioning of *grk* in the condensates. Instead, both Me31B and *grk* co-existed together inside the condensates (Figure 5.18). This is likely because of the faster gelation induced by *grk*; in the absence of frequent fusion events over time, the strength of Me31B-RNA interactions likely outcompetes RNA-RNA interactions.

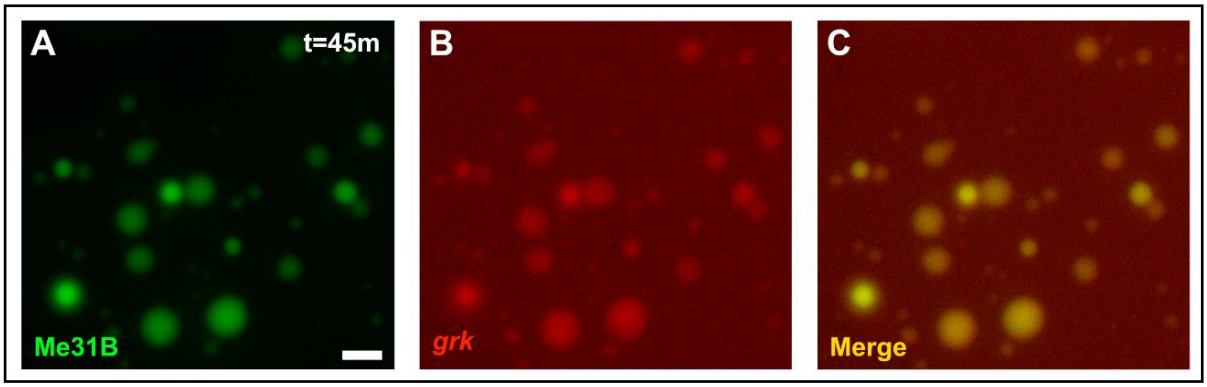

Figure 5.18: *grk* RNA co-localises with Me31B condensates. (A-C) Purified GFP-Me31B condensates (7.5 µm) in the presence of *grk* RNA (75ng/µl) imaged at different time points; *grk* is detected by F22 RNA binding dye. Although *grk* homogeneously partitions inside Me31B condensates as revealed by their colocalisation **(C)**, most of *grk* is in the bulk phase **(B)**. Scale bar: 5 µm.

Conclusions: Presence of *grk* RNA accelerates gelation of Me31B condensates. Unlike *polyA* RNA, *grk* does not cause Me31B dissolution or sub-structure formation inside Me31b condensates. Caveat: Since molarity of RNAs were not controlled for, further experiments are required to further compare the effects of *polyA* RNA versus *grk* RNA.

5.11 $MgCl_2$ promotes rapid condensate fusion and delays gelation

A prominent inter-molecular interaction that regulates phase separation of biomolecular condensates is electrostatic forces. Electrostatics play a key role in driving condensation through interactions between negatively charged RNA molecules and charged protein residues within RNP granules. Besides RNA, an additional source of electrostatic interactions can also be derived from ions (salts). As demonstrated in the previous chapter, ionic concentrations play a crucial role in regulating Me31B granule integrity and material properties. To test how changes in ionic concentration affects Me31B *in vitro*, condensates were treated with the divalent salt, $MgCl_2$. Time

lapse imaging of Me31B condensates showed an increase in condensate size over time, indicating condensate coalescence (Figure 5.19A-C).

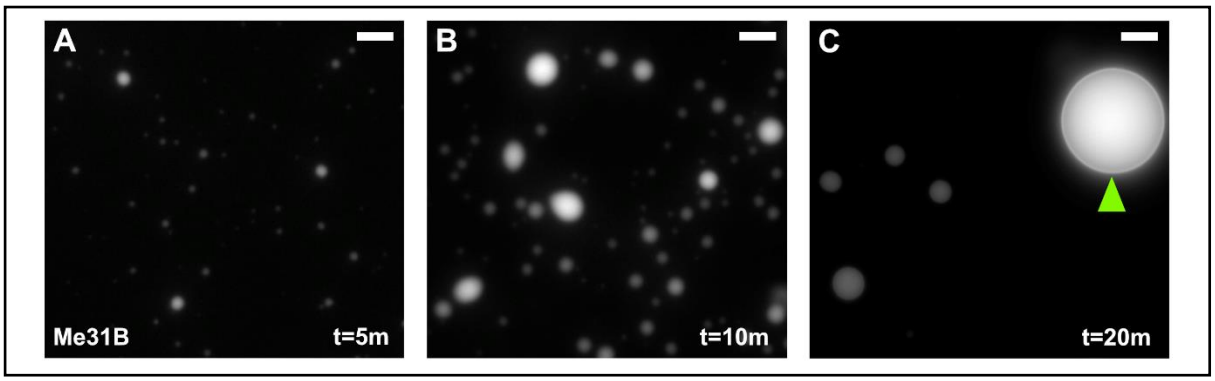

Figure 5.19: $MgCl_2$ increases surface tension of Me31B condensates. (A-C) Purified GFP-Me31B condensates (7.5 µm) in the presence of $MgCl_2$ (5mM) imaged at different time points. Me31B condensate size increases over time, resulting in giant condensates (green arrowhead). Scale bar: 5 µm (A-C).

Enormous condensates could be observed shortly after condensation (Figure 5.19C), suggesting rapid fusion events, significantly faster than WT Me31B condensates in the absence of $MgCl_2$. To confirm if gelation is delayed in these condensates, fusions were quantified by optical tweezers which showed a significantly delayed gelation compared to WT Me31B condensates in the absence of $MgCl_2$, as exemplified by scaled fusion kinetics (Figure 5. 20). These results suggest that $MgCl_2$, like *polyA* RNA, increases surface tension of Me31B condensates and delays gelation.

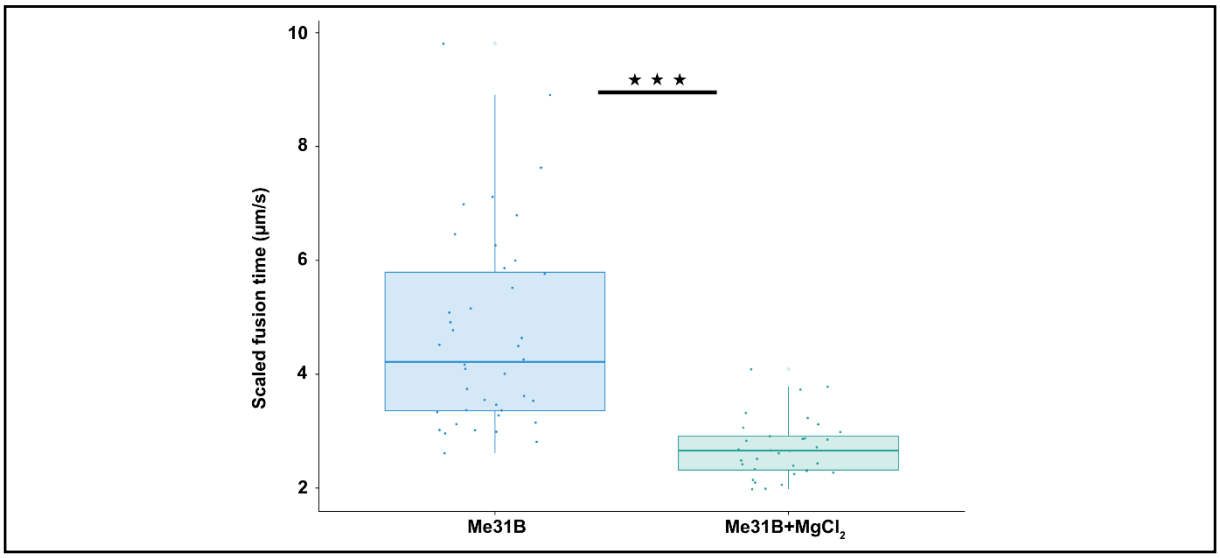

Figure 5.20: Me31B condensates display faster scaled fusion kinetics in the presence of $MgCl_2$. Quantification of scaled fusion time for GFP-Me31B condensates in the absence and presence of $MgCl_2$; $p<0.0001$.

Conclusion: Presence of divalent ion $MgCl_2$ delays Me31B condensate gelation.

5.12 Presence of both *polyA* RNA and $MgCl_2$ accelerates the reentrant phase transition of Me31B condensates

Independent experiments with *polyA* RNA and $MgCl_2$ showed similar effects of delaying Me31B condensate gelation. In the oocyte cytoplasm, however, both these conditions would be expected to co-exist together, giving rise to promiscuous interactions and varied effects on RNP condensates, including P bodies. Therefore, to partially simulate *in vivo* conditions, I used a three-component *in vitro* system of RNA, Me31B and salt to examine how *polyA* RNA and $MgCl_2$, together, would affect Me31B condensates. Addition of *polyA* and $MgCl_2$ induced increased fusion events and resulted in the formation of large condensates (Figure 5.21A,B). However, 30 minutes post condensation, multiple sub-domains inside Me31B condensates could already be observed (Figure 5.22C), similar to the reentrant phase transition previously observed in the presence of *polyA* RNA.

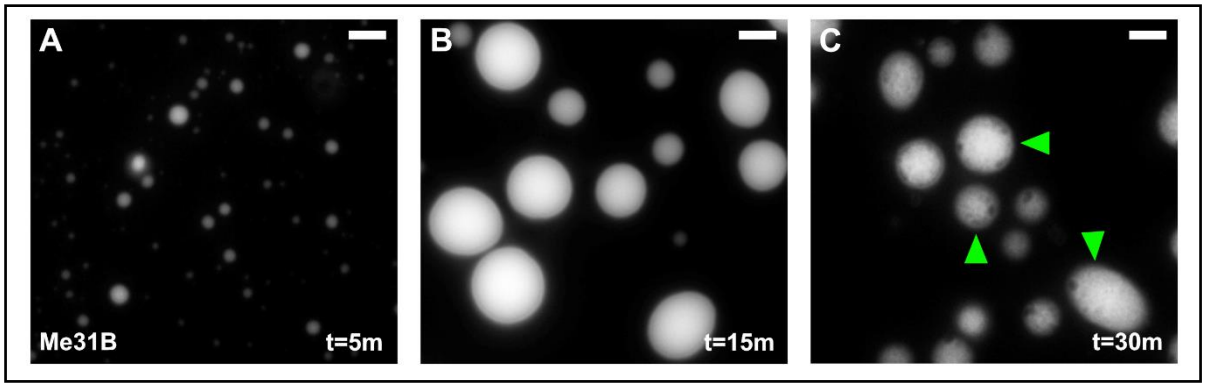

Figure 5.21: $MgCl_2$ and *polyA* RNA, over time, induce compartmentalisation inside Me31B condensates. (A-C) Purified GFP-Me31B condensates (7.5 µm) in the presence of $MgCl_2$ (5mM) and *polyA* RNA (75ng/µl) imaged at different time points. **(B)** Condensates exhibit increased droplet size and appear homogeneous at 15 minutes post condensation. **(C)** 30 minutes post condensation, condensates begin to display multiple sub-domains (green arrowheads), indicative of heterogeneous internal structuring. Scale bar: 5 µm (A-C).

To test if *polyA* RNA is compartmentalised inside these sub-domains, condensates were treated with the F22 dye. While *polyA* RNA and Me31B co-existed together inside condensates shortly post condensation (Figure 5.22A-C), over time, *polyA* RNA was localised inside sub-domains devoid of Me31B (Figure 5.22D-F). It is likely that increased electrostatic interactions contributed by both *polyA* and $MgCl_2$ are stronger

and, therefore, more favourable than Me31B-Me31B interactions, which causes internal compartmentalisation by gradual dissolution of Me31B.

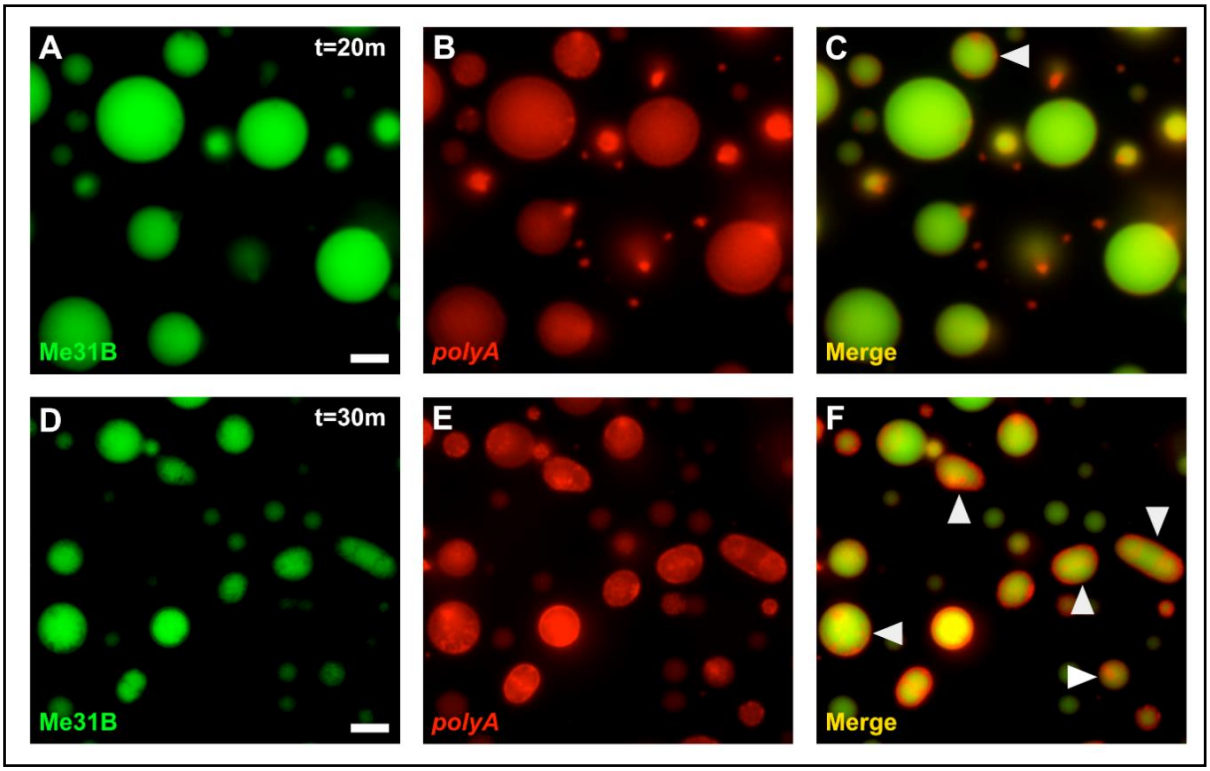

Figure 5.22: *polyA* RNA is differentially partitioned inside Me31B condensate sub-domains. (A-F) Purified GFP-Me31B condensates (7.5 µm) in the presence of $MgCl_2$ (5mM) and *polyA* RNA (75ng/µl) imaged at different time points. **(A-C)** While in majority of the condensates *polyA* RNA and Me31B partitioned at similar levels as revealed by the colocalisation, some condensates already display sub-domains where *polyA* is partitioned (white arrowhead). **(D-F)** 30 minutes post condensation, most condensates exhibit multiple sub-domains inside which *polyA* is preferentially segregated (white arrowheads). Scale bar: 5 µm (A-F).

Presence of $MgCl_2$ alone did not induce compartmentalisation, suggesting that *polyA* RNA is essential for the induction of this reentrant phase transition, while $MgCl_2$ simply accelerates the process.

Conclusion: Presence of *polyA* RNA and $MgCl_2$ induce compartmentalisation inside Me31B condensates, resulting in preferential segregation of *polyA* into these compartments.

5.13 Me31B contains two short disordered regions

Having tested the effect of various factors on Me31B condensates, the underlying question was: 'what sequence/structural features of Me31B contribute to condensate phase separation and material properties?'. IDRs of several RBPs have been shown to greatly influence RNP phase behaviour (Elbaum-Garfinkle et al. 2015; Nott et al. 2015; Smith et al. 2016; Wang et al. 2018). Whether proteins contain IDRs or not can be determined using IDR prediction algorithms. To determine if Me31B protein contains IDRs, I used the disorder prediction algorithm, IUPred (Dosztányi 2018; Dosztányi et al. 2005). Sequence analysis revealed that the N terminal region (~50 residues) and the C terminal region (~17 residues of Me31B) are highly disordered compared to the remaining structured proportion of Me31B (Figure 5.23).

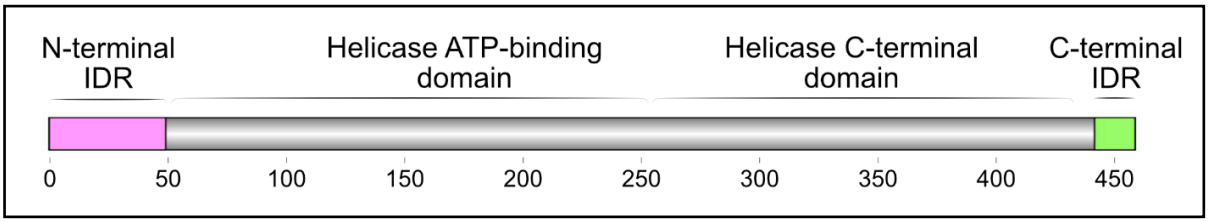

Figure 5.23: Overview of Me31B domain architecture. Schematic representation of Me31B domain architecture displaying two short disordered regions, one in the N-terminus (magenta) and one in the C-terminus (green), on either side of the structured helicase domains.

Me31B belongs to a conserved class of DEAD-box RNA helicases that regulate various aspects of RNA metabolism. Sequence analysis of Me31B orthologues DDX6 (humans) and Dhh1 (yeast) revealed long disordered regions in their N and/or C terminal domains, albeit with considerable variations in the IDR lengths (Figure 5.24). While our understanding of the sequence determinants for phase separation is still rudimentary, it is widely accepted that IDRs can exist in different forms. Sequence variations are thought to influence IDR length, which likely determine emergent properties and material states of condensates.

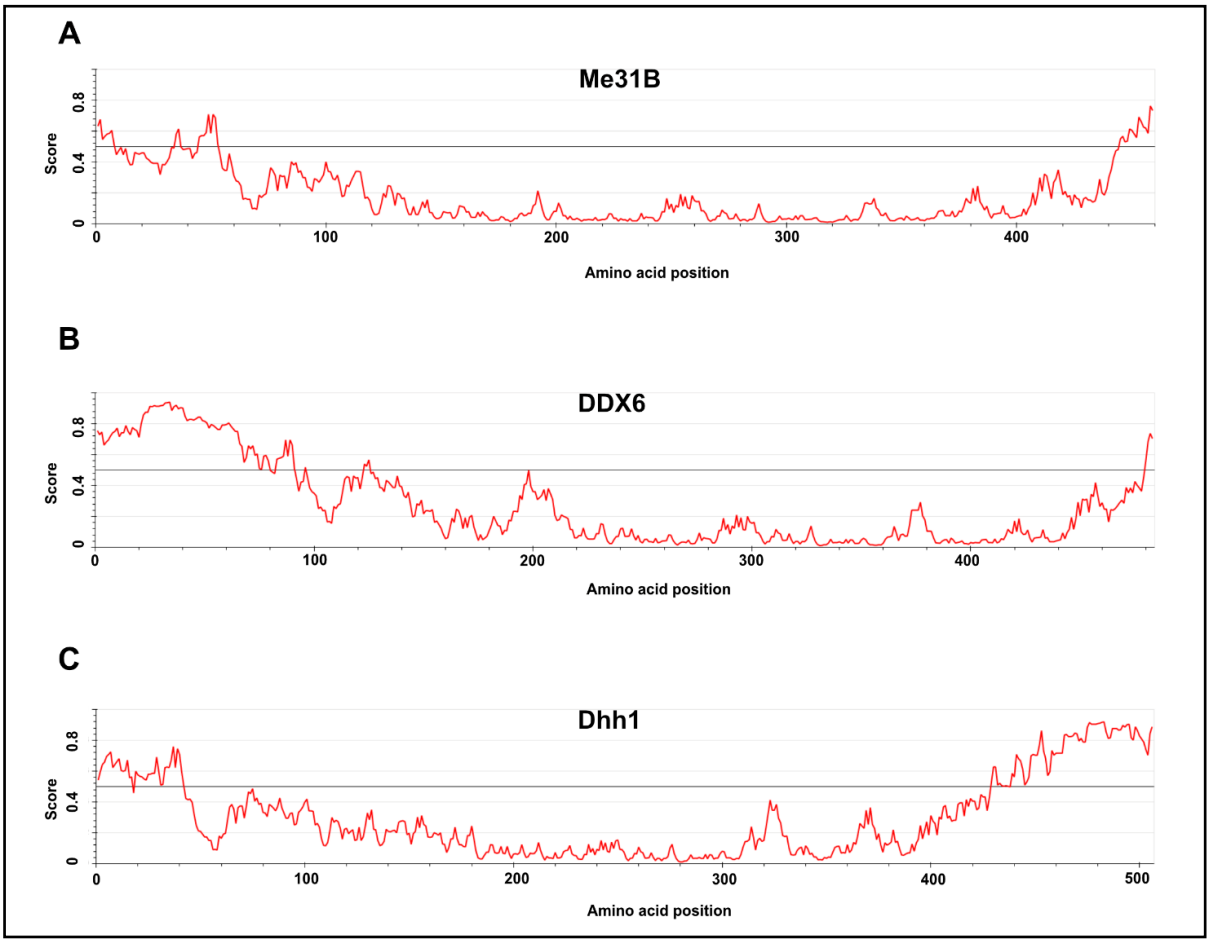

Figure 5.24: IDRs of different DDX6 orthologues have diverged significantly. (A-C) Schematic displaying domain architecture of different orthologues of DDX6 family of RNA helicases analysed by IUPred. A score above 0.5 represents strong disorder. While Me31B contains two short disordered regions on the N and C-terminus **(A)**, human DDX6 exhibits a long N-terminal and a short C terminal disordered region **(B)**. Contrary to DDX6, yeast Dhh1 exhibits a long C-terminal and a short N-terminal disordered region **(C)**.

Conclusion: Me31B contains two disordered regions which are significantly shorter than the human (DDX6) and yeast orthologues (Dhh1).

5.14 Loss of IDRs causes aggregation of Me31B condensates

In the majority of RNP phase separation studies *in vitro*, IDRs have been shown to be important for driving phase separation (Franzmann and Alberti 2019; Lin, Currie, and Rosen 2017). However, in some cases, IDRs also regulate the material properties of condensates. Since Me31B possesses significantly shorter disordered regions than conventional IDRs, I hypothesised that IDRs may help regulate condensate properties rather than drive their assembly. To test the role of IDRs, Me31B lacking both N- and

C-terminal IDRs (Me31BΔNC) were purified. First, I examined whether Me31BΔNC could form condensates in the absence of PEG. Live imaging revealed that Me31BΔNC failed to form condensates (Figure 5.25A), indicating no role for IDRs in Me31B condensation. To test if loss of IDRs affected condensate material properties, Me31BΔNC protein was added to the protein buffer containing 1% PEG. Shortly post-condensation, Me31BΔNC formed tiny condensates which readily showed signs of gelation (Figure 5.25B). To examine if condensates coalescence occurs over time, condensates were imaged over a time course of 30 minutes. Time lapse imaging revealed that Me31BΔNC condensates failed to undergo any fusion. Instead, they displayed multiple networks of condensates sticking to each other, suggesting aggregation-like property, rather than gelation (Figure 5.25C).

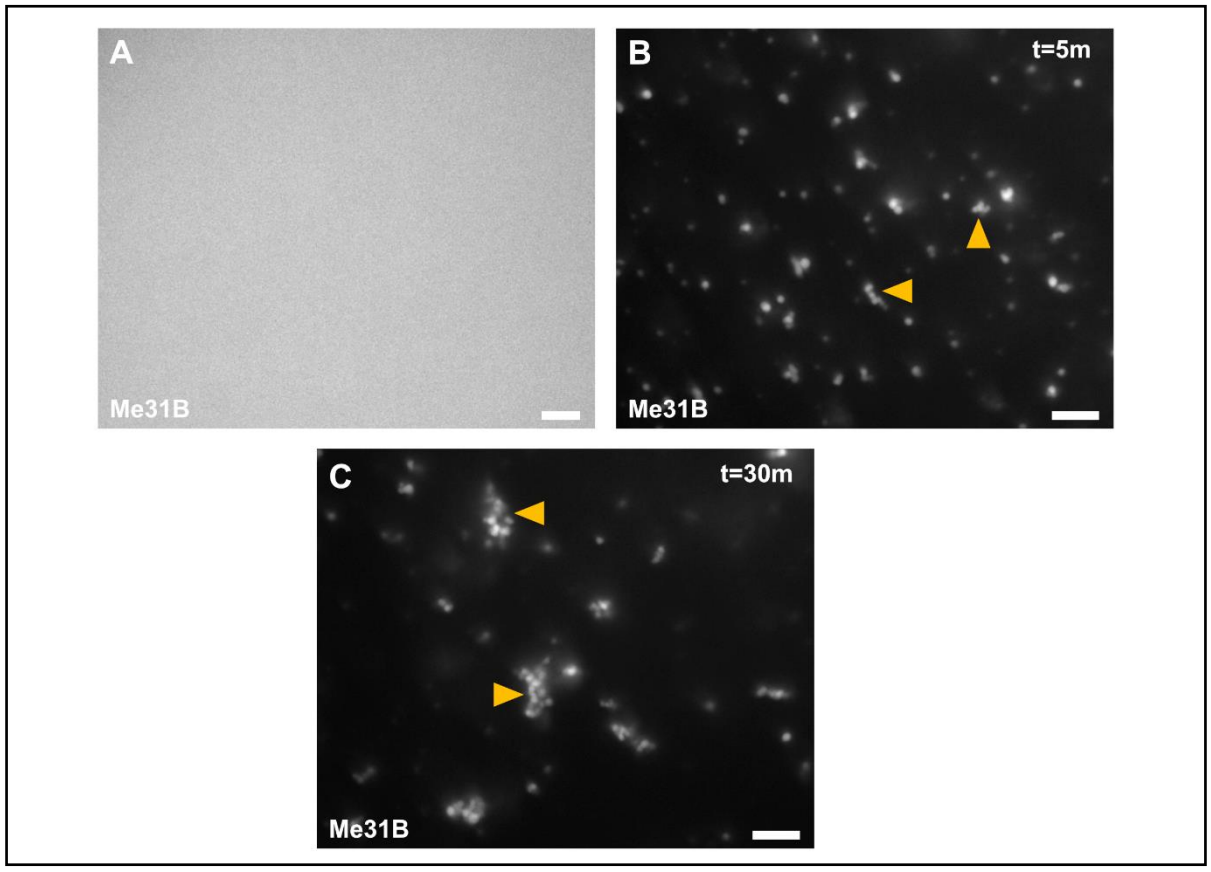

Figure 5.25: Loss of IDRs prevents Me31B condensate coalescence. (A) Purified GFP-Me31BΔNC (7.5 µm) does not form condensates by itself; scale bar: 5 µm. **(B,C)** Purified Me31BΔNC (7.5 µm) in the presence of 1% PEG form condensates; shortly post condensation, condensates start forming network of aggregates (yellow arrowheads). Scale bar: 5 µm (B,C).

To verify whether these condensates exhibited accelerated gelation, Me31BΔNC condensate fusion events were examined using optical tweezers. Strikingly, shortly after condensation, condensates began sticking to each other with deformed morphologies (Figure 5.26), indicative of aggregation.

These results suggest that IDRs likely regulate condensate material properties by preventing aggregation of Me31B. Furthermore, since IDRs are not necessary to induce Me31B condensation, folded domains of Me31B may play a primary role in driving phase separation of Me31B condensates.

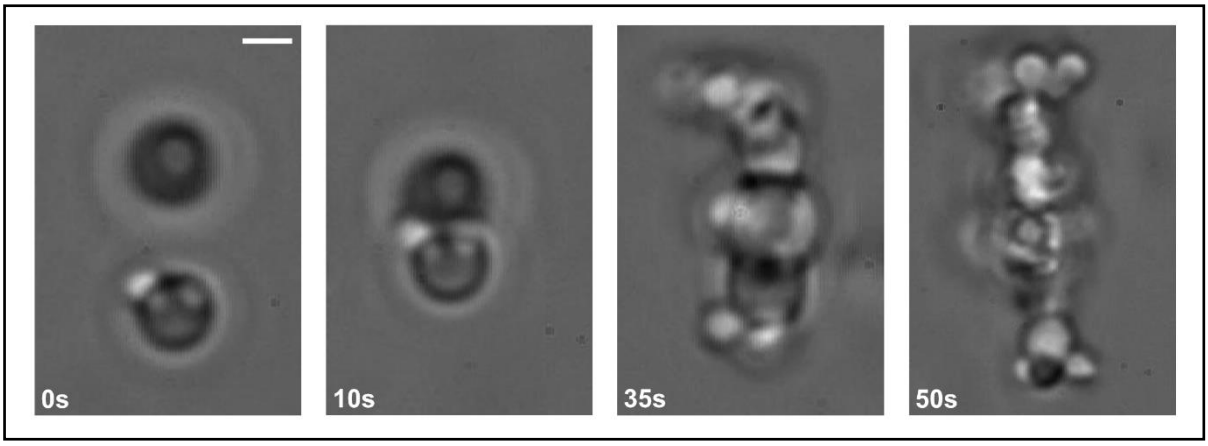

Figure 5.26: Me31B condensates display aggregation behaviour in the absence of N- and C-terminal IDRs. Image sequence of GFP-Me31BΔNC condensates using optical traps displaying multiple condensates sticking to each other shortly after condensation, indicating aggregation. Scale bar: 1.5 µm.

Conclusion: IDRs are not required to drive Me31B condensation, however, loss of IDRs causes aggregation of PEG-induced Me31B condensates.

5.15 Addition of *polyA* RNA prevents accelerated gelation of Me31BΔNC condensates

Results from the previous section showed that while IDRs are not required to drive Me31B condensation, loss of IDRs caused aggregation of Me31B condensates. This suggests that the folded domains of Me31B likely facilitate condensation of Me31B. In previous sections, I have demonstrated the role of the long homopolymeric *polyA* RNA (3K) in delaying Me31B condensate gelation. To test if addition of RNA prevents or delays aggregation of Me31BΔNC, *polyA* RNA was added to Me31BΔNC condensates. Interestingly, the presence of *polyA* RNA induced the formation of phase

separated condensates similar to the WT Me31B condensates (Figure 5.27A). The observed result is likely due to the resulting multivalent interactions between *polyA* and Me31B folded domains, thereby preventing aggregation.

However, over a time course of 30 minutes, Me31BΔNC condensates undergo gelation (Figure 5.27B), contrary to frequent fusion events observed for WT Me31B condensates in the presence of *polyA* RNA along the same time course. This indicates that while the presence of RNA alone is sufficient to prevent accelerated aggregation of Me31B condensates, IDRs are important to regulate material properties over longer periods of time.

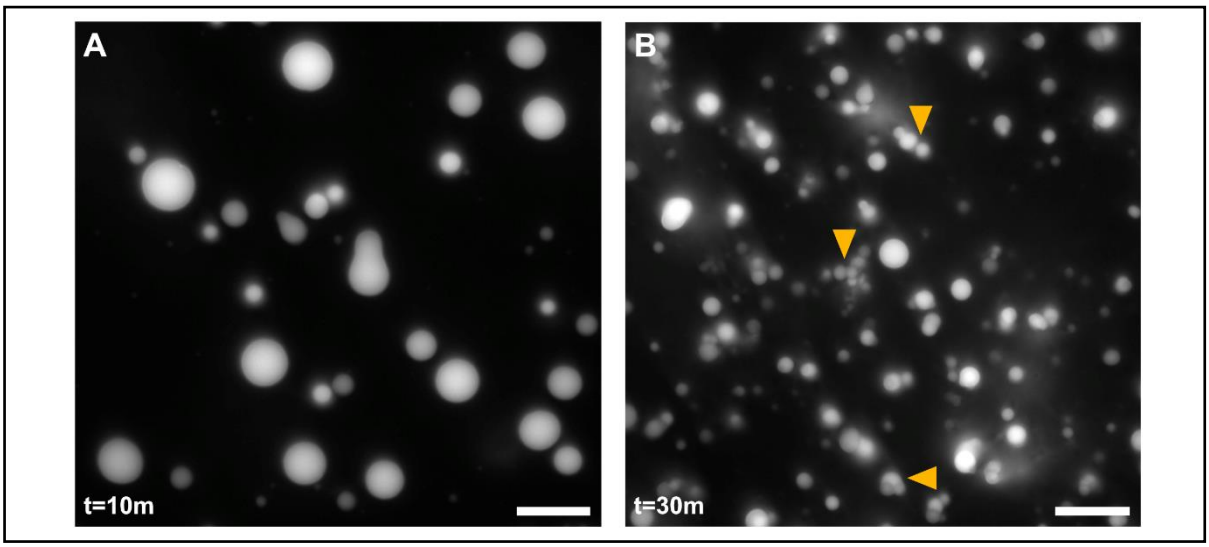

Figure 5.27: *polyA* RNA prevents aggregation of Me31BΔNC condensates. (A,B) Purified GFP-Me31BΔNC (7.5 µm) condensates in the presence of 1%PEG and *polyA* RNA (75ng/µl). **(A)** Me31BΔNC forms liquid-like condensates shortly post condensation. **(B)** 30 minutes post condensation, Me31BΔNC condensates undergo gelation (yellow arrowheads). Scale bar: 10 µm (A,B).

Conclusion: Presence of *polyA* RNA prevents the aggregation of Me31BΔNC condensates.

5.16 Summary of results

In the previous chapters, I described the biophysical properties exhibited by Me31B granules (representative of P bodies) in the mature oocyte and early embryo, providing insights into the potential role of granule material states in RNA regulation. To better understand the factors and sequence determinants that regulate P body material properties, I have studied the phase separation and material properties of *in vitro* reconstituted Me31B. Using live imaging, my data shows that purified Me31B undergoes phase separation in the presence of very low concentrations of crowders such as PEG and Ficoll. Using optical tweezers and live imaging, my data shows that Me31B condensates exhibit high viscosity and undergo gelation, over time. While addition of unstructured *polyA* RNA and $MgCl_2$ independently delay gelation, presence of the structured *grk* RNA promoted faster gelation of Me31B condensates. Longer exposure to *polyA* RNA, but not *grk* RNA, induced reentrant phase behaviour of RNA, resulting in the dissolution of Me31B and enrichment of *polyA* RNA inside the condensates. Finally, two short disordered regions within the Me31B protein were identified, one in the N-terminus and the other in the C-terminus. Both IDRs are not necessary for Me31B condensation, however, they are important to prevent the aggregation of Me31B condensates.

5.17 Discussion

5.17.1 Similarities between *in vitro* and *in vivo* Me31B condensates

Since Me31B is an essential protein for oocyte development and survival, studying the intrinsic properties of Me31B *in vitro* provided a more direct and easier approach to understand how P body material states could be regulated *in vivo*. However, it is key to evaluate the similarities of *in vitro* reconstituted condensates to *in vivo* Me31B granules to draw meaningful interpretations:

1. *In vitro* Me31B condensation is strongly dependent on crowding, which helps increase local concentration of Me31B protein, which likely contributes to condensate assembly. Me31B condensates also exhibit liquid-like characteristics including spherical morphology and frequent fusion events. Similar results were found for *in vivo* P bodies extruded into oil, indicating that the observed liquid-like features are likely an intrinsic property of Me31B.

2. Addition of RNA not only increased surface tension, but also increased the size of Me31B condensates, indicating that RNA may influence condensate size. *In vivo*, P body size is significantly larger in the mature oocyte compared to the early embryo. While P bodies in the mature oocyte contain several maternal RNAs, it is likely that embryonic P bodies are devoid of RNAs. This idea was supported by observations for the maternal mRNA, *bcd*, which did not associate with P bodies re-formed post activation, indicating that RNA likely influences P body size during early development. Additional evidence for Me31B granule dissociation post RNase A treatment also corroborates the likely regulation of granule size by RNA.

3. Me31B granules in the mature oocyte exist in an arrested state and exhibit negligible exchange of molecules between the P bodies and cytoplasm, while embryonic Me31B granules exhibit significantly more exchange of Me31B molecules. Interestingly, *in vitro* reconstituted Me31B exhibits exchange of molecules between the condensate and bulk solution but this exchange is significantly reduced in the presence of *polyA* RNA. These results strongly support the model that embryonic P bodies are devoid of RNA, which likely contributes to their differential exchange kinetics compared to the mature oocyte.

These observations suggest that despite the absence of several factors which regulate Me31B granules *in vivo*, *in vitro* reconstituted Me31B displays characteristics that substantially simulate *in vivo* behaviour.

5.17.2 Effects of structured versus unstructured RNA

RNA has recently emerged as an important biomolecule in driving and regulating RNP phase separation. Much of RNA's control over the material properties of condensates is largely attributed either to the intrinsic features of the RNA itself such as length and structure, or modulation of interaction network or strength of interaction with the associated proteins. Addition of *polyA* RNA and *grk* RNA affected Me31B condensates in contrasting manners, one delayed gelation while the other promoted faster gelation.

Due to its length, *polyA* RNA can adopt multiple configurations, thereby establishing an interactive network that supports condensation, while sequences hidden within structured regions of *grk* RNA are much less likely to interact with other molecules, thereby preventing additional interactions and driving gelation. RNA is normally considered as a fairly transient molecule with short half-life; however, this is not the case in mature oocytes which rely heavily on stable maternal mRNAs. It is therefore possible that a combination of highly structured and less-structured RNAs regulate P body viscosity, size, and material properties during oogenesis.

5.17.3 Reentrant phase transition and condensate compartmentalisation

Several multicomponent systems have been shown to display reentrant phase transition behaviour, often induced by factors such as temperature and oppositely charged ions which create a state of mutual miscibility of multiple phases at specific concentration ranges. RNA also has been proposed to act as a buffer system that regulates the assembly and disassembly of condensates at specific concentrations (Banerjee et al. 2017; Maharana et al. 2018). My results show that long exposures to *polyA* RNA resulted in the formation of vacuoles inside Me31B condensates which were preferentially enriched for *polyA* RNA. This indicates a reentrant phase transition induced by excess *polyA* RNA concentration, likely as a result of continuous condensate fusions, resulting in the subsequent dissolution of Me31B. Interestingly, this reentrant phase transition was accelerated in the presence of both *polyA* RNA and

$MgCl_2$ indicating that such reentrant phase transitions may more generally allow the formation of dynamic sub-compartments inside *in vivo* RNP condensates.

5.17.4 Regulation of Me31B condensate material properties by IDRs

Disordered regions often serve as linker sequences that connect folded domains of proteins and participate in both driving and regulating phase separation. Deletion of both disordered regions causes aggregation of Me31B condensates, indicating that IDRs likely function in regulating Me31B material properties. Alternatively, IDRs may play a regulatory role by preventing folded domains of multiple Me31B proteins from interacting/-sticking to each other, thereby preventing aggregation. Whether both IDRs are essential for this regulation is unclear and requires further investigation. It is possible that individual IDRs may contribute differentially as has been demonstrated for IDRs in the stress granule protein Ded1p (Iserman et al. 2020). Due to their positioning on the N- and C- terminal ends of the Me31B protein, IDRs may induce a closed loop structural conformation by interacting with each other. This idea is supported by results which revealed the prevention of Me31BΔNC aggregation in the presence of RNA. Multivalent interactions induced by RNA mirror the likely function of IDRs by preventing 'sticking' of folded domains. Extending this model to the *in vivo* context, a closed loop conformation may promote the gel-like material state of P bodies in the mature oocyte by minimizing the frequency of weak interactions that facilitate LLPS. Furthermore, in the early embryo, the closed loop conformation induced by IDRs likely prevents aggregation of P bodies in the absence of stored RNAs.

5.18 Future directions

5.18.1 Investigating Me31B properties using phase diagrams

Currently, Me31B phase separation and material properties have been tested under fairly fixed conditions as demonstrated by the usage of PEG, RNA, and salt at recommended concentrations used for other RBPs, to study Me31B phase behaviour. Understanding Me31B condensation and the underlying inter-molecular forces in further detail requires systematic testing of different conditions such as temperature, pH, salt, and RNA/protein concentration using a phase diagram, a schematic way of representing phase behaviours of molecules and how the propensity for condensation

or dissolution is affected across different conditions (Alberti, Gladfelter, and Mittag 2019).

5.18.2 Examining the molecular determinants underlying reentrant phase transition

Reentrant phase transition observed for Me31B condensates in the presence of *polyA* only and *polyA* RNA and $MgCl_2$ opens up several interesting trajectories for further investigation. Varying the concentrations of *polyA* RNA or salts ($MgCl_2$ or NaCl) could be used to determine if internal structuring of Me31B condensates can be modulated as a function of RNA or salt levels. Heating *in vitro* transcribed *grk* RNA at high temperatures would disrupt its secondary structures. Therefore, addition of less structured *grk* RNA could provide insights into the role of RNA structure in the induction of reentrant phase transition. Finally, excess Me31B protein could be added to the condensates post induction of reentrant phase transition to see if vacuolization could be reversed. This will help demonstrate whether the observed reentrant phase behaviours are reversible or not.

5.18.3 Testing the roles of individual IDRs and their functions

Deletion of short IDRs on either end of Me31B promotes the aggregation of condensates, indicating their role in regulating Me31B material state. However, whether both IDRs are required to accomplish this regulation is not clear. It is also important to validate and test the functional implications of the closed loop conformation model of Me31B condensates proposed earlier.

Testing Me31B condensate properties in the absence of individual IDRs (Me31BΔC and Me31BΔN) could be used to determine whether N- and C-terminal disordered regions have differential effects. Additionally, using solution-state NMR spectroscopy, the closed loop conformation model could be tested by studying the intermediate conformations adopted by Me31B condensates in the different IDR mutants. Since IDRs appear to prevent Me31B aggregation, likely by burying folded domains, a key question is whether this might have any functional relevance. Using extracts from mature oocytes, *in vitro* translation assays in the presence of WT Me31B condensates or different IDR mutants whether IDRs and the proposed structural conformation have a functional role in translational regulation. Additionally, generating transgenic mutant

flies with the different combinations of IDR deletions could inform the significance and functions of the IDRs in regulating P body assembly and properties, *in vivo*.

Chapter 6

Investigating Trailer hitch granule properties and function in the mature oocyte.

6.1 Introduction

The formation of RNP granules such as P bodies is largely governed by multiple multivalent interactions. While the precise mechanistic details underlying their formation is not fully clear, P bodies contain thousands of proteins and RNAs (Hubstenberger et al. 2013), and it is likely that diverse components act in concert to promote P body assembly and integrity. In *Drosophila*, several components which localise to P bodies have been identified, however much less is understood in terms of whether specific scaffold or client proteins exist. Throughout the thesis thus far, I have visualised and demonstrated the properties of P bodies using Me31B, a highly structured protein as revealed by its domain architecture. Since P bodies contain several structurally distinct proteins, I wanted to examine whether disordered proteins within P bodies exhibited properties different to that of Me31B. To address this, I have studied the properties of Trailer hitch (Tral), a highly conserved member of the LSm protein family (RAP55 in vertebrates, CAR-1 in *C-elegans*) and a key component of *Drosophila* P bodies (Bouveret 2000; Decker and Parker 2006; Götze et al. 2017; Monzo et al. 2006; Tanaka et al. 2006; Wilhelm, Buszczak, and Sayles 2005). Tral has been implicated in multiple functions during *Drosophila* oogenesis which include: (a) secretion of gurken protein, key dorso-ventral patterning factor and yolkless, the vitellogenin receptor (Herpers and Rabouille 2004; Wilhelm et al. 2005); (b) translational repression of maternal mRNAs as part of the P body complex (Bouveret 2000; Hara et al. 2018) and; (c) normal endoplasmic reticulum exit site formation. Tral expression is not just confined to the germ line but is also found in cultured *Drosophila* S2 cells (as a component of somatic P bodies) and neurons (as a component of neuronal transport granules). The presence and role of Tral in the germline and somatic P bodies, and neuronal granules suggests a more general role for Tral in RNA metabolism, in addition to regulating maternal RNAs during *Drosophila* oogenesis (Tritschler et al. 2007, 2008, 2009).

Both Me31B and Tral are thought to contain a modular domain architecture that facilitates their interaction with additional P body proteins and RNAs. In fact, structural studies have shown that Me31B interacts with a conserved domain of Tral and interfering with this, impairs P body formation in cells (Tritschler et al. 2007, 2008, 2009). Deletion of Tral in *Drosophila* S2 cells did not affect P body formation, suggesting that Tral is dispensable for the assembly of P bodies and therefore, may

act as a client protein. Biochemical studies of P body components show that Me31B and Tral are part of the same RNP complex in the mature oocyte and early embryo (Hara et al. 2018; McCambridge et al. 2020; Wang et al. 2017). In contrast to Me31B, Tral protein has been shown to contain several disordered regions and therefore, presents an ideal disordered protein to investigate if it exhibits properties different to or similar to Me31B. This can provide insights into the role of structurally distinct proteins and how they eventually contribute to the overall assembly, organisation, and material properties of P bodies during early *Drosophila* development.

6.2 Chapter objectives

In this chapter, I have studied the properties of Tral granules in the mature oocyte and the early embryo. The specific questions addressed are as follows:

1. Do Tral granules have similar or different material properties in the mature oocyte compared to Me31B?
2. What happens to Tral granules during and post egg activation?
3. Do Tral granules have different biochemical properties prior to and after activation?
4. Is Tral necessary for the regulation of Me31B granule formation and material properties in the mature oocyte?

6.3 Tral domain architecture

Disordered regions within Me31B were identified using the intrinsically disordered region (IDRs) prediction algorithm, IUPred. While low complexity domains in Tral have been highlighted in a few studies, the nature of disordered-ness across the protein is unclear. Using the IUPred algorithm, sequence analysis of Tral was performed. A significant proportion of the Tral protein was unstructured (Figure 6.1), thereby classifying Tral as a highly disordered protein. Tral's orthologous proteins across different species CAR-1 in *C.elegans*, RAP55 in vertebrates and Scd6p in *S.cerevisiae* have also been shown to contain long disordered regions (Jonas and Izaurralde 2013), indicating that the unstructured feature of Tral is evolutionarily conserved.

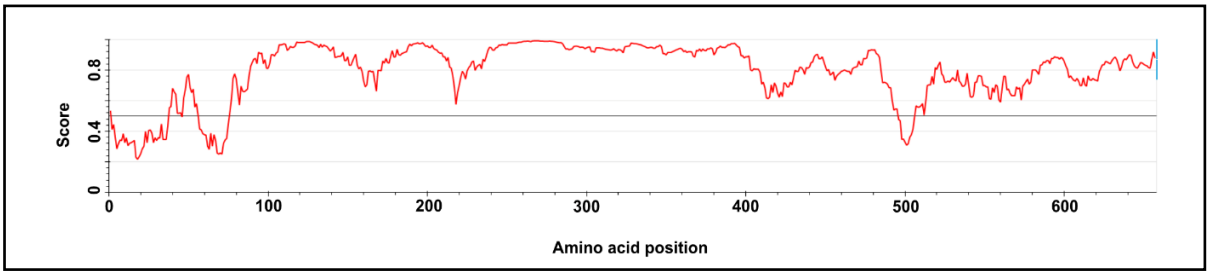

Figure 6.1: Overview of Tral domain architecture. Schematic representation of Tral disorderedness analysed by IUPred. Score above 0.5 represents disorder.

Conclusion: Tral is a highly disordered protein.

6.4 Tral granules exist as heterogeneous elastic condensates

Since Tral is a key component of P bodies and has been shown to co-localise with Me31B associated granules throughout early and mid-oogenesis, I hypothesised that Tral would display similar granular properties as Me31B in the mature oocyte as well. To visualise Tral granules, I imaged mature oocytes expressing Tral protein fused to a GFP tag (Tral::GFP). Live imaging revealed that, like Me31B, Tral granules exhibited a broad range of morphologically spherical and amorphous granules (Figure 6.2A,B).

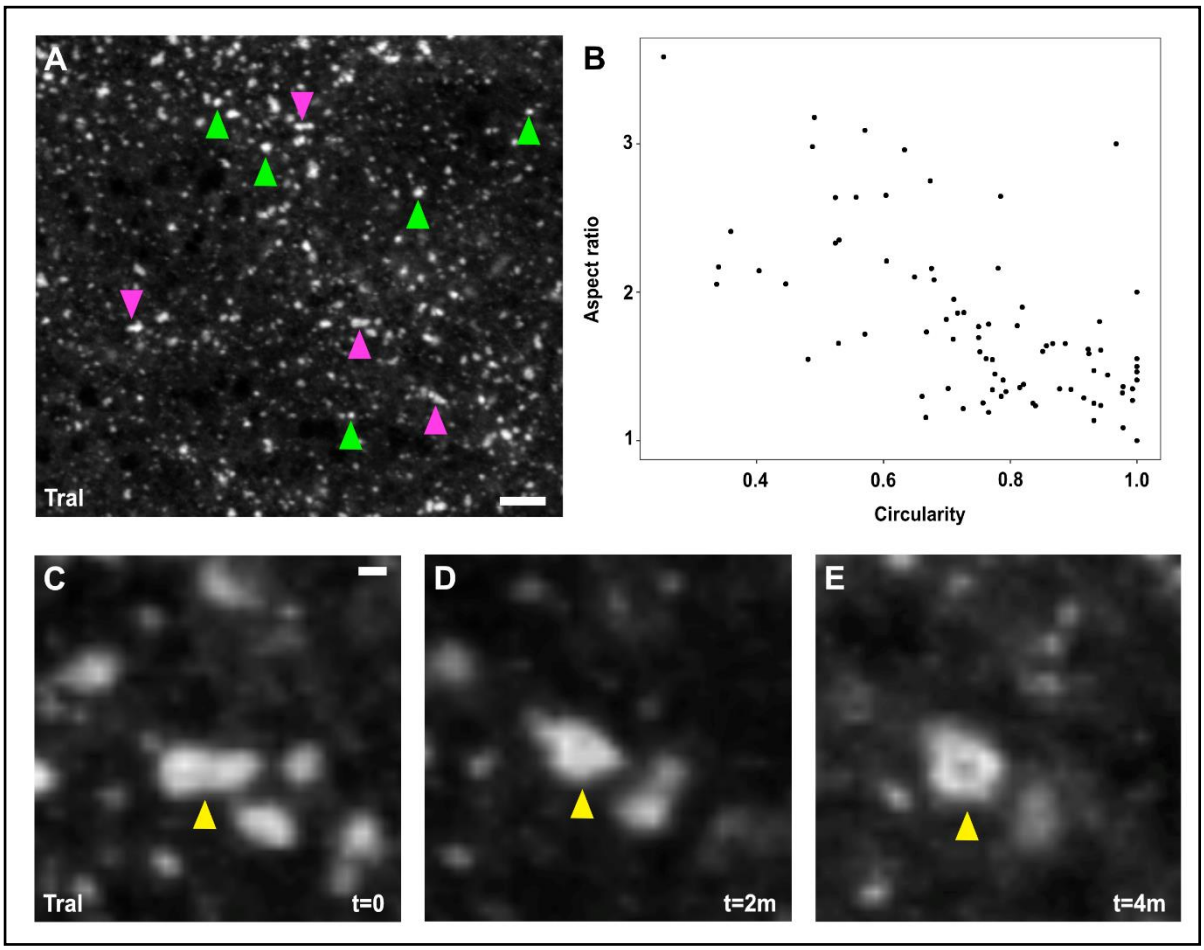

Figure 6.2: Tral granules exist as elastic condensates in the mature oocyte. (A,C-E) Mature oocytes expressing Tral::GFP. **(A)** Differential morphologies, spherical (green arrowheads) and amorphous (magenta arrowheads), morphologies in the mature oocyte exhibited by Tral. Scale bar: 20 µm. **(B)** Quantification of circularity and aspect ratio reveal a distribution of Tral granules tending towards a liquid-like state. **(C-E)** Representative image sequence of Tral granules exhibiting elastic recovery (yellow arrowheads). Scale bar: 5 µm.

Although time lapse imaging of Tral granules did not reveal significant elasticity as observed for Me31B, they did, however, display occasional expansion and relaxation while exhibiting controlled spatial dynamics (Figure 6.2C-E). The relaxation events also revealed sub-domains within Tral granules (Figure 6.2E), indicating heterogeneous organisation.

Conclusion: Tral granules in the mature oocyte are morphologically similar to Me31B and exhibit limited dynamics across space. Additionally, Tral granules exhibit multi-layered organisation and elastic properties, suggesting that these features are an intrinsic property of P bodies in the mature oocyte.

6.5 Tral granules do not exhibit exchange of molecules with the cytoplasm

A key feature observed with Me31B granules is the ability to prevent exchange of molecules between the granule and cytoplasm due to the gel-like material state. To test if Tral granules also exhibited similar behaviour, I performed whole particle FRAP of Tral granules. Over time, granules displayed very little or no recovery post photobleaching (Figure 6.3A). The percentage of mobile Tral particles was very minimal (Figure 6.3B) suggesting that exchange of molecules between the granule and cytoplasmic Tral in the mature oocyte is rate limiting. This is consistent with the idea that P bodies in the mature oocyte exist in an arrested state as a means to protect the stored maternal mRNAs.

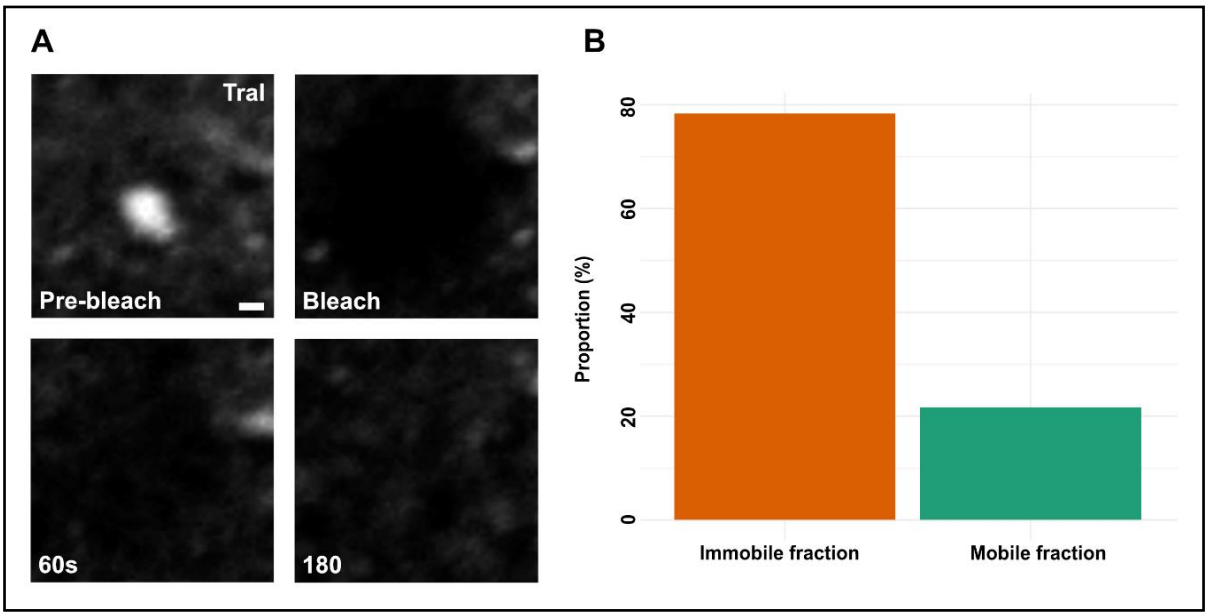

Figure 6.3: Tral granules do not display exchange of molecules between the granule and cytoplasm. (A) Mature oocytes expressing Tral::GFP. Time lapse images of Tral granule before and after photobleaching whole granule; scale bar: 3 µm. **(B)** Quantification of mobile and immobile proportions of Tral molecules post granule photobleaching.

Conclusion: Tral granules, like Me31B, exist in an arrested state in the mature oocyte and prevent exchange of molecules between the granule and the cytoplasm.

6.6 1,6 Hexanediol causes phase transition of Tral granules to a liquid-like state

Hexanediol, an amphipathic alcohol compound used to distinguish between liquid-like and solid-like states, was shown to induce an aberrant phase transition of Me31B granules from gel to liquid-like state in the mature oocyte. The ability of hexanediol to dissolve liquids and not solids is based on its ability to disrupt weak hydrophobic forces. To test if Tral granules also display a similar phase transition, mature oocytes were treated with 5% 1,6 hexanediol solution. Interestingly, Tral granules underwent a dramatic shape change from less circular to highly spherical morphology post hexanediol treatment (Figure 6.4A,B). This change was accompanied by fusion events of individual Tral granules resulting in relatively larger sized Tral granules post treatment (Figure 6.4B). This suggests that like Me31B, Tral granules in the mature oocyte also display liquid-like properties upon hexanediol treatment.

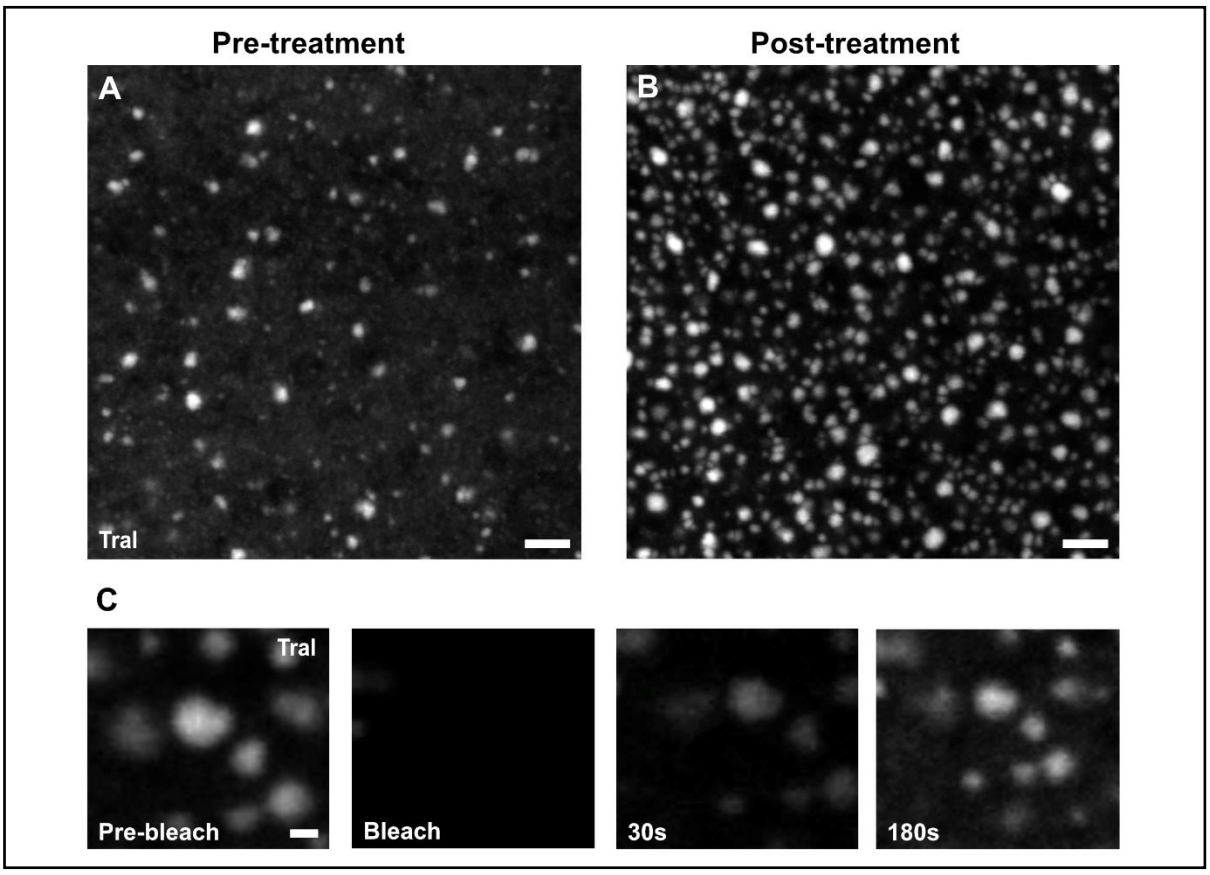

Figure 6.4: Hexanediol causes Tral granules to transition into a liquid-like material state. **(A-F)** Mature oocytes expressing Tral::GFP. **(A,B)** Representative image of Tral granules before **(A)** and after hexanediol treatment **(B)** exhibiting changes in morphology and size. Scale bar: 10 µm. **(C)** Time lapse images of hexanediol treated Tral granule before and after photobleaching whole granules reveal exchange of Tral molecules between the granule and cytoplasm. Scale bar: 6 µm.

To confirm if the biophysical state of altered Tral granules is liquid-like, I performed whole particle FRAP of hexanediol treated Tral granules to test their exchange kinetics. Consistent with the liquid-like behaviour, hexanediol treated Tral granules exhibited rapid exchange of Tral molecules with the cytoplasmic pool (Figure 6.4C), confirming the liquid-like material state.

Conclusion: Tral, like Me31B granules, undergo a phase transition to liquid-like state upon disruption of hydrophobic interactions by hexanediol, indicating that hydrophobicity primarily contributes to the gel state of P bodies in the mature oocyte.

6.7 Tral granules disperse upon *ex vivo* egg activation

Placing mature oocytes in a hypotonic 'activation' buffer causes them to hydrate and swell, resulting in egg activation. Using this method, I have previously demonstrated that Me31B granules undergo dispersion upon *ex vivo* activation. This dispersion results in the release of stored maternal mRNAs such as *bicoid*, likely for translational activation.

To test if Tral granules also dispersed upon activation, mature oocytes expressing Tral::GFP were dissected into oil and activation buffer was added. Shortly after treatment, Tral granules underwent rapid dispersion at a similar rate as observed for Me31B (Figure 6.5A,B). Additionally, prolonged imaging showed that shortly post dispersion, Tral re-forms into condensed granules post activation (Figure 6.5C).

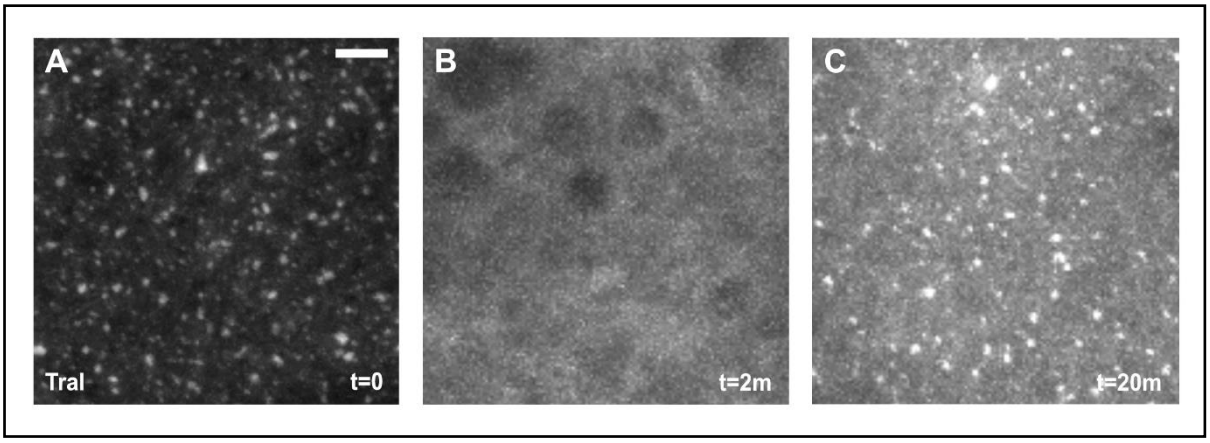

Figure 6.5: Tral granules rapidly disperse at activation and reform shortly post dispersion. (A-C) Mature oocytes expressing Tral::GFP. **(A,B)** Addition of activation buffer causes rapid dispersion of Tral granules. **(C)** Shortly post dispersion, Tral phase separates into condensed granules. Scale bar: 10 µm (A-C).

Conclusion: Tral granules undergo dispersion from granular to cytoplasmic phase upon *ex vivo* egg activation, indicating that P body dispersion at egg activation is accompanied by dissolution of RBPs present in P bodies, irrespective of their structural features.

6.8 Tral reforms into small sized condensed granules in the early embryo

Me31B was shown to reform into smaller sized granules in the early embryo, post egg activation. Biochemical studies have shown that Tral associates with Me31B in the same RNP complex in the early embryo. To test if Tral granules are present in the early embryo, I imaged 0-1hour old embryos expressing Tral::GFP. Live imaging revealed that Tral is distributed as condensed granules throughout the embryo (Figure 6.6). The size and distribution of Tral granules in the early embryo are similar to those observed with Me31B.

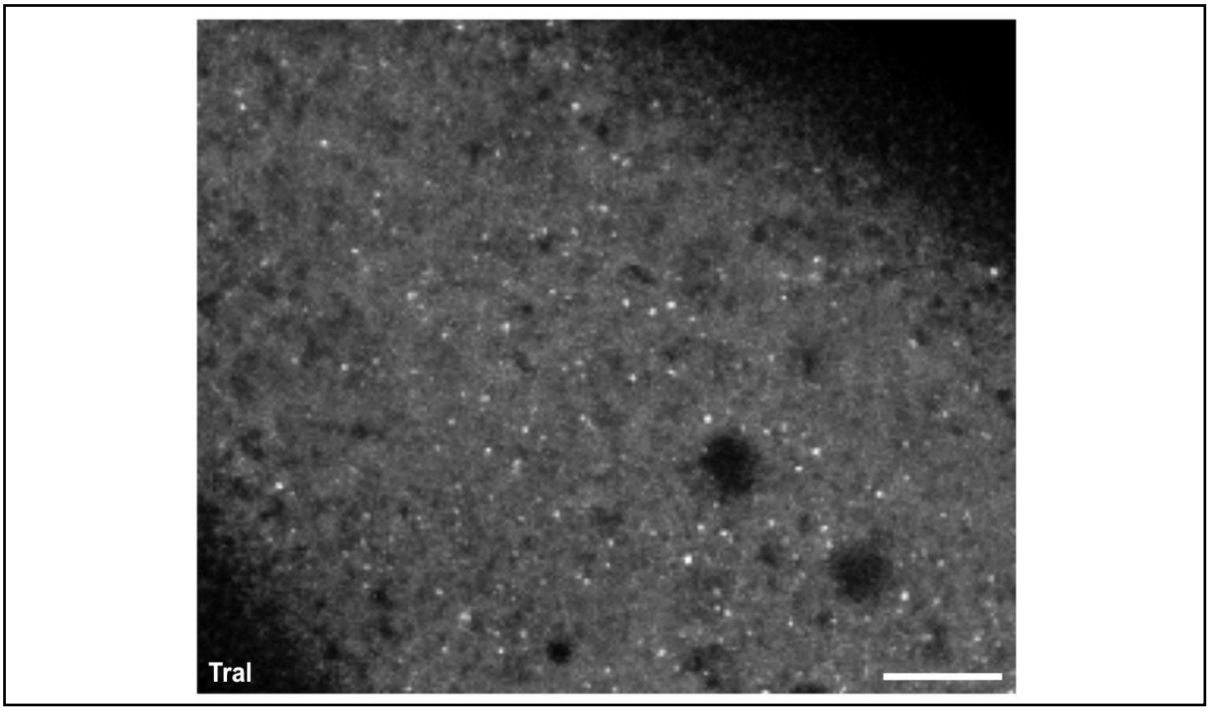

Figure 6.6: Tral exist as small sized condensed granules in the early embryo. 1 hour-old embryo expressing Tral::GFP displays Tral present in smaller sized condensed granules distributed throughout the embryo. Scale bar: 10 µm.

Conclusion: Tral, like Me31B, is present as small sized, condensed granules in the early embryo.

6.9 Tral exhibits differential biochemical properties between the mature oocyte and early embryo

Perhaps, the most striking difference observed between the oocyte and embryonic Me31B granules is the varying degree of complex density; oocyte Me31B was present in lower and high molecular weight complexes, while embryonic Me31B was present predominantly in high molecular weight forms. Since Tral has been shown to be present in the same RNP complex as Me31B in both stages, I hypothesised that Tral also may exhibit similar biochemical behaviour.

Firstly, western blot analysis of lysates obtained from mature oocytes and early embryos were performed to test the relative levels of Tral protein between the mature oocyte and early embryo. Lysates from both samples displayed fairly similar amounts of Tral protein (Figure 6.7), indicating that the Tral protein levels do not significantly vary between the mature oocyte and early embryo.

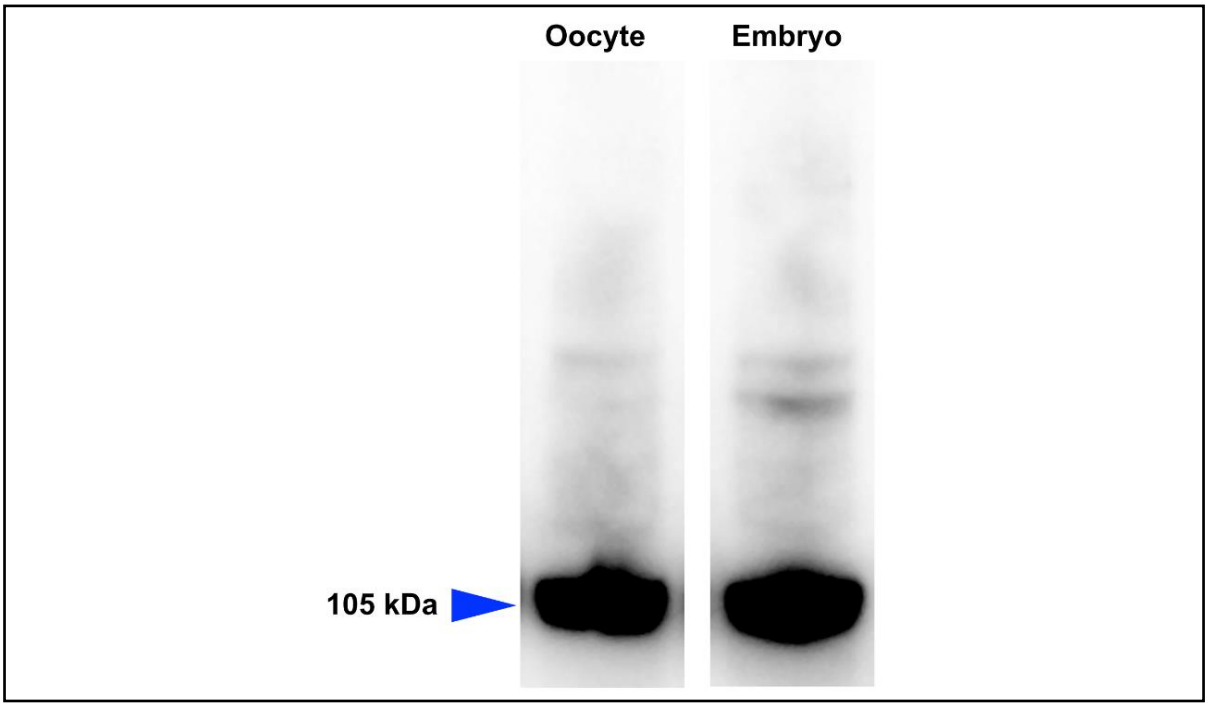

Figure 6.7: Tral protein levels remain similar between the mature oocyte and early embryo. Lysates from mature oocytes and 0-3-hour old embryos expressing Tral::GFP were subjected to SDS-PAGE. Tral::GFP (105 kDa) was detected by western blot against GFP.

To investigate the density of Tral complexes, a continuous sucrose gradient assay of lysates obtained from the mature oocyte and early embryo was performed, followed by western blot analysis. Interestingly, Tral from the mature oocyte sedimented

through the sucrose gradient as low molecular weight entities whereas the embryonic Tral was restricted predominantly to high molecular weight fractions, similar to Me31B (Figure 6.8). However, while Me31B from mature oocyte lysates was also present in high molecular weight complexes, Tral appears to be predominantly present only in low molecular weight complexes. Based on results from cell culture studies and Tral distribution in the mature oocyte, it is possible that Tral acts as a client molecule, and the low molecular weight complexes (which largely includes monomeric forms) mostly represent the cytoplasmic fraction of Tral in the mature oocyte.

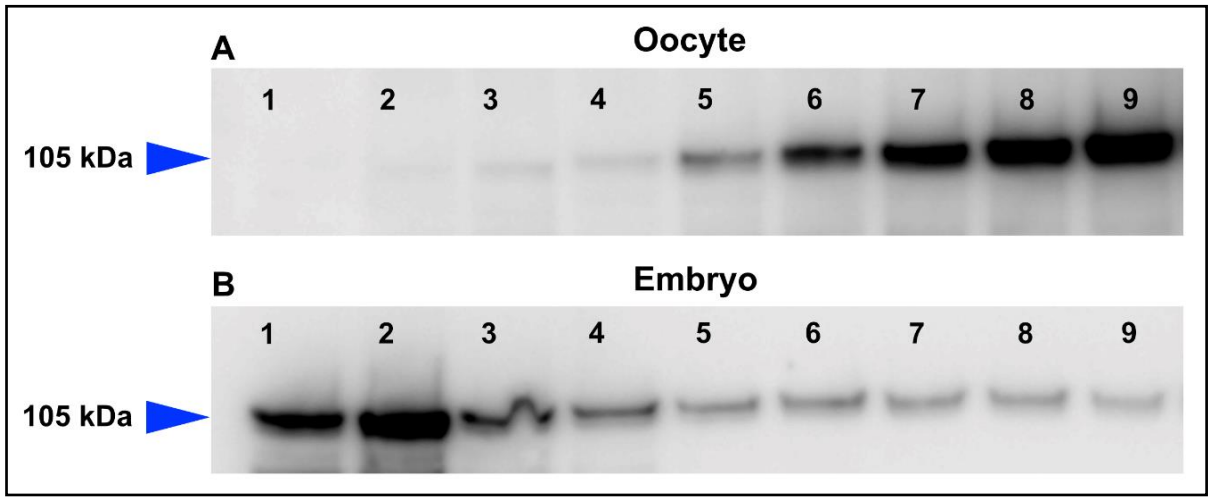

Figure 6.8: Tral is present in distinct molecular weight complexes in the mature oocyte and early embryo. Lysates obtained from mature oocytes (A) and 0-3-hour old embryos (B) expressing Tral::GFP were subjected to a 15-40% continuous sucrose gradient. Tral::GFP in different lanes was detected by western blot against GFP.

Conclusion: Tral protein levels do not vary between the mature oocyte and early embryo. However, Tral in the early embryo is present largely in high molecular weight complexes while Tral in the mature oocyte is present only in low molecular weight complexes. These results suggest that P body complexity is drastically altered between the mature oocyte and the early embryo.

6.10 Tral deficiency affects Me31B granule morphology and dynamics

Despite being structurally different from Me31B, granules formed by Tral behave in a very similar way to Me31B granules, indicating that structured and disordered proteins likely work synergistically to contribute to overall material properties of P bodies. The follow up question therefore was: ‘is Tral important for Me31B granule property and function?’. To test the role of Tral, I used a Tral mutant allele over deficiency ($Tral^{1}$/Df)

which has been previously used to reduce Tral expression to undetectable levels during oogenesis (Wilhelm et al. 2005).

To examine if Tral influences Me31B granule integrity and properties, I performed live imaging of mature oocytes expressing Me31B::GFP and Tral^{1} deficiency. Me31B granules in the mature oocytes displayed dramatically altered morphologies: doughnut and rod-shaped structures (Figure 6.9A,B). These abnormal morphological features of Me31B granules were observed across different stages of oogenesis (Figure 6.9C).

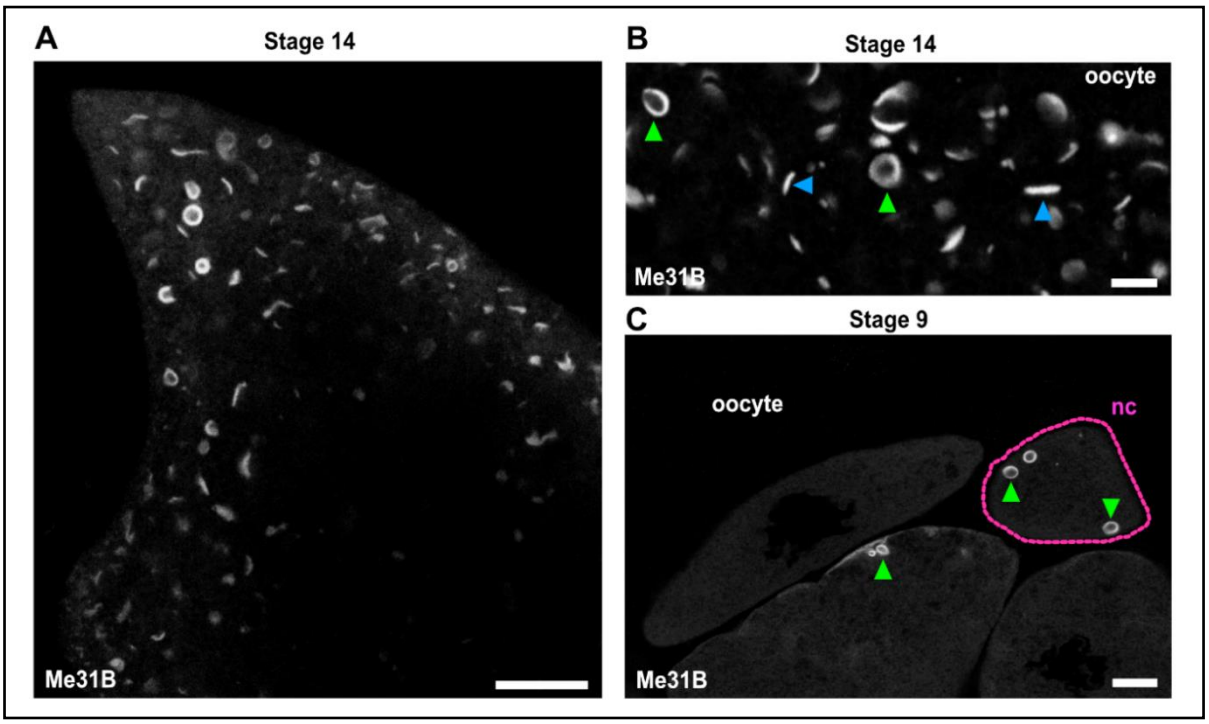

Figure 6.9: Me31B granule integrity and morphology are dramatically disrupted in Tral^{1} mutants. (A-C) Egg chambers expressing Me31B::GFP and Trail^{1} deficiency. **(A)** Representative image of Me31B granules displaying diverse morphologies in the mature stage 14 oocyte. Scale bar: 20 µm. **(B)** High resolution image of the different morphologies, doughnut (green arrowheads) and rod-like (blue arrowheads), exhibited by Me31B granules in the stage 14 oocyte. Scale bar: 10 µm. **(C)** Representative image of a mid-staged egg chamber (stage 9) displaying doughnut shaped Me31B granules in the nurse cells (green arrowheads); an entire nurse cell (nc) is outlined with magenta dotted lines. Scale bar: 10 µm.

Interestingly, shortly post photobleaching of mutant Me31B granules, fluorescence recovery up to at least 50% was observed (Figure 6.10), significantly more than WT Me31B granules. Loss of Tral interaction, therefore, drives Me31B granules to transition into morphologically abnormal and dynamic compartments. Alternatively,

these granules may also represent liquid crystals, which have properties between those of conventional liquids and solid crystals.

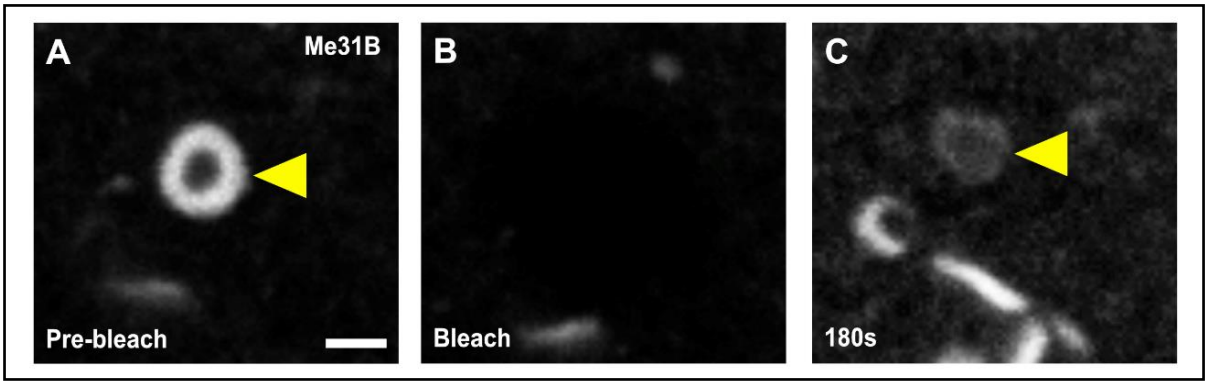

Figure 6.10: Me31B granules in Tral mutants exchange components between the granule and cytoplasm. (A-C) Tral^{1}/Df egg chambers expressing GFP::Me31B. Image sequence of whole Me31B granule FRAP (yellow arrowhead) shows Me31B fluorescence recovery post photobleaching. Scale bar: 12 µm.

Furthermore, ovaries from the Tral mutants contained significantly less mature oocytes compared to ovaries from Tral::GFP females (data not shown). While previous studies which had utilised this mutant line reported abnormalities in the morphology of oocytes or the number of dorsal appendages, there was no mention about defects in the production of mature oocytes (Wilhelm et al. 2005). My observations suggest that deficiency of Tral dramatically affects oocyte maturation.

Conclusion: Absence of Tral results in the formation of geometrically irregular and highly dynamic Me31B granules throughout oogenesis. The absence of Tral also appears to affect oocyte maturation. While it is not clear whether oocyte maturation is prevented by Me31B granule formation or due to the absence of signals and factors regulated by Tral, it is possible that a combination of both events affects maturation of developing egg chambers.

6.11 Summary of results

In previous chapters, I demonstrated P body material and biochemical properties using a structured protein, Me31B, in both the mature oocyte and early embryo. Since P body contains several other structurally distinct proteins, I wanted to test if the disordered P body protein Trailer hitch displayed different properties Me31B. Using a combination of live imaging and pharmacological treatments, my data demonstrates the elastic property and gel-like state of Tral granules in the mature oocyte. Upon *ex vivo* egg activation, Tral granules transitioned from granular to cytoplasmic phase, similar to Me31B. Furthermore, using live imaging and standard biochemical assays, my data shows that Tral granules in the early embryo exhibit properties different from Tral in the mature oocyte. Finally, live imaging of Me31B granules in the absence of Tral revealed the formation of morphologically aberrant and dynamic granule, indicating the importance of Me31B-Tral interaction in maintaining overall P body integrity and material properties in the mature oocyte.

6.12 Discussion

Multivalent protein-protein interactions are key to RNP granule assembly and integrity. Me31B and Tral are highly conserved RBPs, whose orthologues in other species have similar functions (Jonas and Izaurralde 2013) and are likely associated with evolutionarily preserved RNP complexes across metazoan species. A key role for Me31B is translational repression of maternal mRNAs during oogenesis. Tral on the other hand has multiple functions, one of which includes association with Me31B and other P body proteins to repress translation of maternal mRNAs. Indeed, structural studies have shown that Me31B and Tral interact at a molecular level through a conserved FDF motif within the Tral protein (Tritschler et al. 2008, 2009). Despite being structurally distinct to Me31B, Tral exhibits strikingly similar biophysical and biochemical properties as Me31B granules, both in the mature oocyte and early embryo. However, loss of Tral results in structurally deformed and biophysically altered P bodies. Similar observations were reported for the germ granule P bodies in arrested *C. elegans* oocytes; loss of CGH-1 (Me31B orthologue) resulted in the formation of morphologically deformed CAR-1 (Tral orthologue) structures with altered material properties (Hubstenberger et al. 2013, 2015). These observations reveal a plausible, evolutionarily conserved molecular principle: the synergistic effect of individual components in a multi-protein system has a greater influence on the overall material state than contributions of its individual components. Therefore, Me31B and Tral interaction synergistically regulate P body integrity and material properties during early *Drosophila* development.

6.13 Future directions

6.13.1 Investigating Tral granule properties and dynamics in the mature oocyte and early embryo

Using key experiments including whole particle FRAP, hexanediol treatment and *ex vivo* egg activation, I have demonstrated that Tral granules in the mature oocyte have similar properties as Me31B, despite being structurally distinct. However, it is important to characterise material properties of Tral granules in greater detail to further confirm the similarities in their material properties to Me31B. Testing the effects of actin or/and microtubules depolymerizing drugs, divalent and monovalent salts, and RNase A, both in the mature oocyte and early embryo, will be important.

6.13.2 Examining Me31B granule properties in Tral mutants

Me31B granules exhibited remarkable deformities in their morphology and increased exchange kinetics with the cytoplasm, in the absence of Tral protein. However, further experiments are required to understand how the absence of Tral affects Me31B properties and function during development. Live imaging of Me31B granules, in Tral mutants, at egg activation and the early embryo could inform whether changes in Me31B granule properties are specific to the mature oocyte or extend to later stages of development as well. Rescue experiments with wild-type Tral could help ascertain if the modified Me31B granule properties are specifically due to loss of interaction with Tral protein. Additionally, comparing the number of mature oocytes from 'rescued' ovaries to ovaries from Tral mutants could inform whether Tral is essential for oocyte maturation.

6.13.3 Testing the effects of Tral mutant on mRNA storage and regulation

A striking phenotype among Me31B granules across different stages of oogenesis in Tral mutants is the abnormal morphologies, including doughnut and rod-shaped structures. This raises questions about the regulation of several maternal RNAs associated with Me31B granules throughout oogenesis. Are maternal mRNAs such as *gurken* and *bicoid* still stored and regulated in Me31B granules? Does granule morphology affect mRNA translational repression? Fluorescent *in situ* hybridisation or live imaging of fluorescently labelled maternal mRNAs such as *gurken* and *bicoid* would be useful to determine their localisation or dynamics relative to Me31B granules. Additionally, immunohistochemistry or western blot analysis to detect protein products of *gurken* and *bicoid,* which are differentially translated at different stages of oogenesis, could confirm whether maternal mRNA translation is efficiently regulated in Tral mutants.

Chapter 7

Summary and Conclusion

7.1 Summary and working model

Our current understanding of how biomolecular condensates are regulated has been primarily elucidated through *in vitro* studies of purified RNA and/or protein components under idealised conditions. In my thesis, I have investigated the *in vivo* material properties and functions of processing (P) bodies, a class of conserved cytoplasmic biomolecular condensates. To visualise and study P bodies during early *Drosophila* development, I utilised fluorescently labeled Me31B, a highly conserved and structured RNA helicase. My data shows that P bodies in the mature oocyte are multilayered viscoelastic condensates exhibiting a gel-like material state which is important for the storage of *bicoid*, a key maternal transcript needed for embryonic development.

Through live imaging and pharmacological disruption, my results indicate that that a combination of changes in egg volume, ionic strength, and cytoskeletal rearrangements in the mature oocyte cause P body dispersal at egg activation. Post activation, P bodies re-form into highly dynamic, semi-liquid condensates which are biochemically distinct from P bodies in the mature oocyte. Using fluorescent *in situ* hybridisation to visualise embryonic transcripts, my data also describes the transient association of the pair-rule mRNAs *hairy* and *fushi tarazu* with P bodies, indicating a regulatory role for P bodies in the early embryo.

My data also shows a role for crowding, ionic concentration, and RNA structure in regulating the biophysical state of *in vitro* reconstituted Me31B condensates. Additionally, my data demonstrates that short disordered regions within Me31B are required for regulating Me31B condensate material state.

Finally, my data examining *Drosophila* P bodies further shows that Trailer hitch, a highly disordered protein, exhibits similar material properties to Me31B in P bodies and is required for P body assembly, integrity, and material properties in the mature oocyte.

Taken together, my data suggests a model for RNA regulation via P body phase transitions during early *Drosophila* development. The gel state of P bodies in the mature oocyte, regulated by synergistic, multivalent interactions between structurally

distinct proteins and RNAs, allows for the storage of translationally repressed mRNAs. Disrupting aspects of these interactions leads to the formation of physiologically abnormal P bodies with modified material properties, affecting RNA storage and oocyte maturation. At egg activation, cytoplasmic modifications cause P body dispersal to allow the translation of the stored maternal mRNAs, thereby preparing the egg for fertilisation. In the early embryo, P bodies re-form into smaller sized, highly dynamic condensates with altered post-translational and biochemical modifications. Since several maternal RNAs undergo large scale degradation during early embryogenesis and P bodies are enriched in RNA degradation proteins, it is likely that the dynamic state of P bodies allows the controlled release of degradation factors to facilitate clearance of maternal RNAs.

Overall, developmental cues coordinate synergistic macromolecular interactions and cytoplasmic modifications to differentially regulate RNAs through P body phase transitions during early *Drosophila* development.

7.2 Significance

Substantial progress has been made towards deciphering the physicochemical rules regulating biomolecular condensate assembly, organisation, and material properties. While majority of the data is derived from *in vitro* reconstitution and cell culture studies, why cells need these condensates and what their biological functions are remain largely unanswered. Results from my thesis have provided a first step towards addressing this question by demonstrating the underlying material properties and their relation to the function of P bodies in achieving RNA regulation during early *Drosophila* development. Below, I have highlighted a few major findings from my work that have furthered our current understanding of the *in vivo* significance of P body condensation in early *Drosophila* development.

(1) How localised RNAs are faithfully stored and translationally repressed for long durations during oogenesis has remained unclear. My results show that P bodies exist in an arrested, gel-like material state that allows for the storage and regulation of RNAs, providing evidence for the *in vivo* significance of condensate material state. Similar modes of regulation may also apply to mRNAs stored and translationally repressed in ribonucleoprotein (RNP) granules at the pre-synapse of neuronal cells.

More importantly, impaired RNP granule regulation in *Drosophila* adult neurons has been shown to affect long term memory formation and present phenotypes implicated in neurodegenerative diseases such as Amyotrophic lateral sclerosis (Bakthavachalu et al. 2018; McCann et al. 2011). Therefore, stable RNP granule material states may be more generally prevalent across cell types to facilitate RNA regulation.

(2) Recent biochemical studies have shown that P bodies in the embryo may function in RNA degradation, transitioning from their translational repression role in the mature oocytes (Wang et al. 2017). How P bodies accomplish this change in functional properties was unclear. My work shows that P bodies undergo a phase transition from gel-like to semi-liquid material state during the oocyte to embryo transition, including an intermediate soluble phase at egg activation. This phase transition was also accompanied changes in phosphorylation and biochemical properties of P bodies, likely to facilitate different functions at various stages of development. Such phase changes have also been observed with other membrane-less organelles as well; for instance, the Balbiani body (storage sites for multiple organelles during oocyte dormancy) exists as a stable amyloid-like compartment in the early oocyte but either disappears or disperses into smaller sized granules during later stages of development (Kloc, Bilinski, and Etkin 2004). Modified organisation and properties of granules after fertilisation were also observed in the *C.elegans* P bodies (Hubstenberger et al. 2013). Therefore, remodelling of membrane-less granules during later stages of development is likely a conserved mechanism to allow differential regulation of RNP components and functions in response to developmental cues.

(3) How the transcriptional regulation of genes in the early embryo is achieved is well studied. However, detailed understanding of the post-transcriptional regulation of early embryonic mRNAs is completely lacking. My work shows that apically localised pair-rule mRNAs specifically associate with P bodies and this association is important for P body condensation in cellularised embryos. This provides a first step towards understanding the regulatory crosstalk between P bodies and embryonic mRNAs in the early embryo. Together with the semi-liquid biophysical state of P bodies and relatively short half-lives of pair-rule mRNAs, it is likely that embryonic P bodies act as sites of mRNA degradation.

(4) Weak inter-molecular forces are critical to maintaining the structural integrity, organisation, and material properties of RNP granules. How different types of interactions individually contribute to the overall material property and organisation of RNP granules is less clear. My results show that P body material state and integrity is primarily contributed by weak electrostatic and hydrophobic interactions. However, while disrupting hydrophobic interactions altered the material state, the integrity of P bodies remained fairly intact. This is most crucial for P bodies during *Drosophila* oogenesis which allow differential regulation of stored maternal mRNAs. Therefore, by modulating the strengths of different inter-molecular interactions, certain mRNAs could be released into the cytoplasm, while maintaining the structural integrity of P bodies, at different stages of development. This mechanism is likely ubiquitous among RNP granules which perform similar functions, such as such stress granules, and provides a controllable switch to modulate material properties in response to different stimuli without significantly altering granule integrity.

7.3 Future directions

Although the field of liquid-liquid phase separation has made significant progress in the last decade, there is still much to learn about the physiological functions of biomolecular condensates in cell and developmental biology. In a recently published article, I have reviewed how *Drosophila* oocytes could be used as a model system to study the underlying molecular and physicochemical principles of maternal RNP granule phase separation and their functional implications in development (Sankaranarayanan and Weil 2020). Below, I discuss a few questions/ ideas that require thorough investigation to better understand the functional implications of RNP granules in physiology and disease.

7.3.1 P body regulation and function across cell types

RNP condensates such as P bodies contain structurally diverse protein and RNA macromolecules. Interestingly, intrinsically disordered sequences of key P body proteins such as Me31B have significantly diverged across higher order eukaryotes. Whether such changes in the disordered sequence length or composition confer structural or functional specificity requires further investigation.

Although the molecular composition of P bodies across cell types, such as oocytes or neurons, are mostly similar, it is possible that local tissue dynamics or cellular fluctuations may influence P body material properties and function. It is therefore important to examine whether differential regulation of P bodies occurs in a cell specific manner and what functional variance might they have.

Recent studies have attributed the liquid-like material state for P bodies in all contexts (Luo, Na, and Slavoff 2018). However, my results argue that P body material states are not universally liquid-like but are regulated in a context-dependent manner. Examining how different material states contribute to the resulting function is, therefore, crucial to understand the similarities and differences of P body functions across cell types.

7.3.2 Fate of RNAs inside RNP condensates

Many RNP condensates such as P bodies and stress granules are optimised for sequestering RNAs, either transient or long-term storage depending on the cell type. In the case of P bodies, while they are known to protect stored RNAs from degradation, ironically, P bodies are also enriched in RNA decay and degradation enzymes. Understanding how stored RNAs are preferentially protected from these enzymes will be important. One possible mechanism could be through microRNAs, which have been shown to localise to P bodies.

Similarly, stress granules which form during cellular stress are thought to insulate cytoplasmic RNAs and proteins from being mis-folded or degraded during the stress. However, because stress granules lack a physical membrane and behave as liquid-like droplets, how sequestered RNAs are faithfully stored and protected from damage or decay requires extensive examination.

Since multiple RNP granules are thought to be involved in the translational regulation of stored RNAs, can translation be achieved within condensates? Do protein (and possibly RNA molecules) shuttling between different RNPs exhibit different functions dependent on the RNP granule they are present in? If so, how is this functional specificity achieved? Taken together, investigating how RNP condensates regulate stored RNAs is critical to understanding how they function.

7.3.3 Implications for RNP condensates in translational research

A classic hallmark prevalent across several disease phenotypes, especially neurodegenerative diseases, is RNP aggregation (Ramaswami, Taylor, and Parker 2013). However, highly ordered and stable RNP aggregates or assemblies are not always pathological (Boke et al. 2016). Since similar multivalent interactions mediate both normal and pathological RNP aggregates, it is crucial to understand the underlying molecular mechanisms of RNP assembly and maintenance, and whether pathological inclusions emerge from normal RNP assemblies. Due to their ability to concentrate molecules, utilising RNP condensates as drug targets is an exciting possibility, as demonstrated in a recent paper from Young and colleagues (Klein et al. 2020).

Additionally, the abundance of RNP condensates and their roles in translational regulation in oocytes, mostly characterised in invertebrate systems, highlight their importance in regulating early development. However, they are relatively less understood in higher order vertebrates such as mouse and human eggs, and therefore require further examination to test whether RNP granules exhibit similar properties and functions.

Besides RNA regulation, it will be exciting to test if RNP condensates associate with the spindle assembly components, and function in regulating meiosis in oocytes. This will not only help understand the role of RNP condensates in chromosomal segregation, but also have potential medical implications. A large majority of unsuccessful (*in vitro*) fertilisations arise from meiotic errors, and therefore investigating the role of RNP condensates could provide an attractive therapeutic target for fertility treatments.

7.4 Concluding remarks

In the past decade, extensive studies on membrane-less organelles have provided cell biologists a new line of thinking to understand cytoplasmic organisation, and how multiple cellular processes may be coordinated and regulated. By deriving principles and concepts from the field of polymer physics and physical chemistry, the field of liquid-liquid phase separation, in biology, has emerged as a novel paradigm for

understanding the physical, chemical, and biological role of biomolecular condensates in physiology and disease.

While several protein and RNA molecules have been shown to undergo phase separation, mostly using cell culture and *in vitro* systems, caution must be exercised in labelling any molecule forming micron sized structures as ‘phase separated’ entities (McSwiggen et al. 2019). Extensive quantitative measurements and novel *in vivo* assays that faithfully reproduce the properties of *in vitro* reconstituted phase separated components must be employed. Even though the field is relatively new, and therefore, the excitement in exploring the potential of this conceptual framework in biological processes cannot be criticised, it is crucial to evaluate the reliability and reproducibility of studies reporting phase separation of biological molecules and monitor future advancements in the topic. Despite considerable progress in our understanding of the molecular grammar underlying the biophysical properties of biomolecular condensates, what phase separation means at a functional level is considerably lacking. Therefore, investigating the physiological roles of biomolecular condensates in living organisms is an important step towards understanding to what extent phase-separation influences, and impacts cellular processes and functions.

Chapter 8

References

1. Abbondanzieri, E. A., & Meyer, A. S. (2019). More than just a phase: the search for membraneless organelles in the bacterial cytoplasm. *Current Genetics*, *65*(3), 691–694. https://doi.org/10.1007/s00294-018-00927-x
2. Aguilera-Gomez, A., & Rabouille, C. (2017). Membrane-bound organelles versus membrane-less compartments and their control of anabolic pathways in Drosophila. *Developmental Biology*, *428*(2), 310–317. https://doi.org/10.1016/j.ydbio.2017.03.029
3. Aguzzi, A., & Altmeyer, M. (2016). Phase Separation: Linking Cellular Compartmentalization to Disease. *Trends in Cell Biology*, *26*(7), 547–558. https://doi.org/10.1016/j.tcb.2016.03.004
4. Aizer, A., Brody, Y., Ler, L. W., Sonenberg, N., Singer, R. H., & Shav-Tal, Y. (2008). The dynamics of mammalian P body transport, assembly, and disassembly in vivo. *Molecular Biology of the Cell*, *19*(10), 4154–4166. https://doi.org/10.1091/mbc.e08-05-0513
5. Al-Husini, N., Tomares, D. T., Bitar, O., Childers, W. S., & Schrader, J. M. (2018). α-Proteobacterial RNA Degradosomes Assemble Liquid-Liquid Phase-Separated RNP Bodies. *Molecular Cell*, *71*(6), 1027-1039.e14. https://doi.org/10.1016/j.molcel.2018.08.003
6. Alberti, 2009. (2009). Suppl 1. *Cell*, *137*(1), 146–158. https://doi.org/10.1016/j.cell.2009.02.044.A
7. Alberti, S., & Dormann, D. (2019). Liquid–Liquid Phase Separation in Disease. *Annual Review of Genetics*, *53*(1), 171–194. https://doi.org/10.1146/annurev-genet-112618-043527
8. Alberti, S., Gladfelter, A., & Mittag, T. (2019). Considerations and Challenges in Studying Liquid-Liquid Phase Separation and Biomolecular Condensates. *Cell*, *176*(3), 419–434. https://doi.org/10.1016/j.cell.2018.12.035
9. Alberti, S., & Hyman, A. A. (2016). Are aberrant phase transitions a driver of cellular aging? *BioEssays*, *38*(10), 959–968. https://doi.org/10.1002/bies.201600042
10. Alberti, S., Saha, S., Woodruff, J. B., Franzmann, T. M., Wang, J., & Hyman, A. A. (2018). A User's Guide for Phase Separation Assays with Purified Proteins. *Journal of Molecular Biology*, *430*(23), 4806–4820. https://doi.org/10.1016/j.jmb.2018.06.038
11. Alshareedah, I., Moosa, M. M., Raju, M., Potoyan, D., & Banerjee, P. R. (2020). Phase Transition of RNA-protein Complexes into Ordered Hollow Condensates. *BioRxiv*, 2020.01.10.902353. https://doi.org/10.1101/2020.01.10.902353
12. Avilés-Pagán, E. E., & Orr-Weaver, T. L. (2018). Activating embryonic

development in Drosophila. *Seminars in Cell and Developmental Biology*, *84*, 100–110. https://doi.org/10.1016/j.semcdb.2018.02.019

13. Ayache, J., Bénard, M., Ernoult-Lange, M., Minshall, N., Standart, N., Kress, M., & Weil, D. (2015). P-body assembly requires DDX6 repression complexes rather than decay or Ataxin2/2L complexes. *Molecular Biology of the Cell*, *26*(14), 2579–2595. https://doi.org/10.1091/mbc.E15-03-0136
14. Bakthavachalu, B., Huelsmeier, J., Sudhakaran, I. P., Hillebrand, J., Singh, A., Petrauskas, A., Thiagarajan, D., Sankaranarayanan, M., Mizoue, L., Anderson, E. N., Pandey, U. B., Ross, E., VijayRaghavan, K., Parker, R., & Ramaswami, M. (2018). RNP-Granule Assembly via Ataxin-2 Disordered Domains Is Required for Long-Term Memory and Neurodegeneration. *Neuron*, *98*(4), 754-766.e4. https://doi.org/10.1016/j.neuron.2018.04.032
15. Banani, S. F., Lee, H. O., Hyman, A. A., & Rosen, M. K. (2017). Biomolecular condensates: Organizers of cellular biochemistry. *Nature Reviews Molecular Cell Biology*, *18*(5), 285–298. https://doi.org/10.1038/nrm.2017.7
16. Banani, S. F., Rice, A. M., Peeples, W. B., Lin, Y., Jain, S., Parker, R., & Rosen, M. K. (2016). Compositional Control of Phase-Separated Cellular Bodies. *Cell*, *166*(3), 651–663. https://doi.org/10.1016/j.cell.2016.06.010
17. Banerjee, P. R., Milin, A. N., Moosa, M. M., Onuchic, P. L., & Deniz, A. A. (2017). Reentrant Phase Transition Drives Dynamic Substructure Formation in Ribonucleoprotein Droplets. *Angewandte Chemie - International Edition*, *56*(38), 11354–11359. https://doi.org/10.1002/anie.201703191
18. Bard, F., & Chia, J. (2016). Cracking the Glycome Encoder: Signaling, Trafficking, and Glycosylation. *Trends in Cell Biology*, *26*(5), 379–388. https://doi.org/10.1016/j.tcb.2015.12.004
19. Bastock, R., & St Johnston, D. (2008). Drosophila oogenesis. *Current Biology*, *18*(23), 1082–1087. https://doi.org/10.1016/j.cub.2008.09.011
20. Batty, E. C., Jensen, K., & Freemont, P. S. (2012). PML nuclear bodies and other TRIM-defined subcellular compartments. *Advances in Experimental Medicine and Biology*, *770*, 39–58. https://doi.org/10.1007/978-1-4614-5398-7_4
21. Becalska, A. N., & Gavis, E. R. (2009). Lighting up mRNA localization in Drosophila oogenesis. *Development*, *136*(15), 2493–2503. https://doi.org/10.1242/dev.032391
22. Becker, K., Balsa-Canto, E., Cicin-Sain, D., Hoermann, A., Janssens, H., Banga,

J. R., & Jaeger, J. (2013). Reverse-Engineering Post-Transcriptional Regulation of Gap Genes in Drosophila melanogaster. *PLoS Computational Biology*, *9*(10), 37–40. https://doi.org/10.1371/journal.pcbi.1003281

23. Bentley, E. P., Frey, B. B., & Deniz, A. A. (2019). Physical Chemistry of Cellular Liquid-Phase Separation. *Chemistry - A European Journal*, *25*(22), 5600–5610. https://doi.org/10.1002/chem.201805093
24. Berry, J., Weber, S. C., Vaidya, N., Haataja, M., Brangwynne, C. P., & Weitz, D. A. (2015). RNA transcription modulates phase transition-driven nuclear body assembly. *Proceedings of the National Academy of Sciences of the United States of America*, *112*(38), E5237–E5245. https://doi.org/10.1073/pnas.1509317112
25. Boeynaems, S., Alberti, S., Fawzi, N. L., Mittag, T., Polymenidou, M., Rousseau, F., Schymkowitz, J., Shorter, J., Wolozin, B., Van Den Bosch, L., Tompa, P., & Fuxreiter, M. (2018). Protein Phase Separation: A New Phase in Cell Biology. *Trends in Cell Biology*, *28*(6), 420–435. https://doi.org/10.1016/j.tcb.2018.02.004
26. Boeynaems, S., Bogaert, E., Kovacs, D., Konijnenberg, A., Timmerman, E., Volkov, A., Guharoy, M., De Decker, M., Jaspers, T., Ryan, V. H., Janke, A. M., Baatsen, P., Vercruysse, T., Kolaitis, R. M., Daelemans, D., Taylor, J. P., Kedersha, N., Anderson, P., Impens, F., … Van Den Bosch, L. (2017). Phase Separation of C9orf72 Dipeptide Repeats Perturbs Stress Granule Dynamics. *Molecular Cell*, *65*(6), 1044-1055.e5. https://doi.org/10.1016/j.molcel.2017.02.013
27. Boeynaems, S., Holehouse, A. S., Weinhardt, V., Kovacs, D., Van Lindt, J., Larabell, C., Bosch, L. Van Den, Das, R., Tompa, P. S., Pappu, R. V., & Gitler, A. D. (2019). Spontaneous driving forces give rise to protein−RNA condensates with coexisting phases and complex material properties. *Proceedings of the National Academy of Sciences of the United States of America*, *116*(16), 7889–7898. https://doi.org/10.1073/pnas.1821038116
28. Boke, E., Ruer, M., Wühr, M., Coughlin, M., Lemaitre, R., Gygi, S. P., Alberti, S., Drechsel, D., Hyman, A. A., & Mitchison, T. J. (2016). Amyloid-like Self-Assembly of a Cellular Compartment. *Cell*, *166*(3), 637–650. https://doi.org/10.1016/j.cell.2016.06.051
29. Bonifacino, J. S., & Glick, B. S. (2004). The Mechanisms of Vesicle Budding and Fusion. *Cell*, *116*(2), 153–166. https://doi.org/10.1016/S0092-8674(03)01079-1
30. Bouveret, E. (2000). A Sm-like protein complex that participates in mRNA degradation. *The EMBO Journal*, *19*(7), 1661–1671. https://doi.org/10.1093/emboj/19.7.1661

31. Bracha, D., Walls, M. T., & Brangwynne, C. P. (2019). Probing and engineering

liquid-phase organelles. *Nature Biotechnology*, *37*(12), 1435–1445. https://doi.org/10.1038/s41587-019-0341-6

32. Brangwynne, C. P., Eckmann, C. R., Courson, D. S., Rybarska, A., Hoege, C., Gharakhani, J., Jülicher, F., & Hyman, A. A. (2009). Germline P granules are liquid droplets that localize by controlled dissolution/condensation. *Science*, *324*(5935), 1729–1732. https://doi.org/10.1126/science.1172046
33. Brangwynne, C. P., Mitchison, T. J., & Hyman, A. A. (2011). Active liquid-like behavior of nucleoli determines their size and shape in Xenopus laevis oocytes. *Proceedings of the National Academy of Sciences of the United States of America*, *108*(11), 4334–4339. https://doi.org/10.1073/pnas.1017150108
34. Brangwynne, C. P., Tompa, P., & Pappu, R. V. (2015). Polymer physics of intracellular phase transitions. *Nature Physics*, *11*(11), 899–904. https://doi.org/10.1038/nphys3532
35. Bullock, S. L., & Ish-Horowicz, D. (2001). Conserved signals and machinery for RNA transport in Drosophila oogenesis and embryogenesis. *Nature*, *414*(6864), 611–616. https://doi.org/10.1038/414611a
36. Bullock, Simon L., Zicha, D., & Ish-Horowicz, D. (2003). The Drosophila hairy RNA localization signal modulates the kinetics of cytoplasmic mRNA transport. *EMBO Journal*, *22*(10), 2484–2494. https://doi.org/10.1093/emboj/cdg230
37. Burke, K. A., Janke, A. M., Rhine, C. L., & Fawzi, N. L. (2015). Residue-by-Residue View of In Vitro FUS Granules that Bind the C-Terminal Domain of RNA Polymerase II. *Molecular Cell*, *60*(2), 231–241. https://doi.org/10.1016/j.molcel.2015.09.006
38. Buszczak, M., Paterno, S., Lighthouse, D., Bachman, J., Planck, J., Owen, S., Skora, A. D., Nystul, T. G., Ohlstein, B., Allen, A., Wilhelm, J. E., Murphy, T. D., Levis, R. W., Matunis, E., Srivali, N., Hoskins, R. a., & Spradling, A. C. (2007). The carnegie protein trap library: A versatile tool for drosophila developmental studies. *Genetics*, *175*(3), 1505–1531. https://doi.org/10.1534/genetics.106.065961
39. Case, L. B., Zhang, X., Ditlev, J. A., & Rosen, M. K. (2019). Stoichiometry controls activity of phase-separated clusters of actin signaling proteins. *Science*, *363*(6431), 1093–1097. https://doi.org/10.1126/science.aau6313
40. Cha, B. J., Koppetsch, B. S., & Theurkauf, W. E. (2001). In vivo analysis of drosophila bicoid mRNA localization reveals a novel microtubule-dependent axis specification pathway. *Cell*, *106*(1), 35–46. https://doi.org/10.1016/S0092-8674(01)00419-6
41. Chantarachot, T., & Bailey-Serres, J. (2018). Polysomes, stress granules, and

processing bodies: A dynamic triumvirate controlling cytoplasmic mRNA fate and function. *Plant Physiology*, *176*(1), 254–269. https://doi.org/10.1104/pp.17.01468

42. Chen, C.-Y. A., & Shyu, A.-B. (2013). Deadenylation and P-Bodies. In E. K. L. Chan & M. J. Fritzler (Eds.), *Ten Years of Progress in GW/P Body Research* (pp. 183–195). Springer New York. https://doi.org/10.1007/978-1-4614-5107-5_11
43. Choi, H. M. T., Beck, V. A., & Pierce, N. A. (2014). Next-generation in situ hybridization chain reaction: Higher gain, lower cost, greater durability. *ACS Nano*, *8*(5), 4284–4294. https://doi.org/10.1021/nn405717p
44. Choi, H. M. T., Schwarzkopf, M., Fornace, M. E., Acharya, A., Artavanis, G., Stegmaier, J., Cunha, A., & Pierce, N. A. (2018). Third-generation in situ hybridization chain reaction: Multiplexed, quantitative, sensitive, versatile, robust. *Development (Cambridge)*, *145*(12), 1–10. https://doi.org/10.1242/dev.165753
45. Choi, J.-M., Holehouse, A. S., & Pappu, R. V. (2020). Physical Principles Underlying the Complex Biology of Intracellular Phase Transitions. *Annual Review of Biophysics*, *49*(1), 107–133. https://doi.org/10.1146/annurev-biophys-121219-081629
46. Choi, J. M., Dar, F., & Pappu, R. V. (2019). LASSI: A lattice model for simulating phase transitions of multivalent proteins. In *PLoS Computational Biology* (Vol. 15, Issue 10). https://doi.org/10.1371/journal.pcbi.1007028
47. Choi, U. B., Sanabria, H., Smirnova, T., Bowen, M. E., & Weninger, K. R. (2019). Spontaneous switching among conformational ensembles in intrinsically disordered proteins. *Biomolecules*, *9*(3), 1–16. https://doi.org/10.3390/biom9030114
48. Clark, A., Meignin, C., & Davis, I. (2007). A Dynein-dependent shortcut rapidly delivers axis determination transcripts into the Drosophila oocyte. *Development*, *134*(10), 1955–1965. https://doi.org/10.1242/dev.02832
49. Clark, E. (2017). Dynamic patterning by the Drosophila pair-rule network reconciles long-germ and short-germ segmentation. *PLOS Biology*, *15*(9), 1–38. https://doi.org/10.1371/journal.pbio.2002439
50. Conicella, A. E., Dignon, G. L., Zerze, G. H., Schmidt, H. B., D'Ordine, A. M., Kim, Y. C., Rohatgi, R., Ayala, Y. M., Mittal, J., & Fawzi, N. L. (2020). TDP-43 α-helical structure tunes liquid–liquid phase separation and function. *Proceedings of the National Academy of Sciences of the United States of America*, *117*(11), 5883–5894. https://doi.org/10.1073/pnas.1912055117

51. Decker, C. J., & Parker, R. (2006). CAR-1 and trailer hitch: Driving mRNP granule

function at the ER? *Journal of Cell Biology*, *173*(2), 159–163. https://doi.org/10.1083/jcb.200601153

52. Decker, C. J., & Parker, R. (2012). P-bodies and stress granules: Possible roles in the control of translation and mRNA degradation. *Cold Spring Harbor Perspectives in Biology*, *4*(9). https://doi.org/10.1101/cshperspect.a012286
53. Decker, C. J., Teixeira, D., & Parker, R. (2007). Edc3p and a glutamine/asparagine-rich domain of Lsm4p function in processing body assembly in Saccharomyces cerevisiae. *Journal of Cell Biology*, *179*(3), 437–449. https://doi.org/10.1083/jcb.200704147
54. DeHaan, H., McCambridge, A., Armstrong, B., Cruse, C., Solanki, D., Trinidad, J. C., Arkov, A. L., & Gao, M. (2017). An in vivo proteomic analysis of the Me31B interactome in Drosophila germ granules. *FEBS Letters*, *591*(21), 3536–3547. https://doi.org/10.1002/1873-3468.12854
55. Delanoue, R., Herpers, B., Soetaert, J., Davis, I., & Rabouille, C. (2007). Drosophila Squid/hnRNP Helps Dynein Switch from a gurken mRNA Transport Motor to an Ultrastructural Static Anchor in Sponge Bodies. *Developmental Cell*, *13*(4), 523–538. https://doi.org/10.1016/j.devcel.2007.08.022
56. Delarue, M., Brittingham, G. P., Pfeffer, S., Surovtsev, I. V., Pinglay, S., Kennedy, K. J., Schaffer, M., Gutierrez, J. I., Sang, D., Poterewicz, G., Chung, J. K., Plitzko, J. M., Groves, J. T., Jacobs-Wagner, C., Engel, B. D., & Holt, L. J. (2018). mTORC1 Controls Phase Separation and the Biophysical Properties of the Cytoplasm by Tuning Crowding. *Cell*, *174*(2), 338-349.e20. https://doi.org/10.1016/j.cell.2018.05.042
57. Derrick, C. J., & Weil, T. T. (2017). Translational control of gurken mRNA in Drosophila development. *Cell Cycle*, *16*(1), 23–32. https://doi.org/10.1080/15384101.2016.1250048
58. Dine, E., Gil, A. A., Uribe, G., Brangwynne, C. P., & Jared, E. (2019). *transient spatial stimuli*. *6*(6), 655–663. https://doi.org/10.1016/j.cels.2018.05.002.Protein
59. Ditlev, J. A., Case, L. B., & Rosen, M. K. (2018). Who's In and Who's Out—Compositional Control of Biomolecular Condensates. *Journal of Molecular Biology*, *430*(23), 4666–4684. https://doi.org/10.1016/j.jmb.2018.08.003
60. dos Santos, G., Simmonds, A. J., & Krause, H. M. (2008). A stem-loop structure in the wingless transcript defines a consensus motif for apical RNA transport. *Development*, *135*(1), 133–143. https://doi.org/10.1242/dev.014068
61. Dosztányi, Z. (2018). Prediction of protein disorder based on IUPred. *Protein Science*, *27*(1), 331–340. https://doi.org/10.1002/pro.3334
62. Dosztányi, Z., Csizmok, V., Tompa, P., & Simon, I. (2005). IUPred: Web server for

the prediction of intrinsically unstructured regions of proteins based on estimated energy content. *Bioinformatics*, *21*(16), 3433–3434. https://doi.org/10.1093/bioinformatics/bti541

63. Douglas, P. M., Treusch, S., Ren, H. Y., Halfmann, R., Duennwald, M. L., Lindquist, S., & Cyr, D. M. (2008). Chaperone-dependent amyloid assembly protects cells from prion toxicity. *Proceedings of the National Academy of Sciences of the United States of America*, *105*(20), 7206–7211. https://doi.org/10.1073/pnas.0802593105
64. Du, T. G., Schmid, M., & Jansen, R. P. (2007). Why cells move messages: The biological functions of mRNA localization. *Seminars in Cell and Developmental Biology*, *18*(2), 171–177. https://doi.org/10.1016/j.semcdb.2007.01.010
65. Edgar, B. A., Odell, G. M., & Schubiger, G. (1989). A genetic switch, based on negative regulation, sharpens stripes in Drosophila embryos. *Developmental Genetics*, *10*(3), 124–142. https://doi.org/10.1002/dvg.1020100303
66. Edgar, B. A., Weir, M. P., Schubiger, G., & Kornberg, T. (1986). Repression and turnover pattern fushi tarazu RNA in the early Drosophila embryo. *Cell*, *47*(5), 747–754. https://doi.org/10.1016/0092-8674(86)90517-9
67. Eichhorn, S. W., Subtelny, A. O., Kronja, I., Kwasnieski, J. C., Orr-Weaver, T. L., & Bartel, D. P. (2016). mRNA poly(A)-tail changes specified by deadenylation broadly reshape translation in Drosophila oocytes and early embryos. *ELife*, *5*(JULY), 1–24. https://doi.org/10.7554/eLife.16955
68. Elbaum-Garfinkle, S., Kim, Y., Szczepaniak, K., Chen, C. C. H., Eckmann, C. R., Myong, S., & Brangwynne, C. P. (2015). The disordered P granule protein LAF-1 drives phase separation into droplets with tunable viscosity and dynamics. *Proceedings of the National Academy of Sciences of the United States of America*, *112*(23), 7189–7194. https://doi.org/10.1073/pnas.1504822112
69. Espinosa, J. R., Joseph, J. A., Sanchez-Burgos, I., Garaizar, A., Frenkel, D., & Collepardo-Guevara, R. (2020). Liquid network connectivity regulates the stability and composition of biomolecular condensates with many components. *Proceedings of the National Academy of Sciences*, 201917569. https://doi.org/10.1073/pnas.1917569117
70. Eulalio, A., Behm-Ansmant, I., & Izaurralde, E. (2007). P bodies: At the crossroads of post-transcriptional pathways. *Nature Reviews Molecular Cell Biology*, *8*(1), 9–22. https://doi.org/10.1038/nrm2080
71. Eulalio, A., Behm-Ansmant, I., Schweizer, D., & Izaurralde, E. (2007). P-Body

Formation Is a Consequence, Not the Cause, of RNA-Mediated Gene Silencing. *Molecular and Cellular Biology*, *27*(11), 3970–3981. https://doi.org/10.1128/mcb.00128-07

72. Farrell, J. A., & O'Farrell, P. H. (2014). From Egg to Gastrula: How the Cell Cycle Is Remodeled During the Drosophila Mid-Blastula Transition . *Annual Review of Genetics*, *48*(1), 269–294. https://doi.org/10.1146/annurev-genet-111212-133531
73. Feric, M., Vaidya, N., Harmon, T. S., Mitrea, D. M., Zhu, L., Richardson, T. M., Kriwacki, R. W., Pappu, R. V., & Brangwynne, C. P. (2016). Coexisting Liquid Phases Underlie Nucleolar Subcompartments. *Cell*, *165*(7), 1686–1697. https://doi.org/10.1016/j.cell.2016.04.047
74. Franzmann, T. M., & Alberti, S. (2019). Protein phase separation as a stress survival strategy. *Cold Spring Harbor Perspectives in Medicine*, *9*(6), 1–18. https://doi.org/10.1101/cshperspect.a034058
75. Franzmann, T. M., Jahnel, M., Pozniakovsky, A., Mahamid, J., Holehouse, A. S., Nüske, E., Richter, D., Baumeister, W., Grill, S. W., Pappu, R. V., Hyman, A. A., & Alberti, S. (2018). Phase separation of a yeast prion protein promotes cellular fitness. *Science*, *359*(6371). https://doi.org/10.1126/science.aao5654
76. Gagnon, J. A., & Mowry, K. L. (2011). Molecular motors: Directing traffic during RNA localization. *Critical Reviews in Biochemistry and Molecular Biology*, *46*(3), 229–239. https://doi.org/10.3109/10409238.2011.572861
77. Garcia-Jove Navarro, M., Kashida, S., Chouaib, R., Souquere, S., Pierron, G., Weil, D., & Gueroui, Z. (2019). RNA is a critical element for the sizing and the composition of phase-separated RNA–protein condensates. *Nature Communications*, *10*(1), 1–13. https://doi.org/10.1038/s41467-019-11241-6
78. Gasior, K., Zhao, J., McLaughlin, G., Forest, M. G., Gladfelter, A. S., & Newby, J. (2019). Partial demixing of RNA-protein complexes leads to intradroplet patterning in phase-separated biological condensates. *Physical Review E*, *99*(1). https://doi.org/10.1103/PhysRevE.99.012411
79. Gibson, B. A., Doolittle, L. K., Schneider, M. W. G., Jensen, L. E., Gamarra, N., Henry, L., Gerlich, D. W., Redding, S., & Rosen, M. K. (2019). Organization of Chromatin by Intrinsic and Regulated Phase Separation. *Cell*, *179*(2), 470-484.e21. https://doi.org/10.1016/j.cell.2019.08.037
80. Gomes, E., & Shorter, J. (2019). The molecular language of membraneless organelles. *Journal of Biological Chemistry*, *294*(18), 7115–7127. https://doi.org/10.1074/jbc.TM118.001192

81. Götze, M., Dufourt, J., Ihling, C., Rammelt, C., Pierson, S., Sambrani, N., Temme,

C., Sinz, A., Simonelig, M., & Wahle, E. (2017). Translational repression of the Drosophila nanos mRNA involves the RNA helicase Belle and RNA coating by Me31B and Trailer hitch. *Rna*, *23*(10), 1552–1568. https://doi.org/10.1261/rna.062208.117

82. Greenblatt, E. J., Obniski, R., Mical, C., & Spradling, A. C. (2019). Prolonged ovarian storage of mature drosophila oocytes dramatically increases meiotic spindle instability. *ELife*, *8*, 1–17. https://doi.org/10.7554/eLife.49455
83. Gui, X., Luo, F., Li, Y., Zhou, H., Qin, Z., Liu, Z., Gu, J., Xie, M., Zhao, K., Dai, B., Shin, W. S., He, J., He, L., Jiang, L., Zhao, M., Sun, B., Li, X., Liu, C., & Li, D. (2019). Structural basis for reversible amyloids of hnRNPA1 elucidates their role in stress granule assembly. *Nature Communications*, *10*(1). https://doi.org/10.1038/s41467-019-09902-7
84. Guillén-Boixet, J., Kopach, A., Holehouse, A. S., Wittmann, S., Jahnel, M., Schlüßler, R., Kim, K., Trussina, I. R. E. A., Wang, J., Mateju, D., Poser, I., Maharana, S., Ruer-Gruß, M., Richter, D., Zhang, X., Chang, Y. T., Guck, J., Honigmann, A., Mahamid, J., … Franzmann, T. M. (2020). RNA-Induced Conformational Switching and Clustering of G3BP Drive Stress Granule Assembly by Condensation. *Cell*, *181*(2), 346-361.e17. https://doi.org/10.1016/j.cell.2020.03.049
85. Halfmann, R., & Lindquist, S. (2008). Screening for amyloid aggregation by semi-denaturing detergent-agarose gel electrophoresis. *Journal of Visualized Experiments*, *17*, 11–13. https://doi.org/10.3791/838
86. Hamm, D. C., & Harrison, M. M. (2018). Regulatory principles governing the maternal-to-zygotic transition: Insights from Drosophila melanogaster. *Open Biology*, *8*(12). https://doi.org/10.1098/rsob.180183
87. Hanazawa, M., Yonetani, M., & Sugimoto, A. (2011). PGL proteins self associate and bind RNPs to mediate germ granule assembly in C. elegans. *Journal of Cell Biology*, *192*(6), 929–937. https://doi.org/10.1083/jcb.201010106
88. Hara, M., Lourido, S., Petrova, B., Lou, H. J., Von Stetina, J. R., Kashevsky, H., Turk, B. E., & Orr-Weaver, T. L. (2018). Identification of PNG kinase substrates uncovers interactions with the translational repressor TRAL in the oocyte-to-embryo transition. *ELife*, *7*, 1–19. https://doi.org/10.7554/eLife.33150
89. Hara, M., Petrova, B., & Orr-Weaver, T. L. (2017). Control of PNG kinase, a key regulator of mrna translation, is coupled to meiosis completion at egg activation. *ELife*, *6*, 1–22. https://doi.org/10.7554/eLife.22219

90. Heald, R., & Cohen-Fix, O. (2014). Morphology and function of membrane-bound

organelles. *Current Opinion in Cell Biology*, *26*(1), 79–86. https://doi.org/10.1016/j.ceb.2013.10.006

91. Heifetz, Y., Yu, J., & Wolfner, M. F. (2001). Ovulation triggers activation of Drosophila oocytes. *Developmental Biology*, *234*, 416–424. https://doi.org/10.1006/dbio.2001.0246

92. Herpers, B., & Rabouille, C. (2004). mRNA localization and ER-based protein sorting mechanisms dictate the use of transitional endoplasmic reticulum-golgi units involved in gurken transport in Drosophila oocytes. *Molecular Biology of the Cell*, *15*(12), 5306–5317. https://doi.org/10.1091/mbc.e04-05-0398

93. Hillebrand, J., Barbee, S. A., & Ramaswami, M. (2007). P-body components, microRNA regulation, and synaptic plasticity. *TheScientificWorldJournal*, *7*(SUPPL. 2), 178–190. https://doi.org/10.1100/tsw.2007.206

94. Hofweber, M., & Dormann, D. (2019). Friend or foe-Post-translational modifications as regulators of phase separation and RNP granule dynamics. *Journal of Biological Chemistry*, *294*(18), 7137–7150. https://doi.org/10.1074/jbc.TM118.001189

95. Hofweber, M., Hutten, S., Bourgeois, B., Spreitzer, E., Niedner-Boblenz, A., Schifferer, M., Ruepp, M. D., Simons, M., Niessing, D., Madl, T., & Dormann, D. (2018). Phase Separation of FUS Is Suppressed by Its Nuclear Import Receptor and Arginine Methylation. *Cell*, *173*(3), 706-719.e13. https://doi.org/10.1016/j.cell.2018.03.004

96. Hondele, M., Sachdev, R., Heinrich, S., Wang, J., Vallotton, P., Fontoura, B. M. A., & Weis, K. (2019). DEAD-box ATPases are global regulators of phase-separated organelles. *Nature*, *573*(7772), 144–148. https://doi.org/10.1038/s41586-019-1502-y

97. Horner, V. L., & Wolfner, M. F. (2008a). Transitioning from egg to embryo: Triggers and mechanisms of egg activation. *Developmental Dynamics*, *237*(3), 527–544. https://doi.org/10.1002/dvdy.21454

98. Hu, Q., & Wolfner, M. F. (2019). The Drosophila Trpm channel mediates calcium influx during egg activation. *Proceedings of the National Academy of Sciences*, *116*(38), 18994–19000. https://doi.org/10.1073/pnas.1906967116

99. Hubstenberger, A., Cameron, C., Noble, S. L., Keenan, S., & Evans, T. C. (2015). Modifiers of solid RNP granules control normal RNP dynamics and mRNA activity in early development. *Journal of Cell Biology*, *211*(3), 703–716. https://doi.org/10.1083/jcb.201504044

100. Hubstenberger, A., Courel, M., Bénard, M., Souquere, S., Ernoult-Lange, M.,

Chouaib, R., Yi, Z., Morlot, J. B., Munier, A., Fradet, M., Daunesse, M., Bertrand, E., Pierron, G., Mozziconacci, J., Kress, M., & Weil, D. (2017). P-Body Purification Reveals the Condensation of Repressed mRNA Regulons. *Molecular Cell*, *68*(1), 144-157.e5. https://doi.org/10.1016/j.molcel.2017.09.003

101. Hubstenberger, A., Noble, S. L., Cameron, C., & Evans, T. C. (2013). Translation repressors, an RNA helicase, and developmental cues control RNP phase transitions during early development. *Developmental Cell*, *27*(2), 161–173. https://doi.org/10.1016/j.devcel.2013.09.024
102. Hughes, S. C., & Simmonds, A. J. (2019). Drosophila mRNA localization during later development: Past, present, and future. *Frontiers in Genetics*, *10*(MAR), 1–19. https://doi.org/10.3389/fgene.2019.00135
103. Huizar, R. L., Lee, C., Boulgakov, A. A., Horani, A., Tu, F., Marcotte, E. M., Brody, S. L., & Wallingford, J. B. (2018). A liquid-like organelle at the root of motile ciliopathy. *ELife*, *7*, 1–24. https://doi.org/10.7554/eLife.38497
104. Hyman, A. A., Weber, C. A., & Jülicher, F. (2014). Liquid-Liquid Phase Separation in Biology. *Annual Review of Cell and Developmental Biology*, *30*(1), 39–58. https://doi.org/10.1146/annurev-cellbio-100913-013325
105. Iserman, C., Desroches Altamirano, C., Jegers, C., Friedrich, U., Zarin, T., Fritsch, A. W., Mittasch, M., Domingues, A., Hersemann, L., Jahnel, M., Richter, D., Guenther, U. P., Hentze, M. W., Moses, A. M., Hyman, A. A., Kramer, G., Kreysing, M., Franzmann, T. M., & Alberti, S. (2020). Condensation of Ded1p Promotes a Translational Switch from Housekeeping to Stress Protein Production. *Cell*, *181*(4), 818-831.e19. https://doi.org/10.1016/j.cell.2020.04.009
106. Jahnel, M., Behrndt, M., Jannasch, A., Schäffer, E., & Grill, S. W. (2011). Measuring the complete force field of an optical trap. *Optics Letters*, *36*(7), 1260. https://doi.org/10.1364/ol.36.001260
107. Jain, A., & Vale, R. D. (2017). RNA phase transitions in repeat expansion disorders. *Nature*, *546*(7657), 243–247. https://doi.org/10.1038/nature22386
108. Jain, S., Wheeler, J. R., Walters, R. W., Agrawal, A., Barsic, A., & Parker, R. (2016). ATPase-Modulated Stress Granules Contain a Diverse Proteome and Substructure. *Cell*, *164*(3), 487–498. https://doi.org/10.1016/j.cell.2015.12.038
109. Jansova, D., Tetkova, A., Koncicka, M., Kubelka, M., & Susor, A. (2018). Localization of RNA and translation in the mammalian oocyte and embryo. *PLoS ONE*, *13*(3), 1–25. https://doi.org/10.1371/journal.pone.0192544
110. Johnston, D. S., & Nüsslein-Volhard, C. (1992). The origin of pattern and polarity

in the Drosophila embryo. *Cell*, *68*(2), 201–219. https://doi.org/10.1016/0092-8674(92)90466-P

111. Jonas, S., & Izaurralde, E. (2013). The role of disordered protein regions in the assembly of decapping complexes and RNP granules. *Genes and Development*, *27*(24), 2628–2641. https://doi.org/10.1101/gad.227843.113

112. Jung, H. Il, Shin, I., Park, Y. M., Kang, K. W., & Ha, K. S. (1997). Colchicine Activates Actin Polymerization by Microtubule Depolymerization. *Molecules and Cells*, *7*(3), 431–437.

113. Kaneuchi, T., Sartain, C. V, Takeo, S., Horner, V. L., Buehner, N. a, Aigaki, T., & Wolfner, M. F. (2015). Calcium waves occur as Drosophila oocytes activate. *Proceedings of the National Academy of Sciences of the United States of America*, *112*(3), 791–796. https://doi.org/10.1073/pnas.1420589112

114. Kato, M., Han, T. W., Xie, S., Shi, K., Du, X., Wu, L. C., Mirzaei, H., Goldsmith, E. J., Longgood, J., Pei, J., Grishin, N. V., Frantz, D. E., Schneider, J. W., Chen, S., Li, L., Sawaya, M. R., Eisenberg, D., Tycko, R., & McKnight, S. L. (2012). Cell-free formation of RNA granules: Low complexity sequence domains form dynamic fibers within hydrogels. *Cell*, *149*(4), 753–767. https://doi.org/10.1016/j.cell.2012.04.017

115. Kato, Y., & Nakamura, A. (2012). Roles of cytoplasmic RNP granules in intracellular RNA localization and translational control in the Drosophila oocyte. *Development Growth and Differentiation*, *54*(1), 19–31. https://doi.org/10.1111/j.1440-169X.2011.01314.x

116. Kaur, T., Alshareedah, I., Wang, W., Ngo, J., Moosa, M. M., & Banerjee, P. R. (2019). Molecular crowding tunes material states of ribonucleoprotein condensates. *Biomolecules*, *9*(2), 1–17. https://doi.org/10.3390/biom9020071

117. Kim, T. H., Tsang, B., Vernon, R. M., Sonenberg, N., Kay, L. E., & Forman-Kay, J. D. (2019). Phospho-dependent phase separation of FMRP and CAPRIN1 recapitulates regulation of translation and deadenylation. *Science*, *365*(6455), 825–829. https://doi.org/10.1126/science.aax4240

118. Klein, I. A., Boija, A., Afeyan, L. K., Hawken, S. W., Fan, M., Dall'Agnese, A., Oksuz, O., Henninger, J. E., Shrinivas, K., Sabari, B. R., Sagi, I., Clark, V. E., Platt, J. M., Kar, M., McCall, P. M., Zamudio, A. V., Manteiga, J. C., Coffey, E. L., Li, C. H., … Young, R. A. (2020). Partitioning of cancer therapeutics in nuclear condensates. *Science (New York, N.Y.)*, *368*(6497), 1386–1392. https://doi.org/10.1126/science.aaz4427

119. Kloc, M., Bilinski, S., & Etkin, L. D. (2004). The Balbiani body and germ cell

determinants: 150 years later. *Current Topics in Developmental Biology*, *59*, 1–36. https://doi.org/10.1016/S0070-2153(04)59001-4

120. Kloc, M., & Etkin, L. D. (2005). RNA localization mechanisms in oocytes. *Journal of Cell Science*, *118*(2), 269–282. https://doi.org/10.1242/jcs.01637

121. Krauchunas, A. R., & Wolfner, M. F. (2013). Molecular Changes During Egg Activation. *Current Topics in Developmental Biology*, *102*, 267–292. https://doi.org/10.1016/B978-0-12-416024-8.00010-6

122. Kroschwald, S., Maharana, S., Mateju, D., Malinovska, L., Nüske, E., Poser, I., Richter, D., & Alberti, S. (2015). Promiscuous interactions and protein disaggregases determine the material state of stress-inducible RNP granules. *ELife*, *4*(AUGUST2015), 1–32. https://doi.org/10.7554/eLife.06807

123. Kulkarni, M., Ozgur, S., & Stoecklin, G. (2010). On track with P-bodies. *Biochemical Society Transactions*, *38*(Pt 1), 242–251. https://doi.org/10.1042/BST0380242

124. Lall, S., Francis-Lang, H., Flament, A., Norvell, A., Schüpbach, T., & Ish-Horowicz, D. (1999). Squid hnRNP protein promotes apical cytoplasmic transport and localization of Drosophila pair-rule transcripts. *Cell*, *98*(2), 171–180. https://doi.org/10.1016/S0092-8674(00)81012-0

125. Langdon, E. M., Qiu, Y., Niaki, A. G., Mclaughlin, G. A., Weidmann, C. A., Gerbich, T. M., Smith, J. A., Crutchley, J. M., Termini, C. M., Weeks, K. M., Myong, S., & Gladfelter, A. S. (2018). *phase separation*. *1*(May), 922–927.

126. Lasko, P. (2012). mRNA localization and translational control in Drosophila oogenesis. *Cold Spring Harbor Perspectives in Biology*, *4*(10), 1–15. https://doi.org/10.1101/cshperspect.a012294

127. Lee, C. F., & Wurtz, J. D. (2018). Novel physics arising from phase transitions in biology. *Journal of Physics D: Applied Physics*, *52*(2). https://doi.org/10.1088/1361-6463/aae510

128. Lee, K. H., Zhang, P., Kim, H. J., Mitrea, D. M., Sarkar, M., Freibaum, B. D., Cika, J., Coughlin, M., Messing, J., Molliex, A., Maxwell, B. A., Kim, N. C., Temirov, J., Moore, J., Kolaitis, R. M., Shaw, T. I., Bai, B., Peng, J., Kriwacki, R. W., & Taylor, J. P. (2016). C9orf72 Dipeptide Repeats Impair the Assembly, Dynamics, and Function of Membrane-Less Organelles. *Cell*, *167*(3), 774-788.e17. https://doi.org/10.1016/j.cell.2016.10.002

129. Li, P., Banjade, S., Cheng, H. C., Kim, S., Chen, B., Guo, L., Llaguno, M.,

Hollingsworth, J. V., King, D. S., Banani, S. F., Russo, P. S., Jiang, Q. X., Nixon, B. T., & Rosen, M. K. (2012). Phase transitions in the assembly of multivalent signalling proteins. *Nature*, *483*(7389), 336–340. https://doi.org/10.1038/nature10879

130. Li, Q., & Chang, Y.-T. (2006). A protocol for preparing, characterizing and using three RNA-specific, live cell imaging probes: E36, E144 and F22. *Nature Protocols*, *1*(6), 2922–2932. https://doi.org/10.1038/nprot.2006.484
131. Lin, M. Der, Jiao, X., Grima, D., Newbury, S. F., Kiledjian, M., & Chou, T. Bin. (2008). Drosophila processing bodies in oogenesis. *Developmental Biology*, *322*(2), 276–288. https://doi.org/10.1016/j.ydbio.2008.07.033
132. Lin, Y., Currie, S. L., & Rosen, M. K. (2017). Intrinsically disordered sequences enable modulation of protein phase separation through distributed tyrosine motifs. *Journal of Biological Chemistry*, *292*(46), 19110–19120. https://doi.org/10.1074/jbc.M117.800466
133. Lin, Y., Protter, D. S. W., Rosen, M. K., & Parker, R. (2015a). Formation and Maturation of Phase-Separated Liquid Droplets by RNA-Binding Proteins. *Molecular Cell*, *60*(2), 208–219. https://doi.org/10.1016/j.molcel.2015.08.018
134. Luo, Y., Na, Z., & Slavoff, S. A. (2018). P-Bodies: Composition, Properties, and Functions. *Biochemistry*, *57*(17), 2424–2431. https://doi.org/10.1021/acs.biochem.7b01162
135. Maharana, S., Wang, J., Papadopoulos, D. K., Richter, D., Pozniakovsky, A., Poser, I., Bickle, M., Rizk, S., Guillén-boixet, J., Franzmann, T. M., Jahnel, M., Marrone, L., Chang, Y., Sterneckert, J., Tomancak, P., Hyman, A. A., & Alberti, S. (2018). *binding proteins*. *921*(March), 918–921.
136. Mahowald, A. (1985). Genetics of Drosophila Embryogenesis. *Annual Review of Genetics*, *19*(1), 149–177. https://doi.org/10.1146/annurev.genet.19.1.149
137. Mahowald, A. P., Goralski, T. J., & Caulton, J. H. (1983). In vitro activation of Drosophila eggs. *Developmental Biology*, *98*(2), 437–445. https://doi.org/10.1016/0012-1606(83)90373-1
138. Mahowald, A. P., Illmensee, K., & Turner, F. R. (1976). *DROSOPHILA*. *70*(18), 358–373.
139. Martin, E. W., Holehouse, A. S., Grace, C. R., Hughes, A., Pappu, R. V., & Mittag, T. (2016). Sequence Determinants of the Conformational Properties of an Intrinsically Disordered Protein Prior to and upon Multisite Phosphorylation. *Journal of the American Chemical Society*, *138*(47), 15323–15335. https://doi.org/10.1021/jacs.6b10272
140. Martin, E. W., Holehouse, A. S., Peran, I., Farag, M., Incicco, J. J., Bremer, A.,

Grace, C. R., Soranno, A., Pappu, R. V., & Mittag, T. (2020). Valence and patterning of aromatic residues determine the phase behavior of prion-like domains. *Science*, *367*(6478), 694–699. https://doi.org/10.1126/science.aaw8653

141. Martin, E. W., & Mittag, T. (2018). Relationship of Sequence and Phase Separation in Protein Low-Complexity Regions. *Biochemistry*, *57*(17), 2478–2487. https://doi.org/10.1021/acs.biochem.8b00008

142. McCambridge, A., Solanki, D., Olchawa, N., Govani, N., Trinidad, J. C., & Gao, M. (2020). Comparative Proteomics Reveal Me31B's Interactome Dynamics, Expression Regulation, and Assembly Mechanism into Germ Granules during Drosophila Germline Development. *Scientific Reports*, *10*(1), 1–13. https://doi.org/10.1038/s41598-020-57492-y

143. McCann, C., Holohan, E. E., Das, S., Dervan, A., Larkin, A., Lee, J. A., Rodrigues, V., Parker, R., & Ramaswami, M. (2011). The ataxin-2 protein is required for microRNA function and synapse-specific long-term olfactory habituation. *Proceedings of the National Academy of Sciences of the United States of America*, *108*(36). https://doi.org/10.1073/pnas.1107198108

144. McSwiggen, D. T., Mir, M., Darzacq, X., & Tjian, R. (2019). Evaluating phase separation in live cells: diagnosis, caveats, and functional consequences. *Genes & Development*, *33*(23–24), 1619–1634. https://doi.org/10.1101/gad.331520.119

145. Medioni, C., Mowry, K., & Besse, F. (2012). Principles and roles of mRNA localization in animal development. *Development (Cambridge)*, *139*(18), 3263–3276. https://doi.org/10.1242/dev.078626

146. Milin, A. N., & Deniz, A. A. (2018). Reentrant Phase Transitions and Non-Equilibrium Dynamics in Membraneless Organelles. *Biochemistry*, *57*(17), 2470–2477. https://doi.org/10.1021/acs.biochem.8b00001

147. Mitrea, D. M., & Kriwacki, R. W. (2016). Phase separation in biology; Functional organization of a higher order Short linear motifs - The unexplored frontier of the eukaryotic proteome. *Cell Communication and Signaling*, *14*(1), 1–20. https://doi.org/10.1186/s12964-015-0125-7

148. Molliex, A., Temirov, J., Lee, J., Coughlin, M., Kanagaraj, A. P., Kim, H. J., Mittag, T., & Taylor, J. P. (2015a). Phase Separation by Low Complexity Domains Promotes Stress Granule Assembly and Drives Pathological Fibrillization. *Cell*, *163*(1), 123–133. https://doi.org/10.1016/j.cell.2015.09.015

149. Monzo, K., Papoulas, O., Cantin, G. T., Wang, Y., Yates, J. R., & Sisson, J. C.

(2006). Fragile X mental retardation protein controls trailer hitch expression and cleavage furrow formation in Drosophila embryos. *Proceedings of the National Academy of Sciences of the United States of America*, *103*(48), 18160–18165. https://doi.org/10.1073/pnas.0606508103

150. Murakami, T., Qamar, S., Lin, J. Q., Schierle, G. S. K., Rees, E., Miyashita, A., Costa, A. R., Dodd, R. B., Chan, F. T. S., Michel, C. H., Kronenberg-Versteeg, D., Li, Y., Yang, S. P., Wakutani, Y., Meadows, W., Ferry, R. R., Dong, L., Tartaglia, G. G., Favrin, G., … St George-Hyslop, P. (2015). ALS/FTD Mutation-Induced Phase Transition of FUS Liquid Droplets and Reversible Hydrogels into Irreversible Hydrogels Impairs RNP Granule Function. *Neuron*, *88*(4), 678–690. https://doi.org/10.1016/j.neuron.2015.10.030

151. Murray, D. T., Kato, M., Lin, Y., Thurber, K. R., Hung, I., McKnight, S. L., & Tycko, R. (2017). Structure of FUS Protein Fibrils and Its Relevance to Self-Assembly and Phase Separation of Low-Complexity Domains. *Cell*, *171*(3), 615-627.e16. https://doi.org/10.1016/j.cell.2017.08.048

152. Nakamura, A., Amikura, R., Hanyu, K., & Kobayashi, S. (2001). Me31B silences translation of oocyte-localizing RNAs through the formation of cytoplasmic RNP complex during Drosophila oogenesis. *Development*, *128*(17), 3233–3242. http://www.ncbi.nlm.nih.gov/entrez/query.fcgi?cmd=Retrieve&db=PubMed&dopt=Citation&list_uids=11546740

153. Nakamura, H., Lee, A. A., Afshar, A. S., Watanabe, S., Rho, E., Razavi, S., Suarez, A., Lin, Y. C., Tanigawa, M., Huang, B., DeRose, R., Bobb, D., Hong, W., Gabelli, S. B., Goutsias, J., & Inoue, T. (2018). Intracellular production of hydrogels and synthetic RNA granules by multivalent molecular interactions. *Nature Materials*, *17*(1), 79–88. https://doi.org/10.1038/NMAT5006

154. Nishihara, T., Zekri, L., Braun, J. E., & Izaurralde, E. (2013). MiRISC recruits decapping factors to miRNA targets to enhance their degradation. *Nucleic Acids Research*, *41*(18), 8692–8705. https://doi.org/10.1093/nar/gkt619

155. Nott, T. J., Petsalaki, E., Farber, P., Jervis, D., Fussner, E., Plochowietz, A., Craggs, T. D., Bazett-Jones, D. P., Pawson, T., Forman-Kay, J. D., & Baldwin, A. J. (2015). Phase Transition of a Disordered Nuage Protein Generates Environmentally Responsive Membraneless Organelles. *Molecular Cell*, *57*(5), 936–947. https://doi.org/10.1016/j.molcel.2015.01.013

156. Owen, I., & Shewmaker, F. (2019). The role of post-translational modifications in the phase transitions of intrinsically disordered proteins. *International Journal of Molecular Sciences*, *20*(21). https://doi.org/10.3390/ijms20215501

157. Parker, R., & Sheth, U. (2007). P Bodies and the Control of mRNA Translation

and Degradation. *Molecular Cell*, *25*(5), 635–646. https://doi.org/10.1016/j.molcel.2007.02.011

158. Patel, A., Lee, H. O., Jawerth, L., Maharana, S., Jahnel, M., Hein, M. Y., Stoynov, S., Mahamid, J., Saha, S., Franzmann, T. M., Pozniakovski, A., Poser, I., Maghelli, N., Royer, L. A., Weigert, M., Myers, E. W., Grill, S., Drechsel, D., Hyman, A. A., & Alberti, S. (2015). A Liquid-to-Solid Phase Transition of the ALS Protein FUS Accelerated by Disease Mutation. *Cell*, *162*(5), 1066–1077. https://doi.org/10.1016/j.cell.2015.07.047
159. Patel, A., Malinovska, L., Saha, S., Wang, J., Alberti, S., Krishnan, Y., & Hyman, A. A. (2017). Biochemistry: ATP as a biological hydrotrope. *Science*, *356*(6339), 753–756. https://doi.org/10.1126/science.aaf6846
160. Patel, P. H., Barbee, S. a., & Blankenship, J. T. (2016). GW-bodies and P-bodies constitute two separate pools of sequestered non-translating RNAs. *PLoS ONE*, *11*(3), 1–23. https://doi.org/10.1371/journal.pone.0150291
161. Patterson, J. R., Wood, M. P., & Schisa, J. A. (2011). Assembly of RNP granules in stressed and aging oocytes requires nucleoporins and is coordinated with nuclear membrane blebbing. *Developmental Biology*, *353*(2), 173–185. https://doi.org/10.1016/j.ydbio.2011.02.028
162. Perry, S. L. (2019). Phase separation: Bridging polymer physics and biology. *Current Opinion in Colloid and Interface Science*, *39*, 86–97. https://doi.org/10.1016/j.cocis.2019.01.007
163. Piccioni, F., Zappavigna, V., & Verrotti, A. C. (2005). Translational regulation during oogenesis and early development: The cap-poly(A) tail relationship. *Comptes Rendus - Biologies*, *328*(10–11), 863–881. https://doi.org/10.1016/j.crvi.2005.05.006
164. Protter, D. S. W., Rao, B. S., Treeck, B. Van, Lin, Y., Mizoue, L., Rosen, M. K., & Parker, R. (2018). Intrinsically Disordered Regions Can Contribute Promiscuous Interactions to RNP Granule Assembly. *Cell Reports*, *22*(6), 1401–1412. https://doi.org/https://doi.org/10.1016/j.celrep.2018.01.036
165. Putnam, A., Cassani, M., Smith, J., & Seydoux, G. (2019). A gel phase promotes condensation of liquid P granules in Caenorhabditis elegans embryos. *Nature Structural and Molecular Biology*, *26*(3), 220–226. https://doi.org/10.1038/s41594-019-0193-2
166. Ramaswami, M. (2018). RNP-Granule Assembly via Ataxin-2 Disordered Domains Is Required for Long-Term Memory and Neurodegeneration. *Neuron*, *98*(4), 754-766.e4. https://doi.org/10.1016/j.neuron.2018.04.032
167. Riback, J. A., Katanski, C. D., Kear-Scott, J. L., Pilipenko, E. V., Rojek, A. E.,

Sosnick, T. R., & Drummond, D. A. (2017). Stress-Triggered Phase Separation Is an Adaptive, Evolutionarily Tuned Response. *Cell*, *168*(6), 1028-1040.e19. https://doi.org/10.1016/j.cell.2017.02.027

168. Roovers, E. F., Kaaij, L. J. T., Redl, S., Bronkhorst, A. W., Wiebrands, K., de Jesus Domingues, A. M., Huang, H. Y., Han, C. T., Riemer, S., Dosch, R., Salvenmoser, W., Grün, D., Butter, F., van Oudenaarden, A., & Ketting, R. F. (2018). Tdrd6a Regulates the Aggregation of Buc into Functional Subcellular Compartments that Drive Germ Cell Specification. *Developmental Cell*, *46*(3), 285-301.e9. https://doi.org/10.1016/j.devcel.2018.07.009
169. Rosowski, K. A., Sai, T., Vidal-Henriquez, E., Zwicker, D., Style, R. W., & Dufresne, E. R. (2020). Elastic ripening and inhibition of liquid–liquid phase separation. *Nature Physics*. https://doi.org/10.1038/s41567-019-0767-2
170. Runft, L. L., Jaffe, L. a, & Mehlmann, L. M. (2002). Egg activation at fertilization: where it all begins. *Developmental Biology*, *245*(2), 237–254. https://doi.org/10.1006/dbio.2002.0600
171. Saha, S., Weber, C. A., Nousch, M., Adame-Arana, O., Hoege, C., Hein, M. Y., Osborne-Nishimura, E., Mahamid, J., Jahnel, M., Jawerth, L., Pozniakovski, A., Eckmann, C. R., Jülicher, F., & Hyman, A. A. (2016). Polar Positioning of Phase-Separated Liquid Compartments in Cells Regulated by an mRNA Competition Mechanism. *Cell*, *166*(6), 1572-1584.e16. https://doi.org/10.1016/j.cell.2016.08.006
172. Sankaranarayanan, M., & Weil, T. T. (2020). Granule regulation by phase separation during Drosophila oogenesis. *Emerging Topics in Life Sciences*. https://doi.org/10.1042/ETLS20190155
173. Sartain, C. V., & Wolfner, M. F. (2013). Calcium and egg activation in Drosophila. *Cell Calcium*, *53*(1), 10–15. https://doi.org/10.1016/j.ceca.2012.11.008
174. Saxton, W. M. (2001). Microtubules, motors, and mRNA localization mechanisms: Watching fluorescent messages move. *Cell*, *107*(6), 707–710. https://doi.org/10.1016/S0092-8674(01)00602-X
175. Schisa, J. A. (2012). New Insights into the Regulation of RNP Granule Assembly in Oocytes. In *International Review of Cell and Molecular Biology* (1st ed., Vol. 295). Elsevier Inc. https://doi.org/10.1016/B978-0-12-394306-4.00013-7
176. Schmidt, H. B., Barreau, A., & Rohatgi, R. (2019). Phase separation-deficient TDP43 remains functional in splicing. *Nature Communications*, *10*(1), 1–14. https://doi.org/10.1038/s41467-019-12740-2

177. Schwartz, J. C., Wang, X., Podell, E. R., & Cech, T. R. (2013). RNA Seeds

Higher-Order Assembly of FUS Protein. *Cell Reports*, *5*(4), 918–925. https://doi.org/10.1016/j.celrep.2013.11.017

178. Scott, M. P., & Carroll, S. B. (1987). The segmentation and homeotic gene network in early Drosophila development. *Cell*, *51*(5), 689–698. https://doi.org/10.1016/0092-8674(87)90092-4

179. Smith, J., Calidas, D., Schmidt, H., Lu, T., Rasoloson, D., & Seydoux, G. (2016). Spatial patterning of P granules by RNA-induced phase separation of the intrinsically-disordered protein MEG-3. *ELife*, *5*(DECEMBER2016), 1–18. https://doi.org/10.7554/eLife.21337

180. Snead, W. T., & Gladfelter, A. S. (2019). The Control Centers of Biomolecular Phase Separation: How Membrane Surfaces, PTMs, and Active Processes Regulate Condensation. *Molecular Cell*, *76*(2), 295–305. https://doi.org/10.1016/j.molcel.2019.09.016

181. Söding, J., Zwicker, D., Sohrabi-Jahromi, S., Boehning, M., & Kirschbaum, J. (2020). Mechanisms for Active Regulation of Biomolecular Condensates. *Trends in Cell Biology*, *30*(1), 4–14. https://doi.org/10.1016/j.tcb.2019.10.006

182. Spradling, A. (1993). Developmental genetics of oogenesis. *The Development of Drosophila Melanogaster*.

183. St. Johnston, D. (2005). Moving messages: The intracellular localization of mRNAs. *Nature Reviews Molecular Cell Biology*, *6*(5), 363–375. https://doi.org/10.1038/nrm1643

184. Standart, N., & Weil, D. (2018). P-Bodies: Cytosolic Droplets for Coordinated mRNA Storage. *Trends in Genetics*, *34*(8), 612–626. https://doi.org/10.1016/j.tig.2018.05.005

185. Tadros, W., & Lipshitz, H. D. (2009). The maternal-to-zygotic transition: A play in two acts. *Development*, *136*(18), 3033–3042. https://doi.org/10.1242/dev.033183

186. Tanaka, K. J., Ogawa, K., Takagi, M., Imamoto, N., Matsumoto, K., & Tsujimoto, M. (2006). RAP55, a cytoplasmic mRNP component, represses translation in Xenopus oocytes. *Journal of Biological Chemistry*, *281*(52), 40096–40106. https://doi.org/10.1074/jbc.M609059200

187. Titus, A. R., Ferreira, L. A., Belgovskiy, A. I., Kooijman, E. E., Mann, E. K., Mann, J. A., Meyer, W. V., Smart, A. E., Uversky, V. N., & Zaslavsky, B. Y. (2020). Interfacial tension and mechanism of liquid-liquid phase separation in aqueous media. *Physical Chemistry Chemical Physics*, *22*(8), 4574–4580. https://doi.org/10.1039/c9cp05810a

188. Trcek, T., Grosch, M., York, A., Shroff, H., Lionnet, T., & Lehmann, R. (2015).

Drosophila germ granules are structured and contain homotypic mRNA clusters. *Nature Communications*, *6*. https://doi.org/10.1038/ncomms8962

189. Tritschler, F., Braun, J. E., Eulalio, A., Truffault, V., Izaurralde, E., & Weichenrieder, O. (2009). Structural Basis for the Mutually Exclusive Anchoring of P Body Components EDC3 and Tral to the DEAD Box Protein DDX6/Me31B. *Molecular Cell*, *33*(5), 661–668. https://doi.org/10.1016/j.molcel.2009.02.014
190. Tritschler, F., Eulalio, A., Helms, S., Schmidt, S., Coles, M., Weichenrieder, O., Izaurralde, E., & Truffault, V. (2008). Similar Modes of Interaction Enable Trailer Hitch and EDC3 To Associate with DCP1 and Me31B in Distinct Protein Complexes. *Molecular and Cellular Biology*, *28*(21), 6695–6708. https://doi.org/10.1128/mcb.00759-08
191. Tritschler, F., Eulalio, A., Truffault, V., Hartmann, M. D., Helms, S., Schmidt, S., Coles, M., Izaurralde, E., & Weichenrieder, O. (2007). A Divergent Sm Fold in EDC3 Proteins Mediates DCP1 Binding and P-Body Targeting. *Molecular and Cellular Biology*, *27*(24), 8600–8611. https://doi.org/10.1128/mcb.01506-07
192. Trovisco, V., Belaya, K., Nashchekin, D., Irion, U., Sirinakis, G., Butler, R., Lee, J. J., Gavis, E. R., & St Johnston, D. (2016). bicoid mRNA localises to the Drosophila oocyte anterior by random Dynein-mediated transport and anchoring. *ELife*, *5*(OCTOBER2016), 1–34. https://doi.org/10.7554/eLife.17537
193. Valentin, G. (1837). *Repertorium für anatomie und physiologie*.
194. Van Treeck, B., & Parker, R. (2018). Emerging Roles for Intermolecular RNA-RNA Interactions in RNP Assemblies. *Cell*, *174*(4), 791–802. https://doi.org/10.1016/j.cell.2018.07.023
195. Voronina, E., Seydoux, G., Sassone-Corsi, P., & Nagamori, I. (2011). RNA granules in germ cells. *Cold Spring Harbor Perspectives in Biology*, *3*(12). https://doi.org/10.1101/cshperspect.a002774
196. Wagner, R. (1835). Einige bemerkungen und fragen über das keimbläschen (vesicular germinativa). *Müller*[illegible]*s Archiv Anat Physiol Wissenschaft Med*, *268*, 373–377.
197. Walter, H., & Brooks, D. E. (1995). Phase separation in cytoplasm, due to macromolecular crowding, is the basis for microcompartmentation. *FEBS Letters*, *361*(2–3), 135–139. https://doi.org/10.1016/0014-5793(95)00159-7
198. Wang, C., Schmich, F., Srivatsa, S., Weidner, J., Beerenwinkel, N., & Spang, A. (2018). Erratum: Correction: Context-dependent deposition and regulation of mRNAs in P-bodies (eLife (2018) 7 PII: e41300). *ELife*, *7*, 1–25. https://doi.org/10.7554/eLife.41300
199. Wang, J., Choi, J. M., Holehouse, A. S., Lee, H. O., Zhang, X., Jahnel, M.,

Maharana, S., Lemaitre, R., Pozniakovsky, A., Drechsel, D., Poser, I., Pappu, R. V., Alberti, S., & Hyman, A. A. (2018a). A Molecular Grammar Governing the Driving Forces for Phase Separation of Prion-like RNA Binding Proteins. *Cell*, *174*(3), 688-699.e16. https://doi.org/10.1016/j.cell.2018.06.006

200. Wang, M., Ly, M., Lugowski, A., Laver, J. D., Lipshitz, H. D., Smibert, C. A., & Rissland, O. S. (2017). ME31B globally represses maternal mRNAs by two distinct mechanisms during the Drosophila maternal-to-zygotic transition. *ELife*, *6*, 1–22. https://doi.org/10.7554/eLife.27891
201. Webster, A., Li, S., Hur, J. K., Wachsmuth, M., Bois, J. S., Perkins, E. M., Patel, D. J., & Aravin, A. A. (2015). Aub and Ago3 Are Recruited to Nuage through Two Mechanisms to Form a Ping-Pong Complex Assembled by Krimper. *Molecular Cell*, *59*(4), 564–575. https://doi.org/10.1016/j.molcel.2015.07.017
202. Weil, T. T. (2014). mRNA localization in the Drosophila germline. *RNA Biology*, *11*(8), 1010–1018. https://doi.org/10.4161/rna.36097
203. Weil, T. T., Parton, R., Davis, I., & Gavis, E. R. (2008). Changes in bicoid mRNA Anchoring Highlight Conserved Mechanisms during the Oocyte-to-Embryo Transition. *Current Biology*, *18*(14), 1055–1061. https://doi.org/10.1016/j.cub.2008.06.046
204. Weil, T. T., Parton, R. M., Herpers, B., Soetaert, J., Veenendaal, T., Xanthakis, D., Dobbie, I. M., Halstead, J. M., Hayashi, R., Rabouille, C., & Davis, I. (2012a). Drosophila patterning is established by differential association of mRNAs with P bodies. *Nature Cell Biology*, *14*(12), 1305–1313. https://doi.org/10.1038/ncb2627
205. Weston, A., & Sommerville, J. (2006). Xp54 and related (DDX6-like) RNA helicases: Roles in messenger RNP assembly, translation regulation and RNA degradation. *Nucleic Acids Research*, *34*(10), 3082–3094. https://doi.org/10.1093/nar/gkl409
206. Wheeler, J. R., Matheny, T., Jain, S., Abrisch, R., & Parker, R. (2016). Distinct stages in stress granule assembly and disassembly. *ELife*, *5*(Se), 1–25. https://doi.org/10.7554/eLife.18413
207. Wilhelm, J. E., Buszczak, M., & Sayles, S. (2005). Efficient protein trafficking requires trailer hitch, a component of a ribonucleoprotein complex localized to the ER in Drosophila. *Developmental Cell*, *9*(5), 675–685. https://doi.org/10.1016/j.devcel.2005.09.015
208. Wilhelm, J. E., & Smibert, C. A. (2005). Mechanisms of translational regulation in Drosophila. *Biology of the Cell*, *97*(4), 235–252. https://doi.org/10.1042/BC20040097
209. Wilkie, G. S., & Davis, I. (2001). Drosophila wingless and pair-rule transcripts

localize apically by dynein-mediated transport of RNA particles. *Cell*, *105*(2), 209–219. https://doi.org/10.1016/S0092-8674(01)00312-9

210. Wilson, E. B. (1899). THE STRUCTURE OF PROTOPLASM. *Science*, *10*(237), 33–45. https://doi.org/10.1126/science.10.237.33

211. Woodruff, J. B., Ferreira Gomes, B., Widlund, P. O., Mahamid, J., Honigmann, A., & Hyman, A. A. (2017). The Centrosome Is a Selective Condensate that Nucleates Microtubules by Concentrating Tubulin. *Cell*, *169*(6), 1066-1077.e10. https://doi.org/10.1016/j.cell.2017.05.028

212. Xing, W., Muhlrad, D., Parker, R., & Rosen, M. K. (2020). A quantitative inventory of yeast P body proteins reveals principles of composition and specificity. *ELife*, *9*. https://doi.org/10.7554/eLife.56525

213. York-Andersen, A. H., Parton, R. M., Bi, C. J., Bromley, C. L., Davis, I., & Weil, T. T. (2015a). A single and rapid calcium wave at egg activation in Drosophila. *Biology Open*, *4*(4), 553–560. https://doi.org/10.1242/bio.201411296

214. Youn, J. Y., Dyakov, B. J. A., Zhang, J., Knight, J. D. R., Vernon, R. M., Forman-Kay, J. D., & Gingras, A. C. (2019). Properties of Stress Granule and P-Body Proteomes. *Molecular Cell*, *76*(2), 286–294. https://doi.org/10.1016/j.molcel.2019.09.014

215. Zhang, H., Elbaum-Garfinkle, S., Langdon, E. M., Taylor, N., Occhipinti, P., Bridges, A. A., Brangwynne, C. P., & Gladfelter, A. S. (2015). RNA Controls PolyQ Protein Phase Transitions. *Molecular Cell*, *60*(2), 220–230. https://doi.org/10.1016/j.molcel.2015.09.017